University of KwaZulu-Natal

Doping Titanium Dioxide with Copper, Nitrogen, or Sulfur: Physico-Chemical Properties and their Photo-catalytic Activity towards Emerging Pollutants

2015

Darrel Sarvesh Naidu

Doping Titanium Dioxide with Copper, Nitrogen, or Sulfur: Physico-Chemical Properties and their Photo-catalytic Activity towards Emerging Pollutants

2015

A Thesis

Submitted in partial fulfilment for the requirements

for the award of the degree of

MASTER OF SCIENCE

in the

School of Chemistry and Physics

College of Agriculture, Engineering & Science

By

Darrel Sarvesh Naidu

2015

Supervisor: Prof. P. Ndungu

Co-Supervisor: Dr S. Singh

Preface

The experimental work described in this dissertation was carried out from February 2013 to November 2015 in the School of Chemistry and Physics, Westville campus, Durban, under the supervision of Prof P Ndungu and Dr S. Singh.

This study represents original work by the author and has not been submitted in any other form to another university. Where use was made of work of others it has been duly acknowledged in the text.

Signed: _____

Darrel Sarvesh Naidu
BSc (Hons)

As the Candidate's supervisor, I have approved this dissertation for submission

Signed: _____

Prof P. Ndungu
Ph.D

Signed: _____

Dr S. Singh
Ph.D

Declaration – Plagiarism

I, **Darrel Sarvesh Naidu**, declare that:

1. The research reported in this thesis, except where otherwise indicated is my original research.
2. This thesis has not been submitted for any degree or examination at any other university.
3. This thesis does not contain other persons' data, pictures, graphs or other information, unless specifically acknowledged as being sourced from other persons.
4. This thesis does not contain other persons' writing, unless specifically acknowledged as being sourced from other researchers. Where other written sources have been quoted, then:
    a) Their words have been re-written but the general information attributed to them has been referenced.
    b) Where their exact words have been used, then their writing has been placed in italics and inside quotation marks, and referenced.
5. This thesis does not contain text, graphics or tables copied and pasted from the internet, unless specifically acknowledged, and the source being detailed in the thesis and in the references sections.

Signed ……..

Declaration – Conference Contributions

Darrel Sarvesh Naidu and Patrick G. Ndungu. 2013. Synthesis And Characterization Of Nitrogen And Sulfur Doped Titanium Dioxide For The Photoreduction Of Carbon Dioxide. Catalysis Society of South Africa (CATSA) conference. Wild Coast Sun, Port Edward, South Africa, November 17-20, 2013.

Darrel Sarvesh Naidu and Patrick G. Ndungu 2014. Copper and Sulphur Doped Titanium Dioxide For The Photo-Reduction Of Carbon Dioxide To Hydrocarbons. Photocatalysis for Energy (PHOTO4E) 2014. IFP Energies nouvelles, Solaize, Lyon, France, October 15-17 2014.

Abstract

Titanium Dioxide (TiO_2) was chosen as a photocatalyst and in order to improve its photo-catalytic properties it was doped with 3 elements copper, nitrogen and sulfur, separately. All catalysts were prepared via sol-gel methods using titanium isopropoxide as a precursor. Copper doping was done in a range of 2-5 mol% whereas nitrogen and sulfur doping was done in a range of 2-4 moles in relation to the number of moles of TiO_2. The physical and chemical properties of these catalysts were studied by inductively coupled plasma optical emissions spectroscopy (ICP-OES), scanning electron microscopy (SEM), electron dispersive X-ray spectroscopy (EDX), transmission electron microscopy (TEM), nitrogen physisorption, powder X-Ray diffraction (XRD), Raman spectroscopy, UV-Vis diffuse reflectance spectroscopy (UV-DRS) and photoluminescence (PL). All dopants were seen to improve the properties of TiO_2 that would affect the rate of photocatalysis; specifically, narrowing of TiO_2 band gap, decrease of the electron hole recombination rate and increase in surface area.

The photocatalytic activity of the prepared materials was tested by degrading a mixture of four compounds with an individual concentration of 5 $mg.L^{-1}$. The four compounds degraded were aspirin, caffeine, phenacetin and salicylic acid, which are classified as emerging contaminants (ECs). These reactions were monitored using high performance liquid chromatography (HPLC) with a UV-Vis detector. The doped catalysts showed an improvement in photocatalytic activity compared to the undoped catalyst, of all of the synthesised catalysts the TiO_2:S 1:4 catalyst was seen to have the best performance. This catalyst was used to optimise operation parameters such as pH, substrate concentration and catalyst mass for the photodegradation reactions.

Keywords: Titanium dioxide, copper doped, nitrogen doped, sulfur doped, photo-catalysis, degradation of emerging pollutants,

Acknowledgements

To my family at home, thank you for creating a happy environment in which to work. Mum thank you for everything, the list of things to thank you for is simply far too long and anything I say simply too insufficient to thank you properly. To my older brother and sister, yes I do see you as my older siblings, thank you for all the ice-cream.

I would like to thank my supervisor, Prof P.G Ndungu, for his help, support and teachings throughout my project. I have learnt a lot during this period from him regarding chemistry and the application of nanomaterials. I have also learnt a great deal from and leant on my senior lab members during the course of my project in particular, Gumbi and Suresh.

I would like to express my gratitude to the technical staff members of both the MMU and the chemistry department. To the members of the MMU I your expertise was much appreciated as was your understanding when making or cancelling bookings. The chemistry technical staff members the use of your equipment when needed and willingness to above and beyond to help is a great example. In this regard a special thank you to Raj Sumaru.

My friends who made this experience a lot less stressful than it could have been. To Amy thank you for all the phone calls to talk about my work and anime. For all the advice regarding the stress of my project and life in general thank you to Christina. To Chrisanne thank you for being an all-around good friend. For all the early morning conversations over coffee thank you to Byron and Strini. To Delon thank you for all our football conversations. To Chandika thank you for all the free coffee.

Honourable mentions my lab members, Surya, Vuyo, Sean, Chima, Mena, Ntseng and the Shabalalas (Nhlanhla and Sebenzile).

Last but not least thank you to the National Research Fund (NRF), for sponsoring me during my project as well as my trip to France for Photocatalysis for Energy (PHOTO4E) conference.

Dedication

This thesis is in dedication of my grandparents, my grandfather the late Paradesy Adari and my grandmother Pravathy Adari.

Contents

List of Abbreviations

TiO_2	Titanium dioxide
MO	Molecular orbital
HOMO	Highest occupied molecular orbital
LUMO	Lowest unoccupied molecular orbital
CB	Conduction band
VB	Valence band
SA	Salicylic acid
SEM	Scanning electron microscopy
EDX	Electron dispersive X-ray
TEM	Transmission electron microscopy
XRD	X-ray diffraction
ICP-OES	Inductively coupled plasma – optical emission spectroscopy
HPLC	High performance liquid chromatography
PL	Photoluminescence
EC	Emerging contaminate

List of Tables

List of Figures

List of Equations

List of Schemes

Chapter 1 Introduction

1.1 Background

Through photocatalysis, sunlight may be used directly to perform reactions that would otherwise require a source of energy that may not be renewable. One of the main advantages of using photocatalysis to carry out a reaction, compared to other methods, is that the reaction may be done at room temperature, meaning that the cost of reactor materials would be low. Photocatalysis can be used for reactions such as hydrogen generation from water splitting, carbon dioxide (CO_2) photoreduction, organic reactions such as benzene to phenol conversion, and degradation of organic pollutants [1-3].

South Africa has an annual rainfall of 495 mm which is lower than most countries [4]. This is further exacerbated by the problem of water delivery to poor and underdeveloped areas. The water being delivered, to households for consumption, must of course be clean and suitable for drinking. Of the types of contaminants in water organics may be of particular concern given that they may be stable and persist in the environment. There are a wide variety of organics, however the group of emerging contaminants (ECs) are of concern as there are no regulations on allowed concentration in the environment and very little is known about their effect on the environment at current levels [5-7]. ECs include compounds such as chemicals from industrial processes, pharmaceuticals and personal care products, but may also include naturally occurring compounds.

There are multiple methods of removing organics from water, namely adsorption on activated carbon, precipitation, ion exchange, membrane filtration (solid state filtration of organic matter) and advanced oxidation processes [8, 9]. One advanced oxidation process that offers an environmentally friendly and potentially cheaper route is photo-oxidation of organics.

This method is advantageous compared to other remediation methods for organics due to the fact that only sunlight and an oxidant, such as oxygen, are needed. It is possible to degrade a wide range of organics using this route and may degrade the organics to less harmful products or, if oxidation is completed, to CO_2 and water. **Figure 1.1** shows the processes that may take place in order to oxidize an organic molecule in solution with an irradiated photocatalyst. Provided that the material is irradiated with energy that is equal to or greater than the energy of the band gap of the photocatalyst then the photocatalyst will generate electron-hole pairs. These electron-hole pairs, as can be seen in **Figure 1.1**, can either react directly with the pollutant or create hydroxyl radicals which would also oxidize the pollutant.

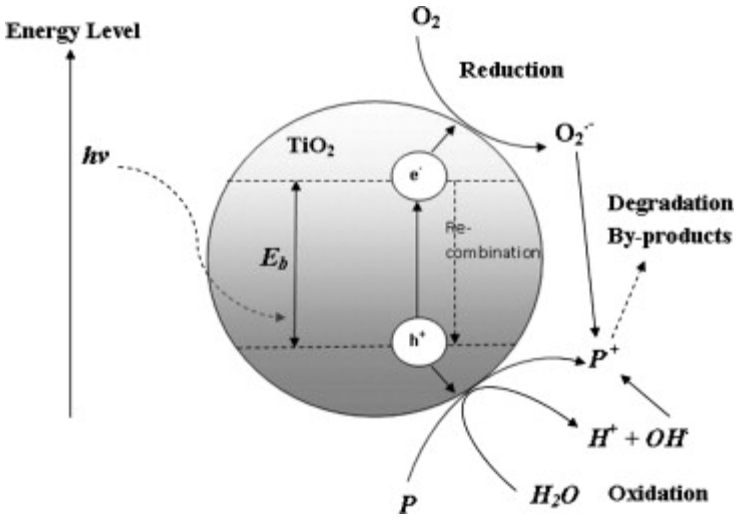

Figure 1.1: Processes for photodegradation of an organic molecule with an irradiated photocatalyst.

(Taken from [10])

There are a wide variety of semiconductors that can be used as photocatalyst such as ZrO_2, ZnS, CdS and CdSe [11]. Titanium dioxide (TiO_2) is one of the most researched semiconductors due to the fact that it is cheap and is resistant to photo-corrosion.

1.2 Problem Statement

Emerging contaminants (ECs) may enter our drinking water through several means such as municipal waste treatment plants, household discharges and discharges by industry [12-15]. Conventional water treatments do not completely remove pollutants, therefore other methods are needed. While TiO_2 may provide a cheap and environmentally friendly alternative to conventional water treatment techniques it suffers from two major drawbacks. Firstly it has wide band gap of 3.0-3.2 eV which means that it only adsorbs light in the ultraviolet region of solar spectrum. The ultraviolet region of the solar spectrum is only about 5% of the solar spectrum energy reaching the surface of the earth. This means that only a small portion of the available solar energy is used and by reducing the band gap more solar energy may be used and more electrons and holes may be produced. The other drawback to TiO_2 is the rate of electron-hole recombination leading to a number of the electron-hole pairs that are generated upon irradiation recombining which reduces the efficiency of the catalyst. Reducing the rate of electron-hole pair recombination will result in longer lifetime for photo-generated electrons and holes, which should lead to greater reaction rates.

1.3 Motivation

Clean drinking water is a necessity for living; however pollution threatens the delivery of clean drinking water. Of concern is that a number of studies have found compounds that have been classified as ECs in South African water bodies [5, 16-18]. Photodegradation of these compounds would provide a cheap and environmentally friendly route to remove them from drinking water. TiO_2 is a good option as a photocatalyst, doping TiO_2 with various elements has been shown to narrow the band gap of the material and in some cases reduce the electron-hole recombination rate. A narrower band gap would result in greater electron-hole

pair generation and a slower electron-hole recombination rate would lead to greater lifetime for generated electrons and holes. Both of effects of doping, smaller band gap as well as a lower electron-hole recombination rate, will improve the rate of photocatalysis in comparison to an undoped catalyst.

1.4 Aims and Objectives

The aims of this project were to develop visible light active TiO_2 photocatalysts, through doping with metals and non-metals for the degradation of emerging contaminants. The selectivity of catalysts based on doping should be determined.

The objectives of this project were as follows:

- Synthesize nitrogen, sulfur and copper doped TiO_2
- Study the chemical and physical properties of the synthesized materials
- Determine the photocatalytic activity of the synthesized materials using ECs as probe molecules.

1.5 Research Approach

Sol-gel methods were used to synthesize all catalysts. Nitrogen and sulfur doped catalysts were synthesised, separately, by a single sol-gel method. A different sol-gel method, from the one used to synthesise the nitrogen and sulfur doped catalysts, was used to synthesise the copper doped catalysts. The chemical and physical properties of the doped catalysts were studied, by various characterization techniques, before applications so as to determine the effect of each dopant on TiO_2. Photocatalytic experiments involving ECs will be carried out

to determine if there is an improvement with doping. The photocatalytic experiments will also help to determine if there is an effect on the selectivity of the catalysts with doping.

1.6 Research Scope

Catalysts were prepared by sol-gel methods using three different types of dopants. The focus was on the change in the material properties with the different types of dopants. Photocatalytic studies will be done using four ECs, to assess the efficacy of the prepared catalysts and the effect of doping. The effect of parameters such as pH of solution, initial concentration of substrates and initial mass of catalyst on the efficiency of photocatalysis will be studied.

1.7 Structure of Dissertation

Chapter one: In this chapter the background of this project and the scope of the project will be discussed

Chapter two: This chapter will provide a background on how semiconductors work, various elements those make up semiconductors. The drawbacks of TiO_2 will be stated and the need for modification. The compounds to be degraded will be discussed in more detail.

Chapter three: Will describe the synthesis procedure of the catalysts as well as the details for the reagents, instrumentation and experimental procedures.

Chapter four: The results for the characterisation of the catalysts will be presented in this chapter and will be discussed. This chapter is separated into two parts, one section for the discussion of the copper doped catalysts and another for sulfur and nitrogen doped catalysts.

Chapter five: The results of the photocatalytic testing will be presented in this chapter and will be discussed. These results will be related to the results in chapter four to show the correlation or lack thereof between the results.

Chapter six: The results obtained will be summarised and overall conclusions will be given. Suggestions, for improvement, will be made for endeavours of a similar nature in the future.

References

1. W.-N. Wang, W.-J. An, B. Ramalingam, S. Mukherjee, D.M. Niedzwiedzki, S. Gangopadhyay, and P. Biswas, *Size and structure matter: Enhanced CO2 photoreduction efficiency by size-resolved ultrafine Pt nanoparticles on TiO2 single crystals.* Journal of the American Chemical Society, 2012. **134**(27): p. 11276-11281.
2. K.A. Connelly and H. Idriss, *The photoreaction of TiO2 and Au/TiO2 single crystal and powder surfaces with organic adsorbates. Emphasis on hydrogen production from renewables.* Green Chemistry, 2012. **14**(2): p. 260-280.
3. Z. Long, Y. Zhou, G. Chen, P. Zhao, and J. Wang, *4, 4'-Bipyridine-modified molybdovanadophosphoric acid: A reusable heterogeneous catalyst for direct hydroxylation of benzene with O 2.* Chemical Engineering Journal, 2014. **239**: p. 19-25.
4. http://data.worldbank.org/indicator/AG.LND.PRCP.MM. [cited 2015 02-09-2015].
5. F.O. Agunbiade and B. Moodley, *Pharmaceuticals as emerging organic contaminants in Umgeni River water system, KwaZulu-Natal, South Africa.* Environmental monitoring and assessment, 2014. **186**(11): p. 7273-7291.
6. M.D. Celiz, J. Tso, and D.S. Aga, *Pharmaceutical metabolites in the environment: analytical challenges and ecological risks.* Environmental Toxicology and Chemistry, 2009. **28**(12): p. 2473-2484.
7. M. Schriks, M.B. Heringa, M.M. van der Kooi, P. de Voogt, and A.P. van Wezel, *Toxicological relevance of emerging contaminants for drinking water quality.* Water Research, 2010. **44**(2): p. 461-476.
8. M.N. Rashed, *Adsorption technique for the removal of organic pollutants from water and wastewater*. Organic Pollutants - Monitoring, Risk and Treatment. 2013.

9. S. Metsämuuronen, M. Sillanpää, A. Bhatnagar, and M. Mänttäri, *Natural organic matter removal from drinking water by membrane technology.* Separation & Purification Reviews, 2014. **43**(1): p. 1-61.

10. M.N. Chong, B. Jin, C.W.K. Chow, and C. Saint, *Recent developments in photocatalytic water treatment technology: A review.* Water Research, 2010. **44**(10): p. 2997-3027.

11. N. Serpone and E. Pelizzetti, *Photocatalysis: fundamentals and applications*. 1989: Wiley New York.

12. D.W. Kolpin, E.T. Furlong, M.T. Meyer, E.M. Thurman, S.D. Zaugg, L.B. Barber, and H.T. Buxton, *Pharmaceuticals, hormones, and other organic wastewater contaminants in US streams, 1999-2000: A national reconnaissance.* Environmental science & technology, 2002. **36**(6): p. 1202-1211.

13. T. Heberer, A. Mechlinski, B. Fanck, A. Knappe, G. Massmann, A. Pekdeger, and B. Fritz, *Field studies on the fate and transport of pharmaceutical residues in bank filtration.* Groundwater Monitoring & Remediation, 2004. **24**(2): p. 70-77.

14. C.H. Swartz, S. Reddy, M.J. Benotti, H. Yin, L.B. Barber, B.J. Brownawell, and R.A. Rudel, *Steroid estrogens, nonylphenol ethoxylate metabolites, and other wastewater contaminants in groundwater affected by a residential septic system on Cape Cod, MA.* Environmental science & technology, 2006. **40**(16): p. 4894-4902.

15. K. Kümmerer, *Drugs in the environment: emission of drugs, diagnostic aids and disinfectants into wastewater by hospitals in relation to other sources–a review.* Chemosphere, 2001. **45**(6): p. 957-969.

16. S. Matongo, G. Birungi, B. Moodley, and P. Ndungu, Occurrence of selected pharmaceuticals in water and sediment of Umgeni River, KwaZulu-Natal, South

Africa. Environmental Science and Pollution Research, 2015. 22(13): p. 10298-10308..

17. B. Gumbi, J.C. Ngila, and P.G. Ndungu, *Direct spectrophotometric detection of the endpoint in metachromatic titration of polydiallyldimethylammonium chloride in water*. Physics and Chemistry of the Earth, Parts A/B/C, 2014. **67–69**: p. 117-124.

18. T. Manickum and W. John, The current preference for the immuno-analytical ELISA method for quantitation of steroid hormones (endocrine disruptor compounds) in wastewater in South Africa. Analytical and bioanalytical chemistry, 2015. 407(17): p. 4949-4970.

Chapter 2 Literature Review

To understand the effect of doping on TiO_2 and why it may induce visible light absorption, it is important to understand the band theory of semiconductors as well as the chemical structure of TiO_2 and the effects of various dopants. Thus this literature review begins with an overview of band theory, and then discusses key parameters that must be investigated in photocatalytic degradation of organic pollutants.

Operational parameters of a photocatalytic reaction are important, parameters such as pH of the reaction medium, substrate concentration, catalyst concentration, temperature, light intensity affect the rate of reaction. Also the nature of the catalyst and the substrate has an effect on the selectivity and rate of reaction. These parameters are discussed in detail within the literature review.

Finally, it is important to discuss the means as to how ECs may find their way into water bodies that are used for drinking water. Not much is known about the individual and collective effect on environmental systems of these ECs.

2.1 Band Theory

The electrical properties of metals, semiconductors and insulators are determined by the distribution of their electrons, a model that describes this distribution is the band theory. This is given by a model of N atoms or molecules of the same type combining, this provides N amount of molecular orbitals (MOs) [1]. Considering just two atoms in a system and applying the Pauli Exclusion Principle, when the atoms approach each other, specific orbitals will start to overlap and split into two discrete energy levels [1]. For a system with N atoms this would lead to 2N number of orbitals with small differences in energy, and because the

energy levels are so close together, the overlapping orbitals form an energy band [1]. Each atom contributes N electrons and there are 2N MOs, and when applying the aufbau principle this leads to some occupied and unoccupied orbitals, the highest occupied MO (HOMO) and the lowest unoccupied MO (LUMO) [2]. Only orbitals of similar symmetry may form MOs, if the available orbitals are s and p, then this would lead to the formation of, s and p bands respectively [1]. For a given system the energy difference between the s band and p bands may be large and this would lead to a band gap. Inside the band gap there are a number of energy states that are forbidden, that is to say energy states at which no electrons can or will occupy [1]. It is the size of the band gap which determines if a material is a metal, semiconductor or insulator [2]. Metals are characterised by two types of energy bands, the first is given by **Figure 2.1** (b), in this case the metal may have a band gap but due to the lower band only being partially filled it will conduct electricity [2]. The second type of energy band that a metal may have is given by **Figure 2.1** (c) whereby the lower band and upper band overlap allowing for conduction of electrons [2]. Insulators have a filled lower band, also called the valance band (VB), and the distance between the upper and lower band is large meaning that electron movement across the two is difficult **Figure 2.1** (a). The difference in the band gaps of metals, insulators and semiconductors can be seen in **Figure 2.1** below.

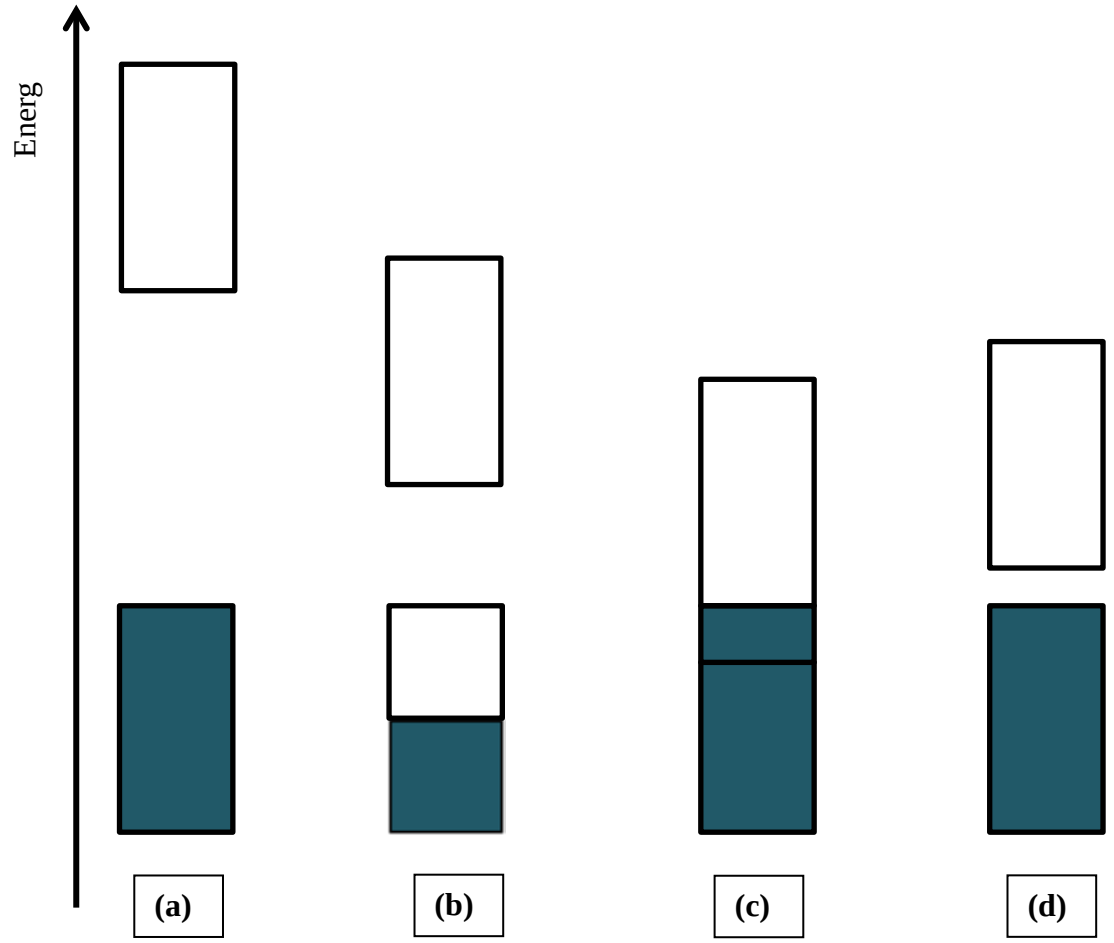

Figure 2.1: An insulator (a), a metal with the lower band partially occupies (b), a metal (in which the occupied and unoccupied bands overlap) (c) and a semiconductor (d)**.**

(Adapted from [2])

A semiconductor, **Figure 2.1** (d) like an insulator has a completely filled lower and a gap of forbidden states between the occupied and unoccupied states, the difference is in the size of the gap with semiconductors having smaller band gaps when compared to insulators. In a semiconductor electrons can be excited from the VB, to the upper band also called the conduction band (CB). Excitation of electrons can occur thorough thermal or optical excitation or with the application of current or potential [3].

2.2 Optical Properties of Semiconductors

When a semiconductor is illuminated with electromagnetic energy (photons) that is equal to or greater than its band-gap it will absorb a photon and an electron will be promoted from its VB to its CB [4]. With the promotion of an electron from the VB to the CB there is a formation of a hole (a positive charge) in the VB. The wavelength of light needed to promote an electron is given by **Equation 2.1** below [4].

$$\lambda = \frac{1240}{E_g} \quad .$$

Equation 2.1: Relationship between band gap and wavelength.

Where λ is the wavelength needed and E_g is the band gap of the material. It can be seen from **Equation 2.1** that as the band gap increases the wavelength, needed to promote an electron from the VB to the CB, decreases i.e. more energy is required.

Semiconductors may either have a direct or an indirect band gap. In order for a semiconductor to possess a direct band gap, **Figure 2.2** (b), the apex of the VB must have the same k (wavenumber) value as that of the CB minimum [5]. A semiconductor with an indirect band gap, **Figure 2.2** (a), however has a two-step mechanism of charge transfer as the VB apex and the CB minimum do not have the same k value [5]. The electrons momentum must match that of the CB to which it is being transferred. In order for an electron to be transferred from the VB to the CB there must either be a gain or a loss of momentum, this is achieved through the interaction of the electron with a phonon [6]. Phonons are quanta of lattice vibration which arise through lattice thermal energy; there are specific frequencies and wavenumbers which characterise each phonon [7]. The phonon will either add momentum to the electron or take away momentum which is then distributed back

to the hole [6, 8]. This is needed as the frequencies, and therefore the wavenumbers, determine the momentum of the electron being transferred.

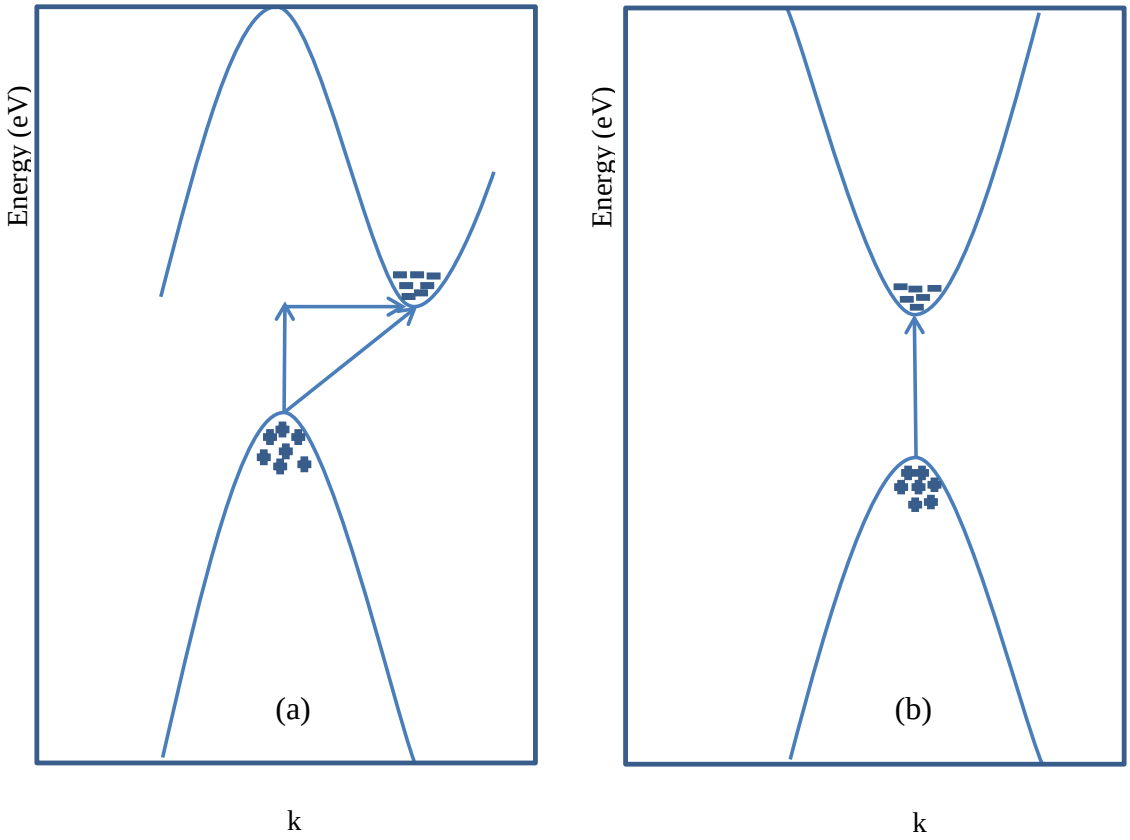

Figure 2.2: Indirect band gap (a) and direct band gap (b).

(Adapted from [9])

One method that can be used to determine the size of the band gap of a substance is via the measurement of the absorbance spectra of the material of interest. Absorbance is normally defined as $\log(I_0/I)$, where I_0 is the incident light intensity and I is the transmitted light intensity [10]. For solid materials, however, reflectance measurements must be used instead, and the value of I must be the intensity of the reflected light [10]. The amount of light lost is taken as the amount of light photoabsorbed by the material [10]. In order to convert the reflectance data into absorbance measurements the Kubleka-Munk function can be used as given below [11].

$$F(R_\infty) = \frac{(1 - R_\infty)^2}{2R_\infty}$$ **Equation 2.2**: Kubelka-Munk function.

Where $F(R_\infty)$ is the absorbance coefficient of the material and R_∞ is the absolute reflectance of the material when it has effectively infinite thickness [11, 12]. The $F(R_\infty)$ term may then be used as the α in the Tauc plot given by **Equation 2.3** below:

$$(\alpha h\nu)^n = A(h\nu - E_g)$$ **Equation 2.3**: Tauc plot equation.

Where A= constant, $h\nu$ = the energy of a photon, E_g= band gap energy, α= absorption coefficient and n= can be 0.5, 1.5, 2 and 3, for indirect, direct allowed, direct forbidden ad indirect forbidden respectively [12-15]. In order to obtain the band gap energy from **Equation 2.3** for an indirect band gap, a plot of $(\alpha h\nu)^{\frac{1}{2}}$ versus $h\nu$ must be used and a linear extrapolation of the curve to $(\alpha h\nu)^{\frac{1}{2}}$ = 0 [14-18].

2.3 General Principles of Heterogeneous Photocatalysis

Considering that the reaction medium would either be gas or liquid one or more of the reactants must be absorbed onto the catalyst surface from either the gas phase or the liquid phase, dependent on the reaction medium [19]. The reaction proceeds with the absorption of a photon with energy of equal or greater than that of the band gap of the photocatalyst being used [19, 20]. The products must then desorb from the catalyst surface and vacate the area immediately around the catalyst [19-21].

Once the photocatalyst is illuminated with light of the appropriate wavelength and electron-hole pairs are created there are several pathways that can be taken, by these pairs. For

example, the electron-hole pair could recombine within the material (along defects, dislocations, or in the bulk phase), or both could migrate to the surface and recombine. In both cases energy is lost by the release of heat [19, 22, 23]. Another option is that both the electron and the hole are trapped by different surface states and thus each is able to come into contact with suitable reactants [19, 23].

The bottom of the CB determines the reduction power of photogenerated electrons and the top of the VB determines the ability of photogenerated holes to oxidize a given molecule [23, 24]. In order to carry out a given reaction the reductive power of photogenerated electrons and the oxidative power of photogenerated holes must be suitable. Organic molecules in an aqueous system may also be oxidised by hydroxyl radicals produced, these hydroxyl radicals are produced through reaction of water molecules with photogenerated holes. The various routes possible are given below in **Scheme 2.1** [25].

$TiO_2 + h\nu\ (UV) \rightarrow TiO_2\ (e_{CB}^- + h_{VB}^+)$ (1)

$TiO_2\ (h_{VB}^+) + H_2O \rightarrow TiO_2 + H^+ + OH^*$ (2)

$TiO_2\ (h_{VB}^+) + OH^- \rightarrow TiO_2 + OH^*$ (3)

$TiO_2\ (e_{CB}^+) + O_2 \rightarrow TiO_2 + O_2^{-*}$ (4)

$O_2^{-*} + H^+ \rightarrow OH_2^*$ (5)

$Organic + OH^* \rightarrow$ degradation product (6)

$Organic + h_{VB} \rightarrow$ oxidation product (7)

$Organic + e_{CB} \rightarrow$ reduction product (8)

Scheme 2.1: Pathways for a photocatalytic reaction upon irradiation.

There are several operational parameters that affect the efficiency of the photocatalytic reactions.

2.3.1 Effect of Photocatalyst Morphology

The reaction is influenced by the particle size, morphology (thin films, fibre, or nanoparticles) and agglomeration. Surface area is directly affected by the morphology of the particles; several morphologies such as nanoparticles, nanoparticulated films, foams and nanotubes have been used in an attempt to improve photocatalytic activity [26]. Particle size and surface area have an inversely proportional relationship, as the particle size decreases the surface to volume ratio increases. The size of agglomerates of the catalyst, in photocatalytic degradation, for example, there is a direct relationship between degradation rate and surface coverage [27]. A number of studies have shown that there is a relationship between the amount of substrate absorbed and the reaction rate [28-30]. A greater surface area would therefore allow for greater amount of substrate absorption and therefore lead to greater reaction rate. Sugimoto *et al* carried out a study in which the shape of the TiO_2 nanoparticles were closely controlled and found that this had a significant effect on the surface area and absorption capacity [31]. In general photocatalytic reactions kinetics follows the Langmuir-Hinshelwood which is a function of surface coverage given by **Equation 2.4** below [20]:

$$r = k\theta = k\left(\frac{KC}{1 + KC}\right)$$

Equation 2.4: Langmuir-Hinshelwood equation.

Where r is the rate of reaction, θ is the surface coverage, k is the true rate constant, K is the adsorption constant and C is the concentration of the reactant [19]. It can be seen from **Equation 2.4** that the amount of surface area is important as it affect surface coverage and therefore reaction rate.

Lin *et al* showed that the reduction of particle size (from bulk) also reduced the size of the band gap, to an optimum value of 17 nm, reduction of the particle size any further from this

resulted in an increase of the band gap.[11] This was attributed to the Bras EMM model given below:

$$E^* \cong E_g + \frac{\hbar^2 \pi^2}{2R^2}\left[\frac{1}{m_e} + \frac{1}{m_e}\right] - \frac{1.8e^2}{\varepsilon R}$$

Equation 2.5: Bras EMM model.

The rate of reaction is determined by the number of photons that reach the surface of the catalyst; therefore reaction only takes place in the absorbed phase [22, 32]. By increasing the amount of surface area of the catalyst this would increase the amount of light reaching the surface of the catalysts and therefore the number of photons hitting the surface of the catalyst. An increase in the number of photons reaching the surface of the catalyst would increase the number of electron-hole pairs generated and therefore would increase the rate of reaction. However as shown in section 2.4.5 later on the amount of photon absorption is only a good thing until a certain level beyond this electron-hole recombination becomes a problem, and retards the reaction rate. Therefore beyond a certain point the surface area may be too high and the amount of photons absorbed will have a negative effect on the reaction rate.

2.3.2 Effect of pH

The activity of the photocatalyst in an aqueous system is affected by the pH. It is possible to adjust the rate of reaction and reaction pathways by adjusting the pH of the solution. The key reason can be attributed to the surface charge of the material under different pH values, which can be determined by the point of zero charge. In the area immediately surrounding a solid in an aqueous solution (on the order of 1 nm) a charge automatically forms, which is controlled by the pH of the solution, the pH at which this charge is neutral is called the point of zero charge (PZC) [33, 34].

A given photocatalyst will have a certain PZC at a specific pH and by adjusting the pH the photocatalyst may have a positive or negative charge on the surface. $TiO_{2,}$ for example, has PZC at pH 6.25, under lower pH values TiO_2 will have a positive surface charge and under higher pH values TiO_2 will have a negative surface charge [35, 36]. The charge on the photocatalyst will affect the attraction and repulsion forces between the photocatalyst, the reactant molecules and the product molecules, which could result in a change in activity [35]. This relates to the surface coverage of the substrate on the photocatalyst surface, if the change in pH results in stronger attraction and therefore greater coverage the reaction rate will increase.

The pH of the medium, in which the photocatalyst is being used, also affects the reduction and oxidation ability of the photocatalyst. With a change in the pH of the solution there is a change in the position of the CB and VB. If a semiconductor follows a Nerstain dependence on the pH of the solution, then for every unit of pH that the solution is reduced by there will be a 59 mV decrease in the potential energy of the CB and VB [37]. At lower pH values a semiconductor should display greater oxidation ability and at higher pH values should display greater reduction ability. Although a semiconductor has greater oxidation ability at low pH values at very low values and excess of H^+ can decrease reaction rate [38]. However it can be seen from **Table 2.1** that this can vary, the work by Sun *et al* and Wei *et al* in particular show the best degradation rates at very low pH values [39, 40]. This increase in reaction rate can be attributed to the nature of the pollutant in question as the pH will influence the amount of absorption of the pollutant, as discussed above (**Equation 2.4**) this greatly influences reaction rate [41].

Table 2.1: Optimum pH operational conditions for various pollutants. Table was adapted from Akpan *et al* [24]**.**

Pollutant type	Light Source	Photocatalyst	Tested pH range	Optimum pH
Fast Green FCF [42]	UV	TiO_2	3.0-11.0	4.4
Patent Blue VF [42]	UV	TiO_2	3.0-11.0	11.0
Orange G [38]	UV	$Sn/TiO_2/AC$	1.0-12	2.0
BRL [43]	UV	$K\text{-}TiO_2$	4.5-11.8	7.2
Methyl Orange [44]	UV	$Pt\text{-}TiO_2$	2.5-11.0	2.5
Orange G [39]	UV	$N\text{-}TiO_2$	1.5-6.5	2.0
Acid Red [40]	UV	$Ce\text{-}TiO_2$	1.5-7.0	1.5
4-Chlorophenol [45]	UV	$N\text{-}TiO_2$	2.0-5.0	3.0
Orange II [46]	UV	$Zn\text{-}TiO_2$	3.0-10.0	3.0
Bromocresol Purple [47]	UV	TiO_2	4.5-8.0	4.5

2.3.3 Effect of Substrate Nature and Concentration

The nature of the substrate reacting with the photocatalyst is very important to the rate of reaction and reaction efficiency. Organic molecules that are more electron withdrawing will adhere more strongly to the surface of the photocatalyst than molecules that are electron donating [48]. The size of the molecule in question is also important as smaller molecules adsorb more easily onto the surface of the catalyst due to a higher driving force [49]. Organic molecules undergoing photo-oxidation are more readily oxidized the more strongly they adhere to the surface of the photocatalyst [50].

Work by Bahnemann *et al* showed that the degradation pathway of the molecule also influences irradiation time. For example, 4-chlorophenol releases a number of intermediates and therefore requires further reaction time to oxidise completely while oxalic acid oxidises directly to carbon dioxide and water.

At high substrate concentration the substrate will absorb light for a given catalyst loading and thereby reduce the number of photons reaching the catalysts surface leading to a reduction in reaction rate [51, 52]. This should only be a factor if the molecules absorb light of the same

wavelengths needed to produce electron-hole pairs in the photocatalyst. Another factor that may lead to a decrease in the rate of reaction is simply that although the number of molecules to be degraded increases the number of electron-hole pairs remain the same (given the same light intensity, catalyst mass and irradiation time) [52]. This means that the number of active species remains the same but the demand has increased a problem that could be made worse if there are intermediate species.

2.3.4 Effect of Catalyst Concentration

At low catalyst concentration the rate of reaction increases linearly with an increase in the concentration of catalyst [53]. However above an optimum value at which the reaction rate reaches a maximum an increase in the amount of catalyst present in the system results in a decrease in the reaction rate [53]. At high catalyst concentration there is a greater amount of light scattering, screening effects and thus a smaller portion of light reaching the catalyst surface which reduces the generation of electron-hole carriers and this leads to a reduction in catalyst activity [35]. At high catalyst concentration the fraction of active particles is low so the increase in number collisions between reactant molecules and catalyst particles will be negated as the likelihood of reactant molecules encountering non-activated catalyst particles is higher [54]. The amount of catalyst in solution is directly proportional to the rate at which substrate molecules will interact with catalyst particles due to the number of times a substrate molecule will encounter a catalyst particle. At low catalyst concentration the percentage of active catalyst particles will be high but the rate of reaction with substrate molecules will be low [54].

2.3.5 Effect of Light Intensity and Wavelength

Light intensity is the amount of Watts of light delivered per a unit area and is defined by **Equation 2.6**:

$$I = \frac{P}{4\pi r^2}$$ **Equation 2.6**: Light intensity equation.

Where P is the amount of Watts that the area in question is being irradiated with and r is the distance of the light source from the object being irradiated. A Watt is defined as the number of Joules per a unit time. In the case of light the number of Joules can be determined by **Equation 2.7**:

$$Q = hc/\lambda$$ **Equation 2.7**: Calculation for number of Joules at a given wavelength.

Where Q represents the number of Joules, h is Planck's constant, c is the speed of light and λ is the wavelength of the light.

Light intensity determines the amount of light absorbed by the catalyst at a particular wavelength [52]. Similarly to catalyst concentration at low light intensities there is a linear increase in the reaction rate with an increase in the light intensity (0-20 $mW.cm^{-2}$) [25]. This is as the number of electron-hole pairs generated increases but there is not a great increase in the rate of electron-hole pair recombination. At high light intensities there is a decrease in the observed reaction rate > 25 $mW.cm^{-2}$ [20, 25]. The decrease in the reaction rate at high light intensity is due to the increase in the rate of electron hole recombination. Although at high light intensity the generation of electron-hole pairs increases, the secondary and parallel process also increases i.e. electron-hole recombination, thus the increase in the recombination

rate, this will result in fewer photogenerated electron-hole pairs reaching the surface and therefore fewer active species generated for any reactants at the surface of the catalyst [19].

At low light intensity (0-20 $mW.cm^{-2}$) the reaction rate is proportional to ϕ (radiant flux), a linear increase in reaction rate [55]. At high light intensities (>25 $mW.cm^{-2}$) the reaction rate is proportional to $\phi^{1/2}$, the rate of reaction is proportional to the square root of the light intensity [55]. However above a certain light intensity the reaction then becomes independent of the light intensity, this is to say that the rates of electron-hole pair generation and recombination will be in equilibrium and any further increase will not change the rate of reaction [56].

2.3.6 Effect of Temperature

In section 2.3.1 the importance of reactants adsorption onto the surface of the catalyst was discussed. The temperature of the solution has an effect on the reactants rate of adsorption. The Langmuir-Hinshelwood model is followed by most photocatalytic systems. The effect of temperature on this model is described below.

$k = k_0 \exp(E_a/RT)$ **Equation 2.8**: Arrhenius law.

Equation 2.8 above describes the dependence of the true rate constant, given in the Langmuir-Hinshelwood model, on temperature. Where E_a stands for the true activation energy, it can be seen by **Equation 2.8** that the rate constant is depend on the variation of temperature only [57]. The true activation energy of a photocatalytic system, is nil due to the activation energy of the system being provided photonic activation [19].

The adsorption constant given by the Langmuir-Hinshelwood model has a dependence on temperature as well given below.

$K_i = (K_i)_0 exp(-\Delta H_i / RT)$ **Equation 2.9**: Hoff's law.

Where ΔH_i is the enthalpy of the adsorption of reactant of interest. This shows that even though the true rate constant r is independent of temperature in a photocatalytic system, because the rate constant is still dependent on the adsorption constant the rate of reaction will still be affected by temperature.

At temperatures greater than 80 °C the recombination of charge carriers is favoured and adsorption of organics is more difficult [22]. Therefore the optimum temperature range for photo-mineralisation in which to work in is 20-80 °C.

2.4 Oxide Photocatalyst Band Gap Engineering

Figure 2.3 below gives the elements that have been used to synthesise photocatalytic materials. From **Figure 2.3** it is possible to see that there are two types of elements that can be used to construct a photocatalyst, elements that only contribute to the crystal structure and elements that contribute to both the crystal and energy bands [58]. The first group are elements used to make up perovskites and the second group will be materials such as oxides, sulphides, oxysulfides. For example lithium oxide could not be used as a photocatalyst whereas lithium has been used in a perovskite type structure as a photocatalyst to split water [59]. Likewise sodium has been used in a perovskite structure to degrade gaseous formaldehyde [60]. Elements from groups 1, 2 and 3 fall into the first bracket whereas elements with d orbitals of d^0 and d^{10} configurations fall into the second bracket [58].

The commonly used photocatalyst are metal oxides, metal sulphides, oxysulfides, oxynitrides or composites thereof [61]. The d and p orbitals of the metal cation make up the bottom of the conduction band and in the case of metal oxides the 2p orbitals from oxygen make up the top of the valance band [62, 63]. The valance band made up from the 2p orbitals of oxygen is normally located at +3 eV (vs. NHE) or higher [61]. In the cases of metal sulphides and nitrides the VB is formed by sulfur 3p and nitrogen 2p orbitals respectively [62].

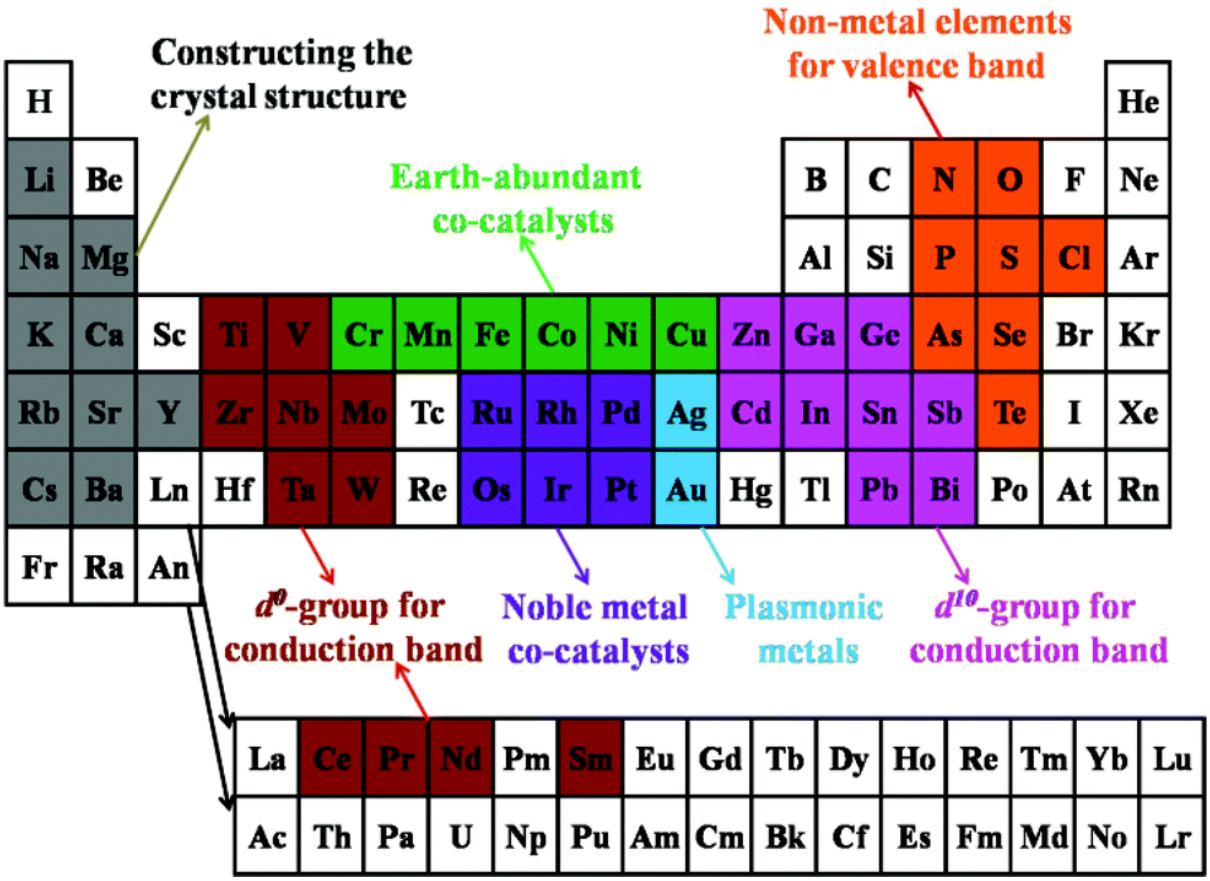

Figure 2.3: Elements and their roles in photocatalysis.

(Taken from [64])

The band positions of a number of photocatalysts is given by **Figure 2.4**, this gives an indication as to the ability of these photocatalysts oxidation and reduction abilities. Discussed previously was that the top of the VB determines the oxidation ability of a

photocatalyst and the bottom of the CB determines the reduction ability of a photocatalyst. Also shown in **Figure 2.4** are the band gaps of a number of photocatalysts.

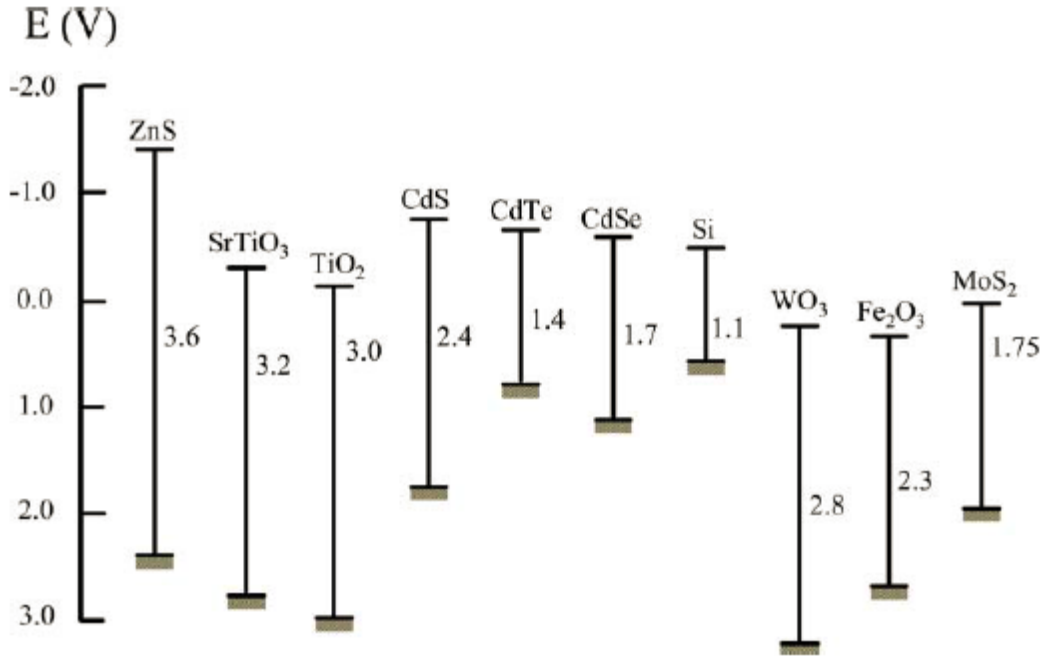

Figure 2.4: The band positions of several semiconductors vs normal hydrogen electrode (NHE) at pH 1.

(Taken from [65])

A semiconductor such as zinc oxide (ZnO) is very easily photocorroded by photogenerated holes [60]. Cadmium sulphide while having a narrow band gap also suffers from photocorrosion, the S^{2-} is oxidised by the photogenerated holes and the Cd^{2+} is eluted into the solution [61].

The ideal photocatalyst should be photoactive, be biologically and chemically inert, resistant towards photocorrosion, be able to harvest light in the visible and near UV light regions and be of low cost [66].

Of all the photocatalysts available the most commonly used and the one that fits the requirements of an ideal photocatalyst the best is TiO_2.

2.5 Titanium Dioxide

TiO_2 is a readily available material, since the metal titanium (Ti) from which it is made, is the fourth most abundant metal on Earth and the ninth most abundant element overall [67]. From ancient times TiO_2 has found application as a white pigment [68]. In more recent times TiO_2 has found wider applications such as, anti-reflecting coatings, cosmetics, chemical sensors, microelectronics and ultra-thin films [69-72]. One of the major applications of TiO_2 due to its physical properties is in catalysis either as a support or as a catalyst, as a catalyst it can be used in photocatalysis. TiO_2 fulfils most of the requirements for an ideal photocatalyst, as it is non-toxic, cheap and resistive to photo-corrosion [21, 73].

2.5.1 Chemical Structure of TiO_2

TiO_2 has polymorphs found in nature, anatase, brookite, rutile and TiO_2 (B); these take the tetragonal, orthorhombic, tetragonal and monoclinic crystal structures respectively [67]. However the TiO_2 (B) form is only found in trace amounts [74]. Two further forms have been synthesised from the rutile polymorph namely TiO_2 (II) and TiO_2 (H) which have PbO_2 (hexagonal) and hollandite structures respectively [75, 76]. In addition to the aforementioned phases of TiO_2 there have been a number of other forms of TiO_2 that have been experimentally and computationally made [77-82].

Figure 2.5 gives the structures of three naturally occurring polymorphs of TiO_2, namely rutile, anatase and brookite [67]. It can be seen that the structures of these polymorphs are formed by the stacking of octahedra; these octahedra are made up of one Ti atom surrounded by 6 oxygen atoms.

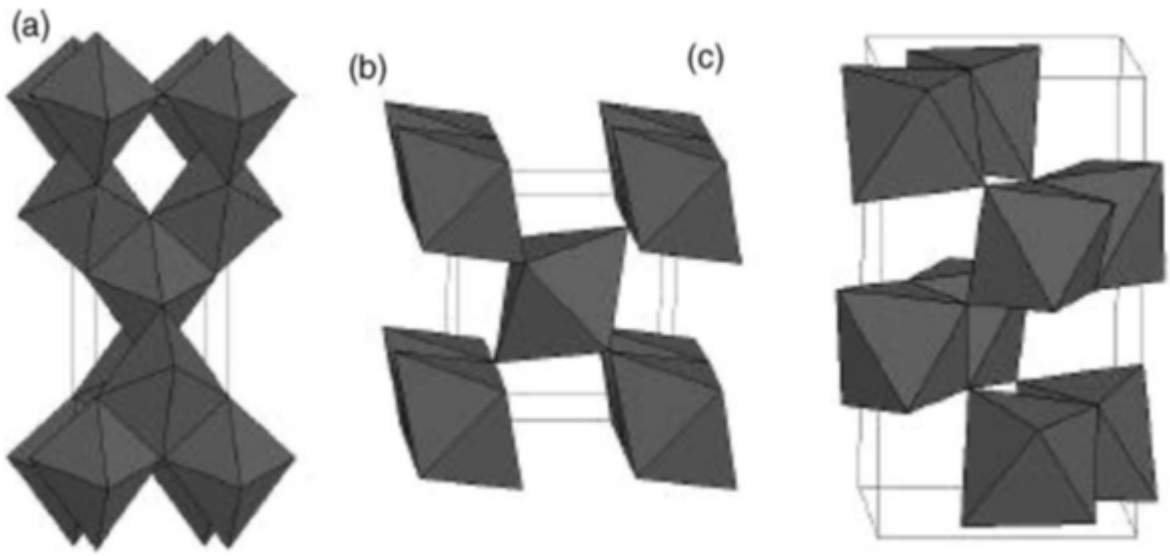

Figure 2.5: Bulk structures of anatase (a), rutile (b) and brookite (c).

(Taken form [67])

Out of these three polymorphs brookite is very difficult to synthesis and there are only a few reported cases [83, 84]. Only the rutile and anatase polymorphs find application [85].

In bulk form rutile is the only stable phase, while in bulk form brookite and anatase are metastable and will irreversibly transform into rutile upon heating [86]. However phase stability is different on the nanoscale. Anatase is the most stable phase for particles under 11 nm, brookite is the most stable phase for particles in the range of 11-35 nm and rutile is the most stable phase for particles of 35 nm and greater [87, 88].

The parameters for the crystals of each of the polymorphs; rutile (tetragonal, a = b = 4.584 Å, c = 2.953 Å), anatase (tetragonal, a = b =3.782 Å, c = 9.502 Å) and brookite (rhombohedrical, a = 5.436 Å, b = 9.166 Å, c = 5.135 Å) [85, 89]. The bond angles for each polymorph is rutile (81.2° and 90.0°), anatase (77.7° and 92.6°) and brookite (77.0-105°) [85, 89].

2.5.2 Drawbacks of TiO_2 as a Photocatalyst

The anatase phase of TiO_2 has a band gap of 3.2 eV, whereas the rutile phase has a band gap of 3.00 eV and brookite displays a band gap of 3.27 eV [90-92]. Even though the rutile phase has a shorter band gap meaning that it will generated electron-hole pairs at longer wavelengths (lower energies), the anatase phase has been found to be the best phase for photocatalytic application [93]. The reasoning for the higher photocatalytic activity the anatase phase has been attributed to a number of things such as, higher adsorption of substrate and lower electron-hole recombination rate of anatase [94, 95]. The longest wavelength permitted for the activation of TiO_2 anatase phase is 387 nm [96, 97]. This wavelength falls in the ultra-violet (UV) region of the electromagnetic spectrum. Of the solar flux incident to the earth's surface only ~5% is in the UV region (~5% UV, ~43% visible and ~52% harvesting infrared) [98]. Therefore TiO_2 anatase phase only absorbs a small portion of the solar flux reaching the earth's surface. This lack of absorption in the solar spectrum is the main drawback of TiO_2 as a photocatalyst.

In section 2.3 it was briefly shown that oxidation of reactants occur through reaction of reactants with photogenerated holes and reduction of reactants occurs through reaction of reactants with photogenerated electrons. Therefore the concentration of the photogenerated electron-hole pairs is very important to the reaction rate. However not all photogenerated electron-hole pairs are able to react with the substrate some as some electron-hole pairs recombined. There are three main modes in which electron-hole pairs can recombine [99]. Band-to-band recombination, this is when an electron from the CB (after photoexcitation) moves to a hole in the VB [99]. The second type of recombination is trap assisted

recombination, this occurs when an electron and hole recombined at a trap state [99]. The third type of recombination is Auger recombination when an electron-hole pair recombine in a band-to-band transition, though the energy is not given off as heat but rather transferred to a third charge carrier either and electron or hole [100, 101]. A further drawback to using TiO_2 is the rate of electron-hole recombination, trapping of electrons on Ti^{3+} sites occur within 30 ps and 90% of photogenerated electrons recombine on a timescale of about 10 ns [102].

There are various ways to increase the range of solar spectrum absorption of TiO_2 and to reduce the recombination rate of electron-hole pairs. One method is thin film formation of TiO_2; work done by Yunxiao *et al* shows TiO_2 films degrades phenol in water better than TiO_2 powder [103]. Morphology control is also a method that has been studied for increased activity, such nanorods and nanotubes, Turki *et al* showed a higher performance for TiO_2 nanowires for formic acid degradation than P25 [104]. TiO_2 immobilised on supports such as graphene oxide and carbon nanotubes has also been explored, Fan *et al* has demonstrated that P25 on graphene oxide is has better activity for hydrogen evolution than P25 nanoparticles [105].

Another way to improve that amount of the solar spectrum that TiO_2 absorbs and the rate of electron-hole recombination is through doping.

2.6 Doping of TiO_2

Doping in the sense of semiconductors means to replace one of the host elements (Ti, O) in the lattice with a foreign element [62]. When doping this foreign element may interact with the host compound lattice in two ways, these two cases are given in **Figure 2.6**. **Figure 2.6** (a) represents a pristine TiO_2 anatase lattice [106]. **Figure 2.6** (b) represents the situation

where the foreign element (red) replaces an atom from lattice, in this case oxygen, of the compound this is called substitutional doping [106]. The second case can be seen in **Figure 2.6** (c) this is when the foreign atom is placed between the natural atoms of the compound this is interstitial doping [106].

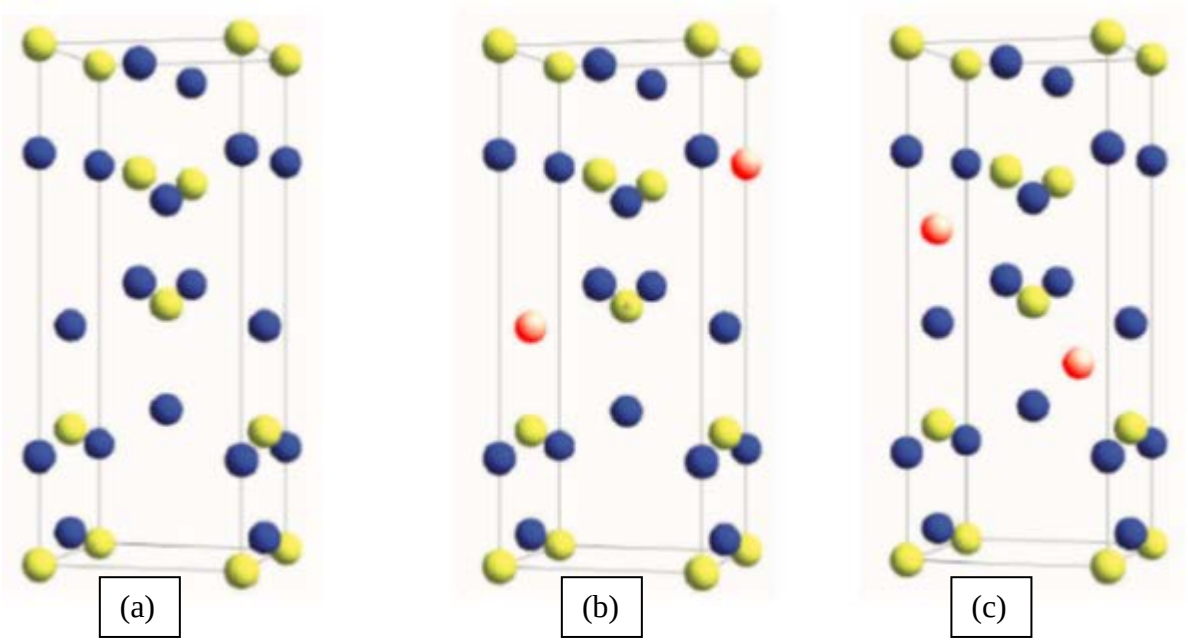

Figure 2.6: Pristine TiO_2 anatase crystal lattice (a), substitutional doped (b) and interstitial doped (c). Where blue is O, yellow is Ti and red is the foreign element.

(Taken from [106])

Doping is carried out so as to induce a *batho-chormic shift* in a semiconductor, that is to say, to decrease the band gap of the semiconductor or to introduce states between the VB and CB which in either case would result in visible light absorption [67]. **Figure 2.7** shows the difference in the band gap of (a) pristine TiO_2, (b) doped TiO_2 and (c) a broadening of the VB resulting in band gap narrowing [107, 108]. **Figure 2.7** (b) shows that doping may induce intermediate states either above the VB or below the CB which in either case there would be a narrowing in the band gap [107, 108]. The broadening of the VB in **Figure 2.7** (c) would also result in band gap narrowing and visible light absorption [107, 108].

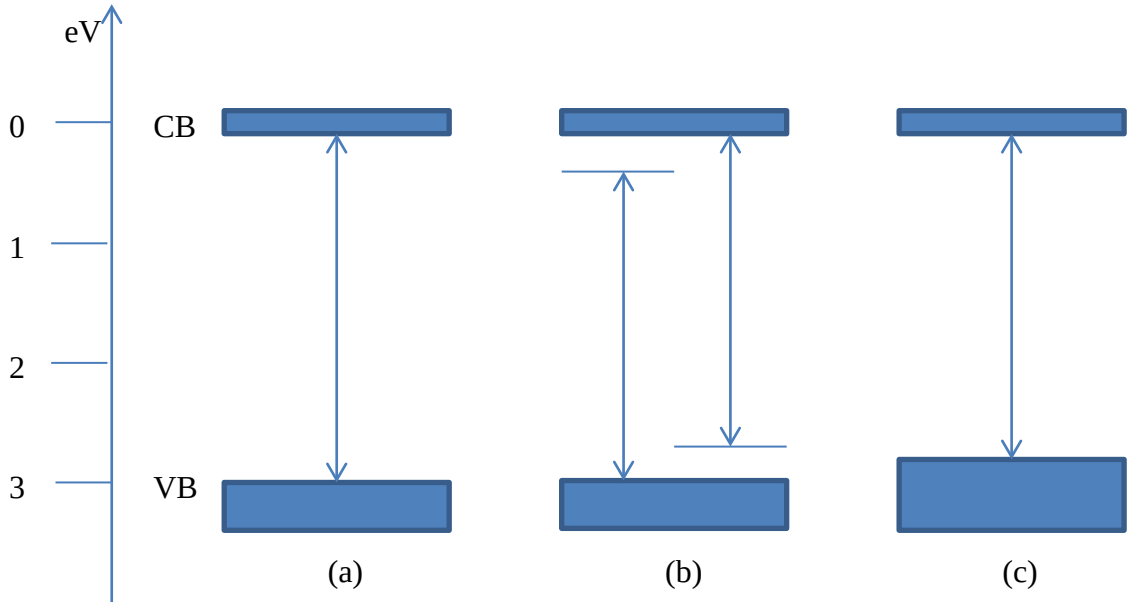

Figure 2.7: Band gap of pristine TiO_2 anatase (a), of doped TiO_2 with intermediate states near either the VB or CB (b) and band gap narrowing through the broadening of the VB (c).

(Taken from [107, 108])

Doping also influences the rate of electron-hole recombination. For optimal separation of charge the potential drop through the space-charge barrier should not be less than 0.2 eV [109]. The space-charge barrier is also known as the space-charge layer or the depletion region, this occurs when an n-type semiconductor is placed in an electrolyte [110]. Electrons may flow out from the donor levels into the electrolyte; this will result in Schottky-type barrier, to stop further electrons from flowing out [110]. This is explained by **Figure 2.8**, where **Figure 2.8** (b) represents the electronic configuration of the semiconductor surface in an electrolyte.

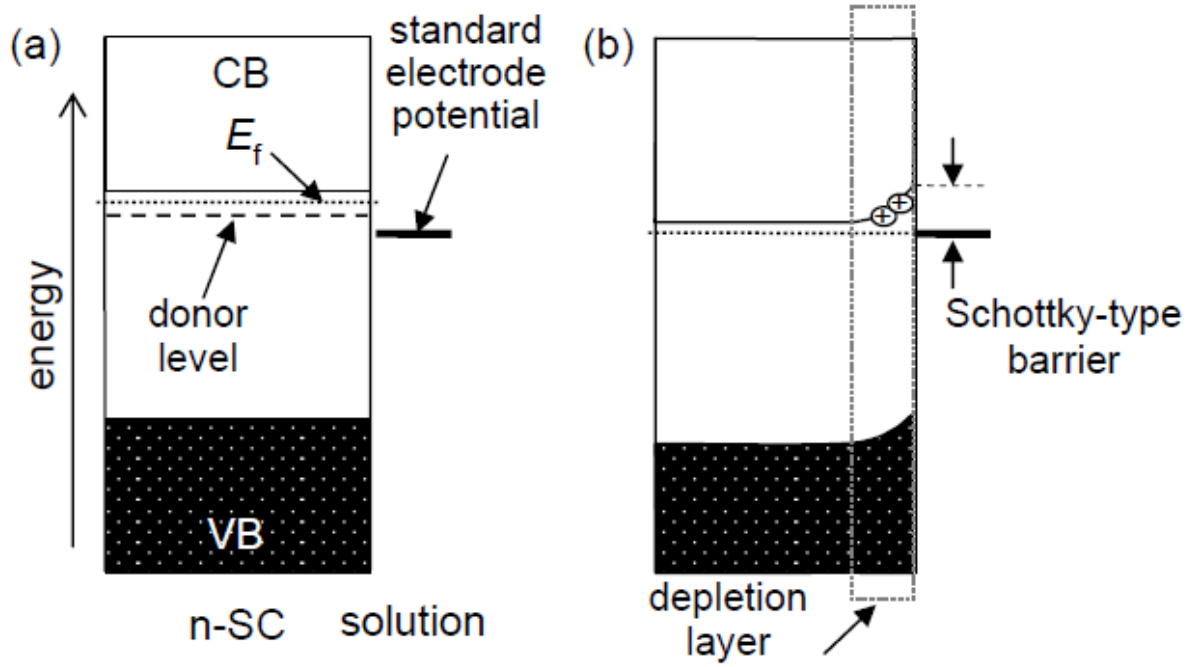

Figure 2.8: N-type semiconductor in solution (a) and Schottky-type barrier where the electrons have flowed out to the lower Fermi level (b).

(Taken from [110])

The effect of dopant concentration on the rate of electron-hole recombination is given by [41].

$$W = \frac{\varepsilon\varepsilon_0 V_s}{eN_d}$$

Equation 2.10: Space charge barrier calculation.

W is the thickness of the space-charge barrier, ε is the static dielectric current of the semiconductor in question, ε_0 is the static dielectric constant in a vacuum, V_s is the surface potential, e is the electron charge and N_d is the number of dopant atoms. When value of W is approximate to the depth of penetration of light into the solid (($l = \frac{1}{a}$), where 'a' is the absorption coefficient at a particular wavelength, then all electrons and holes generated will be separated [67].

With an increase in dopant concentration there is a narrowing in the space-charge barrier and this therefore results in an increase in separation of electrons and holes, lowering recombination. However at high dopant concentrations the barrier becomes too narrow with the space-charge barrier dropping below the recommended 0.2 eV this cause's increased recombination. Therefore there is an optimum level of doping above or below which would result in increased electron-hole recombination.

Doping may be carried out by either metal or non-metal atoms.

2.6.1 Metal Doping

A wide range of metals have been used to dope TiO_2. The metals used range from, transition metals to noble metals to lanthanides [111-118]. Doping TiO_2 with metal ions of higher or lower oxidations states than Ti^{+2} promotes the electrical conductivity of the TiO_2 [119]. **Table 2.2** gives a few of the metal dopants that have been used to improve the activity of TiO_2 with a view to degrade organic pollutants. It can be seen from **Table 2.2** that a wide range of metals have been used in an attempt to improve the activity of TiO_2. In the cases where the final degradation efficiencies of the doped and undoped catalysts were similar or the same, the doped catalyst showed a faster reaction rate.

Table 2.2: A number of metal dopants used to improve the photocatalytic activity of TiO_2 for photo-oxidation.

Dopant	Organic pollutant	Doped TiO_2 efficiency (%)	Undoped TiO_2 efficiency (%)
Fe [120]	Methyl orange	70	50
Pt [121]	Methyl orange	98	90
Ce [122]	4-Chlorophenol	78	20
Sm [123]	Salicylic acid	65	3
Zr [124]	4-chlorophenol	100	90
Ba [125]	4-chlorophenol	100	100
Ag [126]	Crystal violet	100	100
Fe [127]	Orange 16	93	70

A number of studies have been done on copper doping of TiO_2 for various applications. It has been shown to provide good results in relation to photo-oxidation. It is a cheap and non-toxic metal, so in the event of photo-corrosion it will not be harmful to the environment.

2.6.1.1 Copper Doping

Copper doping of TiO_2 has been used to improve photocatalytic activity for many applications [128-138]. A study by Nguyen Thi Thu *et al*, tested the effect of pH on the activity, for the degradation of methylene blue, of Cu-doped TiO_2 compared to undoped TiO_2, it was found that at all pH values Cu doped TiO_2 had better activity [139]. However at higher copper loadings the activity decreased, the best doping level was 0.15 at%. Pham *et al* found greater activity for the degradation of methylene blue using Cu doped TiO_2 on reduced graphene oxide than with the undoped TiO_2; the greater activity was attributed to a smaller band gap and an increase in the hydrophilicity with doping [140]. Chaing *et al* produced Cu doped TiO_2 nanorods for the photodegradation of bisphenol A, the reaction rate of the doped nanorods was nearly 7 times greater than the undoped nanorods, and the optimum wt% Cu was 7% [141]. Wang *et al* used mesoporous Cu doped TiO_2 to degrade methyl orange which

showed a significant improvement to the degradation rate of the undoped mesoporous TiO_2 [142]. Yadav *et al* used copper doped TiO_2 for antibacterial activity and found that it worked better than the undoped TiO_2 [133].

B. Choudhury *et al* used a sol-gel method to synthesis copper doped TiO_2, with titanium isopropoxide as a precursor and copper nitrate hexahydrate as a source of copper [143]. Samples were calcined at 450 °C however it was found that the copper induced the formation of brookite phase TiO_2. The copper doped catalysts show a decrease in band gap and increased absorption in the visible light region. Yoong *et al* studied the difference in hydrogen production rates of copper doped TiO_2 catalysts prepared via either a sol gel or wet impregnation method in a range 2-15 mol% [128]. It was found that both preparation methods induced a reduction in band gap, the catalysts prepared by wet impregnation had narrower band gaps but the band gap did not decrease linearly with the addition of copper. It was seen that hydrogen production was best with copper doped samples prepared by the sol gel method, 10 mol% doping was found to be the most active. Wang *et al* reported the use of copper doped TiO_2 for the degradation of Rhodamine B, the catalysts were synthesised using a sol gel method and catalysts were doped with copper in range of 0-3 mol% [129]. It was found that up to 0.06 mol% copper reduced the rate of electron-hole recombination but thereafter the copper increased the amount of electron-hole recombination. Copper doping induced visible light absorption. Initially doping increased photocatalytic activity but at doping levels greater than 0.06 mol% there was a rapid decrease in activity. The reduction in photocatalytic activity was attributed to the formation of Cu_2O on the surface of the TiO_2

Y. Liu *et al* found that interstitial doping of copper into TiO_2 is more stable than the substitution of Ti with Cu, meaning that interstitial doping is easier than substitutional doping [144]. In another study done by B. Choudhury it was proposed that the visible light

absorption of copper doped samples originates from the hybridization of the copper d-states and oxygen 2p levels [145].

2.6.2 Non-metal Doping

Non-metals affect change in the band gap by interaction with the oxygen 2p orbitals [146]. A wide range of non-metals have been used to dope TiO_2. **Table 2.3** shows various non-metals that have been used to dope TiO_2 in an effort to improve photocatalytic activity towards degradation of organic pollutants.

Table 2.3: Various non-metals used to dope TiO2 for the degradation of organic pollutants.

Dopant	**Organic pollutant**	**Doped TiO_2 efficiency (%)**	**Undoped TiO_2 efficiency (%)**
B [147]	Benzene	100	70
B [148]	Phenol	80	6
C [149]	4-Chlorophenol	71	56
Cl [150]	Phthalate ester	92	16
I [151]	Phenol	87	62
P [152]	Bisphenol A	65	59

2.6.2.1 Nitrogen Doping

Nitrogen doping of TiO_2 has attracted increased recently due to the increase in visible light absorption and photocatalytic activity of N-Doped TiO_2 [153-158]. Yang *et al* found that nitrogen doped TiO_2 catalysts irradiated only by wavelengths above 420 nm could completely degrade 10 ppm of methylene blue within 100 min [159]. Li *et al* also demonstrated the degradation of Rhodamine B with nitrogen doped TiO_2 under visible light irradiation, these catalyst showed improvement of the undoped catalyst and had absorption 400-800nm region [156]. This shows that nitrogen doped catalysts would be viable for utilisation of more of the solar spectrum than undoped TiO_2. Chong *et al* found that nitrogen doping improved the

degradation rate of Rhodamine B, the study also looked at various sources of nitrogen and it was found that triethlyamine was the best nitrogen source [158]. Work by Devi *et al* where TiO_2 was doped with nitrogen and used under solar irradiation for the degradation of phenol, the nitrogen doped catalyst showed an increase in activity compared to the undoped catalysts [160]. Samiolo *et al* used N-doped TiO_2 as a photoelectrode for the conversion benzyl and cinnamyl alcohols to the respective aldehydes, 100% selectivity was found using visible light conditions but not under UV irritation, proving the benefit of the visible light activity given by doping [161]. Pan *et al* used nitrogen doped TiO_2 to improve the anti-cancer activity of aluminium phthalocyanine chloride tetrasulfonate, as the UV irradiation necessary for undoped TiO_2 would be harmful for photodynamic therapy [162].

Zeng *et al* investigated the difference between photocatalytic activity of substitutional and interstitial doping of nitrogen in TiO_2 [153]. The difference in the position of the dopant was changed simply by including air upon calcination, creating and oxygen rich environment, the other calcination condition only included ammonia. The difference was proven via XPS. It was found that the substitutional doping provided better photocatalytic activity. These finds were supported by Serpone *et al* whom stated that under oxygen poor conditions substitutional doping is favoured and under oxygen rich conditions interstitial doping is favoured [163].

Asahi *et al* calculated that substitutional doping of nitrogen would result in band gap narrowing through the mixing of the *p* states of nitrogen and the 2*p* states of oxygen [164]. Di Valentin *et al* found that nitrogen doping lowers the energy cost of oxygen vacancies from 4.2 eV to 0.6 eV which means that nitrogen doping should be followed by formation of oxygen vacancies [165].

2.6.2.2 Sulfur Doping

Sulfur doping of TiO_2 has proven to an effect way to increase the absorption of visible light by TiO_2 and increase the rates of reaction for various purposes [166-172]. Devi *et al* reported the use of sulfur doped TiO_2 for the degradation of phenol which showed better activity than undoped TiO_2, this was attributed to a narrower band gap and improvement of electron trapping [166]. Sharotri *et al* used sulfur doped TiO_2 to degrade 2-chlorophenol, it was found that these catalysts worked far better than Degussa P25 or TiO_2 (Merck), the optimum wavelength for the sulfur doped catalysts was found to 660 nm. Goswami *et al* synthesized sulfur doped catalyst with oxalic acid as a controlling agent, it was found that these catalysts had better activity and much narrower band gaps that the undoped catalyst, the sulfur doping also increased surface area [169]. Li *et al* used a non-hydrolytic themolysis synthesis route to make sulfur doped TiO_2 which showed vastly improve degradation of both Rhodamine B and methylene blue, under visible light irradiation (420-770 nm) [170]. These results show that sulfur doping would improve the absorption and activity of TiO_2 under solar .irradiation

According to the study done by Asahi *et al* sulfur doping would result in a similar band gap narrowing to that of nitrogen; however the formation energy required for substitutional doping is very high [164]. In a computational study by Yang *et al* it was shown that S^{6+} or S^{4+} ion will replace Ti in the TiO_2 lattice which is agreement with experimental results found elsewhere [173-175].

Ohno reported that sulfur doped TiO_2 has inferior activity under UV light compared to undoped TiO_2 though under visible light it shows better activity than undoped TiO_2 [176]. Rockafellow *et al* made a similar observation, noting that sulfur doped TiO_2 only worked better in the visible light region compared to undoped TiO_2 [177]. The study further stated

that sulfur doped TiO_2 would only be useful for easily oxidized compounds due to deep trap states and therefore weaker oxidizing power.

2.7 Photodegradation of Emerging Contaminants

In a review by Sauve *et* al, the definition of an emerging contaminant (EC) was given as a naturally occurring or manmade chemical, which may persist in the environment and may alter the metabolism of a living organism [178]. It was further stated that these pollutants may only remain emerging so long as very little is known about their effect on the environment. Amongst emerging contaminants are pharmaceuticals, personal care products and other endocrine disrupting chemicals [179, 180]. Some of the most commonly reported ECs are a pharmaceutical group of chemicals called analgesics (painkillers). There are no regulations regarding the acceptable levels at which these compounds should be present in the environment, although there may be a threshold value at which one of these compounds become toxic. These chemicals can find their way into the environment in multiple ways, such as through municipal treatment plants, household discharges and pharmaceutical discharges [181-184]. There have been a number of studies on compounds that are considered EC in various European countries as well as the United States of America [185-188]. Work by Matongo *et al* shows that the Umegni River (Durban) which feeds a number of dams which provide water for consumption, namely Albert falls, Inanda, Midmar and Nagle dams, contains a number of ECs [189]. It was shown in further work that the Darvill (Pietermaritzburg) waste water treatment plant does not remove all of these pollutants and then this water is fed to the Msunduzi River, which then joins the Umgeni River [190]. This would in turn contaminate the four aforementioned dams which provide drinking water for Durban.

These compounds have low biodegradability, so it is necessary to oxidized via an external source. Some of these compounds may also degrade but into even more harmful compounds in the environment. Photodegradation may be a solution to this issue as it may convert organic compounds to carbon dioxide and water, and as discussed previously if TiO_2 is used as a photocatalyst then it would provide a cheap and non-toxic catalyst. Photocatalyst provides the advantages of being energy efficient and reusable compared to other advanced oxidation techniques. The photodegradation of these compounds has been attributed to the reaction with photo-generated hydroxyl radicals [55, 191].

2.7.1 Caffeine

Caffeine (structure seen in **Figure 2.9**) can be found in a wide range of regularly consumed items, such as coffee, tea, soft drinks and even some sweets. Caffeine also has medicinal uses as it can be used to enhance the effects of painkillers, in cough, cold and headache medication and can further be used as a stimulant for cardiac and respiratory systems [192]. Several studies have been done on the concentration of caffeine in waste water and surface water [193-195]. A study by Moore *et al* suggests that current levels of caffeine concentrations in water bodies do not pose a threat to organisms present [196]. While current levels do not pose a threat acute levels may pose a threat and given the number of compounds in which caffeine can be found it is possible it may pose a threat in the future. Recently the studies by Matongo *et al* as well as Foluso *et al* found caffeine in the Umgeni River, which in turn can be found in drinking water [189, 190, 197]. Marques *et al*, used photodegradation for the remove of caffeine from water, this was done using TiO_2 anchored on CNTs, and the TiO_2 was prepared by three different methods [198]. In this study 1.0 $g.L^{-1}$ of catalyst was used in 250 mL of 50 ppm caffeine solution, and system was continuously bubbled with 20

vol% oxygen. No degradation mechanism was given for this reaction. Klamerth *et al* conducted a test to degrade 9 ECs in the same reactor, one of them being caffeine this test was carried out with both TiO_2 and a photo-Fenton process, in a pilot solar reactor. A concentration of 5 $mg.L^{-1}$ of TiO_2 (P25) was used and 100 ppb of each of the ECs complete degradation of all 9 compounds took place within 200 min.

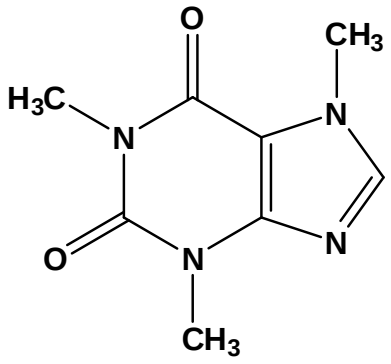

Figure 2.9: Structure of caffeine.

2.7.2 Phenacetin

Phenacetin (**Figure 2.10**) is an analgesic and is also used to reduce fever [199]. It has been proven to cause renal failure and as such has been banned from use in some countries [200]. Despite this there have been reports of phenacetin being detected in wastewater even in countries where it has been banned [201]. Phenacetin was degraded along with 3 other EC in a study done by Benitez *et al* by three different methods namely, hydrogen peroxide, TiO_2 photodegradation and photo-Fenton process [202]. It was found that the TiO_2 worked best for the degradation of these compounds and it was also found that the compound slowest to degrade was phenacetin. Giri *et al* used 7 techniques to degrade 16 different ECs 1 of which was phenacetin in the same solution [203]. In this study phenacetin showed almost no

degradation with UV irradiation and TiO_2, and ozone was needed to effect degradation, complete degradation took place within 1 hour when using ozone.

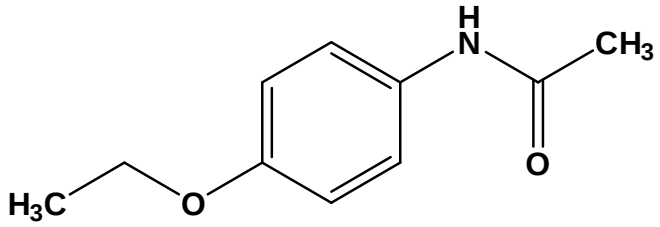

Figure 2.10: Structure of phenacetin.

2.7.3 Aspirin

Aspirin (acetylsalicylic acid), structure shown in **Figure 2.11**, is a readily available in a wide range of over the counter medication. There is evidence that aspirin may reduce the risk of certain types of cancer [204]. A toxic dose of aspirin would be in the range of 200-300 mg/kg, and a dose of 500 mg/kg is potentially lethal [205]. In a study by Takada *et al* of Tokyo wastewater it was found that of the monitored compounds aspirin had the highest concentration [206]. A study by Foluso found aspirin in the water of the Umgeni River, as well as the Inanda and Midmar Dams [197].

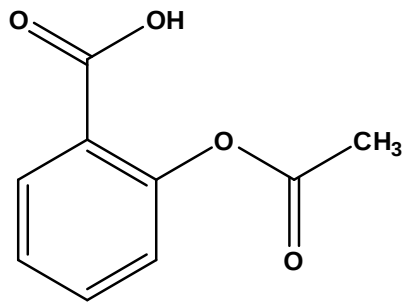

Figure 2.11: Structure of Aspirin.

2.7.4 Salicylic Acid

Salicylic acid (SA), structure is given below in **Figure 2.12**, is a major metabolite of aspirin [207]. A number of studies have found trace concentration of SA in effluent, influent and soil [208-210]. It is used in creams to treat pimples and blemishes [211]. Vilhunen *et al* degraded SA on TiO_2 films, the effect of initial concentration of SA and the initial pH of the solution was studied [212]. The films were placed in a petri dish and the solution of SA poured over it, this setup was the irradiated with a UV lamp, with 85% of it spectrum 250-260 nm range. The best concentration was found to 75 ppm and the best pH to 8. Silva *et al* synthesized TiO_2 anchored on SBA-15 and used these catalysts to photodegrade SA [213]. For each reaction 50 mL of 50 $mmol.L^{-1}$ SA was used, to this 4 mg of the respective catalyst was added, the mixture was irradiated with a 125 W mercury lamp. The maximum degradation observed for this study in a 180 min period was 20% removal of the initial concentration.

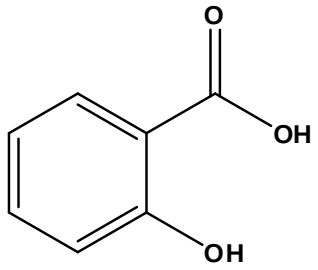

Figure 2.12: Structure of SA.

References

1. P. Atkins and J. De Paula, *Physical Chemistry*. 8 ed. 2006, Hong Kong, China.
2. C.E. Housecroft and A.G. Sharpe, *Inorganic Chemistry*. 3 ed. 2008, Italy: Pearson Education Limited.
3. M. G.L and D. Tarr, *Inoragnic chemistry*, 2004, Pearson Prentice Hall.
4. L. Zhang, H.H. Mohamed, R. Dillert, and D. Bahnemann, *Kinetics and mechanisms of charge transfer processes in photocatalytic systems: A review*. Journal of Photochemistry and Photobiology C: Photochemistry Reviews, 2012(13): p. 263-276.
5. D.A. Neamen, *Semiconductor physics and devices: Basic principles*, ed. P.M. Buschman. 1992, United States of America: Richard D. Irwin, INC.
6. J.I. Pankove, *Optical processes in semiconductors*. Solid State Physical Electronics Series, ed. N. Holoyak. 1971, United States of America: Prentice-Hall.
7. S.M. Sze and K.K. Ng, *Physics of semiconductor devices*. 2006: John Wiley & Sons.
8. B.K. Tanner, *Introduction to the physics of electronic in solids*. 1995, Great Britain Cambridge: Cambridge University Press.
9. S.M. Sze and K.N. Kwok, *Physics of semiconductor devices*. 3rd ed. 2007, United States of America: John Wiley & Sons, Inc.
10. B. Ohtani, *Photocatalysis A to Z—What we know and what we do not know in a scientific sense.* Journal of Photochemistry and Photobiology C: Photochemistry Reviews, 2010. **11**(4): p. 157-178.
11. H. Lin, C.P. Huang, W. Li, C. Ni, S.I. Shah, and Y.-H. Tseng, *Size dependency of nanocrystalline TiO2 on its optical property and photocatalytic reactivity exemplified by 2-chlorophenol.* Applied Catalysis B: Environmental, 2006. **68**(1–2): p. 1-11.
12. C. Colleoni, M.R. Massafra, and G. Rosace, *Photocatalytic properties and optical characterization of cotton fabric coated via sol–gel with non-crystalline TiO2*

modified with poly(ethylene glycol). Surface and Coatings Technology, 2012. **207**(0): p. 79-88.

13. J. Lim, P. Murugan, N. Lakshminarasimhan, J.Y. Kim, J.S. Lee, S.-H. Lee, and W. Choi, *Synergic photocatalytic effects of nitrogen and niobium co-doping in TiO2 for the redox conversion of aquatic pollutants under visible light.* Journal of Catalysis, 2014. **310**(0): p. 91-99.
14. A. Bjelajac, V. Djokic, R. Petrovic, G. Socol, I.N. Mihailescu, I. Florea, O. Ersen, and D. Janackovic, *Visible light-harvesting of TiO2 nanotubes array by pulsed laser deposited CdS.* Applied Surface Science, 2014. **309**(0): p. 225-230.
15. N. Jain, Y. Zhu, D. Maurya, R. Varghese, S. Priya, and M.K. Hudait, *Interfacial band alignment and structural properties of nanoscale TiO2 thin films for integration with epitaxial crystallographic oriented germanium.* Journal of Applied Physics, 2014. **115**(2): p. 1-8.
16. C.-C. Yen, D.-Y. Wang, M.-H. Shih, L.-S. Chang, and H.C. Shih, *A combined experimental and theoretical analysis of Fe-implanted TiO2 modified by metal plasma ion implantation.* Applied Surface Science, 2010. **256**(22): p. 6865-6870.
17. P. Apopei, C. Catrinescu, C. Teodosiu, and S. Royer, *Mixed-phase TiO2 photocatalysts: Crystalline phase isolation and reconstruction, characterization and photocatalytic activity in the oxidation of 4-chlorophenol from aqueous effluents.* Applied Catalysis B: Environmental, 2014. **160–161**(0): p. 374-382.
18. A. Slav, *Optical characterization of TiO2-Ge nanocomposite films obtained by reactive magnetron sputtering.* Digest Journal of Nanomaterials & Biostructures (DJNB), 2011. **6**(3): p. 915-920.
19. J.M. Herrmann, *Heterogeneous photocatalysis: state of the art and present applications In honor of Pr. R.L. Burwell Jr. (1912–2003), Former Head of Ipatieff*

Laboratories, Northwestern University, Evanston (Ill). Topics in Catalysis, 2005. **34**(1-4): p. 49-65.

20. J.-M. Herrmann, *Heterogeneous photocatalysis: Fundamentals and applications to the removal of various types of aqueous pollutants.* Catalysis Today, 1999. **53**(1): p. 115-129.
21. A.L. Linsebigler, G. Lu, and J.T. Yates, *Photocatalysis on TiOn surfaces: Principles, mechanisms, and selected results.* Chemical Reviews, 1995. **95**: p. 735-758.
22. U.I. Gaya and A.H. Abdullah, *Heterogeneous photocatalytic degradation of organic contaminants over titanium dioxide: A review of fundamentals, progress and problems.* Journal of Photochemistry and Photobiology C: Photochemistry Reviews, 2008. **9**: p. 1-12.
23. M.I. Litter, *Heterogeneous photocatalysis Transition metal ions in photocatalytic systems.* Applied Catalysis B: Environmental, 1999. **23**: p. 89-114.
24. U.G. Akpan and B.H. Hameed, *Parameters affecting the photocatalytic degradation of dyes using TiO2-based photocatalysts: A review.* Journal of Hazardous Materials, 2009. **170**: p. 520-529.
25. I.K. Konstantinou and T.A. Albanis, *TiO2-assisted photocatalytic degradation of azo dyes in aqueous solution: kinetic and mechanistic investigations: a review.* Applied Catalysis B: Environmental, 2004. **49**(1): p. 1-14.
26. M.D. Hernández-Alonso, F. Fresno, S. Suárez, and J.M. Coronado, *Development of alternative photocatalysts to TiO2: challenges and opportunities.* Energy & Environmental Science, 2009. **2**(12): p. 1231-1257.
27. C. Guillard, H. Lachheb, A. Houas, M. Ksibi, E. Elaloui, and J.-M. Herrmann, *Influence of chemical structure of dyes, of pH and of inorganic salts on their photocatalytic degradation by TiO2 comparison of the efficiency of powder and*

supported TiO2. Journal of Photochemistry and Photobiology A: Chemistry, 2003. **158**(1): p. 27-36.

28. S. Tunesi and M. Anderson, *Influence of chemisorption on the photodecomposition of salicylic acid and related compounds using suspended titania ceramic membranes.* The Journal of Physical Chemistry, 1991. **95**(8): p. 3399-3405.
29. T. Noguchi, A. Fujishima, P. Sawunyama, and K. Hashimoto, *Photocatalytic degradation of gaseous formaldehyde using TiO2 film.* Environmental science & technology, 1998. **32**(23): p. 3831-3833.
30. K. Tanaka, K. Padermpole, and T. Hisanaga, *Photocatalytic degradation of commercial azo dyes.* Water research, 2000. **34**(1): p. 327-333.
31. T. Sugimoto, X. Zhou, and A. Muramatsu, *Synthesis of uniform anatase TiO2 nanoparticles by gel–sol method: 4. Shape control.* Journal of Colloid and Interface Science, 2003. **259**(1): p. 53-61.
32. K. Kogo, H. Yoneyama, and H. Tamura, *Photocatalytic oxidation of cyanide on platinized titanium dioxide.* The Journal of Physical Chemistry, 1980. **84**(13): p. 1705-1710.
33. G.A. Parks, *The isoelectric points of solid oxides, solid hydroxides, and aqueous hydroxo complex systems.* Chemical Reviews, 1965. **65**(2): p. 177-198.
34. M. Kosmulski, *The pH-dependent surface charging and the points of zero charge.* Journal of Colloid and Interface Science, 2002. **253**(1): p. 77-87.
35. S. Ahmed, M. Rasul, W. Martens, R. Brown, M. Rosen, R. Perryman, S. Dodds, F. Muzi, W. Yuji, and Z. Polkowska. *A review on the role of operating parameters in heterogeneous photo catalytic water purification processes for storm and wastewater reuse*. in *WSEAS International Conference. Proceedings. Mechanical Engineering Series*. 2010. World Scientific and Engineering Academy and Society.

36. X. Zhu, S.R. Castleberry, M.A. Nanny, and E.C. Butler, *Effects of pH and catalyst concentration on photocatalytic oxidation of aqueous ammonia and nitrite in titanium dioxide suspensions.* Environmental science & technology, 2005. **39**(10): p. 3784-3791.

37. M.D. Ward, J.R. White, and A.J. Bard, *Electrochemical investigation of the energetics of particulate titanium dioxide photocatalysts. The methyl viologen-acetate system.* Journal of the American Chemical Society, 1983. **105**(1): p. 27-31.

38. J. Sun, X. Wang, J. Sun, R. Sun, S. Sun, and L. Qiao, *Photocatalytic degradation and kinetics of Orange G using nano-sized Sn (IV)/TiO 2/AC photocatalyst.* Journal of molecular catalysis A: Chemical, 2006. **260**(1): p. 241-246.

39. J. Sun, L. Qiao, S. Sun, and G. Wang, *Photocatalytic degradation of Orange G on nitrogen-doped TiO 2 catalysts under visible light and sunlight irradiation.* Journal of hazardous materials, 2008. **155**(1): p. 312-319.

40. C.-h. Wei, X.-h. Tang, J.-r. Liang, and S.-y. Tan, *Preparation, characterization and photocatalytic activities of boron-and cerium-codoped TiO2.* Journal of Environmental Sciences, 2007. **19**(1): p. 90-96.

41. M.A. Fox and M.T. Dulay, *Heterogeneous photocatalysis.* Chemical reviews, 1993. **93**(1): p. 341-357.

42. M. Saquib, M.A. Tariq, M. Faisal, and M. Muneer, *Photocatalytic degradation of two selected dye derivatives in aqueous suspensions of titanium dioxide.* Desalination, 2008. **219**(1): p. 301-311.

43. L.-C. Chen, C.-M. Huang, and F.-R. Tsai, *Characterization and photocatalytic activity of K+-doped TiO 2 photocatalysts.* Journal of Molecular Catalysis A: Chemical, 2007. **265**(1): p. 133-140.

44. M. Huang, C. Xu, Z. Wu, Y. Huang, J. Lin, and J. Wu, *Photocatalytic discolorization of methyl orange solution by Pt modified TiO 2 loaded on natural zeolite.* Dyes and Pigments, 2008. **77**(2): p. 327-334.

45. Y. Huang, X. Zheng, Y. Zhongyi, T. Feng, F. Beibei, and H. Keshan, *Preparation of nitrogen-doped TiO 2 nanoparticle catalyst and its catalytic activity under visible light.* Chinese Journal of Chemical Engineering, 2007. **15**(6): p. 802-807.

46. Y. Zhiyong, M. Bensimon, V. Sarria, I. Stolitchnov, W. Jardim, D. Laub, E. Mielczarski, J. Mielczarski, L. Kiwi-Minsker, and J. Kiwi, *ZnSO 4–TiO 2 doped catalyst with higher activity in photocatalytic processes.* Applied Catalysis B: Environmental, 2007. **76**(1): p. 185-195.

47. W. Baran, A. Makowski, and W. Wardas, *The effect of UV radiation absorption of cationic and anionic dye solutions on their photocatalytic degradation in the presence TiO 2.* Dyes and Pigments, 2008. **76**(1): p. 226-230.

48. D.S. Bhatkhande, S.P. Kamble, S.B. Sawant, and V.G. Pangarkar, *Photocatalytic and photochemical degradation of nitrobenzene using artificial ultraviolet light.* Chemical Engineering Journal, 2004. **102**(3): p. 283-290.

49. H. Zhang, R.L. Penn, R.J. Hamers, and J.F. Banfield, *Enhanced adsorption of molecules on surfaces of nanocrystalline particles.* The Journal of Physical Chemistry B, 1999. **103**(22): p. 4656-4662.

50. M.A. Tariq, M. Faisal, M. Muneer, and D. Bahnemann, *Photochemical reactions of a few selected pesticide derivatives and other priority organic pollutants in aqueous suspensions of titanium dioxide.* Journal of Molecular Catalysis A: Chemical, 2007. **265**(1–2): p. 231-236.

51. J. Araña, J.L. Martínez Nieto, J.A. Herrera Melián, J.M. Doña Rodríguez, O. González Díaz, J. Pérez Peña, O. Bergasa, C. Alvarez, and J. Méndez, *Photocatalytic*

degradation of formaldehyde containing wastewater from veterinarian laboratories. Chemosphere, 2004. **55**(6): p. 893-904.

52. S. Ahmed, M.G. Rasul, W.N. Martens, R. Brown, and M.A. Hashib, *Heterogeneous photocatalytic degradation of phenols in wastewater: A review on current status and developments.* Desalination, 2010. **261**(1–2): p. 3-18.

53. M. Pera-Titus, V. García-Molina, M.A. Baños, J. Giménez, and S. Esplugas, *Degradation of chlorophenols by means of advanced oxidation processes: a general review.* Applied Catalysis B: Environmental, 2004. **47**(4): p. 219-256.

54. O.K. Dalrymple, E. Stefanakos, M.A. Trotz, and D.Y. Goswami, *A review of the mechanisms and modeling of photocatalytic disinfection.* Applied Catalysis B: Environmental, 2010. **98**(1): p. 27-38.

55. M.N. Chong, B. Jin, C.W. Chow, and C. Saint, *Recent developments in photocatalytic water treatment technology: a review.* Water research, 2010. **44**(10): p. 2997-3027.

56. D. Spasiano, R. Marotta, S. Malato, P. Fernandez-Ibanez, and I. Di Somma, *Solar photocatalysis: Materials, reactors, some commercial and pre-industrialized applications. A comprehensive approach.* Applied Catalysis B: Environmental, 2015.

57. J.-M. Herrmann, *Fundamentals and misconceptions in photocatalysis.* Journal of Photochemistry and Photobiology A: Chemistry, 2010. **216**(2): p. 85-93.

58. G. Luca Chiarello and E. Selli, *Photocatalytic hydrogen production.* Recent Patents on Engineering, 2010. **4**(3): p. 155-169.

59. H. Kato and A. Kudo, *Water splitting into H2 and O2 on alkali tantalate photocatalysts ATaO3 (A= Li, Na, and K).* The Journal of Physical Chemistry B, 2001. **105**(19): p. 4285-4292.

60. X. Li and J. Zang, *Facile hydrothermal synthesis of sodium tantalate (NaTaO3) nanocubes and high photocatalytic properties.* The Journal of Physical Chemistry C, 2009. **113**(45): p. 19411-19418.

61. J. Zhu and M. Zäch, *Nanostructured materials for photocatalytic hydrogen production.* Current Opinion in Colloid & Interface Science, 2009. **14**(4): p. 260-269.

62. A. Kudo and Y. Miseki, *Heterogeneous photocatalyst materials for water splitting.* Chemical Society Reviews, 2009. **38**(1): p. 253-278.

63. R.M. Navarro Yerga, M.C. Álvarez Galván, F. del Valle, J.A. Villoria de la Mano, and J.L.G. Fierro, *Water splitting on semiconductor catalysts under visible-light irradiation.* ChemSusChem, 2009. **2**(6): p. 471-485.

64. X. Li, J. Yu, J. Low, Y. Fang, J. Xiao, and X. Chen, *Engineering heterogeneous semiconductors for solar water splitting.* Journal of Materials Chemistry A, 2015. **3**(6): p. 2485-2534.

65. G. Palmisano, V. Augugliaro, M. Pagliaro, and L. Palmisano, *Photocatalysis: a promising route for 21st century organic chemistry.* Chemical Communications, 2007(33): p. 3425-3437.

66. R.A. Al-Rasheed. *Water treatment by heterogeneous photocatalysis an overview*. in *4th SWCC acquired Experience Symposium held in Jeddah*. 2005.

67. O. Carp, C.L. Huisman, and A. Reller, *Photoinduced reactivity of titanium dioxide.* Progress in solid state chemistry, 2004. **32**(1): p. 33-177.

68. K. Hashimoto, H. Irie, and A. Fujishima, *TiO2 photocatalysis: a historical overview and future prospects.* Japanese journal of applied physics, 2005. **44**(12R): p. 8269.

69. G. An, W. Ma, Z. Sun, Z. Liu, B. Han, S. Miao, Z. Miao, and K. Ding, *Preparation of titania/carbon nanotube composites using supercritical ethanol and their*

photocatalytic activity for phenol degradation under visible light irradiation. Carbon, 2007. **45**(9): p. 1795-1801.

70. Y. Ju, L. Li, Z. Wu, and Y. Jiang, *Effect of oxygen partial pressure on the optical property of amorphous titanium oxide thin films.* Energy Procedia, 2011. **12**: p. 450-455.

71. H. Kangarlou and S. Rafizadeh, *Study the optical properties of titanium oxide thin films deposited on glass substrate at different deposition angles by resistive evaporation method.* Optik-International Journal for Light and Electron Optics, 2013. **124**(17): p. 2787-2790.

72. M. Auffan, M. Pedeutour, J. Rose, A. Masion, F. Ziarelli, D. Borschneck, C. Chaneac, C. Botta, P. Chaurand, and J. Labille, *Structural degradation at the surface of a TiO2-based nanomaterial used in cosmetics.* Environmental science & technology, 2010. **44**(7): p. 2689-2694.

73. P.V. Kamat, *Photochemistry on nonreactive and reactive (semiconductor) surfaces.* Chemical Reviews, 1993. **93**(1): p. 267-300.

74. F. De Angelis, C. Di Valentin, S. Fantacci, A. Vittadini, and A. Selloni, *Theoretical studies on anatase and less common TiO2 phases: Bulk, surfaces, and nanomaterials.* Chemical reviews, 2014. **114**(19): p. 9708-9753.

75. P. Simons and F. Dachille, *The structure of TiO2II, a high-pressure phase of TiO2.* Acta Crystallographica, 1967. **23**(2): p. 334-336.

76. M. Latroche, L. Brohan, R. Marchand, and M. Tournoux, *New hollandite oxides: TiO 2 (H) and K 0.06 TiO 2.* Journal of Solid State Chemistry, 1989. **81**(1): p. 78-82.

77. H. Sato, S. Endo, M. Sugiyama, T. Kikegawa, O. Shimomura, and K. Kusaba, *Baddeleyite-Type High-Pressure Phase of TiO2.* Science, 1991. **251**(4995): p. 786-788.

78. J. Tang and S. Endo, *P–T Boundary of α-PbO2 type and Baddeleyite type high-pressure phases of titanium dioxide.* Journal of the American Ceramic Society, 1993. **76**(3): p. 796-798.

79. L.S. Dubrovinsky, N.A. Dubrovinskaia, V. Swamy, J. Muscat, N.M. Harrison, R. Ahuja, B. Holm, and B. Johansson, *Materials science: The hardest known oxide.* Nature, 2001. **410**(6829): p. 653-654.

80. L. Gerward and J. Staun Olsen, *Post-rutile high-pressure phases in TiO2.* Journal of applied crystallography, 1997. **30**(3): p. 259-264.

81. J.S. Tse and D.D. Klug, *Theoretical studies of structural stability at high pressure.* Canadian Journal of Physics, 1995. **73**(5-6): p. 253-257.

82. K. Lagarec and S. Desgreniers, *Raman study of single crystal anatase TiO2 up to 70 GPa.* Solid State Communications, 1995. **94**(7): p. 519-524.

83. T. Fröschl, U. Hörmann, P. Kubiak, G. Kučerová, M. Pfanzelt, C.K. Weiss, R. Behm, N. Hüsing, U. Kaiser, and K. Landfester, *High surface area crystalline titanium dioxide: potential and limits in electrochemical energy storage and catalysis.* Chemical Society Reviews, 2012. **41**(15): p. 5313-5360.

84. V. Štengl and D. Králová, *Photoactivity of brookite–rutile TiO 2 nanocrystalline mixtures obtained by heat treatment of hydrothermally prepared brookite.* Materials Chemistry and Physics, 2011. **129**(3): p. 794-801.

85. U. Diebold, *The surface science of titanium dioxide.* Surface science reports, 2003. **48**(5): p. 53-229.

86. V.N. Koparde and P.T. Cummings, *Phase transformations during sintering of titania nanoparticles.* ACS nano, 2008. **2**(8): p. 1620-1624.

87. H. Zhang and J.F. Banfield, *Understanding polymorphic phase transformation behavior during growth of nanocrystalline aggregates: Insights from TiO2.* The Journal of Physical Chemistry B, 2000. **104**(15): p. 3481-3487.

88. H. Zhang and J. F. Banfield, *Thermodynamic analysis of phase stability of nanocrystalline titania.* Journal of Materials Chemistry, 1998. **8**(9): p. 2073-2076.

89. F. Grant, *Properties of rutile (titanium dioxide).* Reviews of Modern Physics, 1959. **31**(3): p. 646.

90. T. Hitosugi, N. Yamada, S. Nakao, Y. Hirose, and T. Hasegawa, *Properties of TiO2-based transparent conducting oxides.* physica status solidi (a), 2010. **207**(7): p. 1529-1537.

91. H. Tang, K. Prasad, R. Sanjinès, P.E. Schmid, and F. Lévy, *Electrical and optical properties of TiO2 anatase thin films.* Journal of Applied Physics, 1994. **75**(4): p. 2042-2047.

92. A. Mattsson and L. Österlund, *Adsorption and photoinduced decomposition of acetone and acetic acid on anatase, brookite, and rutile TiO2 nanoparticles.* The Journal of Physical Chemistry C, 2010. **114**(33): p. 14121-14132.

93. J. Zhang, P. Zhou, J. Liu, and J. Yu, *New understanding of the difference of photocatalytic activity among anatase, rutile and brookite TiO2.* Physical Chemistry Chemical Physics, 2014. **16**(38): p. 20382-20386.

94. D.A. Hanaor and C.C. Sorrell, *Review of the anatase to rutile phase transformation.* Journal of Materials science, 2011. **46**(4): p. 855-874.

95. A. Sclafani and J.M. Herrmann, *Comparison of the photoelectronic and photocatalytic activities of various anatase and rutile forms of titania in pure liquid organic phases and in aqueous solutions.* The Journal of Physical Chemistry, 1996. **100**(32): p. 13655-13661.

96. D.M. Han, H.-J. Song, C.-H. Han, and Y.S. Kim, *Enhancement of the outdoor stability of dye-sensitized solar cells by a spectrum conversion layer with 1, 8-naphthalimide derivatives.* RSC Advances, 2015. **5**(41): p. 32588-32593.

97. Y. Peng, J. He, Q. Liu, Z. Sun, W. Yan, Z. Pan, Y. Wu, S. Liang, W. Cheng, and S. Wei, *Impurity concentration dependence of optical absorption for phosphorus-doped anatase TiO2.* The Journal of Physical Chemistry C, 2011. **115**(16): p. 8184-8188.

98. S.G. Kumar and L.G. Devi, *Review on modified TiO2 photocatalysis under UV/visible light: selected results and related mechanisms on interfacial charge carrier transfer dynamics.* The Journal of Physical Chemistry A, 2011. **115**(46): p. 13211-13241.

99. Y. Peter and M. Cardona, *Fundamentals of semiconductors: physics and materials properties*. 2010: Springer Science & Business Media.

100. Z. Zhang and J.T. Yates Jr, *Direct observation of surface-mediated electron− hole pair recombination in TiO2 (110).* The Journal of Physical Chemistry C, 2010. **114**(7): p. 3098-3101.

101. D. Steiauf, E. Kioupakis, and C.G. Van de Walle, *Auger recombination in GaAs from first principles.* Acs Photonics, 2014. **1**(8): p. 643-646.

102. N. Serpone, D. Lawless, R. Khairutdinov, and E. Pelizzetti, *Subnanosecond relaxation dynamics in TiO2 colloidal Sols (particle sizes Rp= 1.0-13.4 nm). relevance to heterogeneous photocatalysis.* The Journal of Physical Chemistry, 1995. **99**(45): p. 16655-16661.

103. B. Yunxiao and W. Xiaochang, *Features and Application of Titanium Dioxide Thin Films in Water Treatment.* Procedia Engineering, 2011. **24**: p. 663-666.

104. A. Turki, H. Kochkar, C. Guillard, G. Berhault, and A. Ghorbel. *Photocatalytic efficiency of TiO2 nanotubes, nanowires and nanorods in water treatment*. in

International Joint Conference CB-WR-MED Conference/2 nd AOP'Tunisia Conference for Sustainable Water Management. 2014.

105. W. Fan, Q. Lai, Q. Zhang, and Y. Wang, *Nanocomposites of TiO2 and reduced graphene oxide as efficient photocatalysts for hydrogen evolution.* The Journal of Physical Chemistry C, 2011. **115**(21): p. 10694-10701.

106. C.W. Dunnill and I.P. Parkin, *Nitrogen-doped TiO 2 thin films: photocatalytic applications for healthcare environments.* Dalton Transactions, 2011. **40**(8): p. 1635-1640.

107. L. Sang, Y. Zhao, and C. Burda, *TiO2 nanoparticles as functional building blocks.* Chemical reviews, 2014. **114**(19): p. 9283-9318.

108. N. Serpone, *Is the band gap of pristine TiO2 Narrowed by anion- and cation-doping of titanium dioxide in second-generation photocatalysts?* The Journal of Physical Chemistry B, 2006. **110**(48): p. 24287-24293.

109. W. Zhou, Q. Liu, Z. Zhu, and J. Zhang, *Preparation and properties of vanadium-doped TiO2 photocatalysts.* Journal of Physics D: Applied Physics, 2010. **43**(3): p. 035301.

110. B. Ohtani, *Titania photocatalysis beyond recombination: A critical review.* Catalysts, 2013. **3**(4): p. 942-953.

111. S. Bingham and W.A. Daoud, *Recent advances in making nano-sized TiO 2 visible-light active through rare-earth metal doping.* Journal of Materials Chemistry, 2011. **21**(7): p. 2041-2050.

112. K.T. Ranjit, I. Willner, S.H. Bossmann, and A.M. Braun, *Lanthanide oxide-doped titanium dioxide photocatalysts: Novel photocatalysts for the enhanced degradation of p-chlorophenoxyacetic acid.* Environmental Science & Technology, 2001. **35**(7): p. 1544-1549.

113. A.-W. Xu, Y. Gao, and H.-Q. Liu, *The preparation, characterization, and their photocatalytic activities of rare-earth-doped TiO 2 nanoparticles.* Journal of Catalysis, 2002. **207**(2): p. 151-157.

114. X.Z. Li and F.B. Li, *Study of Au/Au3+-TiO2 photocatalysts toward visible photooxidation for water and wastewater treatment.* Environmental Science & Technology, 2001. **35**(11): p. 2381-2387.

115. M.K. Seery, R. George, P. Floris, and S.C. Pillai, *Silver doped titanium dioxide nanomaterials for enhanced visible light photocatalysis.* Journal of Photochemistry and Photobiology A: Chemistry, 2007. **189**(2): p. 258-263.

116. L. Andronic, A. Enesca, C. Vladuta, and A. Duta, *Photocatalytic activity of cadmium doped TiO 2 films for photocatalytic degradation of dyes.* Chemical Engineering Journal, 2009. **152**(1): p. 64-71.

117. R.S. Wong, J. Feng, X. Hu, and P.L. Yue, *Discoloration and mineralization of non-biodegradable azo dye orange II by copper-doped TiO2 nanocatalysts.* Journal of Environmental Science and Health, Part A, 2004. **39**(10): p. 2583-2595.

118. C.-y. Wang, D.W. Bahnemann, and J.K. Dohrmann, *A novel preparation of iron-doped TiO2 nanoparticles with enhanced photocatalytic activity.* Chemical Communications, 2000(16): p. 1539-1540.

119. C.W. Dunnill, A. Kafizas, and I.P. Parkin, *CVD production of doped titanium dioxide thin films.* Chemical Vapor Deposition, 2012. **18**(4-6): p. 89-101.

120. T. Tong, J. Zhang, B. Tian, F. Chen, and D. He, *Preparation of Fe3+-doped TiO2 catalysts by controlled hydrolysis of titanium alkoxide and study on their photocatalytic activity for methyl orange degradation.* Journal of Hazardous Materials, 2008. **155**(3): p. 572-579.

121. M. Huang, C. Xu, Z. Wu, Y. Huang, J. Lin, and J. Wu, *Photocatalytic discolorization of methyl orange solution by Pt modified TiO2 loaded on natural zeolite.* Dyes and Pigments, 2008. **77**(2): p. 327-334.

122. J. Xiao, T. Peng, R. Li, Z. Peng, and C. Yan, *Preparation, phase transformation and photocatalytic activities of cerium-doped mesoporous titania nanoparticles.* Journal of Solid State Chemistry, 2006. **179**(4): p. 1161-1170.

123. Y. Ma, J. Zhang, B. Tian, F. Chen, and L. Wang, *Synthesis and characterization of thermally stable Sm,N co-doped TiO2 with highly visible light activity.* Journal of Hazardous Materials, 2010. **182**(1–3): p. 386-393.

124. N. Venkatachalam, M. Palanichamy, B. Arabindoo, and V. Murugesan, *Enhanced photocatalytic degradation of 4-chlorophenol by Zr4+ doped nano TiO2.* Journal of Molecular Catalysis A: Chemical, 2007. **266**(1–2): p. 158-165.

125. N. Venkatachalam, M. Palanichamy, and V. Murugesan, *Sol–gel preparation and characterization of alkaline earth metal doped nano TiO2: Efficient photocatalytic degradation of 4-chlorophenol.* Journal of Molecular Catalysis A: Chemical, 2007. **273**(1–2): p. 177-185.

126. C. Sahoo, A. Gupta, and A. Pal, *Photocatalytic degradation of Crystal Violet (CI Basic Violet 3) on silver ion doped TiO 2.* Dyes and Pigments, 2005. **66**(3): p. 189-196.

127. M. Safari, R. Talebi, M.H. Rostami, M. Nikazar, and M. Dadvar, *Synthesis of iron-doped TiO2 for degradation of reactive Orange16.* Journal of Environmental Health Science and Engineering, 2014. **12**(1): p. 19.

128. L. Yoong, F.K. Chong, and B.K. Dutta, *Development of copper-doped TiO2 photocatalyst for hydrogen production under visible light.* Energy, 2009. **34**(10): p. 1652-1661.

129. B. Xin, P. Wang, D. Ding, J. Liu, Z. Ren, and H. Fu, *Effect of surface species on Cu-TiO 2 photocatalytic activity.* Applied surface science, 2008. **254**(9): p. 2569-2574.

130. M.A. Behnajady, H. Taba, N. Modirshahla, and M. Shokri, *Photocatalytic activity of Cu doped TiO2 nanoparticles and comparison of two main doping procedures.* Micro & Nano Letters, 2013. **8**(7): p. 345-348.

131. J.R. De la Rosa, C.J. Lucio-Ortiz, A.H. Ramirez, G.A. Flores-Escamilla, and C.D. Garcia, *Photocatalytic degradation of trichloroethylene in a continuous annular reactor using Cu-doped TiO 2 catalysts by sol-gel synthesis.* Applied Catalysis B: Environmental, 2015.

132. T. Aguilar, J. Navas, R. Alcántara, C. Fernández-Lorenzo, J. Gallardo, G. Blanco, and J. Martín-Calleja, *A route for the synthesis of Cu-doped TiO 2 nanoparticles with a very low band gap.* Chemical Physics Letters, 2013. **571**: p. 49-53.

133. H.M. Yadav, S.V. Otari, V.B. Koli, S.S. Mali, C.K. Hong, S.H. Pawar, and S.D. Delekar, *Preparation and characterization of copper-doped anatase TiO 2 nanoparticles with visible light photocatalytic antibacterial activity.* Journal of Photochemistry and Photobiology A: Chemistry, 2014. **280**: p. 32-38.

134. X.-j. Yang, W. Shu, H.-m. Sun, X.-b. Wang, and J.-s. Lian, *Preparation and photocatalytic performance of Cu-doped TiO 2 nanoparticles.* Transactions of Nonferrous Metals Society of China, 2015. **25**(2): p. 504-509.

135. A. Hernández-Gordillo and V.R. González, *Silver nanoparticles loaded on Cu-doped TiO2 for the effective reduction of nitro-aromatic contaminants.* Chemical Engineering Journal, 2015. **261**: p. 53-59.

136. C. Liu, J. Wang, W. Chen, C. Dong, and C. Li, *The removal of DON derived from algae cells by Cu-doped TiO2 under sunlight irradiation.* Chemical Engineering Journal, 2015. **280**: p. 588-596.

137. Y. Hong-bin, W. Wen ke, J. Xiu-yan, and Y. Sheng-ke. *Preparation of doped nano-TiO2 by sol-gel method and the study on its photocatalytic performance*. in *Bioinformatics and Biomedical Engineering (iCBBE), 2010 4th International Conference on*. 2010.

138. W. Sangchay, W. Mudtharak, K. Mahamad, and A. Namesai, *The Physical properties and photocatalytic activity of Cu/TEA doped TiO2-nanoparticles prepared by the sol-gel process.* Journal of Chemistry and Chemical Engineering, 2012. **6**(8): p. 744.

139. T. Nguyen Thi Thu, N. Nguyen Thi, V. Tran Quang, K. Nguyen Hong, T. Nguyen Minh, and N. Le Thi Hoai, *Synthesis, characterisation, and effect of pH on degradation of dyes of copper-doped TiO2.* Journal of Experimental Nanoscience, 2015(ahead-of-print): p. 1-13.

140. T.-T. Pham, C. Nguyen-Huy, H.-J. Lee, T.-D. Nguyen-Phan, T.H. Son, C.-K. Kim, and E.W. Shin, *Cu-doped TiO2/reduced graphene oxide thin-film photocatalysts: Effect of Cu content upon methylene blue removal in water.* Ceramics International, 2015. **41**(9, Part A): p. 11184-11193.

141. L.-F. Chiang and R.-a. Doong, *Cu–TiO2 nanorods with enhanced ultraviolet- and visible-light photoactivity for bisphenol A degradation.* Journal of Hazardous Materials, 2014. **277**: p. 84-92.

142. Y. Wang, W. Duan, B. Liu, X. Chen, F. Yang, and J. Guo, *The effects of doping copper and mesoporous structure on photocatalytic properties of TiO 2.* Journal of Nanomaterials, 2014. **2014**.

143. B. Choudhury, M. Dey, and A. Choudhury, *Defect generation, dd transition, and band gap reduction in Cu-doped TiO2 nanoparticles.* International Nano Letters, 2013. **3**(1): p. 1-8.

144. Y. Liu, W. Liang, W. Zhang, J. Zhang, and P. Han, *First principle study of Cu □N, Cu and N-doped anatase TiO 2.* Solid State Communications, 2013. **164**: p. 27-31.

145. B. Choudhury, A. Choudhury, and D. Borah, *Interplay of dopants and defects in making Cu doped TiO 2 nanoparticle a ferromagnetic semiconductor.* Journal of Alloys and Compounds, 2015. **646**: p. 692-698.

146. W. Li, *Influence of electronic structures of doped TiO2 on their photocatalysis.* physica status solidi (RRL)-Rapid Research Letters, 2014. **9999**.

147. M. Zhang, Y. Dai, S. Zhang, and W. Chen, *Highly efficient photocatalytic activity of boron-doped TiO2 for gas phase degradation of benzene.* Rare Metals, 2011. **30**(1): p. 243-248.

148. A. Zaleska, E. Grabowska, J.W. Sobczak, M. Gazda, and J. Hupka, *Photocatalytic activity of boron-modified TiO 2 under visible light: the effect of boron content, calcination temperature and TiO 2 matrix.* Applied Catalysis B: Environmental, 2009. **89**(3): p. 469-475.

149. E.M. Neville, M.J. Mattle, D. Loughrey, B. Rajesh, M. Rahman, J.M.D. MacElroy, J.A. Sullivan, and K.R. Thampi, *Carbon-Doped TiO2 and carbon, tungsten-codoped TiO2 through sol–gel processes in the presence of melamine borate: Reflections through photocatalysis.* The Journal of Physical Chemistry C, 2012. **116**(31): p. 16511-16521.

150. X.-K. Wang, C. Wang, W.-Q. Jiang, W.-L. Guo, and J.-G. Wang, *Sonochemical synthesis and characterization of Cl-doped TiO2 and its application in the photodegradation of phthalate ester under visible light irradiation.* Chemical Engineering Journal, 2012. **189**: p. 288-294.

151. W.-a. Wang, Q. Shi, Y.-p. Wang, J.-l. Cao, G.-q. Liu, and P.-y. Peng, *Preparation and characterization of iodine-doped mesoporous TiO 2 by hydrothermal method.* Applied Surface Science, 2011. **257**(8): p. 3688-3696.

152. C.-Y. Kuo, C.-H. Wu, J.-T. Wu, and Y.-R. Chen, *Synthesis and characterization of a phosphorus-doped TiO2 immobilized bed for the photodegradation of bisphenol A under UV and sunlight irradiation.* Reaction Kinetics, Mechanisms and Catalysis, 2015. **114**(2): p. 753-766.

153. L. Zeng, W. Song, M. Li, X. Jie, D. Zeng, and C. Xie, *Comparative study on the visible light driven photocatalytic activity between substitutional nitrogen doped and interstitial nitrogen doped TiO 2.* Applied Catalysis A: General, 2014. **488**: p. 239-247.

154. X. Cheng, X. Yu, and Z. Xing, *Characterization and mechanism analysis of N doped TiO 2 with visible light response and its enhanced visible activity.* Applied Surface Science, 2012. **258**(7): p. 3244-3248.

155. D. Nassoko, Y.-F. Li, H. Wang, J.-L. Li, Y.-Z. Li, and Y. Yu, *Nitrogen-doped TiO 2 nanoparticles by using EDTA as nitrogen source and soft template: Simple preparation, mesoporous structure, and photocatalytic activity under visible light.* Journal of Alloys and Compounds, 2012. **540**: p. 228-235.

156. X. Li, P. Liu, Y. Mao, M. Xing, and J. Zhang, *Preparation of homogeneous nitrogen-doped mesoporous TiO 2 spheres with enhanced visible-light photocatalysis.* Applied Catalysis B: Environmental, 2015. **164**: p. 352-359.

157. X. Cheng, X. Yu, Z. Xing, and J. Wan, *Enhanced photocatalytic activity of nitrogen doped TiO2 anatase nano-particle under simulated sunlight irradiation.* Energy Procedia, 2012. **16**: p. 598-605.

158. Y. Cong, J. Zhang, F. Chen, and M. Anpo, *Synthesis and characterization of nitrogen-doped TiO2 nanophotocatalyst with high visible light activity.* The Journal of Physical Chemistry C, 2007. **111**(19): p. 6976-6982.

159. G. Yang, Z. Jiang, H. Shi, T. Xiao, and Z. Yan, *Preparation of highly visible-light active N-doped TiO 2 photocatalyst.* Journal of Materials Chemistry, 2010. **20**(25): p. 5301-5309.

160. L.G. Devi, B. Nagaraj, and K.E. Rajashekhar, *Synergistic effect of Ag deposition and nitrogen doping in TiO 2 for the degradation of phenol under solar irradiation in presence of electron acceptor.* Chemical Engineering Journal, 2012. **181**: p. 259-266.

161. L. Samiolo, M. Valigi, D. Gazzoli, and R. Amadelli, *Photo-electro catalytic oxidation of aromatic alcohols on visible light-absorbing nitrogen-doped TiO2.* Electrochimica Acta, 2010. **55**(26): p. 7788-7795.

162. X. Pan, J. Xie, Z. Li, M. Chen, M. Wang, P.-N. Wang, L. Chen, and L. Mi, *Enhancement of the photokilling effect of aluminum phthalocyanine in photodynamic therapy by conjugating with nitrogen-doped TiO 2 nanoparticles.* Colloids and Surfaces B: Biointerfaces, 2015. **130**: p. 292-298.

163. V.N. Kuznetsov and N. Serpone, *On the origin of the spectral bands in the visible absorption spectra of visible-light-active TiO2 specimens analysis and assignments.* The Journal of Physical Chemistry C, 2009. **113**(34): p. 15110-15123.

164. R. Asahi, T. Morikawa, T. Ohwaki, K. Aoki, and Y. Taga, *Visible-light photocatalysis in nitrogen-doped titanium oxides.* Science, 2001. **293**(5528): p. 269-271.

165. C. Di Valentin, G. Pacchioni, A. Selloni, S. Livraghi, and E. Giamello, *Characterization of paramagnetic species in N-doped TiO2 powders by epr spectroscopy and DFT calculations.* The Journal of Physical Chemistry B, 2005. **109**(23): p. 11414-11419.

166. L.G. Devi and R. Kavitha, *Enhanced photocatalytic activity of sulfur doped TiO 2 for the decomposition of phenol: A new insight into the bulk and surface modification.* Materials Chemistry and Physics, 2014. **143**(3): p. 1300-1308.

167. S.-H. Nam, T.K. Kim, and J.-H. Boo, *Physical property and photo-catalytic activity of sulfur doped TiO 2 catalysts responding to visible light.* Catalysis Today, 2012. **185**(1): p. 259-262.

168. N. Sharotri and D. Sud, *A greener approach to synthesize visible light responsive nanoporous S-doped TiO 2 with enhanced photocatalytic activity.* New Journal of Chemistry, 2015. **39**(3): p. 2217-2223.

169. P. Goswami and J.N. Ganguli, *A novel synthetic approach for the preparation of sulfated titania with enhanced photocatalytic activity.* RSC Advances, 2013. **3**(23): p. 8878-8888.

170. N. Li, X. Zhang, W. Zhou, Z. Liu, G. Xie, Y. Wang, and Y. Du, *High quality sulfur-doped titanium dioxide nanocatalysts with visible light photocatalytic activity from non-hydrolytic thermolysis synthesis.* Inorg. Chem. Front., 2014. **1**(7): p. 521-525.

171. M.V. Dozzi, S. Livraghi, E. Giamello, and E. Selli, *Photocatalytic activity of S-and F-doped TiO 2 in formic acid mineralization.* Photochemical & Photobiological Sciences, 2011. **10**(3): p. 343-349.

172. P. Ramacharyulu, J.P. Kumar, G. Prasad, and B. Sreedhar, *Sulphur doped nano TiO 2: Synthesis, characterization and photocatalytic degradation of a toxic chemical in presence of sunlight.* Materials Chemistry and Physics, 2014. **148**(3): p. 692-698.

173. K. Yang, Y. Dai, and B. Huang, *Understanding photocatalytic activity of S-and P-doped TiO2 under visible light from first-principles.* The Journal of Physical Chemistry C, 2007. **111**(51): p. 18985-18994.

174. T. Ohno, M. Akiyoshi, T. Umebayashi, K. Asai, T. Mitsui, and M. Matsumura, *Preparation of S-doped TiO2 photocatalysts and their photocatalytic activities under visible light.* Applied Catalysis A: General, 2004. **265**(1): p. 115-121.

175. T. Ohno, T. Mitsui, and M. Matsumura, *Photocatalytic activity of S-doped TiO2 photocatalyst under visible light.* Chemistry Letters, 2003. **32**(4): p. 364-365.

176. T. Ohno, M. Akiyoshi, T. Umebayashi, K. Asai, T. Mitsui, and M. Matsumura, *Preparation of S-doped TiO 2 photocatalysts and their photocatalytic activities under visible light.* Applied Catalysis A: General, 2004. **265**(1): p. 115-121.

177. E.M. Rockafellow, L.K. Stewart, and W.S. Jenks, *Is sulfur-doped TiO 2 an effective visible light photocatalyst for remediation?* Applied Catalysis B: Environmental, 2009. **91**(1): p. 554-562.

178. S. Sauvé and M. Desrosiers, *A review of what is an emerging contaminant.* Chemistry Central Journal, 2014. **8**(1): p. 1-7.

179. N. Bolong, A.F. Ismail, M.R. Salim, and T. Matsuura, *A review of the effects of emerging contaminants in wastewater and options for their removal.* Desalination, 2009. **239**(1–3): p. 229-246.

180. B. Petrie, R. Barden, and B. Kasprzyk-Hordern, *A review on emerging contaminants in wastewaters and the environment: Current knowledge, understudied areas and recommendations for future monitoring.* Water research, 2015. **72**: p. 3-27.

181. D.W. Kolpin, E.T. Furlong, M.T. Meyer, E.M. Thurman, S.D. Zaugg, L.B. Barber, and H.T. Buxton, *Pharmaceuticals, hormones, and other organic wastewater contaminants in US streams, 1999-2000: A national reconnaissance.* Environmental science & technology, 2002. **36**(6): p. 1202-1211.

182. T. Heberer, A. Mechlinski, B. Fanck, A. Knappe, G. Massmann, A. Pekdeger, and B. Fritz, *Field studies on the fate and transport of pharmaceutical residues in bank filtration.* Groundwater Monitoring & Remediation, 2004. **24**(2): p. 70-77.

183. C.H. Swartz, S. Reddy, M.J. Benotti, H. Yin, L.B. Barber, B.J. Brownawell, and R.A. Rudel, *Steroid estrogens, nonylphenol ethoxylate metabolites, and other wastewater contaminants in groundwater affected by a residential septic system on Cape Cod, MA.* Environmental science & technology, 2006. **40**(16): p. 4894-4902.

184. K. Kümmerer, *Drugs in the environment: emission of drugs, diagnostic aids and disinfectants into wastewater by hospitals in relation to other sources–a review.* Chemosphere, 2001. **45**(6): p. 957-969.

185. R. Hirsch, T.A. Ternes, K. Haberer, A. Mehlich, F. Ballwanz, and K.-L. Kratz, *Determination of antibiotics in different water compartments via liquid chromatography–electrospray tandem mass spectrometry.* Journal of Chromatography A, 1998. **815**(2): p. 213-223.

186. T. Heberer, *Tracking persistent pharmaceutical residues from municipal sewage to drinking water.* Journal of Hydrology, 2002. **266**(3–4): p. 175-189.

187. E. Godfrey, W.W. Woessner, and M.J. Benotti, *Pharmaceuticals in on-site sewage effluent and ground water, Western Montana.* Groundwater, 2007. **45**(3): p. 263-271.

188. D.W. Kolpin, E.T. Furlong, M.T. Meyer, E.M. Thurman, S.D. Zaugg, L.B. Barber, and H.T. Buxton, *Pharmaceuticals, hormones, and other organic wastewater contaminants in U.S. streams, 1999−2000: A National Reconnaissance.* Environmental Science & Technology, 2002. **36**(6): p. 1202-1211.

189. S. Matongo, G. Birungi, B. Moodley, and P. Ndungu, *Occurrence of selected pharmaceuticals in water and sediment of Umgeni River, KwaZulu-Natal, South Africa.* Environmental Science and Pollution Research, 2015: p. 1-11.

190. S. Matongo, G. Birungi, B. Moodley, and P. Ndungu, *Pharmaceutical residues in water and sediment of Msunduzi River, KwaZulu-Natal, South Africa.* Chemosphere, 2015. **134**: p. 133-140.

191. C.-m. Dai, X.-f. Zhou, Y.-l. Zhang, Y.-p. Duan, Z.-m. Qiang, and T.C. Zhang, *Comparative study of the degradation of carbamazepine in water by advanced oxidation processes.* Environmental Technology, 2011. **33**(10): p. 1101-1109.

192. I.J. Buerge, T. Poiger, M.D. Müller, and H.-R. Buser, *Caffeine, an anthropogenic marker for wastewater contamination of surface waters.* Environmental Science & Technology, 2003. **37**(4): p. 691-700.

193. J.L. Santos, I. Aparicio, and E. Alonso, *Occurrence and risk assessment of pharmaceutically active compounds in wastewater treatment plants. A case study: Seville city (Spain).* Environment International, 2007. **33**(4): p. 596-601.

194. C. Potera, *Caffeine in wastewater is a tracer for human fecal contamination.* Environmental Health Perspectives, 2012. **120**(3): p. a108-a109.

195. P.R. Gardinali and X. Zhao, *Trace determination of caffeine in surface water samples by liquid chromatography–atmospheric pressure chemical ionization–mass spectrometry (LC–APCI–MS).* Environment International, 2002. **28**(6): p. 521-528.

196. M. Moore, S. Greenway, J. Farris, and B. Guerra, *Assessing caffeine as an emerging environmental concern using conventional approaches.* Archives of environmental contamination and toxicology, 2008. **54**(1): p. 31-35.

197. F.O. Agunbiade and B. Moodley, *Pharmaceuticals as emerging organic contaminants in Umgeni River water system, KwaZulu-Natal, South Africa.* Environmental monitoring and assessment, 2014. **186**(11): p. 7273-7291.

198. R.R. Marques, M.J. Sampaio, P.M. Carrapiço, C.G. Silva, S. Morales-Torres, G. Dražić, J.L. Faria, and A.M. Silva, *Photocatalytic degradation of caffeine: Developing solutions for emerging pollutants.* Catalysis today, 2013. **209**: p. 108-115.

199. S. Antoni, I. Soerjomataram, S. Moore, J. Ferlay, F. Sitas, D.P. Smith, and D. Forman, *The ban on phenacetin is associated with changes in the incidence trends of upper-urinary tract cancers in Australia.* Australian and New Zealand Journal of Public Health, 2014. **38**(5): p. 455-458.

200. J.K. McLaughlin, L. Lipworth, W.-H. Chow, and W.J. Blot, *Analgesic use and chronic renal failure: A critical review of the epidemiologic literature.* Kidney Int, 1998. **54**(3): p. 679-686.

201. M. Kotti, E. Piliouris, and A. Vlessidis, *A new method for comparing hospital and municipal wastewater.* Journal of Environmental Science and Engineering. A, 2013. **2**(3A): p. 141.

202. F.J. Benitez, J.L. Acero, F.J. Real, and G. Roldán, *Ozonation of pharmaceutical compounds: rate constants and elimination in various water matrices.* Chemosphere, 2009. **77**(1): p. 53-59.

203. R. Giri, H. Ozaki, S. Ota, R. Takanami, and S. Taniguchi, *Degradation of common pharmaceuticals and personal care products in mixed solutions by advanced oxidation techniques.* International Journal of Environmental Science & Technology, 2010. **7**(2): p. 251-260.

204. C. Bosetti, V. Rosato, S. Gallus, J. Cuzick, and C. La Vecchia, *Aspirin and cancer risk: a quantitative review to 2011.* Annals of Oncology, 2012. **23**(6): p. 1403-1415.

205. D.L. Seger and L. Murray, *Aspirin and nonsteroidal agents.* system (CNS), 2013. **4**: p. 5.

206. N. Nakada, T. Tanishima, H. Shinohara, K. Kiri, and H. Takada, *Pharmaceutical chemicals and endocrine disrupters in municipal wastewater in Tokyo and their removal during activated sludge treatment.* Water Research, 2006. **40**(17): p. 3297-3303.

207. S.K. Bae, K.A. Seo, E.J. Jung, H.-S. Kim, C.-W. Yeo, J.-H. Shon, K.-M. Park, K.-H. Liu, and J.-G. Shin, *Determination of acetylsalicylic acid and its major metabolite, salicylic acid, in human plasma using liquid chromatography–tandem mass spectrometry: application to pharmacokinetic study of Astrix® in Korean healthy volunteers.* Biomedical Chromatography, 2008. **22**(6): p. 590-595.

208. A.L. Spongberg and J.D. Witter, *Pharmaceutical compounds in the wastewater process stream in Northwest Ohio.* Science of the total environment, 2008. **397**(1): p. 148-157.

209. L. Lishman, S.A. Smyth, K. Sarafin, S. Kleywegt, J. Toito, T. Peart, B. Lee, M. Servos, M. Beland, and P. Seto, *Occurrence and reductions of pharmaceuticals and personal care products and estrogens by municipal wastewater treatment plants in Ontario, Canada.* Science of the Total Environment, 2006. **367**(2): p. 544-558.

210. H.-B. Lee, T.E. Peart, and M.L. Svoboda, *Determination of endocrine-disrupting phenols, acidic pharmaceuticals, and personal-care products in sewage by solid-phase extraction and gas chromatography–mass spectrometry.* Journal of Chromatography A, 2005. **1094**(1): p. 122-129.

211. O. Lekakh, A.M. Mahoney, K. Novice, J. Kamalpour, A. Sadeghian, D. Mondo, C. Kalnicky, R. Guo, A. Peterson, and R. Tung, *Treatment of Acne Vulgaris With Salicylic Acid Chemical Peel and Pulsed Dye Laser: A Split Face, Rater-Blinded, Randomized Controlled Trial.* Journal of lasers in medical sciences, 2015. **6**(4): p. 167-70.

212. S. Vilhunen, M. Bosund, M.-L. Kääriäinen, D. Cameron, and M. Sillanpää, *Atomic layer deposited TiO 2 films in photodegradation of aqueous salicylic acid.* Separation and Purification Technology, 2009. **66**(1): p. 130-134.

213. J. Martins de Souza e Silva, M. Pastorello, M. Strauss, C.M. Maroneze, F.A. Sigoli, Y. Gushikem, and I.O. Mazali, *Size controlled synthesis of highly dispersed anatase/rutile nanoparticles with photocatalytic activity toward salicylic acid degradation.* RSC Advances, 2012. **2**(12): p. 5390-5397.

Chapter 3 Materials and Methods

This chapter describes the methods used to prepare and characterize the undoped and doped titania powders and the methods used to test the materials as photocatalysts. This chapter also describes the reaction methods as well as the analysis method for all the procedures adapted and developed throughout the dissertation.

3.1 Chemicals

Table 3.1 lists all of the chemicals and reagents that were used for this project as well as the reagent grade and the supplier of each given reagent. All the chemicals were used without any further purification

Table 3.1: List of reagents used.

Chemical	Supplier	Grade/Purity
Methanol	Parlabo laboratories	>99%
Acetic acid glacial	Rochelle Chemicals	99.5%
Sulfuric acid	Promark chemicals	98%
Orthophosphoric acid	Promark Chemicals	85%
Titanium tetraisopropoxide	Alfsa Aesar	>97%
Copper nitrate	Sigma-Aldrich	99%
Urea	Sigma-Aldrich	99%
Thiourea	Sigma-Aldrich	99%
2-propanol	Promark Chemicals	99%
Ti 1000 ppm ICP standard	Industrial Analytical	AR
Phenacetin	BDH laboratory reagents	98%
Caffeine	Sigma-Aldrich	>99%
Aspirin	Merck	>99%
Salicylic acid	Sigma-Aldrich	99%

3.2 Synthesis

This section describes the synthesis method used for the preparation of the undoped and doped catalyst by one of copper, nitrogen or sulfur.

3.2.1 Synthesis of Copper Doped Titanium Dioxide Nanomaterials

The synthesis procedure for copper doped catalysts was adapted from Baltazar *et al* [1]. Reagents were used in a molar ratio of 1: 2: 2: 4 of titanium tetraisopropoxide, acetic acid, water and 2-propanol respectively. The dopant, copper nitrate, was dissolved in water and the amount of copper nitrate used was in the range of 0-5 mol% with respect to the titanium tetraisopropoxide precursor. The masses of the dopant precursor used for each sample prepared are given in **Table 3.2** below. All chemicals used during synthesis were weighed out on an analytical balance.

Table 3.2: Masses of copper nitrate hexahydrate used for copper doped catalysts.

Catalyst/ mol%	Mass of copper nitrate used/ g	Mass of water/ g	Mass of acetic acid/ g
Undoped TiO_2	0	0.6305	2.1015
2% Cu-TiO_2	0.1034	0.6305	2.1015
3% Cu-TiO_2	0.1552	0.6305	2.1015
4% Cu-TiO_2	0.2070	0.6305	2.1015
5% Cu-TiO_2	0.2587	0.6305	2.1015

In a typical experiment, a beaker was placed in an ice bath and to this beaker 2.1015 g of acetic acid was added, followed by 5.0000 g of titanium isopropoxide and then 4.2288 g of 2-propanol. Additions were done with stirring on a magnetic stirrer unit with a magnetic stirrer bar. In a separate beaker an appropriate amount of copper nitrate hexahydrate (see **Table 3.2**) was dissolved in 0.6305 g of water, and then this mixture was added drop wise with stirring to the titanium isopropoxide mixture. Each mixture was stirred for 2 hours so that

gelation took place, the time taken for gelation to occur varied on the amount of dopant used. The gels were aged for 120 hours under reduced pressure; this was done in the fumehood with the extractor fan on. The gels were then placed in the oven (Labcon 1028K Ecoflomu, Labdesign Engineering) at 80 °C for 72 hours. Finally the obtained powders were calcined using a heating rate of 2 °C to a finally temperature of 400 °C, and held at 400 °C 4 hours. The furnace used for the calcinations was a Kittec Squadro SQ50 (**Figure 3.1**). Before calcination all catalysts were white in colour all catalysts containing after calcination all catalysts containing dopant changed colour to green.

Figure 3.1: Kittec Squadro muffle furnace.

3.2.2 Doping of Titanium Dioxide with Either (Nitrogen or Sulfur)

This procedure was adapted from the methods reported by Ananpattarachai *et al* [2]. Depending on the dopant desired either urea (nitrogen doped) or thiourea (sulfur doped) was used. The materials were prepared using a molar ratio of 1:16:0.5:58:2 for titanium tetraisopropoxide: water: acetic acid: ethanol: dopant. The amount of dopant precursor used was dependent on the final level of doping desired while all other reagent masses remained the same. Each of the reagents was weighted out using an analytical balance. To synthesis TiO_2:N 1-2, 2.1142 g of urea was dissolved in 3.168 g of water thereafter 32.4219 g of ethanol and 0.5284 g of acetic acid was added, this was stirred for 20 min. To this solution 5.0000g of titanium tetraisopropoxide was added drop wise, this mixture was then stirred for 2 hours at room temperature.

The resulting mixture was aged at room temperature under reduced pressure for 48h; this was done in the fumehood with the extractor fan switched on. The materials were then dried in the oven, Labcon 1028K Ecoflomu, Labdesign Engineering, for 1 hour at 100 °C. Thereafter the materials were calcined in a muffle furnace, with a ramp rate 2 °C min, to a final temperature of 400 °C and held at that temperature for 4 hours. The same procedure was carried out to prepare an undoped sample of TiO_2 except that no dopant precursor was used. All catalysts containing the nitrogen dopant changed from white to yellow upon calcination.

A similar procedure was used to synthesize the sulfur doped materials. **Table 3.3** lists the masses used for each of the sulfur doped samples. All catalysts containing the sulfur dopant changed from white to yellow upon calcination.

Table 3.3: Masses of urea and thiourea used to achieve desired doping ratios.

Name of catalyst	Dopant used	Mass of dopant used/ g	Mass of water/ g	Mass of acetic acid/ g
Undoped catalyst	N/A	N/A	3.168	0.5284
TiO_2:N 1:2	Urea	2.1142	3.168	0.5284
TiO_2:N 1:3	Urea	3.1713	3.168	0.5284
TiO_2:N 1:4	Urea	4.2284	3.168	0.5284
TiO_2:S 1:2	Thiourea	2.6184	3.168	0.5284
TiO_2:S 1:3	Thiourea	3.9276	3.168	0.5284
TiO_2:S 1:4	Thiourea	5.2368	3.168	0.5284

3.3 Characterization Techniques

3.3.1 Nitrogen Physisorption

Nitrogen physisorption measurements were done using a Tri-star 3030, manufactured by Micrometrics, USA and purchased from Poretech, South Africa. Sample preparation was done on a VacPrep 061 system manufactured by Micrometrics, USA and purchased from Poretech, South Africa. Measurements were done at -196 °C, this was done using liquid nitrogen. Pictures of the instruments can be seen in **Figure 3.2**.

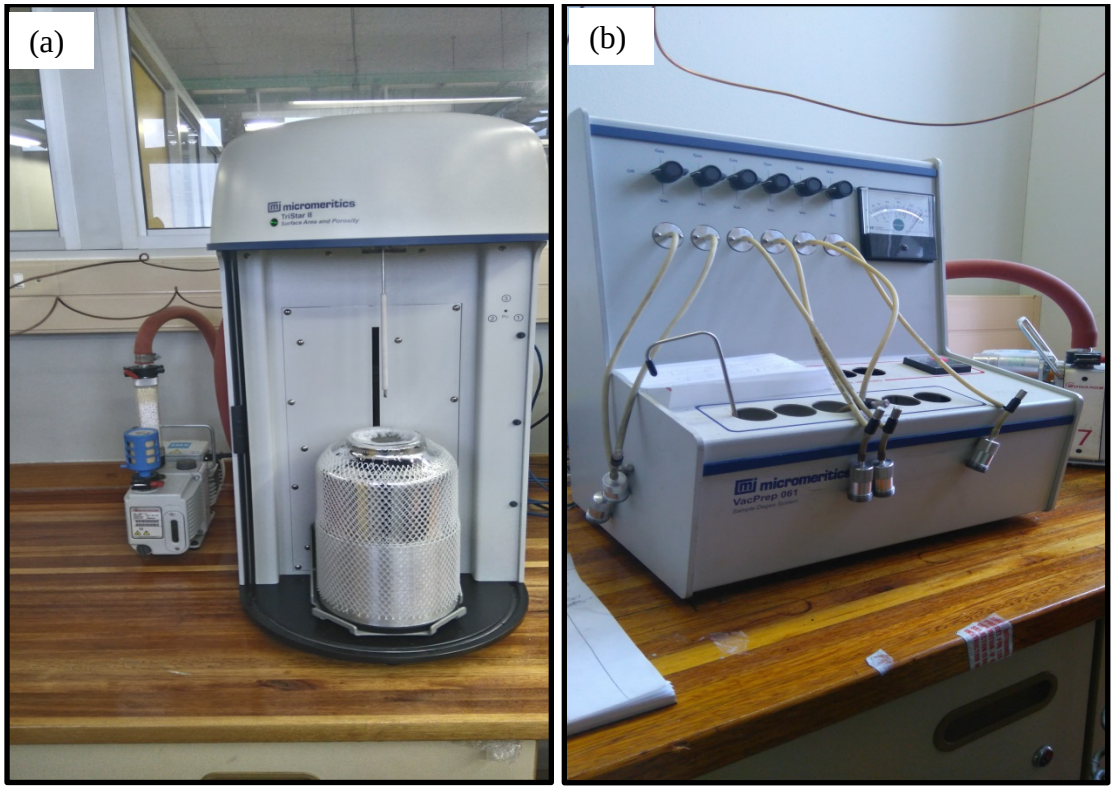

Figure 3.2: Tri-star 3030 instrument used for BET measurements (a) and VacPrep 061 unit (b).

Initially, samples were weighed in the glass sample tubes that are specific to the instrument. Samples were then prepared for analysis by heating all materials under vacuum for 1 hour at 90 °C, and then at 150 °C for 1 hour and then finally overnight at 200 °C under nitrogen flow. Before analysis the temperature was reduced to 90 °C. The samples where then reweighed and fitted onto the instrument.

Based on the isotherms obtained and use of the Brunauer, Emmett and Teller (BET) equation, the surface area, pore volume and pore diameter values of the catalysts were calculated. Pore size distribution was done using the absorption branch of the isotherm based on Barrett-Joyner-Halenda (BJH) method.

3.3.2 Ultraviolet-Visible Diffuse Reflectance Spectroscopy (UV-DRS)

Ultraviolet-Visible diffuse reflectance spectroscopy (UV-DRS) measurements on the catalysts were carried using an Ocean Optics spectrometer, the light source used was a tungsten halogen lamp. Measurements were done using the T300-RT-UV-Vis optical fibre probe, which has a diameter of 300 μm and a length of 2 m. The measurements were done in absorbance mode, the absorbance measurements were then converted to a Tauc plot using **Equation 3.1**. The spectra are the averages of 50 replicates; the boxcar width was set to 10 for all catalysts. Barium sulphate was used as the reference material.

To determine the band gaps of the materials the Tauc plot model was used, this is given by **Equation 3.1**.

$(\alpha h\nu)^2$ **vs** $h\nu$ **Equation 3. 1**: Tuac plot.

Where α is absorbance and $h\nu$ is equal to $\frac{1240}{\lambda}$.

3.3.3 Photoluminescence (PL)

Photoluminescence spectra were obtained from a Perkin Elmer, LS55 Fluorescence Spectrometer (**Figure 3.3**), using LS55 solid probe accessory. The instrument was controlled using the FL WinLab version 4.00.03 Perkin Elmer Inc., and graph server version 1.60 software. The instrument was operated in emission mode. The excitation wavelength was set to 310 nm with an excitation slit width of 5.0 nm and an emission slit width of 0.0 nm at a scan speed of 100 nm min^{-1}, with 10 scans to average.

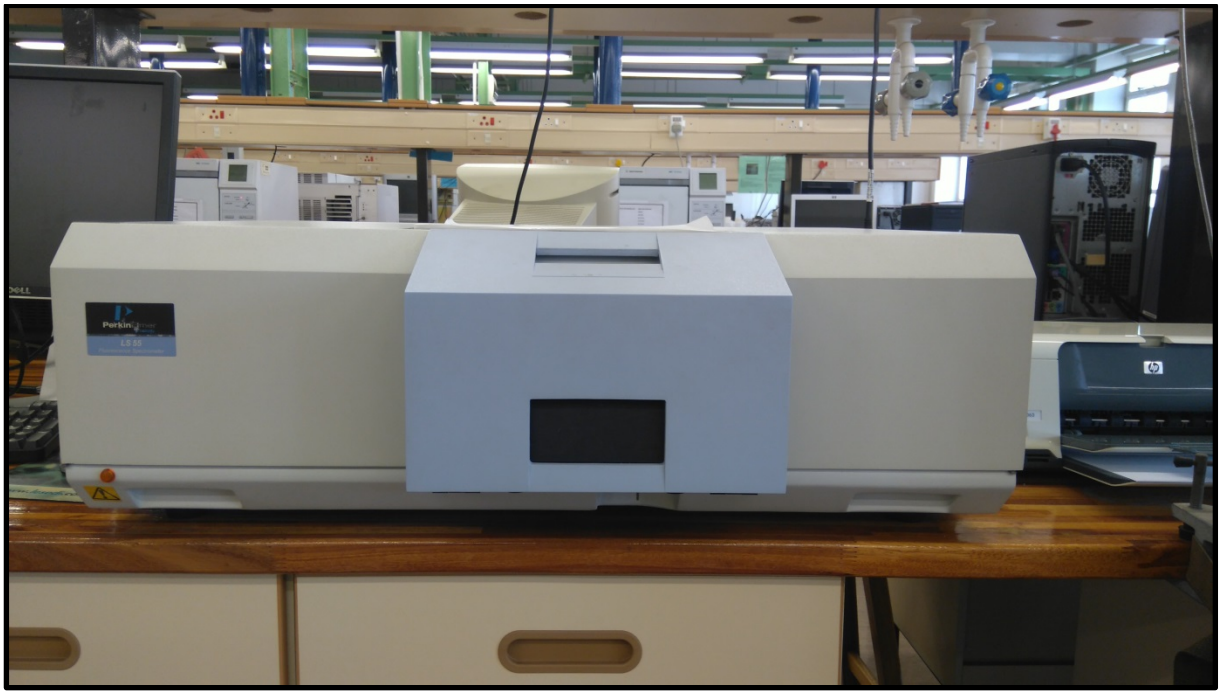

Figure 3.3: Perkin Elmer, LS55 Fluorescence Spectrometer.

3.3.4 Powder X-Ray Diffraction (XRD)

XRD diffractogram patterns were obtained using a Bruker D8 Advance XRD diffractometer employing Cu K_α radiation (λ = 1.5406 Å). The diffractometer operated at 40 kV and 40 mA for the X-ray tube voltage and current respectively. The analysis angles were between 15-90 degrees with a scan rate of 0.5 °.min^{-1} and with divergence slit and scatter widths of 1°. Crystallite size values were calculated for the full width at half maximum (FWHM) values of the 101 diffraction peak using the Debye-Scherrer (**Equation 3.2**).

$$L = \frac{0.9\lambda}{\beta cos\theta}$$

Equation 3. 2: Debye-Scherrer equation.

The interplanar spacing values were calculated using the 101 diffraction peak and the Bragg's law equation given by **Equation 3.3**.

$$d = \frac{n\lambda}{2Sin\theta}$$ **Equation 3. 3**: Bragg's Law.

The unit cell measurements and cells volumes were calculated from **Equation 3.4** and **Equation 3.5** respectively.

$$\frac{1}{d^2} = \frac{h^2+k^2}{a^2} + \frac{l^2}{c^2}$$ **Equation 3. 4**: Lattice parameters for a tetragonal system.

$$V = a^2c$$ **Equation 3. 5**: Cell volume for a tetragonal system.

Samples were sent for analysis to iThemba LABS, Cape Town.

3.3.5 Raman

Raman spectra were acquired using a DeltaNu, Advantage 532 instrument (**Figure 3.4**), the wavelength of the laser was 532 nm, and the instrument was controlled using the Nuspec software. The materials were loaded into clean quartz tubes and then were placed in the appropriate sample holder. Analysis parameters were varied based on the number of scans and time per scan so as to obtain clear and well defined peaks. Parameters where maintained for a particular set of catalysts.

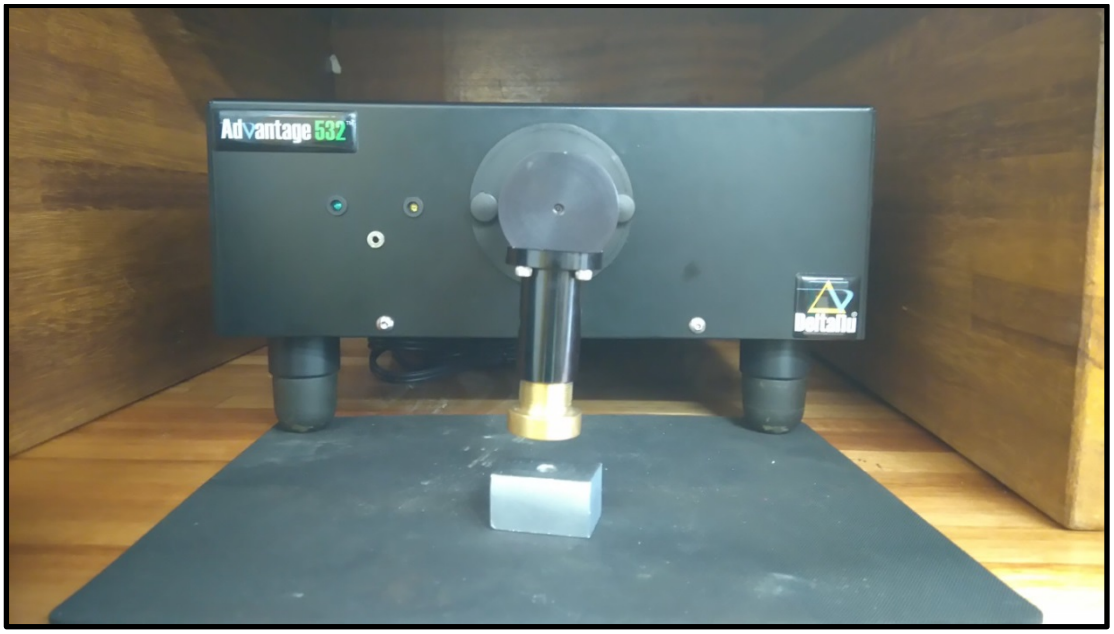

Figure 3.4: DeltaNu Advantage 532 Raman Spectrometer.

3.3.6 Inductively Coupled Plasma Optical Emission Spectroscopy (ICP-OES)

ICP-OES was done using a Perkin Elemer Optical Emission Spectrometer Optima 2100 DV (**Figure 3.5**), which is a sequential scanning instrument. This was used to determine the amount of titanium present in the catalysts as well as the amount of dopant present in the catalysts. Into a 100 mL beaker 20 mg of sample was added to this 20 mL of concentrated acid was added. The beaker was then placed on a heater/stirrer unit in fumehood, with the temperature at 120 °C and 200 rpm, a watch glass was placed over the beaker. The beaker was left on the heater/stirrer unit until the sample was completely digested. The copper doped and nitrogen doped catalysts were digested in hot concentrated sulfuric acid (H_2SO_4). The sulfur doped catalysts were digested in concentrated phosphoric acid (H_3PO_4). The samples regardless of the acid being used were quantitatively transferred from the beaker to a 100 mL

volumetric flask and made up to the mark with double distilled water. The sample were filtered through a 0.45 micron cartridge before analysis.

Figure 3.5: Picture of Optima 2100 DV Perkin Elemer Optical Emission Spectrometer.

3.3.7 Scanning Electron Microscopy (SEM)

SEM imaging was done with a Zeiss Ultra Plus Field Emission Gun SEM (**Figure 3.6**) using a secondary electron detector, the Smart SEM software controlled the instrument and was used to capture images. Sample preparation was done by depositing the materials onto double-sided carbon tape which was placed on an aluminium stub. All materials were coated with gold prior to analysis using Quorum Q150 ε vacuum evaporator to disperse the gold carbon dioxide was used by the instrument. Electron Dispersive X-ray (EDX) analysis was done by Joel JSM-6100.

Figure 3.6: Picture of Zeiss Ultra Plus Field Emission Gun SEM.

3.3.8 Transmission Electron Microscopy (TEM)

TEM imaging was done on Jeol JEM-1010 (**Figure 3.7**) electron microscope, with an accelerating voltage of 100 kV. The software used to control the instrument and take images was iTEM. Sample preparation was done by sonicating the materials in absolute ethanol for 5 min. Formvar coated copper grids were then dipped into the solution containing the sample, this grid was then removed from the solution and allowed to dry before being placed in the instrument.

Figure 3.7: Jeol JEM-1010 TEM.

3.4 Photocatalytic experiments

Stock solutions, 1000 ppm, of aspirin, caffeine and salicylic acid where prepared by dissolving 100 mg of their respective salts in deionised water and then making the solution up to 100 mL in a volumetric flask. The same procedure was followed for phenacetin except that a stock solution of 500 ppm was made by dissolving 50 mg of its salt.

A combined 5 ppm working solution of the above drugs was made in a 1 L beaker by pipetting 5 mL of each 1000ppm solution and 10 mL of phenacetin.

In a typical photocatalytic experiment 100 mL of the 5 ppm working solution was dispensed into a 250 mL beaker. To this solution 50 mg of a given catalyst was added. After the addition of the catalyst the beaker was covered with foil and the mixture was sonicated for 10

min in an ultra-sonication bath. Sonication was carried out using a MRC ultrasonication cleaner model D150H. Thereafter the mixture was stirred in the dark for 30 min on a stirrer/heater unit. The foil was then removed and the lamp switched on. The lamp employed for this was an Applo 32 W day light lamp with a voltage rating of 220-240 V and a colour temperature of 64000 K. The solution was stirred for 120 min with sampling every 20 min. Approximately 1 mL was taken as a sampling aliquot; the catalyst was separated from the solution by passing the mixture through a 0.45 μm PVDF filter and transferred to an HPLC auto-sampler vial. The reaction was monitored by HPLC the procedure for which is given below.

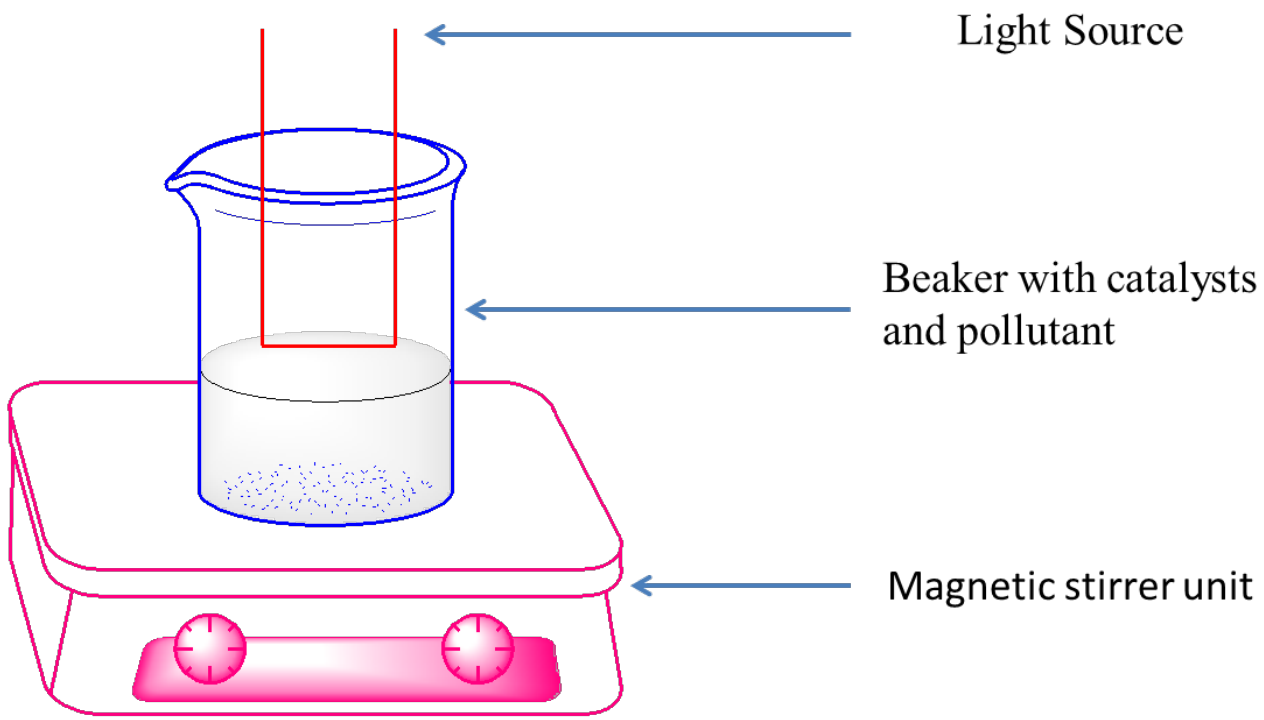

Figure 3.8: Picture of photocatalytic reaction setup.

3.4.1 High Performance Liquid Chromatography

HPLC analysis was done on an Agilent Technologies 1100 series liquid chromatography instrument (**Figure 3.9**). The column employed was a Gemini C18 column from Phenomnex, 15 mm x 2 mm, particle size of 3 µm and pore size of 110 Å. The wavelength used for this analysis was 210 nm. The mobile phase used was 40:60 (V/V) methanol and water acidified with orthtophosphoric acid to a pH 2.30-2.50. The flow rate was 0.180 mL min. The injection volume was 10 µL.

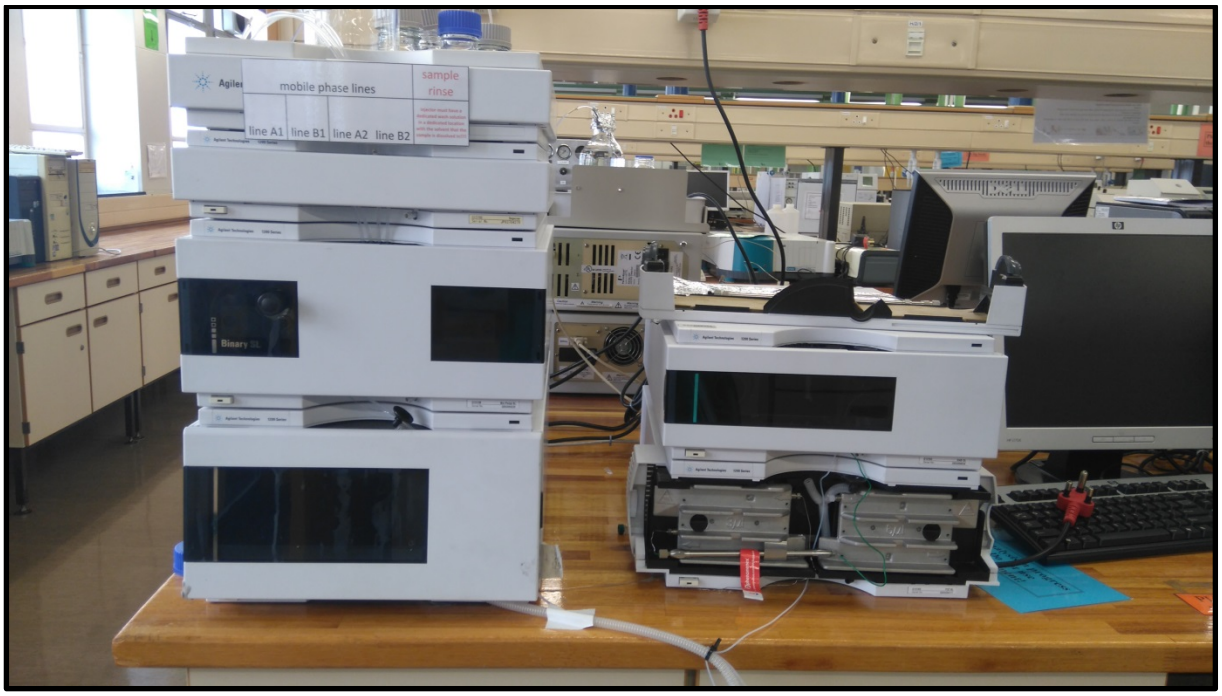

Figure 3.9: HPLC used for analysis.

References

1. Baltazar, P., V. Lara, G. Cordoba, and R. Arroyo, *Kinetics of the amorphous—anatase phase transformation in copper doped titanium oxide.* Journal of sol-gel science and technology, 2006. **37**(2): p. 129-133.
2. Ananpattarachai, J., P. Kajitvichyanukul, and S. Seraphin, *Visible light absorption ability and photocatalytic oxidation activity of various interstitial N-doped TiO2 prepared from different nitrogen dopants.* Journal of Hazardous Materials, 2009. **168**: p. 253-261.

Chapter 4 Characterization Results and Discussion

In this chapter the characterization results of all catalysts are discussed. The catalysts were prepared by sol-gel methods as described in chapter 3. The results for all the catalyst are discussed separately from each other. The techniques presented in this section are nitrogen physisorption, UV-DRS, photoluminescence (PL), XRD, Raman, ICP, TEM and SEM-EDX.

4.1 Copper Doping

Copper doping has been shown to narrow the band gap and increase the hydrophilicity of TiO_2 and therefore increase the photocatalytic activity of TiO_2 [1]. Copper doping can also reduce the rate of electron-hole pair recombination in TiO_2 however at high doping levels copper can promote electron hole recombination [2].

4.1.1 Quantification of Copper Doping Level

The level of copper doping in the titania materials was quantified using inductively coupled plasma optical emission spectroscopy (ICP-OES). **Table 4.1** gives the amount of copper present in the undoped TiO_2 catalyst and the copper doped catalysts as a function of mole percentage, these results were calculated from ICP-OES data. The results for all the copper doped catalysts show that the level of doping for all catalysts is lower than what was originally intended.

Table 4.1: Amount of copper present in catalysts in terms of mol percentage as determined by ICP-OES.

Catalyst	Doping level (mol %)
Undoped	0
2% Cu TiO_2	0.91
3% Cu TiO_2	2.03
4% Cu TiO_2	2.90
5% Cu TiO_2	3.69

The difference between the theoretical doping and the actual doping is about 1% for each sample synthesized. The 3 mol % Cu-TiO_2 catalyst is closest to the intended doping level having 2.03 mol% copper, which is less than the theoretical doping by just under 1%. The 5% Cu-TiO_2 catalyst has the largest difference between the intended and actual amount, with a difference of 1.31%.

4.1.2 Scanning Electron Microscopy Analysis of Copper Doped Samples

Figure 4.1 (a-e) shows the SEM images of the undoped TiO_2 catalyst as well as the copper doped catalysts. It can be seen from these images that all of the catalysts have irregularly shaped particles. On the surface of these irregularly shaped particles shown in **Figure 4.1** (a-e) there are smaller particles.

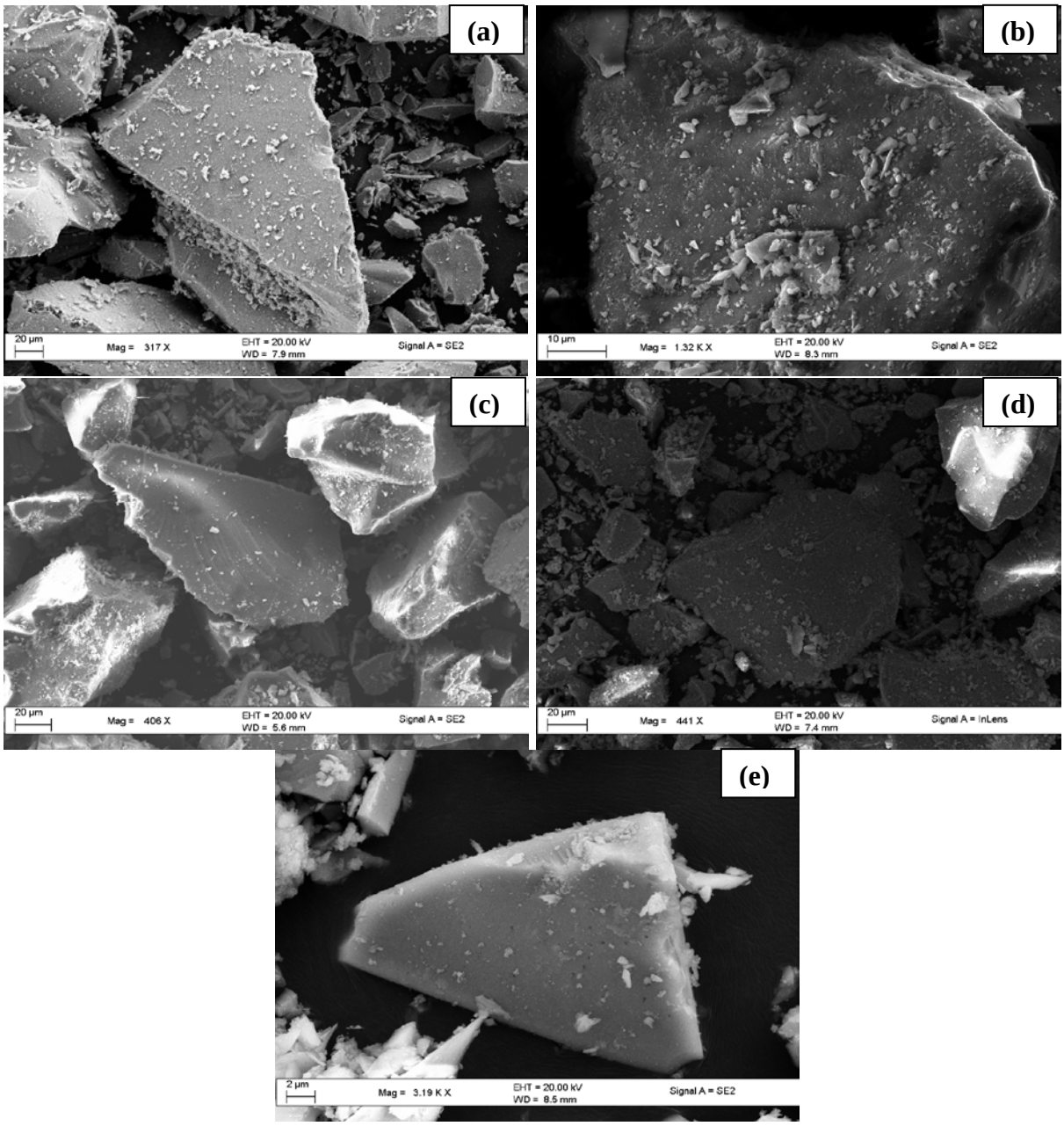

Figure 4.1: SEM images of undoped TiO_2 (a), 2% Cu TiO_2 (b), 3% Cu TiO_2 (c), 4% Cu TiO_2 (d) and 5% Cu TiO_2 (e).

Figure 4.2 (a-e) show higher magnification SEM images of those shown in **Figure 4.1** (a-e) of the undoped catalyst and the copper doped catalysts. These images show the small particles on the surface of the large irregularly shaped particles shown in **Figure 4.1** (a-e); these smaller particles are made up of yet smaller particles. The surfaces of the large

particles shown in **Figure 4.1** (a-e) are also seen in the respective images in **Figure 4.2** (a-e) and it can be seen that this particle is an agglomeration of small particles.

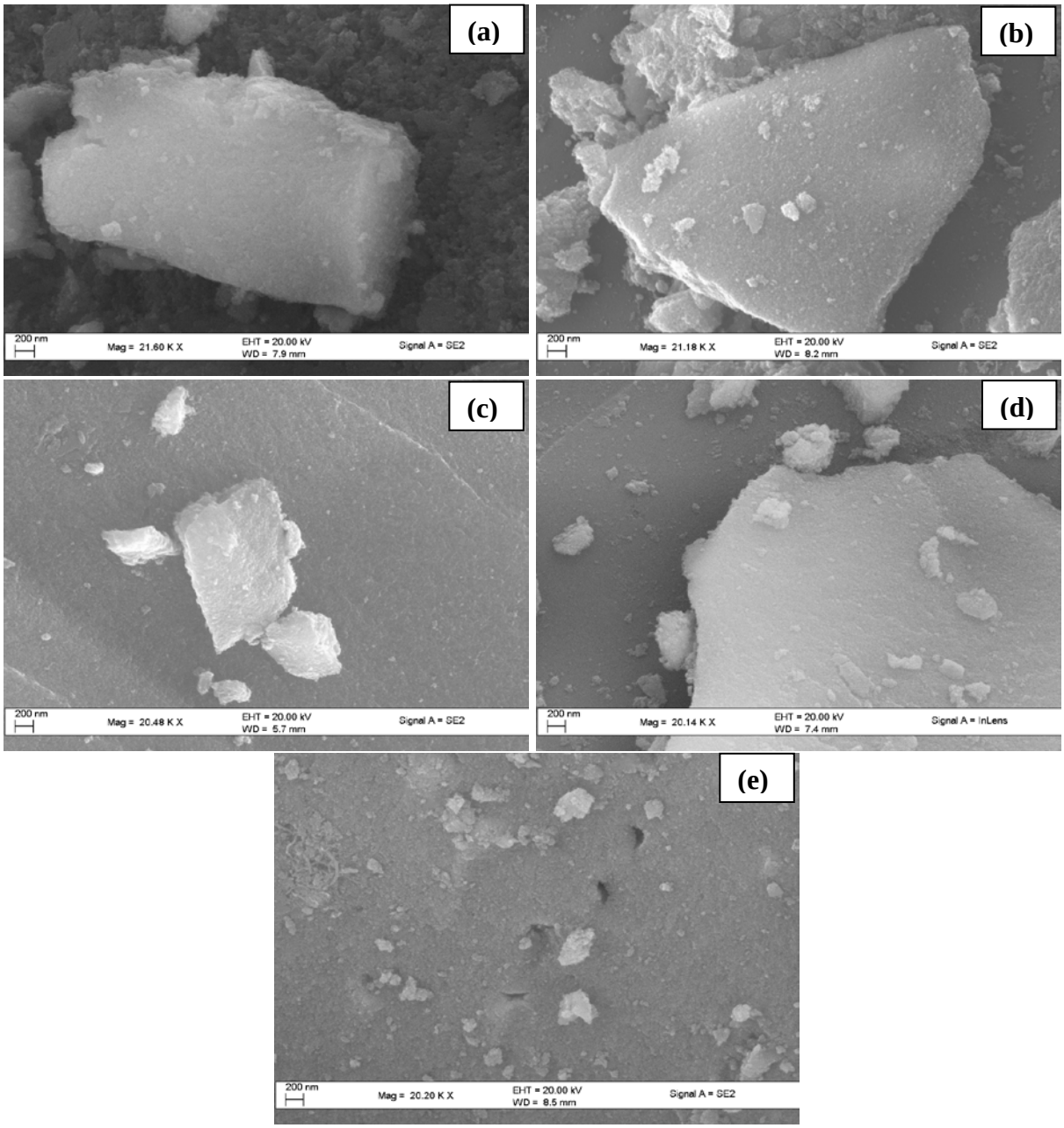

Figure 4.2: Higher magnification images of the particles shown above of undoped TiO_2 (a), 2% Cu TiO_2 (b), 3% Cu TiO_2 (c), 4% Cu TiO_2 (d) and 5% Cu TiO_2 (e).

In **Figure 4.3** (a) showing the undoped TiO_2 catalyst only titanium and oxygen was detected by EDX mapping, this was expected as the material is not modified by copper. In **Figure 4.3**

(b-d) the EDX mapping for the copper doped catalysts are shown, it appears in these images that the copper is well dispersed on the TiO_2 surface and does not agglomerate.

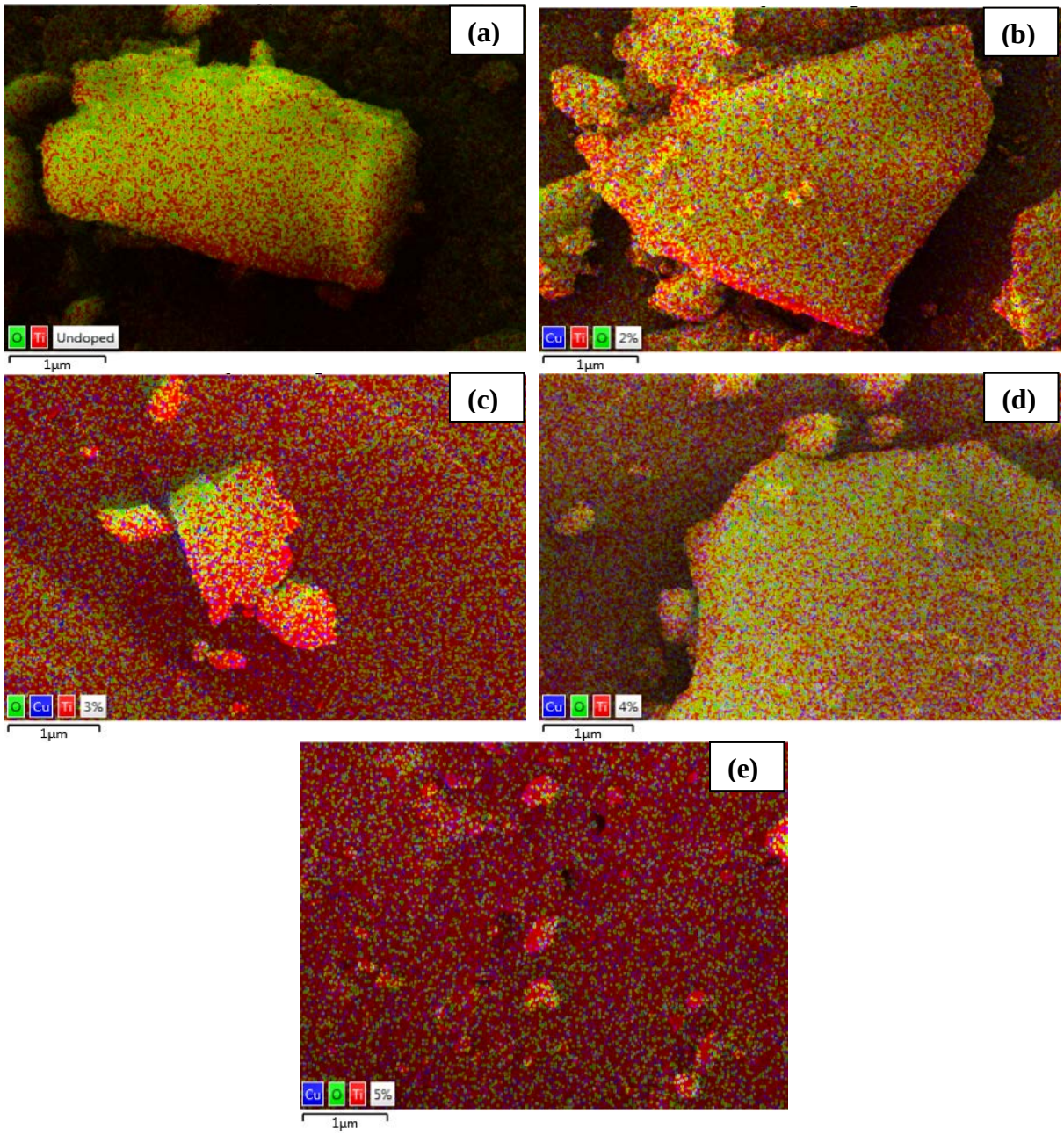

Figure 4.3: SEM-EDX mapping images of the sites shown in **Figure 4.2** undoped TiO_2 (a), 2% Cu TiO_2 (b), 3% Cu TiO_2 (c), 4% Cu TiO_2 (d) and 5% Cu TiO_2 (e).

4.1.3 Transmission Electron Microscopy Observations on the Copper Doped Samples

Figure 4.3 (a-e) shows the TEM images of the undoped TiO_2 catalyst as well as the copper doped catalysts. It can be seen from these images that the particles of all samples are irregularly shaped, the size of these particles vary widely for all the catalysts. This shows that the copper doping does not have any effect on the shape of the particles.

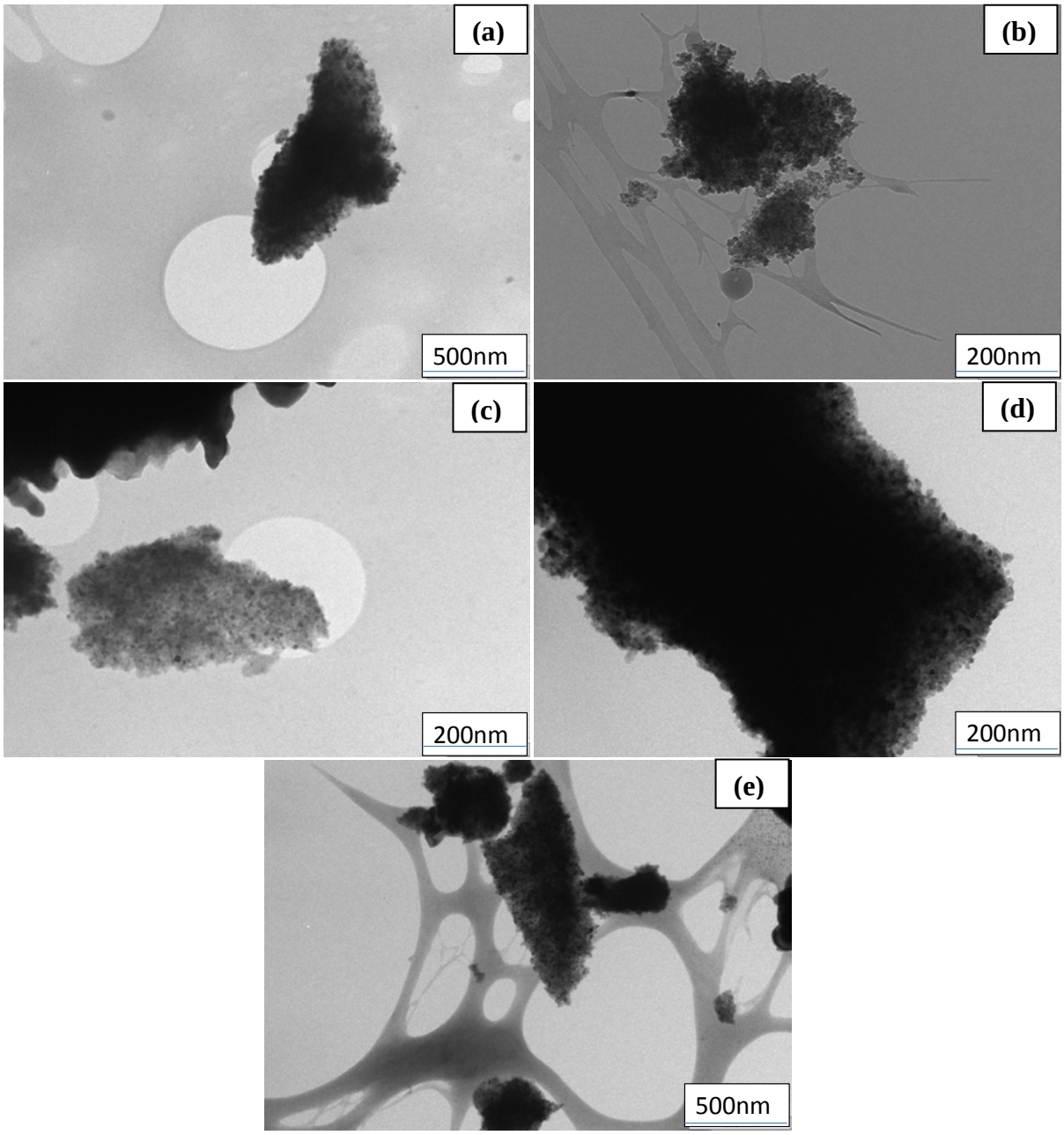

Figure 4.4: TEM images of undoped TiO_2 (a), 2% Cu TiO_2 (b), 3% Cu TiO_2 (c), 4% Cu TiO_2 (d) and 5% Cu TiO_2 (e).

Figure 4.5 show higher magnification images of the undoped TiO_2 and the copper doped catalysts. It appears in these higher magnification images that the particles in **Figure 4.4** are made up of smaller particles. This means that these samples are agglomerations. These small particles that make up the agglomerates are difficult to measure due to overlap and poor definition of boundaries.

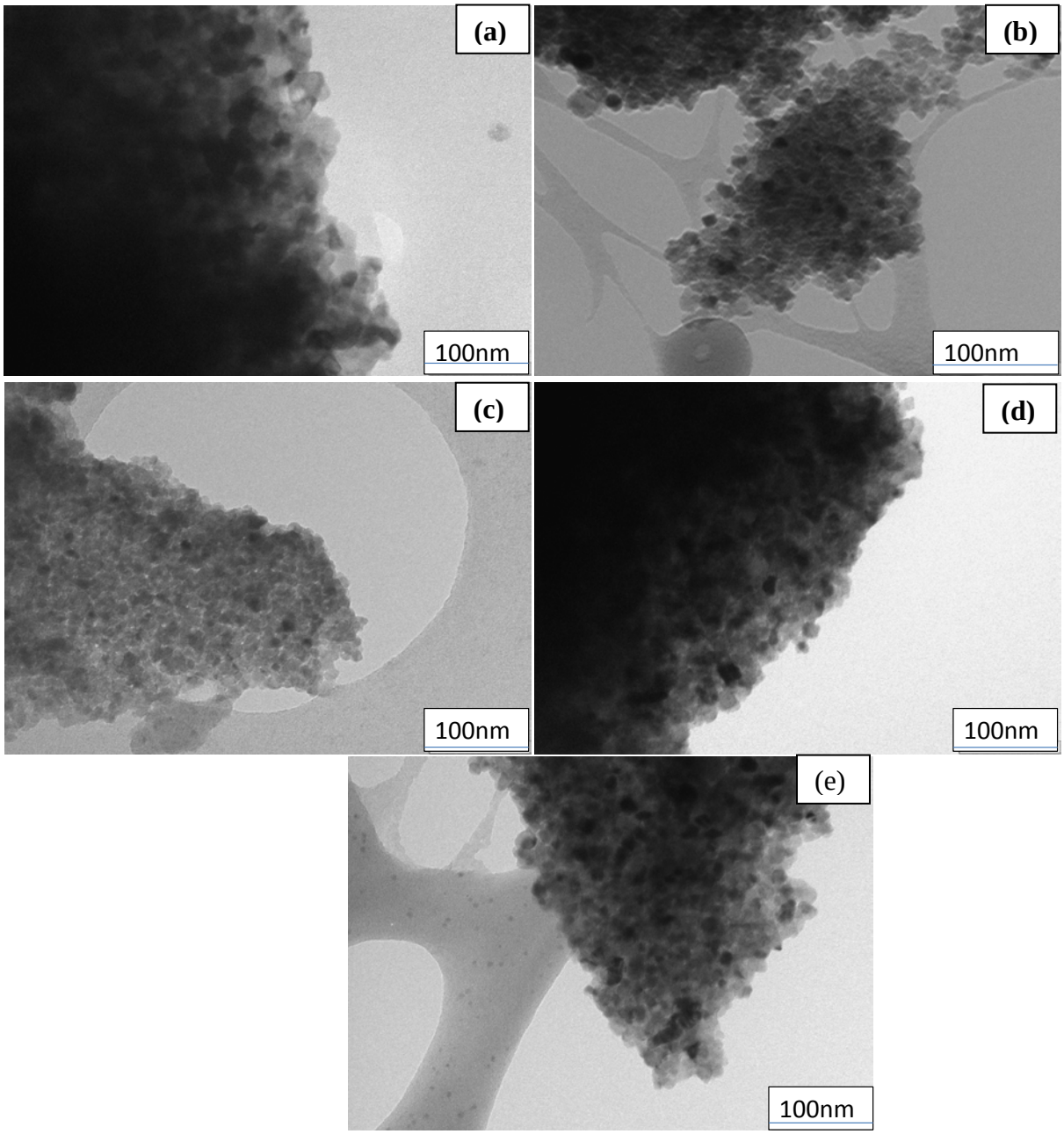

Figure 4.5: Higher magnification TEM images of undoped TiO_2 (a), 2% Cu TiO_2 (b), 3% Cu TiO_2 (c), 4% Cu TiO_2 (d) and 5% Cu TiO_2 (e).

4.1.4 XRD

Figure 4.6 presents the XRD diffractograms of copper doped catalysts. When comparing **Figure 4.6** to the JCPDS (00-021-1272) file for anatase phase of titanium dioxide it can be

seen that the materials are in the anatase form of titania. There are no diffraction peaks that indicate that there is any rutile (JCPDS 00-021-1276) phase present, this is expected as the temperature of calcination was below that required to effect a phase change [3].

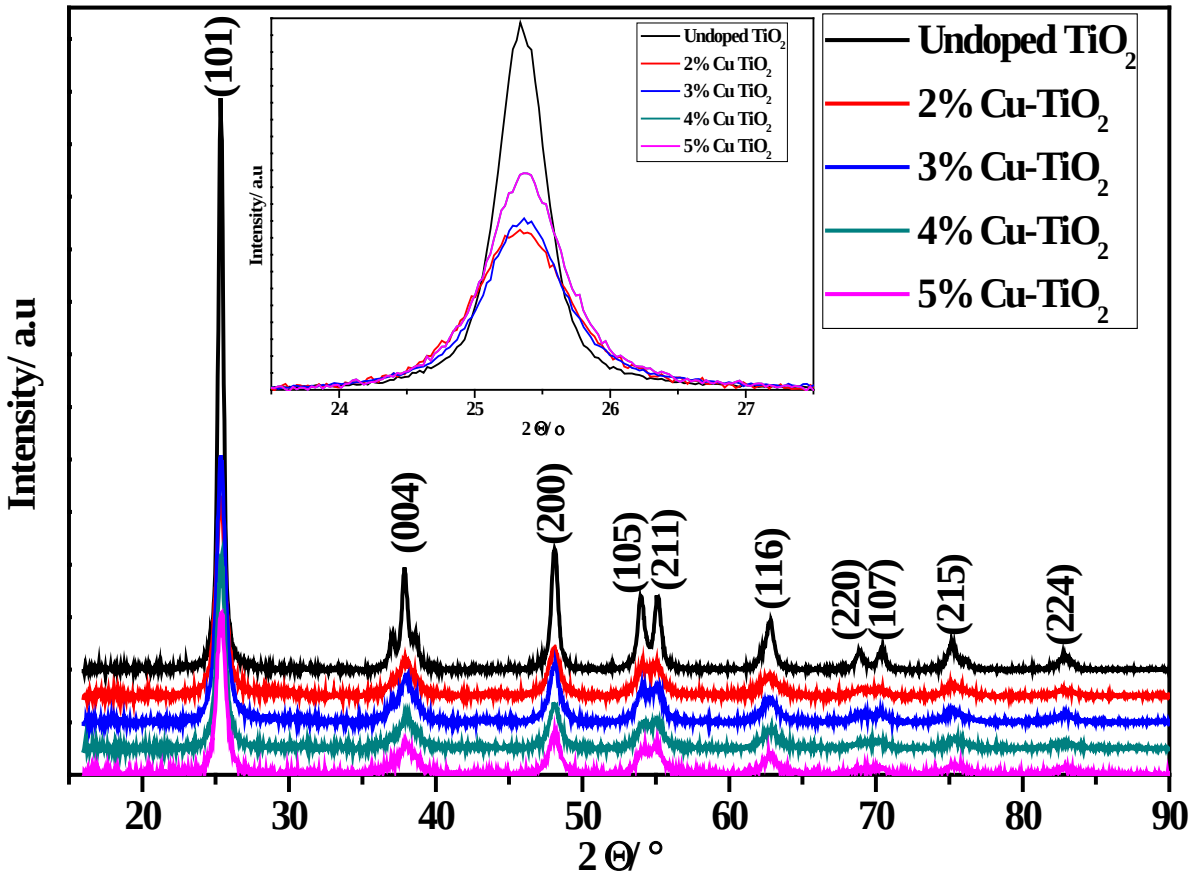

Figure 4.6: XRD diffractogram patterns of undoped and copper doped titanium dioxide materials. Inset magnified view of the 101 peak.

There are no diffraction peaks representing copper or any copper oxides in the diffractograms shown in **Figure 4.6**. Considering that the copper is expected to be doping the TiO_2 as in either the case of copper doping or copper being on the surface of the catalyst the amount of copper used is below the detection limit of XRD [4]. Inset in **Figure 4.6** can be seen a magnified image of the 101 diffraction peak. It can be seen that there is broadening of this diffraction peak with doping and that there is also a decrease in the intensity of this peak. This indicates that there is a loss of structure quality and/or loss of crystallinity caused by

doping [5]. The 4% Cu TiO_2 catalyst has a very similar pattern to the 5% Cu TiO_2 catalyst the 101 diffraction peak for these catalysts appear overlaid.

The d-spacing of undoped catalyst is shown which was calculated from the 101 diffraction peak in **Figure 4.6**, using the Bragg's law equation where n = 1 and $\lambda = 0.15405$ nm.

From the results in **Table 4.2** it can be seen that all of the catalysts have the same d-spacing value of 0.352 nm. This d-spacing value matches that of d-spacing for the 101 diffraction peak give in the JCPDS file for anatase.

Table 4.2: Lattice parameters and cell volume for copper doped photocatalysts.

Catalyst	a (nm)	c (nm)	a^2*c (nm^3)	Crystallite size (nm)	d-spacing (nm)
Undoped	0.3784	0.9501	0.1360	17.75	0.352
2% Cu-TiO_2	0.3787	0.9486	0.1360	9.34	0.352
3% Cu-TiO_2	0.3785	0.9480	0.1358	10.42	0.352
4% Cu-TiO_2	0.3786	0.9470	0.1358	10.75	0.352
5% Cu-TiO_2	0.3786	0.9470	0.1358	10.85	0.352

Table 4.2 lists the lattice parameters and crystallite sizes of the undoped and copper doped titanium dioxide catalysts. The 'a' and 'c' parameters seen in **Table 4.2** were calculated from the 2θ values of the 200 and 004 diffraction peaks respectively, using the Bragg's law equation with miller indices, for a tetragonal system [6]. The d-spacing was calculated as shown above but for either the 200 or 004 diffraction peak. Below is an example of the 'c' parameter calculation for the undoped sample.

The 'a' parameter was calculated in the same way using the 200 diffraction peak.

From the values in **Table 4.2**, the '*a*' lattice parameter is relatively unchanged when comparing all the catalysts. The '*c*' parameter on the other hand shows a slight decrease with increased doping with the undoped catalyst having a 'c' parameter of 0.9501 nm which decreases to 0.9486 for the 2% Cu catalyst. However comparing the cell volume of the

catalysts it can be seen that there is a very small decrease in cell volume for the doped catalysts but the all doped catalysts have the same cell volume of 0.1358 nm^3. There is very little change seen with the lattice parameters due to the similarity in size of the metal ions. Prekajski *et al* doped TiO_2 with Cr^{3+} and found that the lattice parameters of the doped materials showed little change compared to the undoped material, even to high doping levels [7]. The lack of change in lattice parameters was attributed to the similar size of the Ti^{4+} ion and Cr^{3+} ion. A similar finding was made by Trenczek-Zajac *et al*, who also doped TiO_2 with Cr^{3+} and found that the lattice parameters did not change again the reasoning was a similar ionic radius [8]. On the other hand Bartlett *et al* found that doping TiO_2 with Nb resulted in a linear increase in the 'a' parameter with increased doping [9].

Crystallite sizes were calculated from the FWHM of the 101 diffraction peak in **Figure 4.6** using the Scherrer equation.

The crystallite sizes in **Table 4.2** show that all the copper doped catalysts have lower crystallite sizes than the undoped TiO_2 catalyst which has a crystallite size of 17.75 nm. Initially the doping causes a decrease in the crystallite size of the catalysts, as the 2% Cu-TiO_2 catalyst has a crystallite size of 9.24 nm which is smaller than that of the undoped TiO_2 catalyst. However thereafter with increasing doping there is an increase in crystallite size in comparison to the 2% Cu-TiO_2 catalyst. Navas *et al* doped in range of 2.5-7.5 mol % of TiO_2 and reported a linear decrease in the crystallite size [10]. Rajamannan *et al* reported that doping TiO_2 in range of 4-16% Cu (not stated if molar, atom or weight percentage) increases crystallite size compared to that of the undoped catalyst [11]. Considering both these results it could be that after a certain doping level, under the given reaction conditions crystallite growth is promoted.

4.1.5 Raman

Figure 4.7 shows the Raman spectra of copper doped catalysts. The dominant peaks are the B_{1g}, A_{1g} and the E_g at 396, 516 and 642 cm^{-1} respectively. These correspond to the anatase phase of titania [12]. The brookite and rutile phases were not observed. The Raman spectra correlate with the XRD diffractograms; specifically, both the Raman and the XRD analysis show only the anatase phase is present in all the synthesized materials.

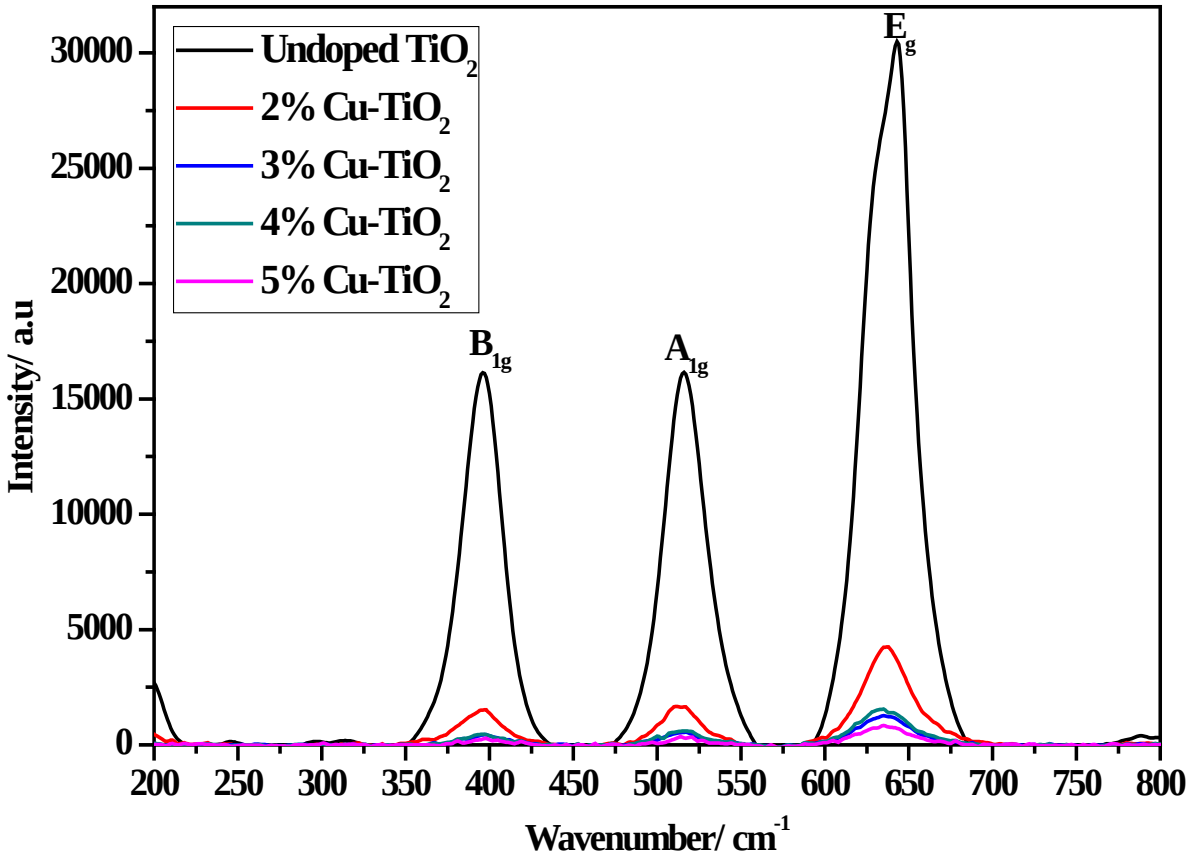

Figure 4.7: Raman spectra of copper doped titanium dioxide catalysts showing the various active modes for the anatase phase.

Table 4.3 shows the FWHM of the E_g peak of the Raman spectra of the copper doped TiO_2 catalysts, this peak was chosen as it showed the highest response factor. Accord to the phonon confinement effect the FWHM should increase with decreasing crystallite size of a material, conversely the FWHM decreases with increasing crystallite size [13-18]. This is given by **Equation 4.1**, according to which a reduction in crystallite size causes a relaxation in the q vector in **Equation 4.1** which leads to a broadening in the Raman spectra [14].

Table 4.3: FWHM of the Eg peak from the Raman spectra of the copper doped TiO_2 catalysts.

Catalyst	**FWHM (cm^{-1})**
Undoped TiO_2	30.85
2% Cu-TiO_2	36.61
3% Cu-TiO_2	35.80
4% Cu-TiO_2	35.35
5% Cu-TiO_2	34.41

$$I(\omega) = \int \frac{d^3q|C(0,q)|^2}{|\omega-\omega(q)|^2+(\Gamma_0/2)^2}$$

Equation 4.1: Gaussian confinement model of first order Raman spectra [14].

Looking at the results in **Table 4.3** it can be said the FWHM of the catalysts follow the phonon confinement effect. The results are in agreement with the crystallite size measurement results shown in **Table 4.2**, which shows an initial decrease in crystallite size upon doping and an increase in crystallite size with further doping. That is to say that the FWHM for the 2% Cu-TiO_2 catalyst increases in relation to the undoped catalyst, going from

30.85 for the undoped catalyst to 36.61 for the 2%Cu-TiO_2 catalyst, thereafter there is a decrease in the FWHM with doping.

4.1.6 Textural Characteristics of the Copper Doped Samples

Figure 4.8 (a-b) shows the isotherms of the undoped TiO_2 catalyst and the copper doped catalysts. It can be seen in **Figure 4.8** (a-b) that all catalysts show type IV isotherms according to IUPAC classfications,[19] this shows that all the catalysts are mesoporous. All the isotherms in **Figure 4.8** (a-b) show H2 type hysterisis, which means that the pores are disordered and there is blockage of the pores [19]. The volume of nitrogen physisorbed onto the copper doped catalysts is greater than the volume physisorbed onto the undoped TiO_2 catalyst synthesised using this particular method. All the doped catalysts showed adsorption up to a value of p/p^0 = 1 showing that there is good interconnect of particles [20]. The undoped catalyst only shows adsorption until a value of p/p^0 = 0.8 which shows particles that are not rigidly joined together [20]. There was no surfactant used in the synthesis of these catalysts so the porsity and surface area of the samples may come from interparticle voids. Interparticle voids can be formed by either aggerates of particles or aggolmerates of particles [21]. Aggerates are loosely packed paricles similar to sand and agglomerates are formed by densely packed particles [21]. From **Figure 4.2** (a-e) and **Figure 4.5** (a-e) it can be seen that the catalysts particles are agglromerated which would result in interparticle voids.

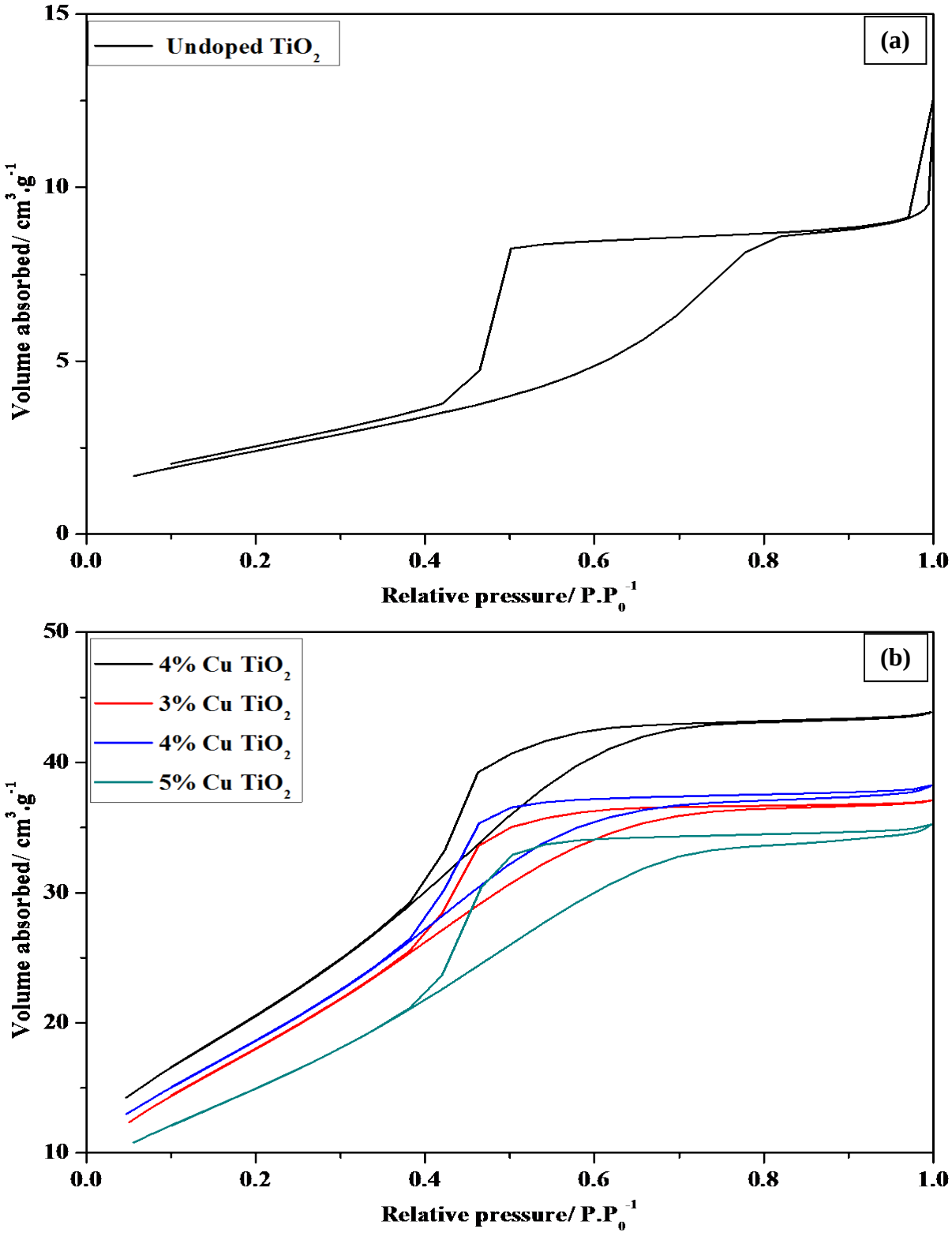

Figure 4.8: Isotherms of catalysts as obtained from nitrogen physisorption of undoped catalyst (a) and copper doped catalysts (b).

The pore size distribution of the copper doped catalysts are shown in **Figure 4.9**. These were calculated using the BJH (Barrett−Joyner−Halenda) method from the desorption branch of the isotherm. The undoped TiO_2 catalyst shows a maxmium distribution centred around 4.5 nm. All the copper doped catalysts show a shift in pore size distribution, with all doped catalyst show maxmium values centred around 3.5 nm. The wider pore size distribution of the doped catalysts in comparsion to the undoped catalyst indcated that there is less homgenity of the pores for doped catalysts [22]. The shift in the maximum values of the doped catalysts compared to the undoped doped catalyst may result from the formation of smaller particles with doping. These smaller particles would be more closely packed and therefore create smaller void spaces leading to smaller pores, however the number of voids and overall void space would increase. That the pore size distribution for all samples is the range of 2-6 nm confirms that all of the catlysts are mesoporous.

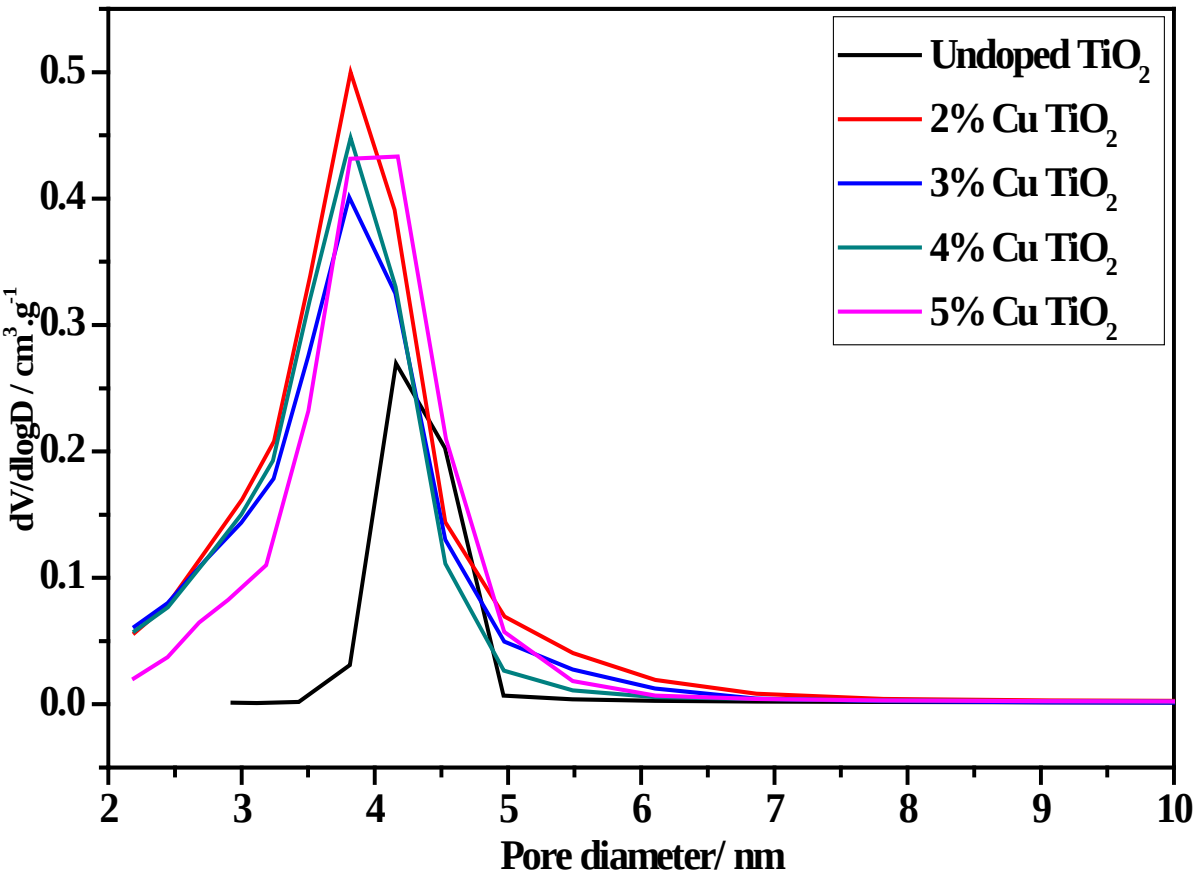

Figure 4.9: Pore size distribution of copper doped catalysts.

Table 4.4 shows a summary of the textrual properties of the copper doped catalysts as obtained form data from nitrogen physisorption. From **Table 4.4**, it can be seen that all the copper doped catalysts show an increase in suraface area compared to the undoped TiO_2 catalyst. The surface area shows an increase from 9.3 $m^3.g^{-1}$ for the undoped TiO_2 catalyst to a maximum value of 78.7 $m^3.g^{-1}$ for the 2% Cu-TiO_2 catalyst. The 3% Cu TiO_2 and 4% Cu TiO_2 catalysts show very similar suface areas of 69 and 71 $m^2.g^{-1}$. The 5% Cu TiO_2 catalyst has the lowest surface are of all the doped catalysts with a surface area of 57.2 $m^2.g^{-1}$. The reduction in surface area with doping greater than the amount of 2% Cu may be due to the morphology of the catalyst with doping. The cause of the low surface area of 5% Cu TiO_2 may be that at this level of doping there may be aggromeration of copper in the pores that would decrease surface area. As can be seen the 2% Cu-TiO_2 catalyst has the highest surface

area, this maybe because the doping loading level is very low. This limited correlation between a change in surface area and the amount of copper used during doping has been reported perviously [23, 24].

Table 4.4: Textural properties of copper doped catalysts.

Catalyst	Surface area ($m^2.g^{-1}$)	Pore diameter (nm)	Pore volume ($cm^3.g^{-1}$)
Undoped TiO_2	9.3	6.0	0.017
2% Cu TiO_2	78.7	3.6	0.082
3% Cu TiO_2	69.4	3.5	0.069
4% Cu TiO_2	71.2	3.5	0.071
5% Cu TiO_2	57.2	3.9	0.067

All copper doped catalysts show a lower pore diameter values than the undoped TiO_2. From the pore size distribution in **Figure 4.9** this was to be expected as the undoped TiO_2 catalyst shows a maxium distribution at a higher pore size.

The pore volume shows the same trend as the surface area, the undoped catalyst shows the lowest pore volume with $0.017 cm^3.g^{-1}$ and the 2% Cu-TiO_2 catalyst has the largest pore volume with 0.082 $cm^3.g^{-1}$. The lower pore volume with increased doping could be due to structural changes at higher doping levels or the accumlation of copper in the pores of the catalyst.

The decrease in pore diameter with doping may be due to the copper causing a change in the structure of the TiO_2 or that there is agglomeration of the copper on the pores. Aggglomeration of copper on the pores may explain the lower surface area of the catalysts with increased doping compared to the 2% Cu TiO_2 catalyst.

4.1.7 Optical Properties Ultra-Violet Diffuse Reflectance Spectroscopy on Copper Doped Samples

The UV-DRS spectra from **Figure 4.10** (a) show that, the absorbance values of copper doped catalysts are much higher than that of the undoped catalyst. The absorbance of the 3% Cu TiO_2 spectrum is clearly the highest and that of the 5% Cu TiO_2 is clearly the lowest of all the copper doped catalysts. The Tauc plots, seen in **Figure 4.10** (b), which was used to obtain the band gaps of the synthesised materials as well as P25 were obtained by converting the UV-DRS spectra seen in **Figure 4.10 (a)**. The commercial catalyst, P25, band gap is shown in **Figure 4.10** (b) the band gap obtained here was 3.2 eV which is the literature value for this catalyst [25].

The undoped TiO_2 catalyst shows a band gap of 3.0 eV which is slightly narrower than the expected 3.2 eV for an anatase phase TiO_2. The doped catalysts had band gap values of 2.6, 2.4, 2.5 and 2.8 eV in the order of 2%, 3%, 4% and 5% Cu TiO_2. The doping initially shows a reduction in band gap in comparison to the undoped catalyst, 2% Cu TiO_2 catalyst has a band gap of 2.6 eV. The 3% Cu shows a further decrease in the size of the band gap with a band gap of 2.4 eV however the 4% Cu catalyst has a larger band gap of 2.5 eV. The 5% Cu TiO_2 catalyst has a further increase in the size of the band gap with a band gap of 2.8 eV. The increase in band gap beyond a certain doping level is due to the doping level moving beyond the Mott critical density level, and hence a Burstein-Moss shift has taken place [26-28]. Burstein-Moss shift takes place when the charge carrier concentration exceeds the conduction band (CB) density of states, with increasing doping the Fermi level is increased causing a blueshift in the absorbance edge [26, 29]. This usually occurs once charge carrier concentration exceeds the Mott critical density [29].

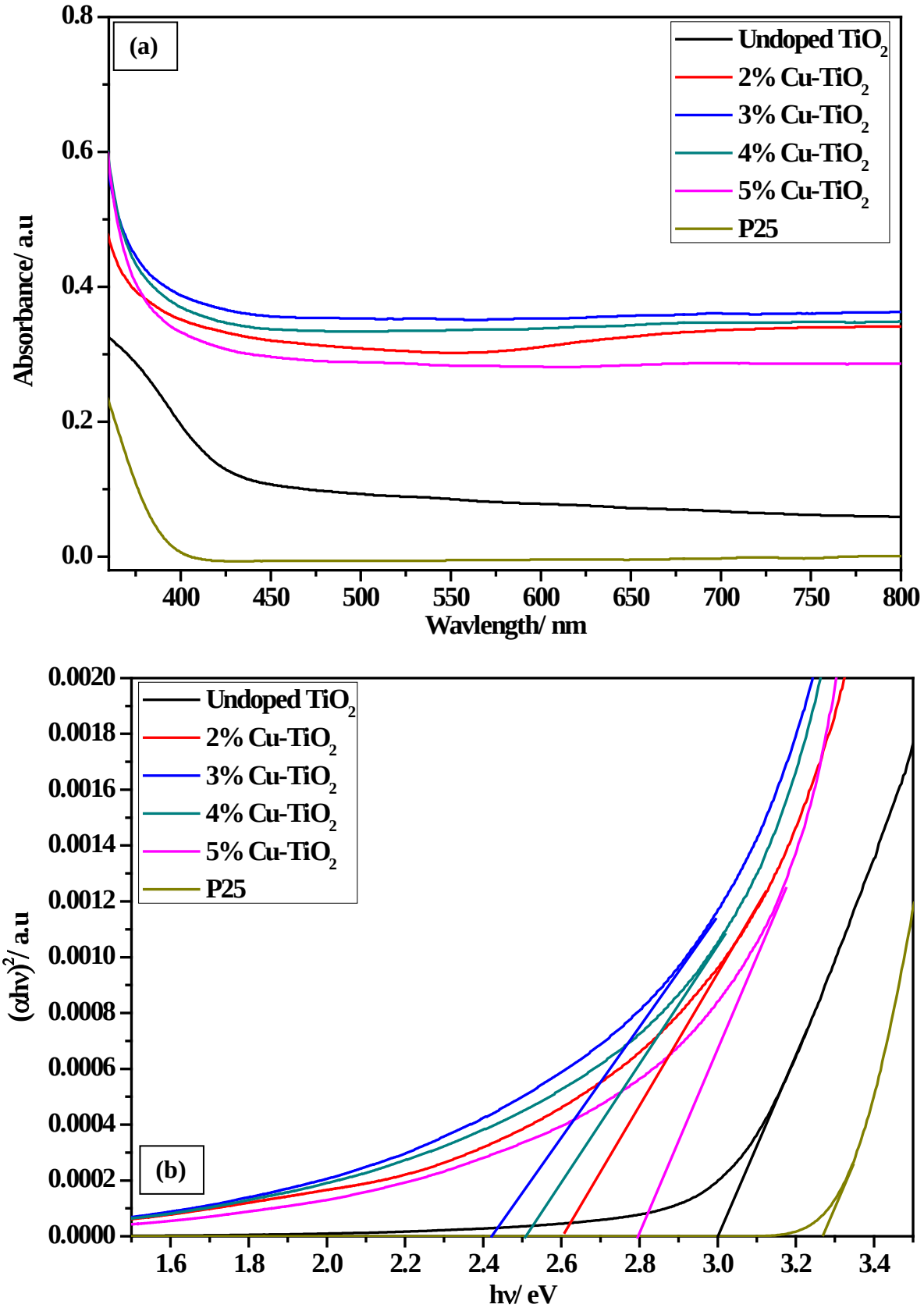

Figure 4.10: UV-DRS spectrum of copper doped materials (a) and Tauc Plot of UV-DRS spectrum of copper doped materials (b).

This shows that in terms of narrowing the band gap and making TiO_2 visible light active doping of 3 mol% Cu would be the optimum level and further doping results in a decrease in the band gap. From these results it is clear that copper doping results in a narrower band gap for TiO_2 and hence allows for visible light absorbance.

4.1.8 Photoluminescence Spectroscopy Studies of Copper Doped Samples

There are a number of peaks in the spectra of **Figure 4.11** which can be assigned to certain events within the catalysts. The peak at 423 nm can be assigned to self-trapped excitons [30-33]. The peak at 447 nm can be attributed to interstitial defects in the TiO_2 catalysts [34]. The peaks at 460 nm and 522 nm can be assigned to oxygen vacancies, which are formed trapping one and two electrons respectively [30-32, 35]. Oxygen vacancies result in donor levels below the CB of TiO_2, this can result in a narrower band gap and result in visible light activity of an undoped TiO_2, this may be the cause of the undoped TiO_2 having a band gap narrower than expected [36-40].

Figure 4.11 shows the photoluminescence (PL) spectra of the undoped TiO_2 catalyst, the copper doped catalysts and P25. The 2% Cu-TiO_2 catalyst shows a drastic reduction in intensity in comparison to the undoped TiO_2 catalyst. There is further decrease in spectrum intensity with increasing doping and therefore further reduction in electron-hole recombination rate with increasing doping. **Figure 4.11** shows the PL spectrum for P25, following the peak at 522 nm it can be seen that, for the peak representing an oxygen vacancy with 2 electrons, the P25 has the lowest intensity of all catalysts. This suggests that P25 may have the lowest recombination rate of all the catalysts.

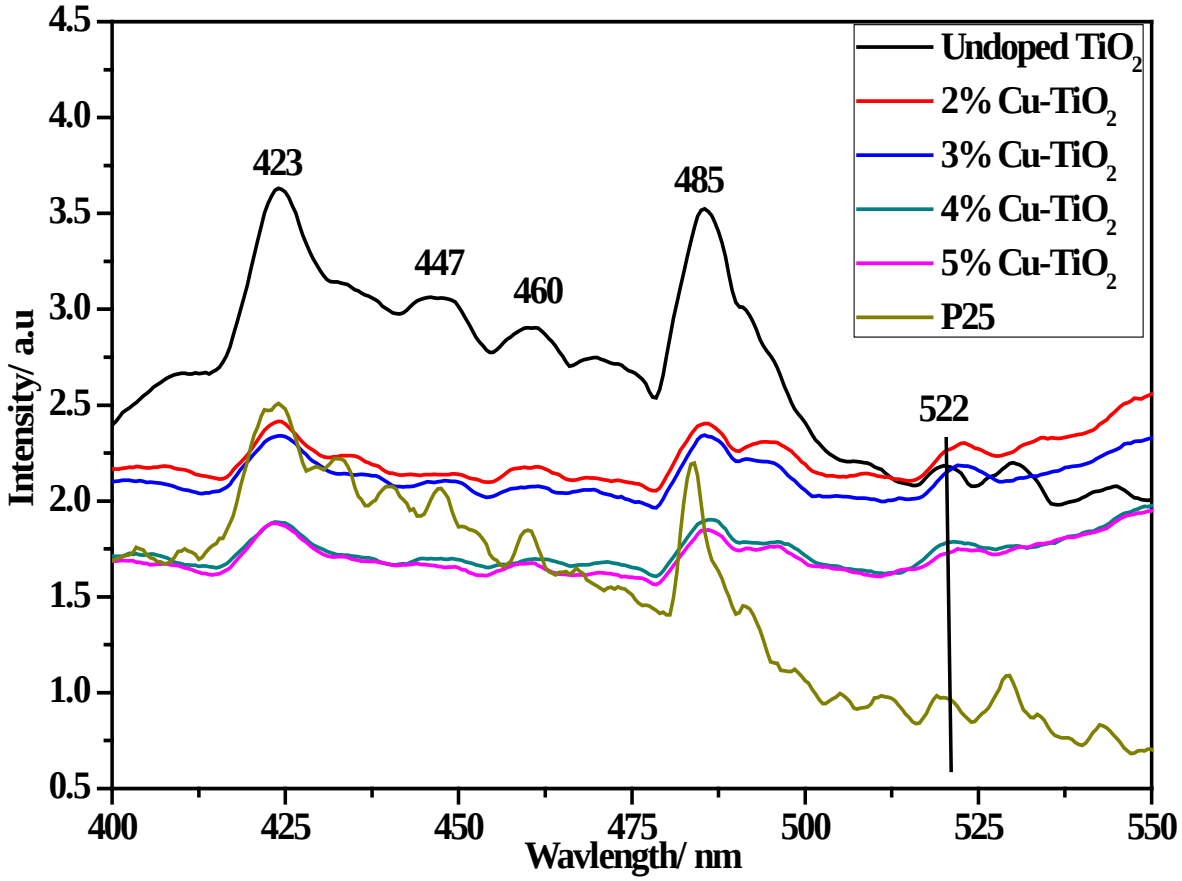

Figure 4.11: Photoluminescence spectra of copper doped materials obtained using, Perkin Elmer, LS55 Fluorescence Spectrometer at 310 nm.

4.1.9 Final Comments on Copper Doping

Copper doping has been shown in this work to improve the properties of TiO_2 that would improve its photocatalytic activity. All catalysts were anatase phase and copper doping showed little to no effect on the structural properties of the TiO_2 lattice, however a loss of crystallinity was observed. Copper has been shown to reduce the band gap of TiO_2 but only to a doping level of 3 mol% Cu. Copper doping in this study has improved the surface area of TiO_2 which should improve reaction rate. The rate of electron-hole pair recombination is reduced by the addition of copper to TiO_2.

4.2 Nitrogen Doped Titanium Dioxide Samples

Nitrogen doping has previously been shown to decrease the band gap of TiO_2 and therefore allow for greater solar spectrum absorption and increase reaction rates of TiO_2 [41, 42]. Nitrogen doping also promotes the formation of oxygen vacancies in TiO_2 [43].

4.2.1 Scanning Electron Microscopy Analysis of Nitrogen Doped Samples

Figure 4.12 (a-d) shows the SEM images of the undoped catalyst and the nitrogen doped catalysts. It can be seen in these images that the undoped catalysts and the nitrogen doped catalysts have irregularly shaped particles and that on the surface of these catalyst particles there are other smaller particles. The nitrogen doping does not appear to offer any shape control of these particles. The size of these particles is very wide ranging for all catalysts.

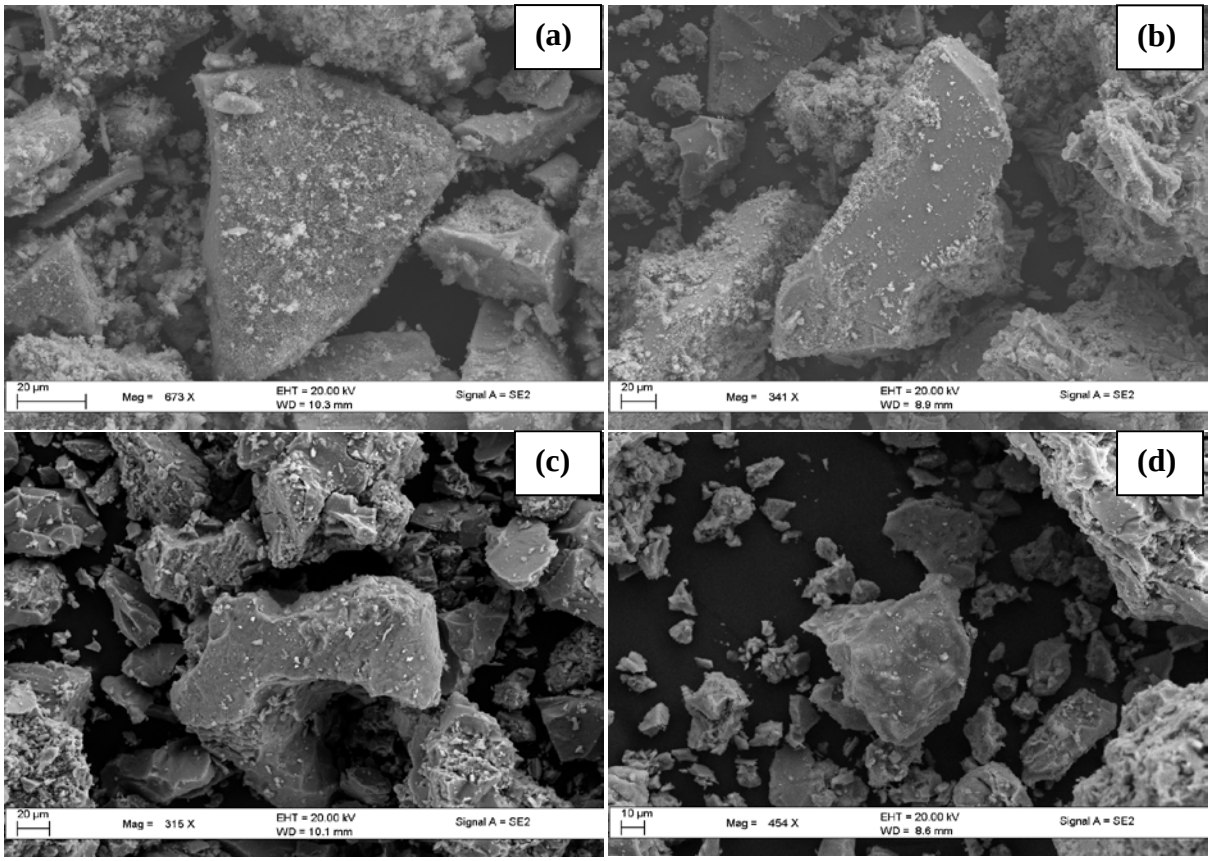

Figure 4.12: SEM images of undoped TiO_2 (a), TiO_2:N 1:2 (b), TiO_2:N 1:3 (c) and TiO_2:N 1:4 (d).

Figure 4.13 (a-d) shows higher magnification images of the particles shown in **Figure 4.12** (a-d) of the undoped catalyst and the nitrogen doped catalysts. **Figure 4.13** (a) and (b) which show images of the undoped and the TiO_2:N 1:2 catalysts respectively show the same morphology. In these images an agglomeration of particles can be seen an interparticle voids can be seen.

For **Figure 4.13** (c) and (d) images of TiO_2:N 1:3 and TiO_2:N 1:4 catalysts respectively show the same morphology, this morphology is different to that of the undoped and TiO_2:N 1:2 catalysts. It is possible that doping changes the morphology of the catalysts. The images for the TiO_2:N 1:3 and TiO_2:N 1:4 catalysts also shows packing of smaller particles to make up the large particles shown in **Figure 4.12** (c) and (d).

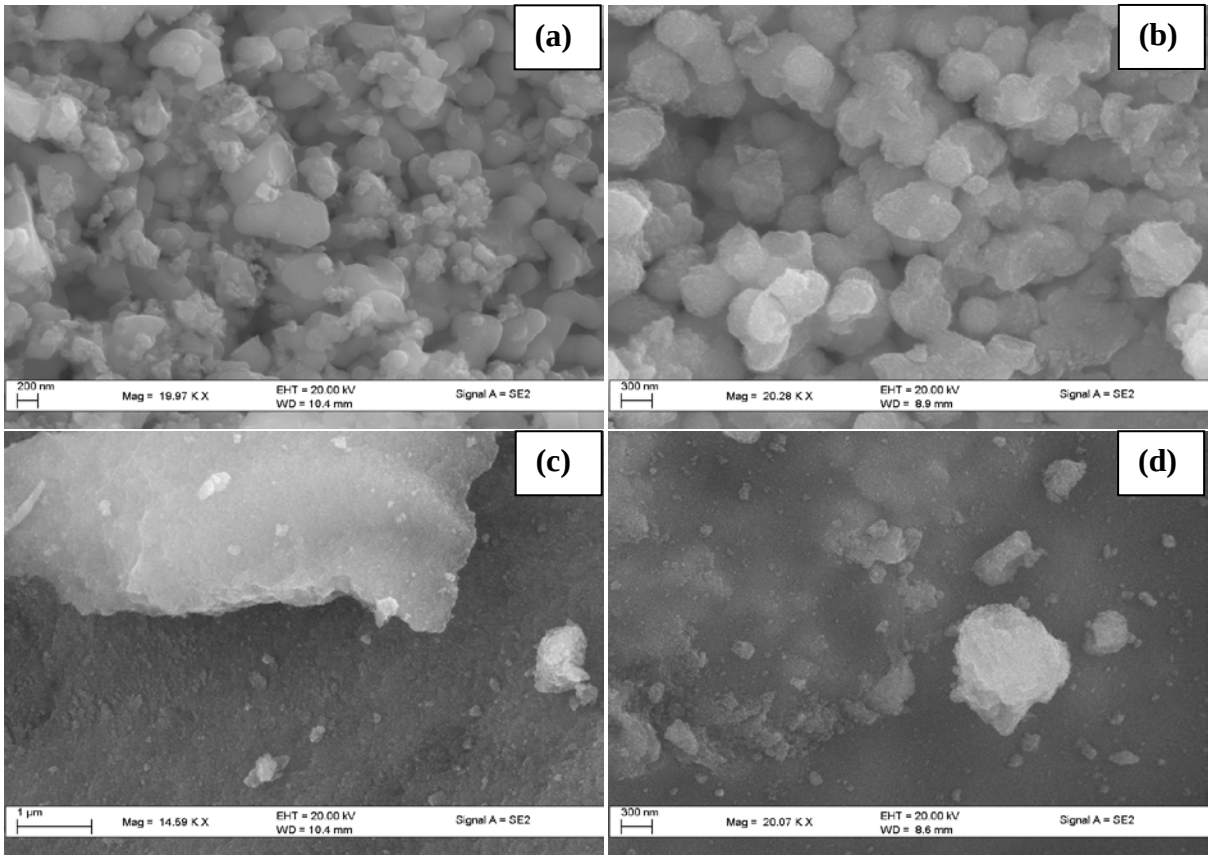

Figure 4.13: Higher magnification SEM images of undoped TiO_2 (a), TiO_2:N 1:2 (b), TiO_2:N 1:3 (c) and TiO_2:N 1:4 (d).

Figure 4.14 (a-d) shows the SEM-EDX mapping of the undoped catalyst and the nitrogen doped catalysts. The undoped catalyst as expected only shows titanium and oxygen on the surface of the catalyst. The nitrogen doped catalysts also only show titanium and oxygen on the surface of the catalysts. The fact that nitrogen is not detected by the instrument is unexpected however the content of nitrogen in the catalyst may be below the instruments detection limit. XPS is needed to prove the presence of nitrogen in the catalysts.

Overall the use of SEM and SEM-EDX may not be a useful method to studying the doping of TiO_2 with nitrogen. This is as nitrogen cannot be seen as particles.

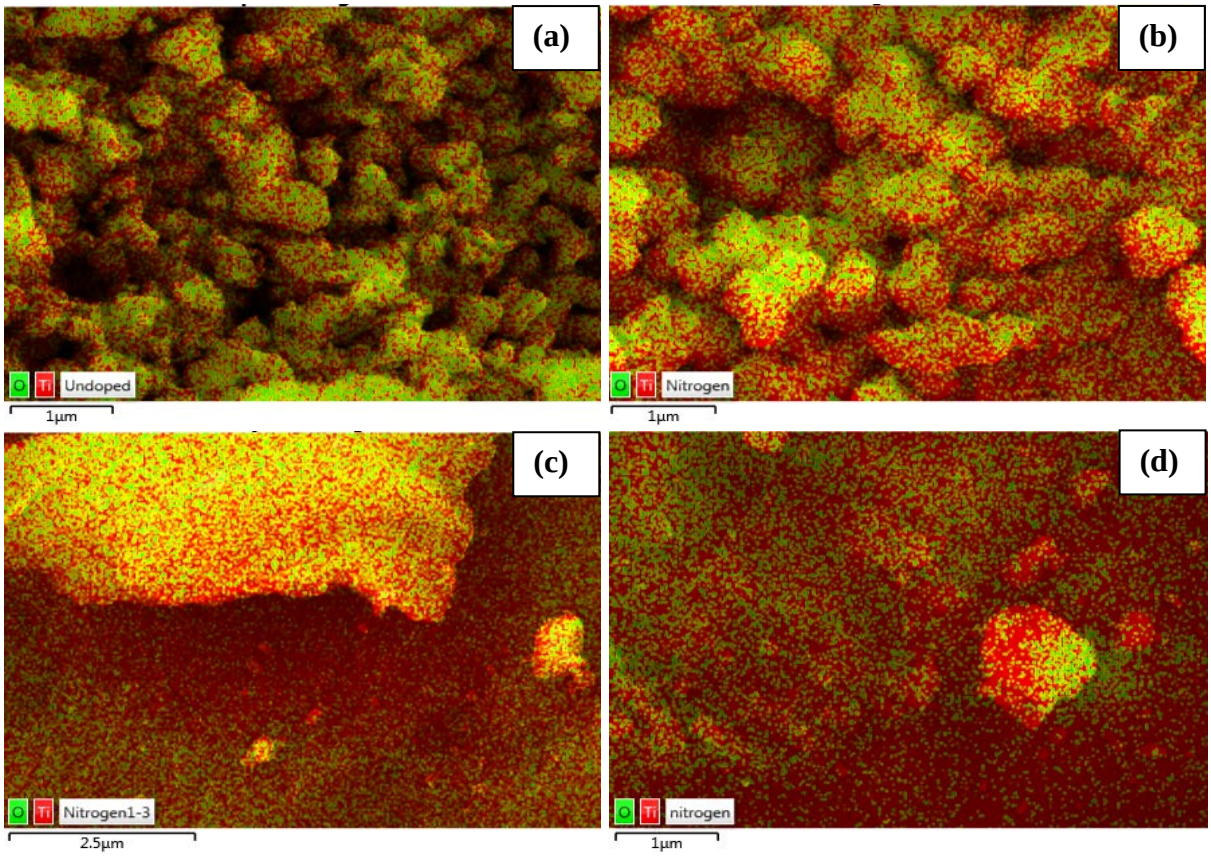

Figure 4.14: SEM-EDX mapping of undoped TiO_2 (a), TiO_2:N 1:2 (b), TiO_2:N 1:3 (c) and TiO_2:N 1:4 (d).

4.2.2 Transmission Electron Microscopy Observations on the Nitrogen Doped Samples

Figure 4.15 (a-d) shows the TEM images of the undoped and nitrogen doped catalysts. The undoped catalyst and all the nitrogen doped catalysts seen in these images show irregular particle shape. The size and shape of these particles vary widely for all catalysts. This shows that doping with nitrogen does not have an effect on the shape of the catalysts which confirms the findings of the SEM images.

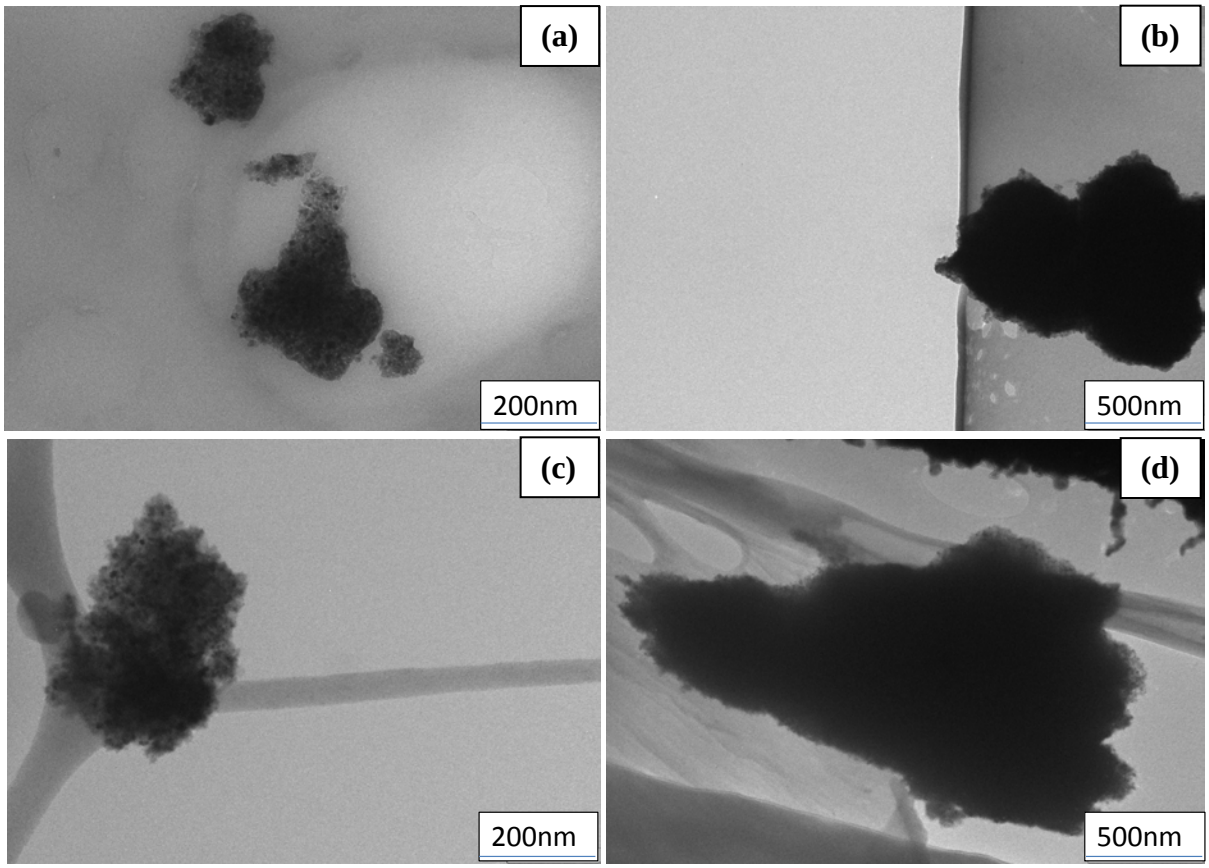

Figure 4.15: TEM Images of undoped TiO_2 (a), TiO_2:N 1:2 (b), TiO_2:N 1:3 (c) and TiO_2:N 1:4 (d).

Figure 4.16 (a-d) show higher magnification TEM images of the particles shown in **Figure 4.15** (a-d) of the undoped catalyst and the nitrogen doped catalysts. It appears in each of the images shown in **Figure 4.16** (a-d) that all of the catalysts are made up of smaller particles. This would support the findings of the SEM high magnification images which show individual particles making up the larger irregular shaped particles.

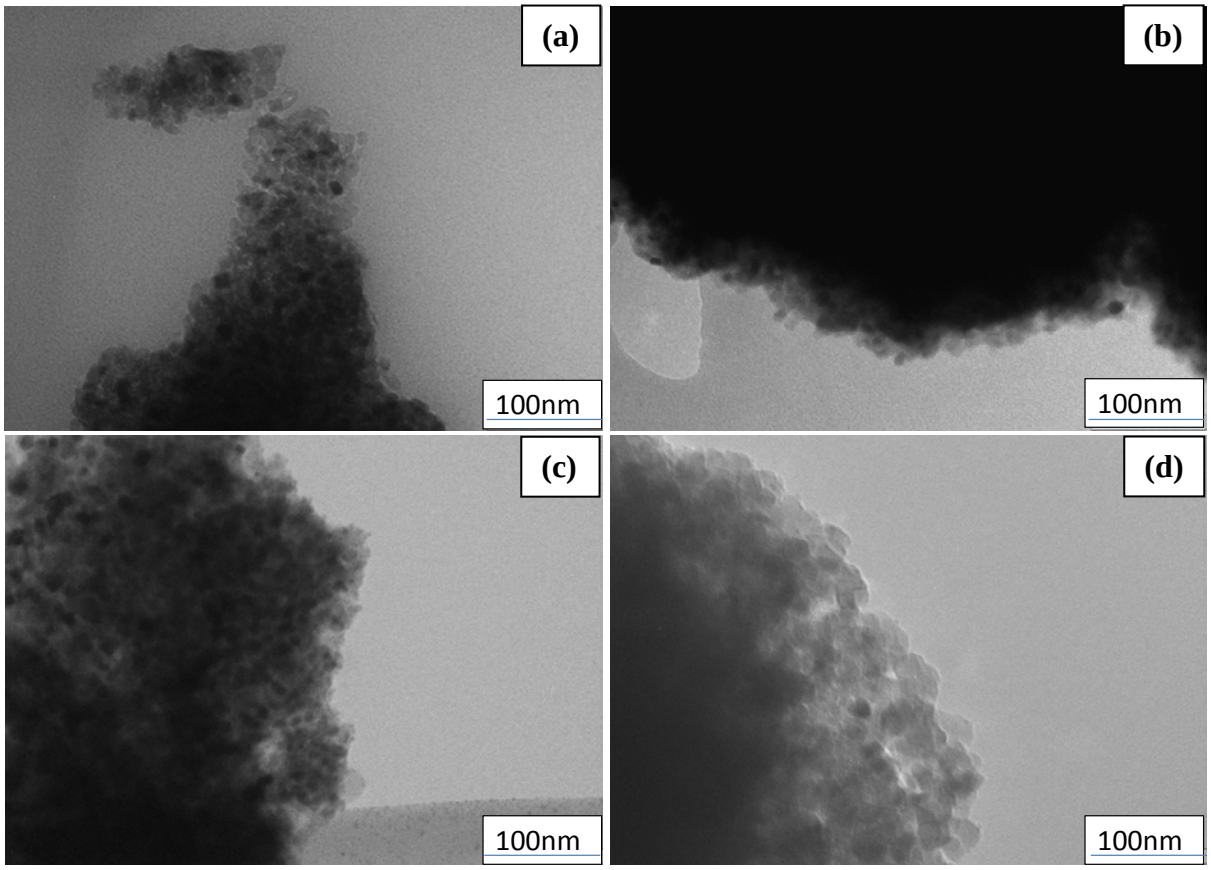

Figure 4.16: Higher magnification TEM Images of undoped TiO_2 (a), TiO_2:N 1:2 (b), TiO_2:N 1:3 (c) and TiO_2:N 1:4 (d).

4.2.3 XRD

Figure 4.17 presents the diffractogram patterns of the nitrogen doped TiO_2 materials. It can be seen that the diffractogram patterns for all of the catalysts match the JCPDS (00-021-1272) file for anatase TiO_2. Matching the diffractogram patterns against rutile phase JCPDS (00-021-1276) file for TiO_2 it can be seen that there are no diffraction peaks belonging to rutile phase present. That anatase is the only phase present is expected as the temperatures used in calcination would not enforce a phase change. Inset is a magnified view of the 101 diffraction peak, it can be seen that this peak decreases in intensity and becomes boarder

upon doping. This implies that there may be a loss of structure quality or crystallinity with doping.

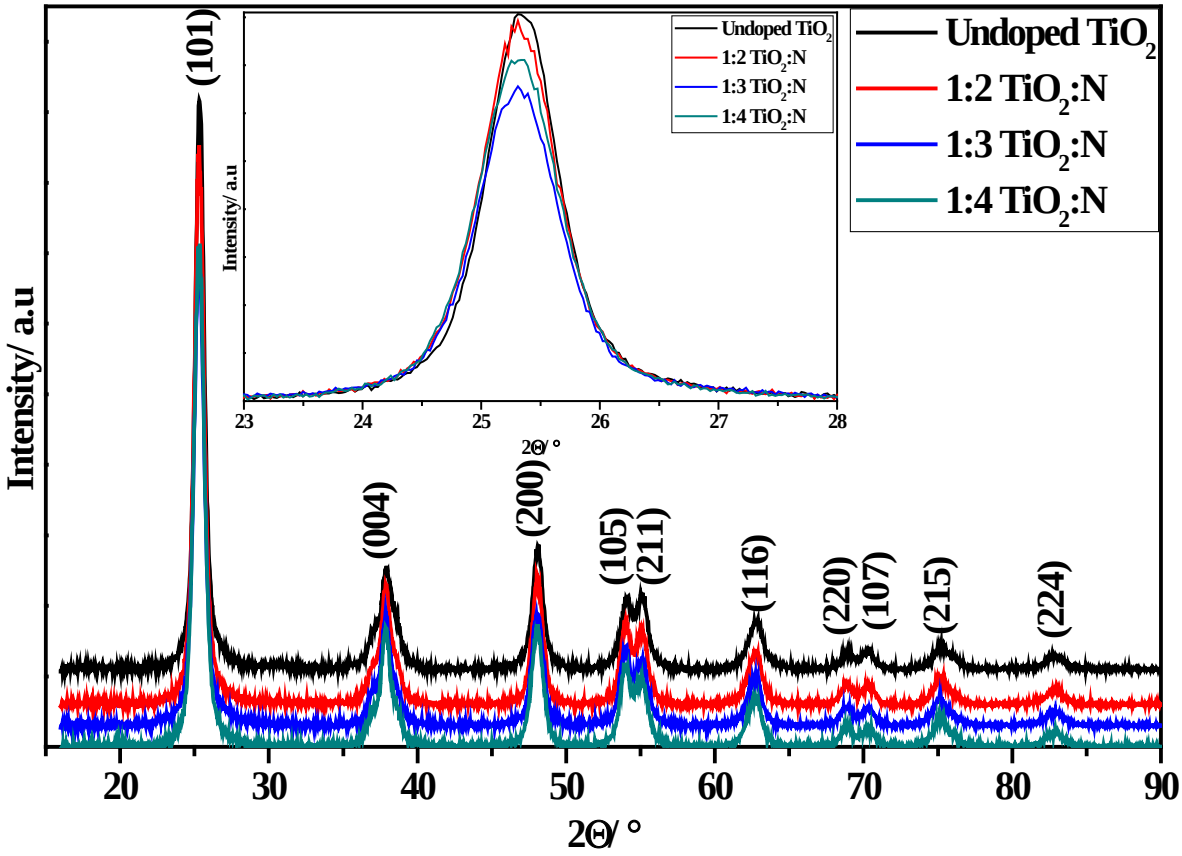

Figure 4.17: XRD diffractogram patterns of undoped and nitrogen doped titanium dioxide materials.

Table 4.5 shows the lattice parameters, cell volume, crystallite size and d-spacing of the copper doped catalysts as calculated from XRD diffractogram patterns. The 'a' and 'c' lattice parameters were calculated from the 2θ values of the 200 and 004 diffraction peaks respectively. It can be seen that there is no change in the 'a' parameter seen for any of the doped catalysts. The 'c' parameter shows only a very slight increase with doping, though this change is constant and increases with doping. Overall the cell volume does not change with increasing doping.

The crystallite sizes shown below in **Table 4.5** were calculated from the FWHM of the 101 diffraction peak of each catalyst. The undoped catalyst has a crystallite size of 10.50 nm upon doping the TiO_2:N 1:2 catalyst has a reduction in crystallite size being 9.85 nm. With increasing doping there is further decrease in the crystallite size. The TiO_2:N 1:3 and TiO_2:N 1:4 catalysts have very similar crystallite sizes of 9.36 and 9.32 nm respectively. The linear reduction of the crystallite size with doping may indicate that doping with nitrogen inhibits the growth of TiO_2 crystals.

Table 4.5: Lattice parameters and cell volume for nitrogen doped photocatalysts.

Catalyst name	Crystallite size (nm)	a = b (nm)	c (nm)	Cell volume (nm^3)	d-spacing (nm)
Undoped TiO_2	10.50	0.3786	0.9492	0.1360	0.352
TiO_2:N 1:2	9.85	0.3787	0.9506	0.1364	0.352
TiO_2:N 1:3	9.36	0.3788	0.9508	0.1364	0.352
TiO_2:N 1:4	9.32	0.3788	0.9510	0.1365	0.352

The d-spacing of the catalysts is also presented in **Table 4.5**. It can be seen that all the catalysts have the same d-spacing (0.352 nm) expected for anatase TiO_2 when using the 101 diffraction peak. This indicates that doping with nitrogen does not induce strain on the structure of TiO_2, as a change in d-spacing would indicate strain [44].

4.2.4 Raman

Figure 4.18 shows the Raman spectra for the nitrogen doped titanium dioxide catalysts. There are three peaks present for the spectrum of each of the catalysts presented below these peaks belong to the B_{1g}, A_{1g} and the E_g modes of anatase TiO_2. These peaks are found at 410, 528 and 649 cm^{-1} respectively and confirm the XRD diffractograms.

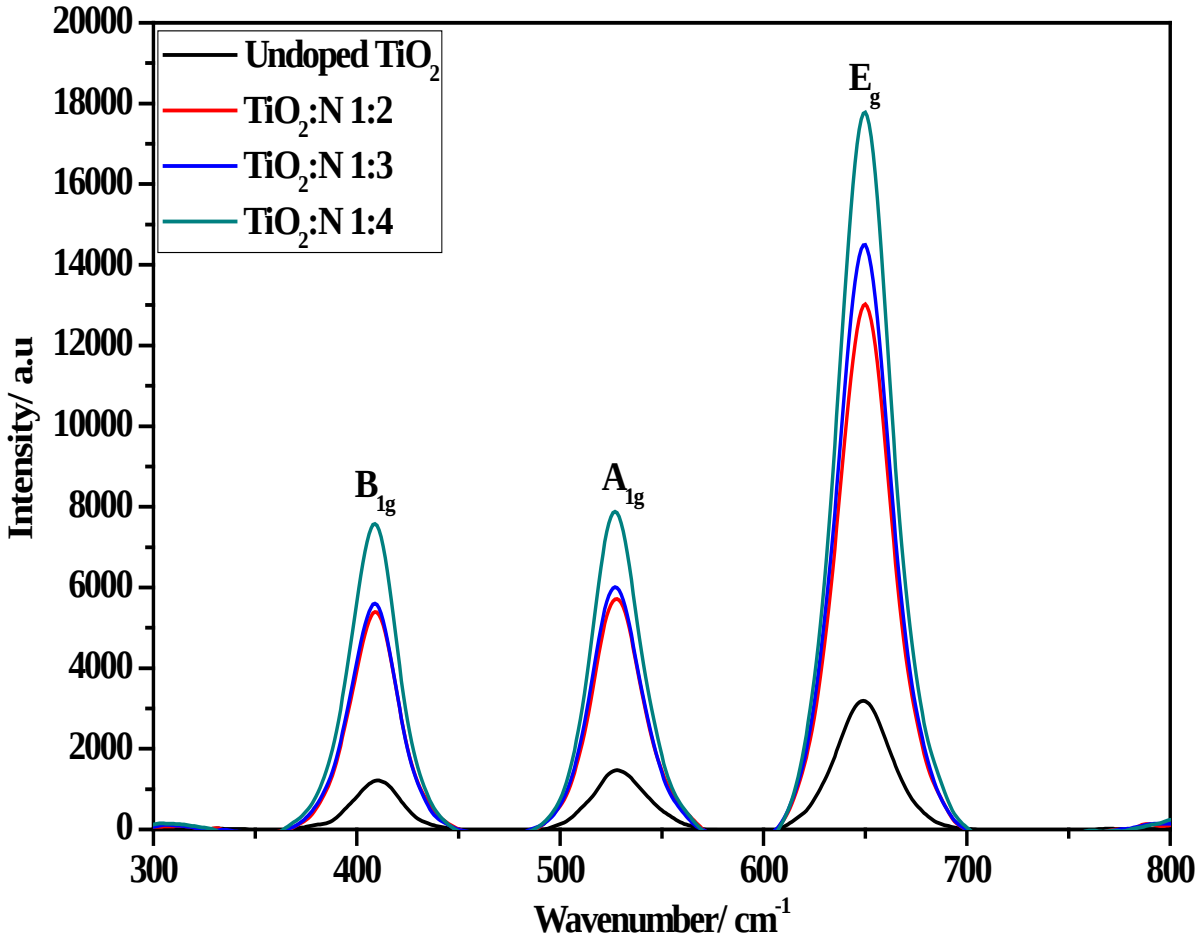

Figure 4.18: Raman spectra of nitrogen doped titanium dioxide catalysts showing the various active modes for the anatase phase.

It can be seen, in **Figure 4.18**, that the intensity of the spectra increase with increasing doping with the undoped catalyst having very low intensity and the TiO_2-N 1-4 catalyst having the highest intensity. This increase in intensity with increasing doping has previously been attributed to an increase in oxygen vacancies [45].

The nitrogen doped catalysts do not show a good agreement with the phonon confinement effect and crystallite size calculated from the XRD data. It can be seen in **Table 4.5** that the crystallite size decreases with increasing nitrogen doping and in **Table 4.6** that the FWHM for nitrogen doped catalysts does not decrease with doping. The disagreement between the

results and the phonon confinement model may be due to the increase in peak intensity with increasing doping which may offset the broadening effects of the phonon confinement.

Table 4.6: FWHM of the Eg peak from the Raman spectra of the nitrogen doped TiO_2 catalysts.

Catalyst	FWHM (cm^{-1})
Undoped TiO_2	31.74
TiO_2:N 1:2	31.39
TiO_2:N 1:3	31.49
TiO_2:N 1:4	31.38

4.2.5 Textural Characteristics of the Nitrogen Doped Samples

Figure 4.19 shows the isotherms of the nitrogen doped catalysts as obtained from nitrogen physisorption. All of the isotherms shown in **Figure 4.19** are type IV by IUPAC classification meaning that all the catalysts are mesoporous [19]. The hysteresis loops of all of the isotherms are H2 according to IUPAC classifications, this means that the pores are disordered and there is blockage of the pores [19]. The porosity of these samples may originate from the interparticle voids seen in **Figure 4.13** (a-d). This is most likely source of the pores as no surfactant was used. The volume of nitrogen adsorbed increases with the amount of doping. The hysteresis loop of all catalysts begins at p/p^0 = 0.42 and none of the samples adsorb beyond a p/p^0 = 0.82, meaning that all catalysts display limited adsorption [20]. This limited adsorption indicates particles that are not rigidly held together.

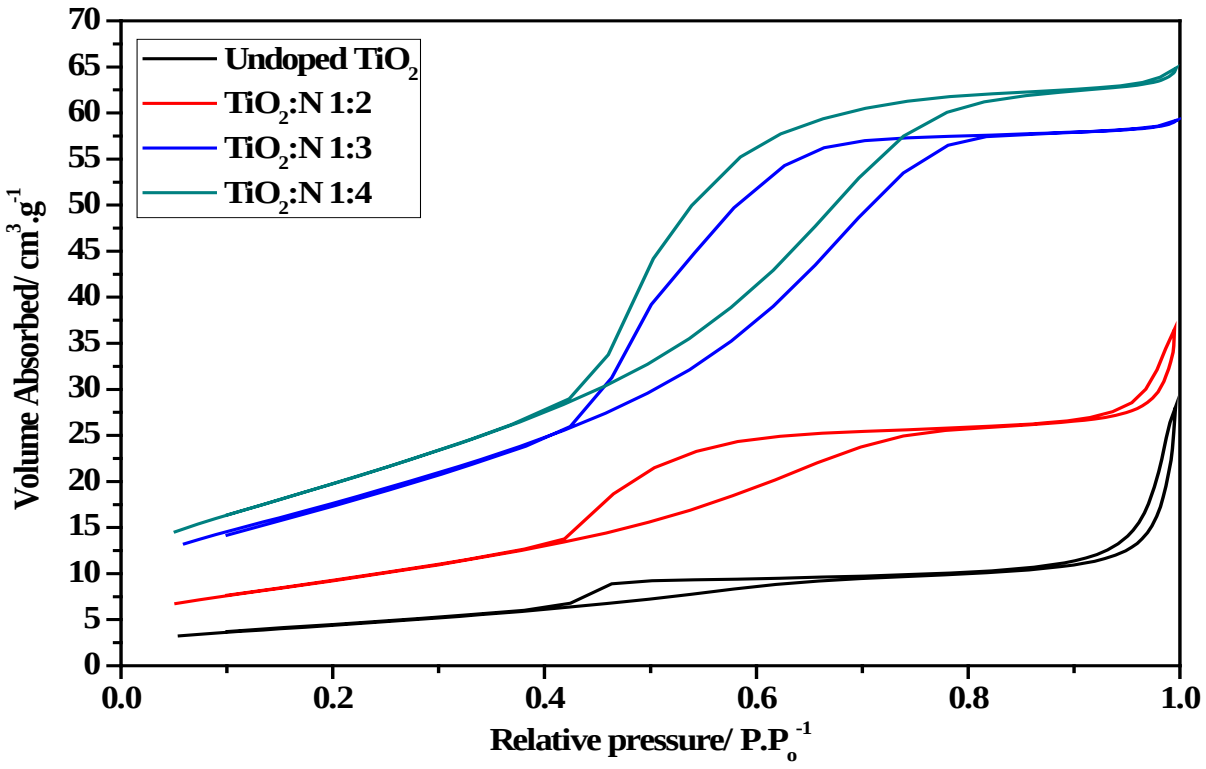

Figure 4.19: Isotherms of nitrogen doped catalysts as obtained from nitrogen physisorption.

Figure 4.20 shows the pore size distribution of the nitrogen doped catalysts as well as the undoped catalyst. These were calculated using the BJH (Barrett−Joyner−Halenda) method from the desorption branch of the isotherm. The undoped TiO_2 catalyst has a maximum centred on 4 nm with a narrow distribution. The TiO_2-N 1-2 catalyst has a wider distribution of pores and the maximum of it pores has shifted slightly in comparison to the undoped catalyst, from 4 nm to slightly more than 4 nm. With increasing doping the range of pore distribution increases and the point around which the pore size is centred increases, this can be seen with the TiO_2-N 1-4 catalyst having the widest pore distribution and peak centred on 5 nm. From these results it is clear that nitrogen doping increases the range over which TiO_2 pores are distributed.

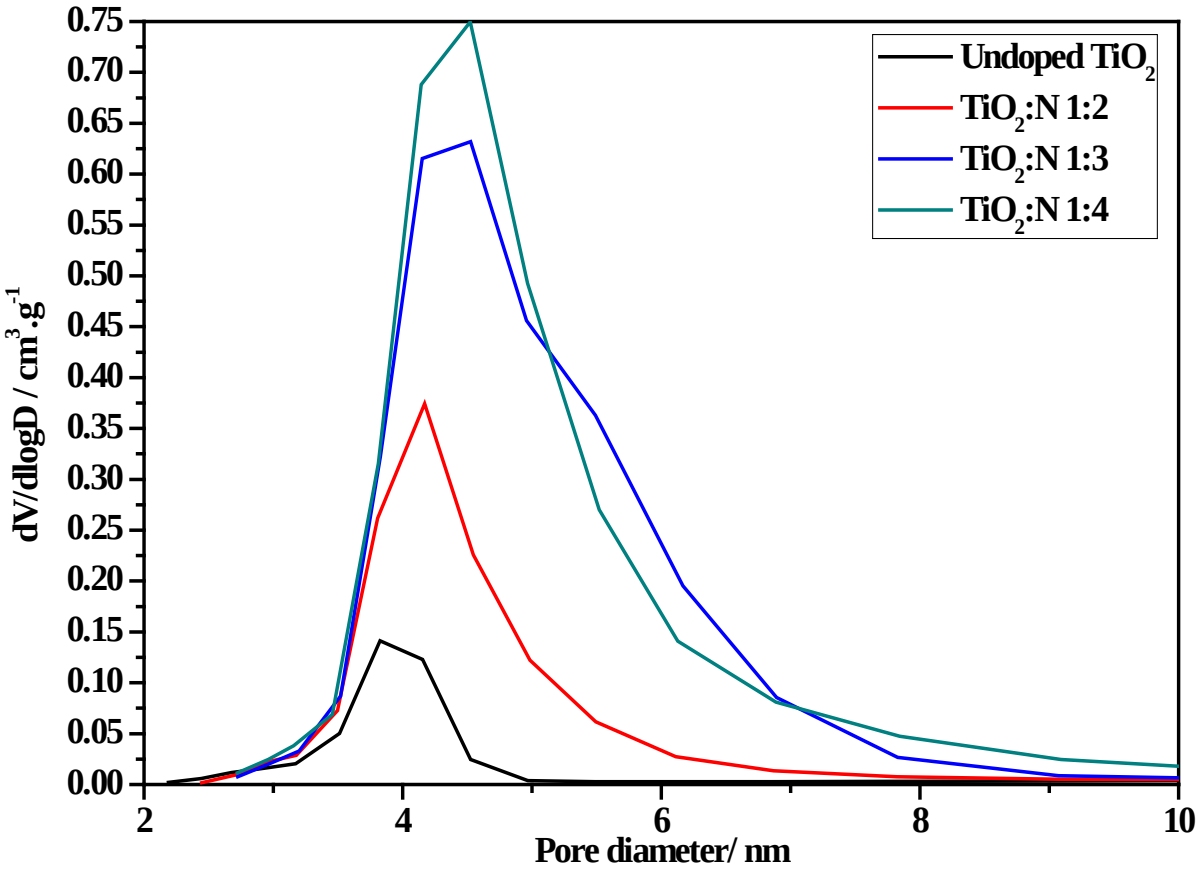

Figure 4.20: Pore size distribution of nitrogen doped catalysts.

This increase in pore size distribution with doping may indicate that doping causes less homogeneity of the pores of the catalyst [22]. The increased range over which the pore sizes are distributed may result from the formation of smaller particles. Smaller particles would result in closer packing and an increase in the amount of void spaces.

Table 4.7 shows the surface area, pore volume and pore size of the nitrogen doped catalysts. The undoped catalyst shows very low surface area of 16 $m^2.g^{-1}$. Upon doping with nitrogen there is a great increase in surface area, the surface area for the TiO_2:N 1:2 catalyst shows double the surface area with 34 $m^2.g^{-1}$. With an increase in doping with nitrogen there is an increase in the surface area of the catalyst, with the TiO_2:N 1:4 catalyst having the highest surface area of 73 $m^3.g^{-1}$. This shows that doping with nitrogen doping improves the surface area of TiO_2 which may improve the photocatalysis of TiO_2.

Table 4.7: Textural properties of nitrogen doped catalysts.

Catalyst name	BET surface area ($m^2 . g^{-1}$)	Pore volume ($cm^3 . g^{-1)}$	Pore size (nm)
Undoped TiO_2	16	0.046	9.41
TiO_2:N 1:2	34	0.066	5.42
TiO_2:N 1:3	65	0.116	4.57
TiO_2:N 1:4	73	0.125	4.61

The pore values in **Table 4.7** show that there is an increase in the pore volume with nitrogen doping. The undoped catalyst has a pore volume of 0.046 $cm^3.g^{-1}$, upon doping with nitrogen with the TiO_2:N 1:2 catalyst there is clearly an increase in pore volume 0.066 $cm^3.g^{-1}$. The pore volume increases greatly with increasing doping with the TiO_2:N 1:4 catalyst having the highest pore volume of 0.125 $cm^3.g^{-1}$ almost.

Table 4.7 also presents the results for the pore size of the catalysts. The undoped catalyst has a pore size of 9.41 nm upon doping however this decreases with the TiO_2:N 1:2 catalyst having a pore size of 5.42 nm. The pore size further decreases with doping but the TiO_2:N 1:3 and TiO_2:N 1:4 catalysts have almost the same pore size with pore sizes of 4.57 and 4.61 nm respectively. Doping with nitrogen produces smaller pore sizes than the undoped catalyst.

4.2.6 Optical Properties Ultra-Violet Diffuse Reflectance Spectroscopy on Nitrogen Doped Samples

The nitrogen doped UV-DRS spectra in **Figure 4.21** (a) show an increase in absorbance with doping. The amount of absorbance increases with increasing doping. The band edge of the absorbance spectrum shifts to longer wavelengths with increasing doping.

The Tauc plots seen in **Figure 4.21** (b) were derived from the UV-DRS spectra seen in **Figure 4.21** (a). It can be seen from **Figure 4.21** (b) that the undoped TiO_2 catalyst has a band gap of 3.0 eV which is narrower than expected of TiO_2 with solely anatase phase present. All nitrogen doped catalysts show lower band gap values than the undoped catalysts. The band gaps of the nitrogen doped catalysts clearly decrease with an increasing amount of nitrogen with the TiO_2: N 1-4 catalyst having the narrowest band gap of 2.7 eV. This indicates that there is an increase in the amount of solar spectrum that the catalysts will absorb with an increase in doping.

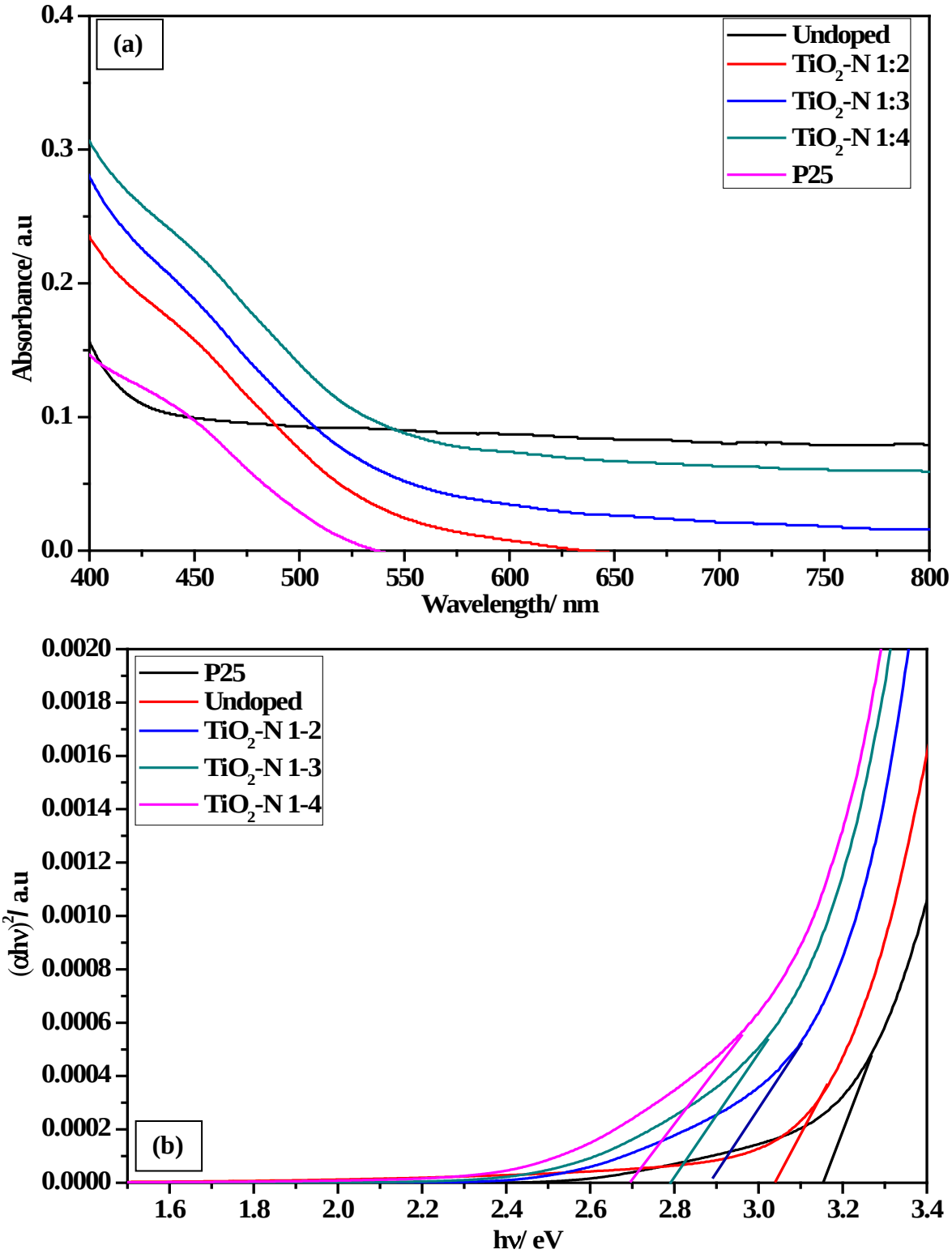

Figure 4.21: UV-DRS spectrum of nitrogen doped materials (a) and Tauc Plot of UV-DRS spectrum of nitrogen doped materials (b).

4.2.7 Photoluminescence Spectroscopy Studies of Nitrogen Doped Samples

In **Figure 4.22** there are 5 peaks of interest, these peaks occur at 422, 424, 460 and 530 nm. The first two peaks at 422 and 424 nm respectively represent self-trapped excitons (STE) localised on a TiO_6 octahedra [30-33]. The peaks at 460 and 530 nm are caused by defects related to oxygen vacancies and trap one and two electrons respectively [30-32, 35]. The peak at 491 nm is due to the charge transfer from a Ti^{3+} site to a TiO_6^{8-} complex [46].

For the nitrogen doped catalysts in **Figure 4.22** it is clear to see that with increasing doping there is a decrease in the intensity of the spectra and therefore a decrease in the rate of electron-hole recombination. This shows that the doping of TiO_2 with nitrogen reduces the rate of electron-hole recombination and therefore should allow more electrons and holes to react with the substrates. The oxygen vacancies seen in the PL spectra may be the cause of the smaller than expected band gap seen for the undoped catalyst. Oxygen vacancies introduce intermediate states between the valance and conduction bands resulting in band gap narrowing.

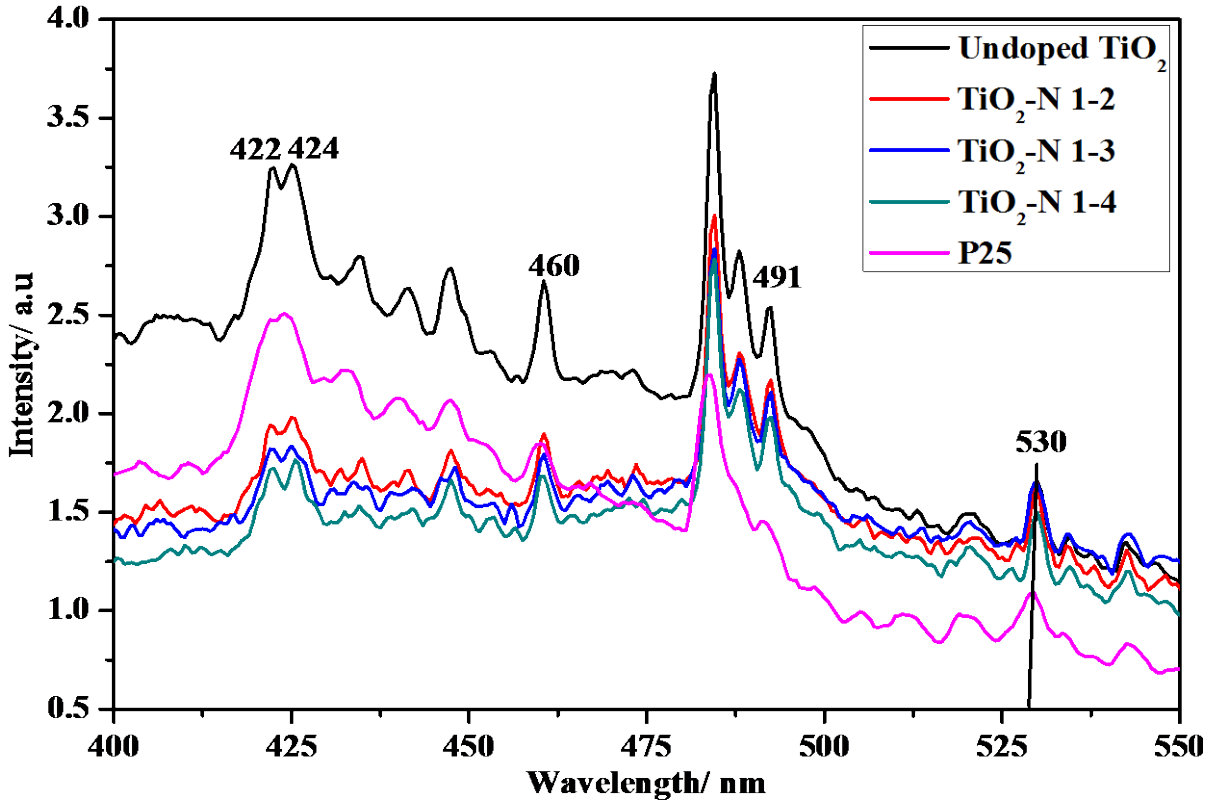

Figure 4.22: Photoluminescence spectra of nitrogen doped materials obtained using, Perkin Elmer, LS55 Fluorescence Spectrometer at 310 nm.

4.2.8 Final Comments on Nitrogen Doping

From the results obtained in this study on nitrogen doping it is expected that the nitrogen doped catalysts will have better photocatalytic activity than the undoped catalysts. The nitrogen doped catalysts all show better higher surface area compared to the undoped catalyst, therefore allowing greater adsorption of substrates. Nitrogen doping caused a narrowing of the TiO_2 band gap which should result in greater adsorption in the visible region and therefore greater electron-hole production leading to faster reaction rates. Nitrogen doping also leads to slower electron-hole recombination rates which should lead to greater lifetime of electron-holes. The greater lifetime for electron-hole pairs means more electrons

and holes will interact with substrates. From XRD it appears that nitrogen doping causes a loss of crystal structure quality and inhibits crystallite size growth.

4.3 Sulfur Doped Titanium Dioxide Samples

Sulfur doping has been shown to improve the band gap of TiO_2 such that it absorbs solar energy in the visible light region [47]. The use of sulfur as a dopant has also been shown to increase the surface area of TiO_2 in comparison of undoped TiO_2 [48]. TiO_2 doped with sulfur has also been reported to only oxidise molecules that are easily oxidised [49].

4.3.1 Quantification of Sulfur Doping Level

Amount of sulfur present in catalysts in terms of mole per mole as determined by ICP-OES

From the results in **Table 4.8** it is clear that the amount of sulfur present in the catalysts is not very close to the amounts intended. There is an increase in the amount of sulfur in the catalyst with an increasing amount of sulfur precursor used in the synthesis. The cause of the lower sulfur content present in the catalysts compared to the amount intended during synthesis, may be due to the loss of sulfur upon calcination.

Table 4.8: Ratio of titanium to sulfur as calculated from ICP-OES results. This was done as moles of sulfur per a mole of TiO_2.

Catalyst	Actually doping ratio (mol/mol)
TiO_2-S 1-2	1:0.579
TiO_2-S 1-3	1:0.675
TiO_2-S 1-4	1:0.851

4.3.2 Scanning Electron Microscopy Analysis of Sulfur Doped Samples

Figure 4.23 (a-d) shows the SEM images of the undoped TiO_2 catalyst as well as the sulfur doped catalysts. From these images it is clear that all of the catalysts have irregularly shaped particles, further there are small particles on the surface of these particles. The sizes of these particles are wide ranging for all catalysts, this shows that sulfur doping does not control the shape of the particles.

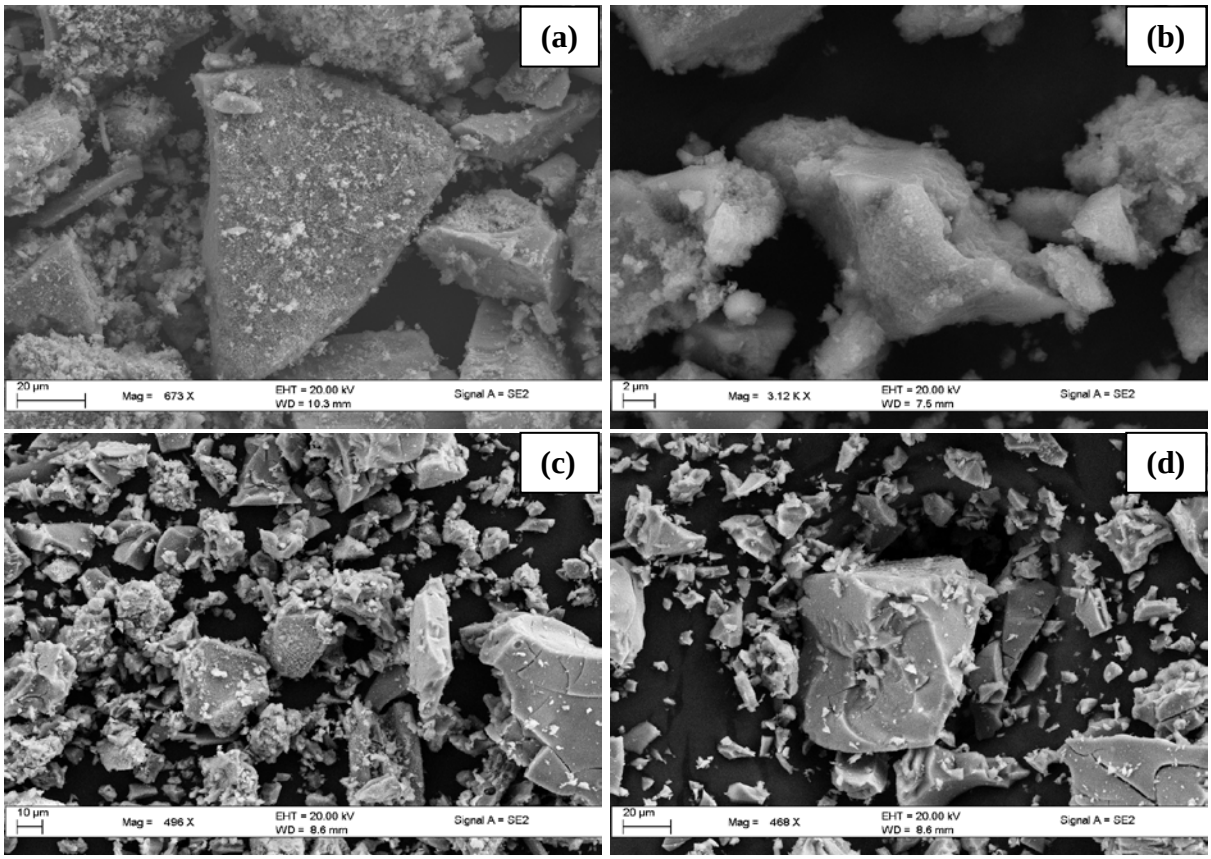

Figure 4.23: SEM images of undoped TiO_2 (a), TiO_2:S 1:2 (b), TiO_2:S 1:3 (c) and TiO_2:S 1:4 (d).

Figure 4.24 (a-d) shows higher magnification SEM images of the undoped TiO_2 catalyst and the sulfur doped catalysts. The undoped catalyst can be seen to have small particles with void space between them. The TiO_2:S 1:2 and TiO_2:S 1:3 catalysts seemingly have progressively smaller particles and void spaces. The TiO_2:S 1:4 catalysts has a different

morphology to the other catalysts and similar void spaces to the other catalysts cannot be seen however there can still be seen small particles on the surface of the catalyst.

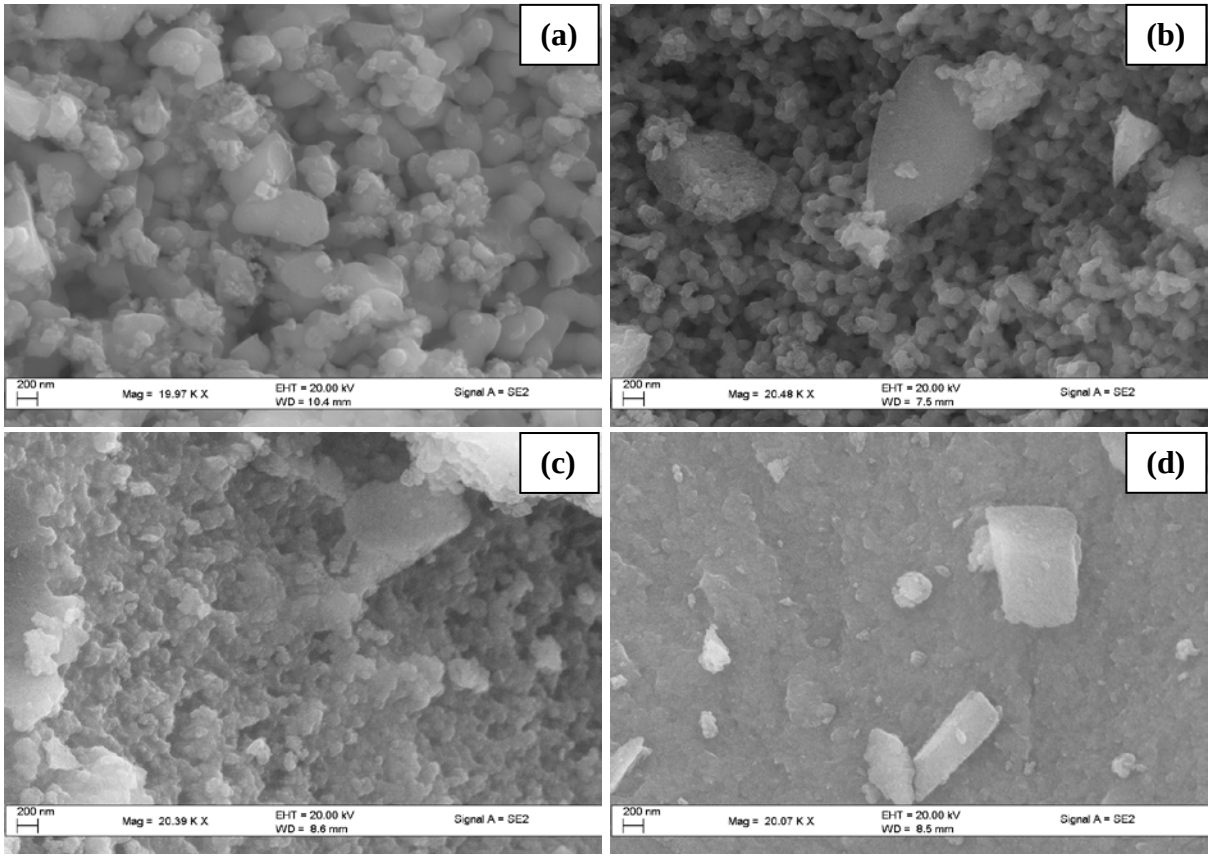

Figure 4.24: Higher magnification SEM images of undoped TiO_2 (a), TiO_2:S 1:2 (b), TiO_2:S 1:3 (c) and TiO_2:S 1:4 (d).

Figure 4.25 (a-d) shows the SEM-EDX mapping of the undoped and sulfur doped catalysts seen in **Figure 4.24** (a-d). There were only two elements detected on the surface of the undoped catalyst, namely titanium and oxygen this was expected. All the sulfur doped catalysts appears to have a high dispersion of sulfur on the surface of the catalysts and agglomeration of sulfur is not apparent.

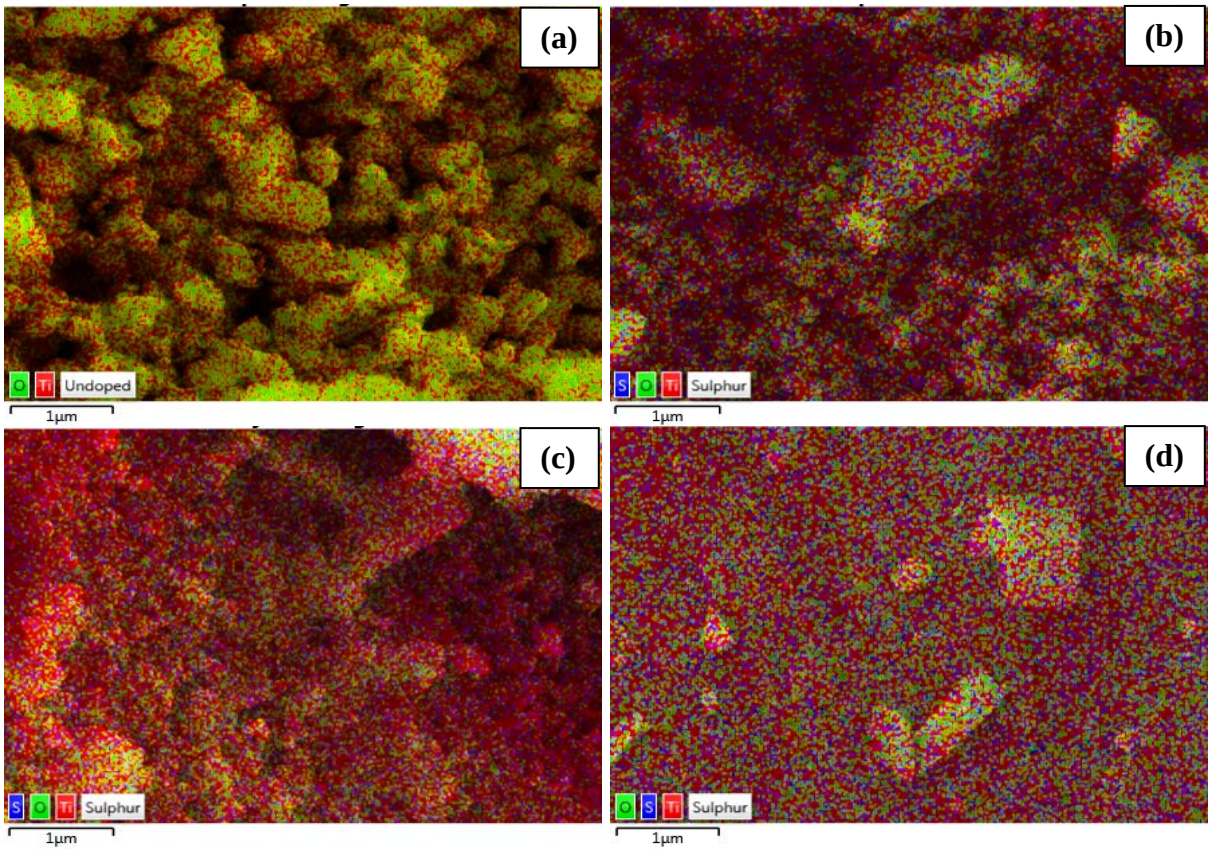

Figure 4.25: SEM-EDX mapping of undoped TiO_2 (a), TiO_2:S 1:2 (b), TiO_2:S 1:3 (c) and TiO_2:S 1:4 (d).

4.3.3 Transmission Electron Microscopy Observations on the Sulfur Doped Samples

Figure 4.26 (a-d) shows the TEM images of the undoped TiO_2 catalyst as well as the all the sulfur doped catalysts. It can be seen in these images that the particles of all catalysts are irregularly shaped, the size of these irregularly shaped particles vary greatly. It can be seen from these images that sulfur doping does not have any effect on the shape of the particles. Making an assessment of the effect of sulfur doping on the size of these particles are difficult given the range of sizes over which these particles are distributed.

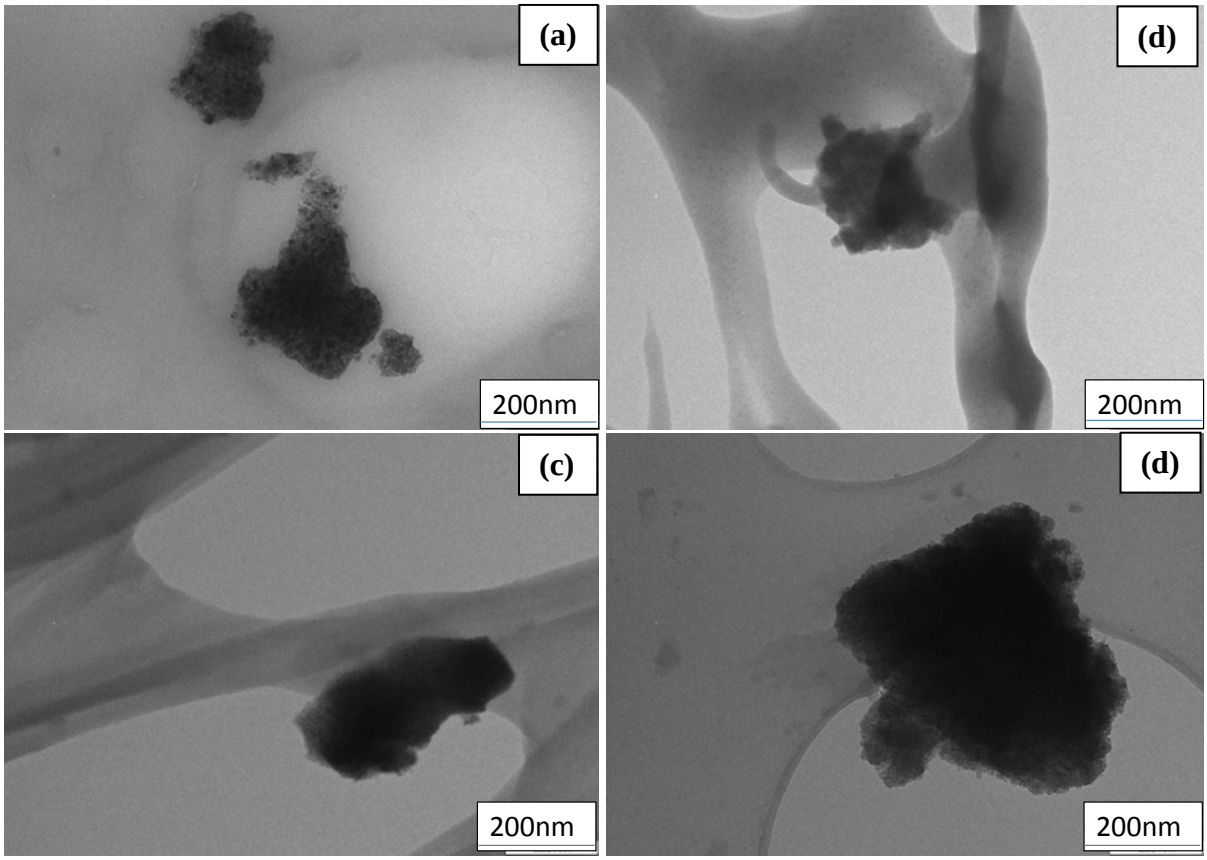

Figure 4.26: TEM images of undoped TiO_2 (a), TiO_2:S 1:2 (b), TiO_2:S 1:3 (c) and TiO_2:S 1:4 (d).

Figure 4.27 (a-d) higher magnification TEM images of the same areas shown in **Figure 4.20** of the undoped catalyst as well as the sulfur doped catalysts. From these images it appears as though the particles shown in **Figure 4.26** (a-d) are made up of smaller particles.

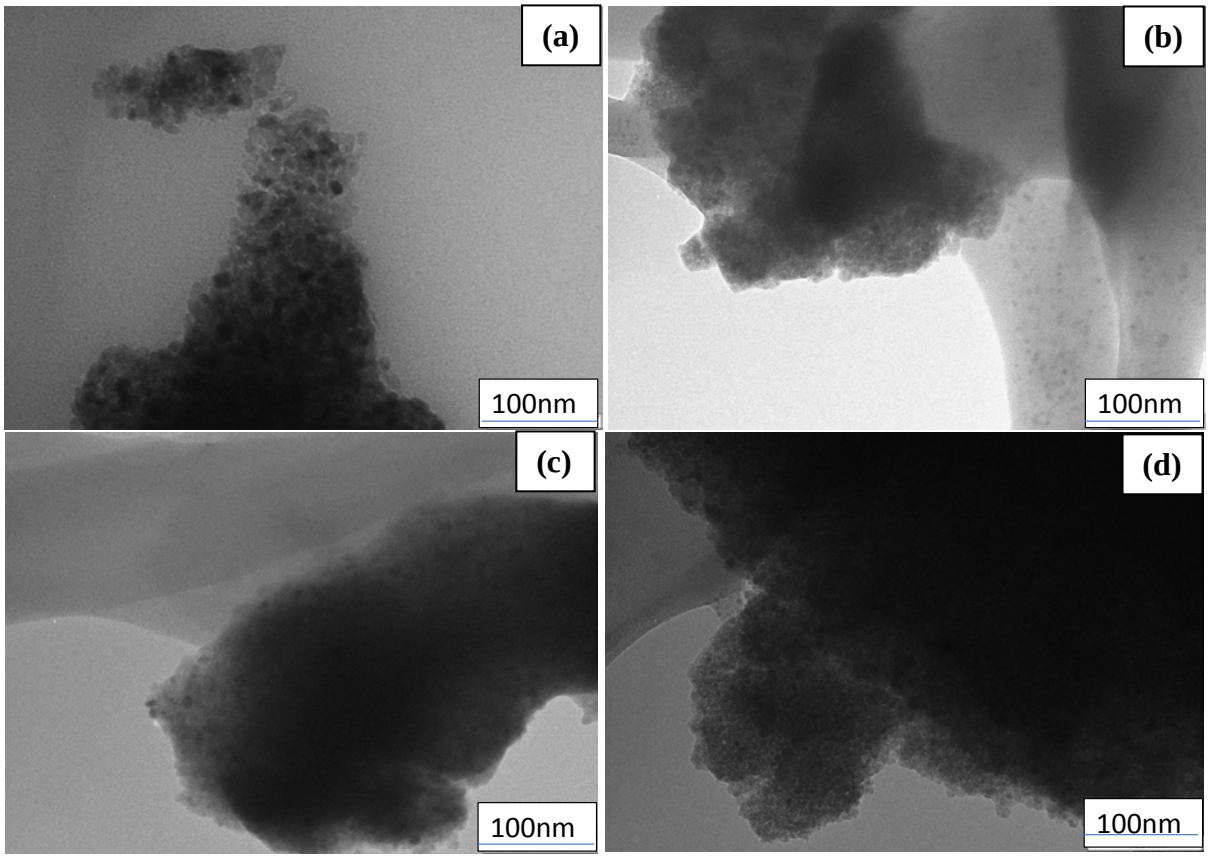

Figure 4.27: Higher magnification TEM images of undoped TiO_2 (a), TiO_2:S 1:2 (b), TiO_2:S 1:3 (c) and TiO_2:S 1:4 (d).

4.3.4 XRD

Figure 4.28 shows the XRD diffractogram patterns for the sulfur doped TiO_2 materials. It can be seen from **Figure 4.28** that the diffractogram patterns of all of the catalysts match that of anatase TiO_2 (JCPDS 00-021-1272). Upon comparing the JCPDS (00-021-1276) file for TiO_2 rutile phase with the diffractogram patterns for the catalysts it can be seen that the rutile phase is not present in any of the catalysts. Inset there is a magnified view of the 101 diffraction peak of the catalysts, it can be seen that with doping there is a decrease in peak intensity and there is a shift to the right.

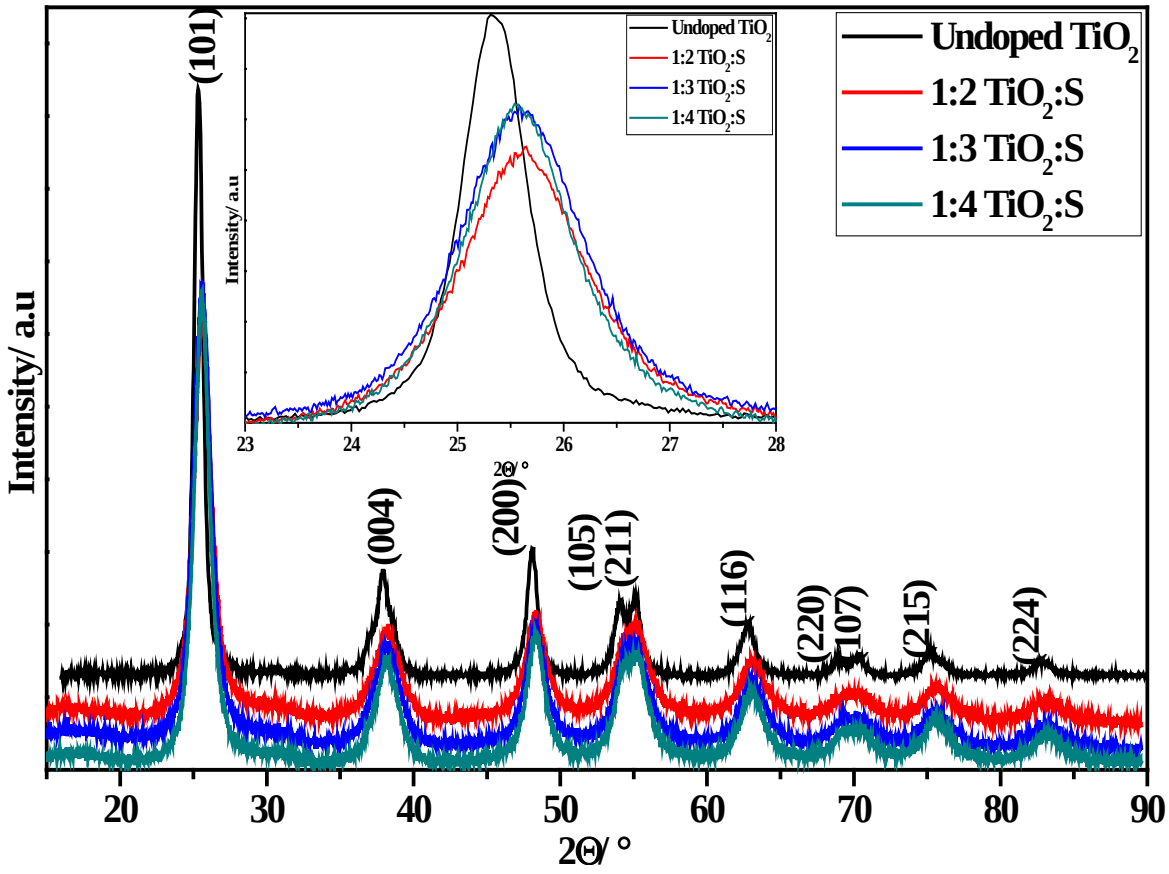

Figure 4.28: XRD diffractogram patterns of undoped and sulfur doped titanium dioxide materials. Inset magnified view of the 101 diffraction peak.

Table 4.9 shows the crystallite size of the sulfur doped catalysts, these values were calculated from the 101 diffraction peak. It can be seen that when that for the lowest sulfur doped catalyst namely TiO_2:S 1:2 there is a reduction in crystallite size compared to the undoped catalyst. However after the initial doping there is an increase in the crystallite size and TiO_2:S 1:3 and TiO_2:S 1:4 have crystallite sizes greater than TiO_2:S 1:2. Yu *et al* reported that sulfur doping inhibits the growth of TiO_2 crystals [50]. Ho *et al* reported increasing crystallite size with increasing sulfur content in TiO_2; a hydrothermal synthesis method was used in this study [51]. Given that the findings of the effect of sulfur on the crystallite size are different, it is possible that for the method used in this study that after a certain doping concentration the crystallite growth was promoted.

The ‘a’ and ‘c’ parameters for the sulfur doped catalysts can be found in **Table 4.9**, these calculations were done using the 200 and 004 diffraction peaks as shown for the copper doped catalysts. The ‘a’ parameter for the sulfur doped catalysts is slightly smaller than that of the undoped catalyst. The ‘a’ parameter for the doped catalysts is nearly identical. The ‘c’ parameter of all sulfur doped catalysts also show a reduction compared to the undoped catalyst. The reduction of the ‘a’ and ‘c’ parameters compared to the undoped catalyst are very small and do not show a continuous decrease with increasing doping.

Table 4.9: Lattice parameters and cell volume for sulfur doped photocatalysts.

Catalyst name	Crystallite size/nm	a = b (nm)	c (nm)	Cell volume (nm^3)	d-spacing/ nm
Undoped TiO_2	10.50	0.3786	0.9492	0.1360	0.352
TiO_2:S 1:2	5.45	0.3767	0.9433	0.1339	0.347
TiO_2:S 1:3	5.58	0.3768	0.9435	0.1340	0.348
TiO_2:S 1:4	6.06	0.3769	0.9437	0.1340	0.348

The d-spacing values of the sulfur doped catalysts are presented in **Table 4.9**; these values were calculated using the 101 diffraction peak as shown for the copper doped catalysts. The d-spacing values of the sulfur doped catalysts shows a slight reduction compared to that of the undoped catalyst. This is supported by the fact that there is a shift to higher 2θ values of the 101 peak for the sulfur doped catalysts in relation to the undoped catalyst, seen inset **Figure 4.28**. This may indicate strain induced by doping.

4.3.5 Raman

Figure 4.29 shows the Raman spectra of the sulfur doped catalysts. The spectra of all catalysts presented in **Figure 4.29** show three dominate peaks; these peaks belong to B_{1g}, A_{1g} and E_g modes of anatase TiO_2. The wavenumbers for these modes are 410, 528 and 649 cm^{-1}

for B1g, A_{1g} and E_g respectively. These results confirm the finds of the XRD diffractograms which show only anatase TiO_2 is present in the catalysts.

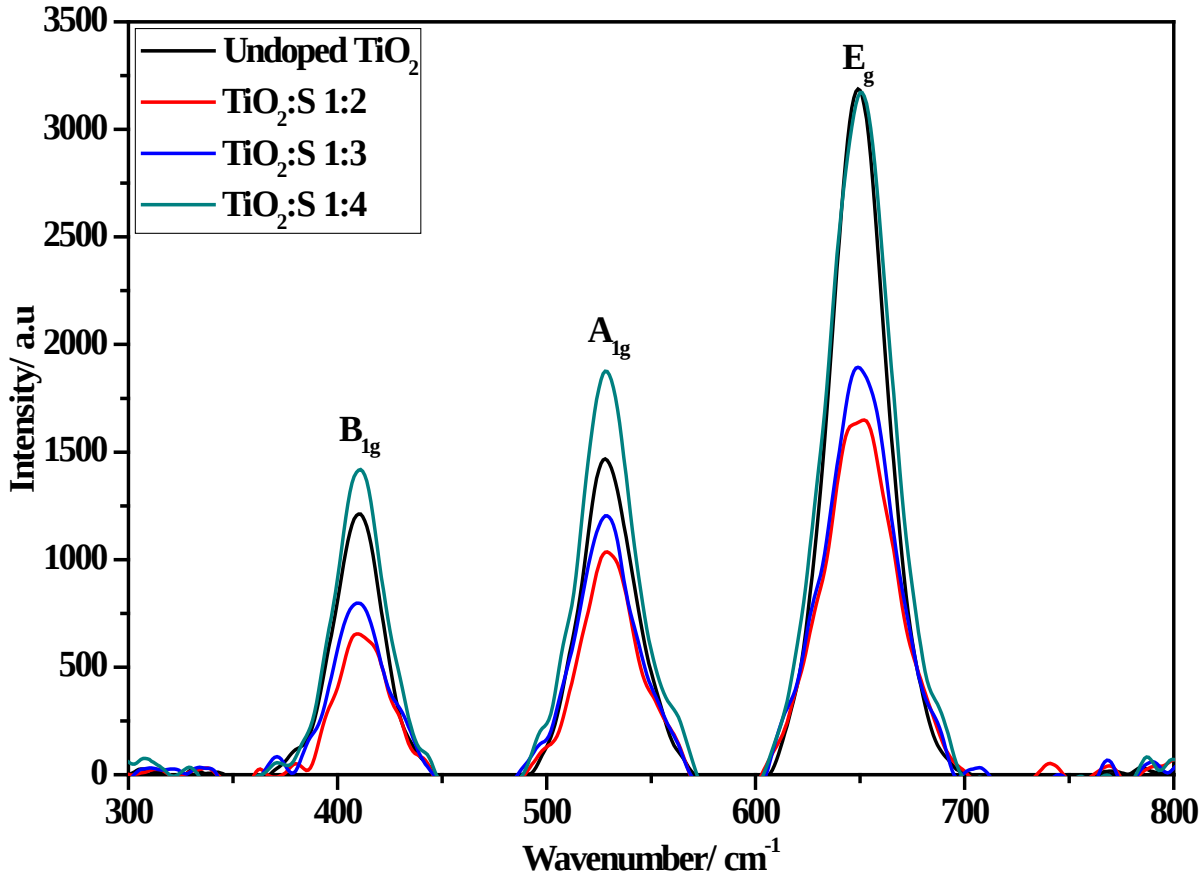

Figure 4.29: Raman spectra of sulfur doped titanium dioxide catalysts showing the various active modes for the anatase phase.

Table 4.10 shows the FWHM for the E_g peak of each catalyst, these results are compared to the results in **Table 4.9**. The FWHM of the TiO_2:S 1:2 catalyst increases from that of the undoped catalyst, there after there is a decrease in the FHWM for the remaining catalysts. Given that according to the phonon confinement effect means that the crystallite size and the FWHM from Raman are inversely related these results are expected. These results confirm the findings of crystallite size from XRD.

Table 4.10: FWHM of the Eg peak from the Raman spectra of the sulfur doped TiO2 catalysts.

Catalyst	FWHM (cm^{-1})
Undoped TiO_2	31.74
TiO_2:S 1:2	40.00
TiO_2:S 1:3	38.03
TiO_2:S 1:4	35.64

4.3.6 Textural Characteristics of the Sulfur Doped Samples

Figure 4.30 shows the isotherms of the sulfur doped catalysts obtained from nitrogen physisorption. The isotherms of all catalysts are type IV according to IUPAC classifications. This means that all of the catalysts are mesoporous [19]. The hysteresis loop of each catalyst is H2 according to IUPAC classifications, this shows that pores of all catalysts are disordered and there is blockage of the pores [19]. No surfactant was used in the making of any of these catalysts so the porosity seen may result from the aggregation of particles and therefore interparticle voids. In **Figure 4.24** interparticle voids are seen and in **Figure 4.26** the aggregation of particles are seen it is possible that the pores originate from this. There is increase in the volume of nitrogen adsorbed with increasing doping. There is a slight shift of the start of the hysteresis loop to lower partial pressures and a slight shift to higher partial pressures for the closure of the hysteresis loop with increasing doping.

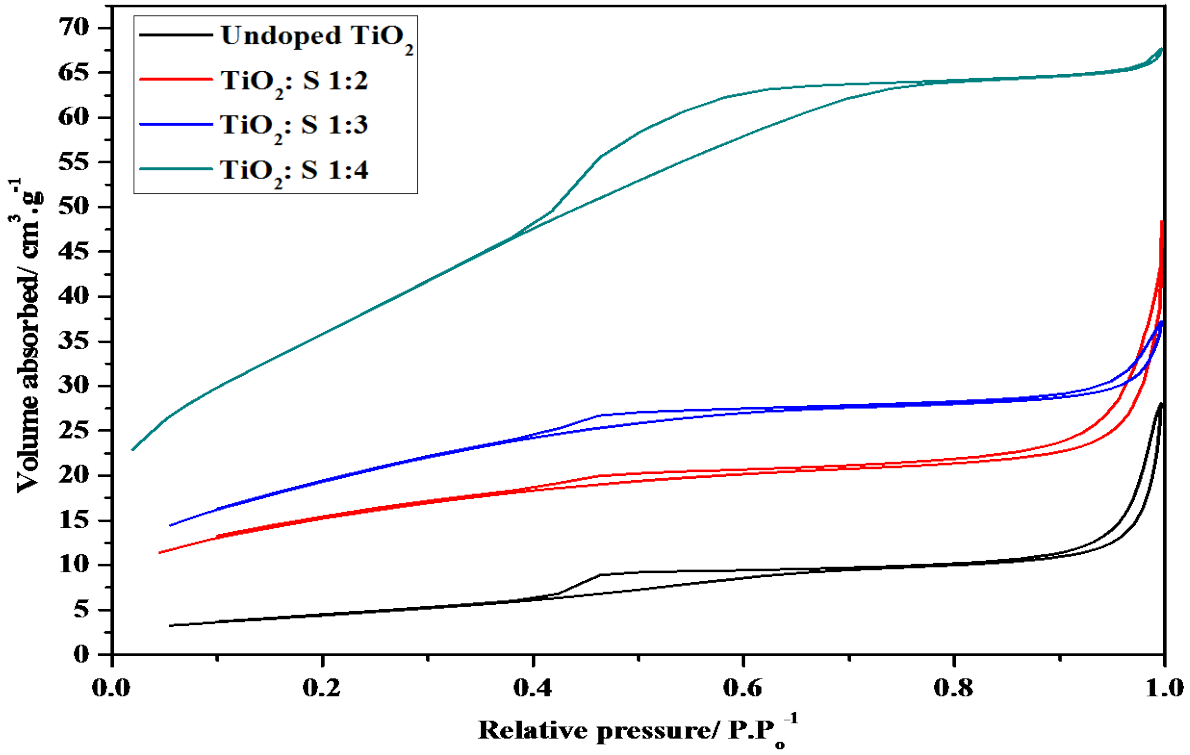

Figure 4.30: Isotherms of nitrogen doped catalysts as obtained from sulfur physisorption.

Figure 4.31 shows the pore size distribution of sulfur doped catalysts as well as the undoped catalyst. The undoped TiO_2 catalyst has a maximum centred on 4 nm, with a distribution range from 2 nm to 5 nm. For the sulfur doped catalysts the pore size distribution of all catalysts are also centred on 4 nm. The TiO_2-S 1-2 and TiO_2-S 1-3 catalysts show the same range of distribution of pores as the undoped catalyst. The TiO_2-S 1-4 catalyst shows a wider range of distribution of pores than all the other catalysts, with pores ranging from 2 nm to 8 nm. No surfactant was used in the making of these catalysts so these pore volumes may result from the void spaces seen in **Figure 4.24** (a-e).

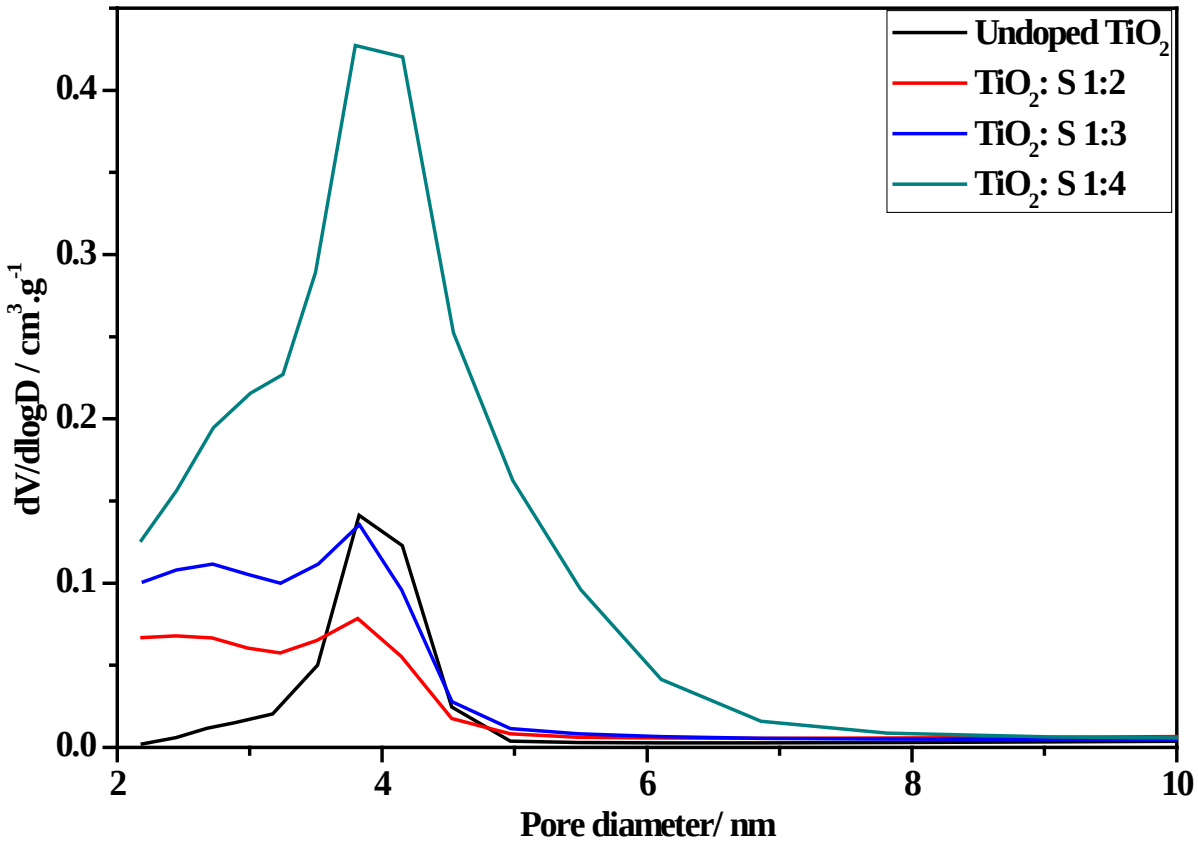

Figure 4.31: Pore size distribution of sulfur doped catalysts.

Table 4.11 presents the surface area of the sulfur doped TiO_2 materials. The TiO_2:S 1:2 catalyst shows more than three times greater surface area than the undoped catalyst with a surface area of 52 $m^2.g^{-1}$ compared to 16 $m^2.g^{-1}$. The surface area shows a linear increase with increasing doping with the TiO_2:S 1:4 catalyst having the highest surface area. From the results in **Table 4.11** it is possible to say that doping TiO_2 with sulfur results in increased surface area.

The pore volume of the sulfur doped catalysts is shown in **Table 4.11**. Sulfur doping appears to increase the pore volume of TiO_2 with all the sulfur doped catalysts having greater pore volumes compared to the undoped catalyst. The TiO_2:S 1:2 and TiO_2:S 1:3 catalysts have very similar pore volumes of 0.059 and 0.051 $cm^3.g^{-1}$ respectively. This may be due to experimental error. The TiO_2:S 1:4 catalyst shows the largest pore volume of 0.108 $cm^3.g^{-1}$.

Table 4.11: Textural properties of sulfur doped catalysts.

Catalyst name	BET surface area ($m^2 . g^{-1}$)	Pore volume ($cm^3 . g^{-1)}$	Pore size (nm)
Undoped TiO_2	16	0.046	9.41
TiO_2:S 1:2	52	0.059	4.70
TiO_2:S 1:3	69	0.051	4.21
TiO_2:S 1:4	130	0.108	3.52

From the pore sizes presented in **Table 4.11** it can be seen that sulfur doping results in lower pore sizes than the undoped catalyst. The decrease in the pore size is linear with increasing doping with the TiO_2:S 1:4 catalyst having the smallest pore size of 3.52 nm. This lower pore size may result from smaller particles packing closer together.

4.3.7 Optical Properties Ultra-Violet Diffuse Reflectance Spectroscopy on Sulfur Doped Samples

Figure 4.32 (a) shows the UV-DRS spectra of the sulfur doped catalysts, the sulfur doped catalysts show a large increase in absorbance with doping. Inset in **Figure 4.32** (a) is the UV-DRS spectra of the TiO_2: S 1-3 catalyst, which has the same absorbance spectrum as the TiO_2: S 1-4 catalyst.

It can be seen in **Figure 4.32** (b), which was obtained by conversion of the UV-DRS spectra in **Figure 4.32** (a), that sulfur doping greatly reduces the band gap of TiO_2. All sulfur doped catalysts have far narrower band gaps than the undoped TiO_2 catalyst. The TiO_2: S 1-3, seen inset of **Figure 4.32** (b), and the TiO_2: S 1-4 catalysts have the same band gap of 2.4 eV. This shows that any increase in doping level will not result in a decrease in the band gap. The results prove that sulfur doping improves the amount of the solar spectrum that TiO_2 absorbs.

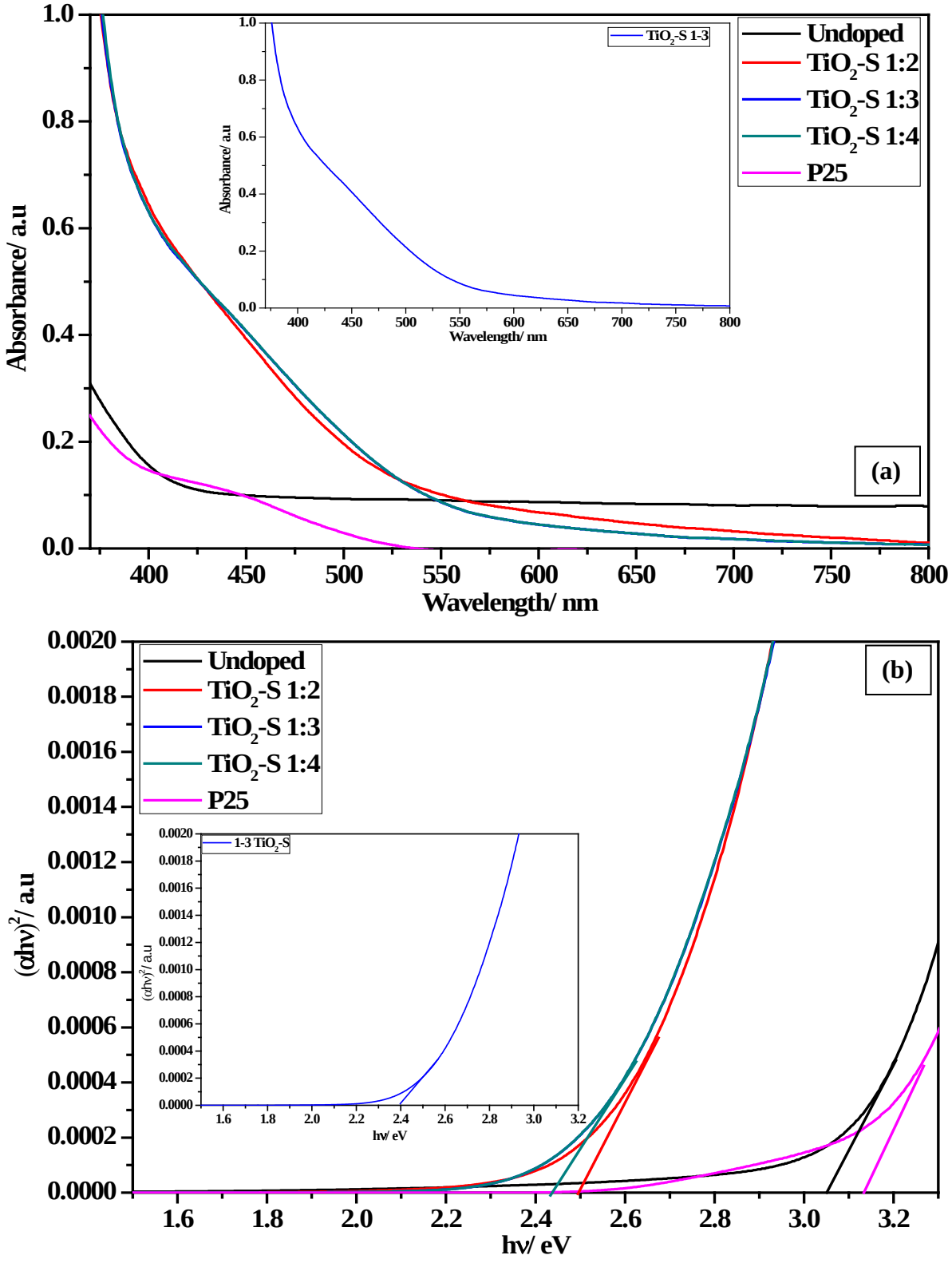

Figure 4.32: UV-DRS spectrum of sulfur doped materials (a) and Tauc Plot of UV-DRS spectrum of sulfur doped materials (b).

4.3.8 Photoluminescence Spectroscopy Studies of Sulfur Doped Samples

Figure 4.33 has 5 peaks of interest, these peaks occur at 422, 424, 460 and 530 nm. The first two peaks at 422 and 424 nm respectively represent self-trapped excitons (STE) localised on a TiO_6 octahedra [30-33]. The peaks at 460 and 530 nm are caused by defects related to oxygen vacancies and trap one and two electrons respectively [30-32, 35]. The peak at 491 nm is due to the charge transfer from a Ti^{3+} site to a TiO_6^{8-} complex [46].

For the sulfur doped catalysts in **Figure 4.33** (b) above it can be seen that initially there is a drastic reduction in the intensity for TiO_2:S 1-2 catalyst compared to the undoped TiO_2 catalyst. However with increasing sulfur doping there is an increase in intensity of the spectra. These results show that with the initial sulfur doping content the electron-hole recombination rate is lowered compared to the undoped catalysts, any further doping results in an increase in the electron-hole recombination in comparison to the TiO2:S 1:4 catalyst.

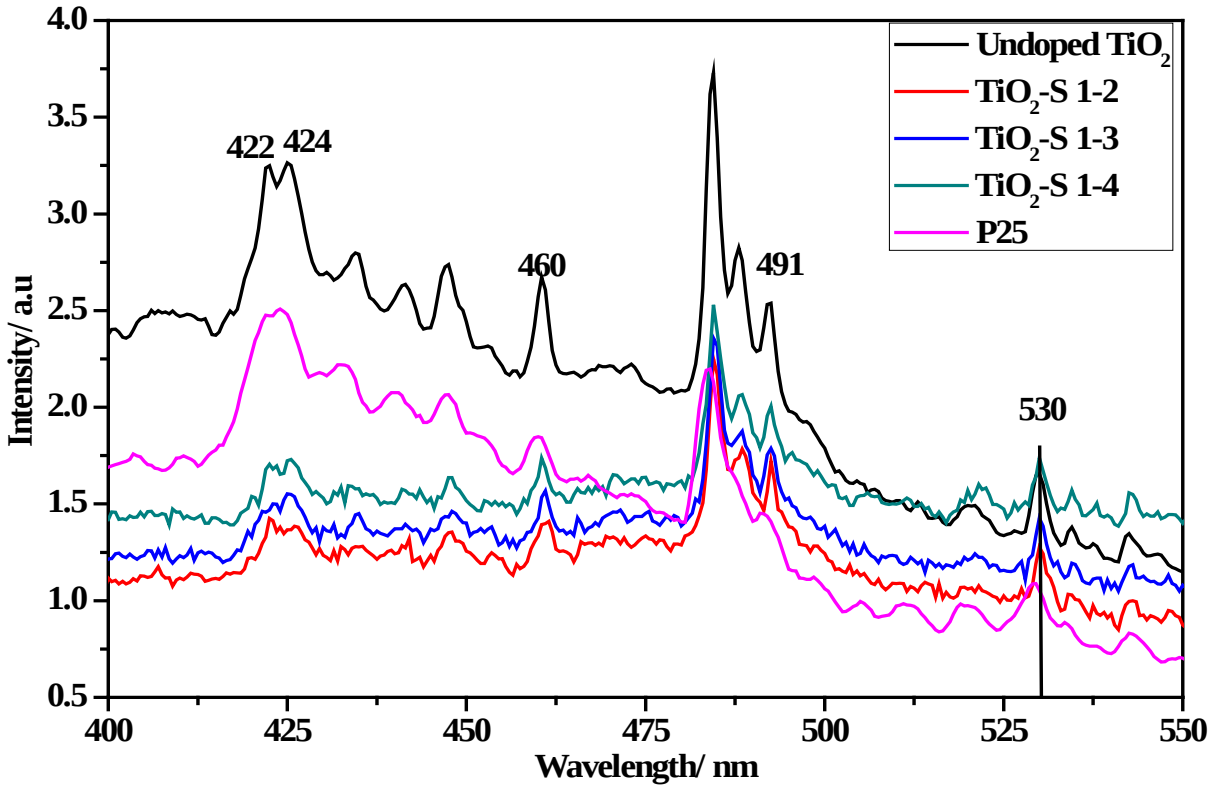

Figure 4.33: Photoluminescence spectra of sulfur doped materials obtained using, Perkin Elmer, LS55 Fluorescence Spectrometer at 310 nm.

4.3.9 Final Comments on Sulfur doping

From the results of this study it is evident that doping TiO_2 with sulfur provides a number of changes in TiO_2 that would improve photocatalytic activity. Sulfur doping improves the surface area of TiO_2 compared to undoped TiO_2 and this change is linear for the series of catalysts. The improvement in surface area should result in an improvement in the amount of substrate adsorbed and the amount of light reaching the surface of the catalyst. Sulfur doping also greatly reduces the band gap of TiO_2 compared to the undoped catalyst, however at a doping a level of TiO_2:S 1:3 this reaches it limit. Further sulfur doping will not narrow the

band gap any further. Sulfur doping also reduces electron-hole pair recombination though at high sulfur concentration it promotes recombination.

References

1. T.-T. Pham, C. Nguyen-Huy, H.-J. Lee, T.-D. Nguyen-Phan, T.H. Son, C.-K. Kim, and E.W. Shin, *Cu-doped TiO2/reduced graphene oxide thin-film photocatalysts: Effect of Cu content upon methylene blue removal in water.* Ceramics International, 2015. **41**(9, Part A): p. 11184-11193.
2. B. Xin, P. Wang, D. Ding, J. Liu, Z. Ren, and H. Fu, *Effect of surface species on Cu-TiO 2 photocatalytic activity.* Applied surface science, 2008. **254**(9): p. 2569-2574.
3. H. Sutrisno and S. Sunarto, *Polymorphic transformation of titanium dioxide caused by heat treatment of protonic lepidocrocite titanate.* Indonesian Journal of Chemistry, 2010. **10**(2): p. 143-148.
4. Slamet, H.W. Nasution, E. Purnama, S. Kosela, and J. Gunlazuardi, *Photocatalytic reduction of CO2 on copper-doped Titania catalysts prepared by improved-impregnation method.* Catalysis Communications, 2005. **6**: p. 313-319.
5. B. Choudhury, M. Dey, and A. Choudhury, *Defect generation, dd transition, and band gap reduction in Cu-doped TiO2 nanoparticles.* International Nano Letters, 2013. **3**(1): p. 1-8.
6. J. Navas, A. Sánchez-Coronilla, T. Aguilar, M. Desireé, N.C. Hernández, R. Alcántara, C. Fernández-Lorenzo, and J. Martín-Calleja, *Thermo-selective Tm x Ti 1− x O 2− x/2 nanoparticles: from Tm-doped anatase TiO 2 to a rutile/pyrochlore Tm 2 Ti 2 O 7 mixture. An experimental and theoretical study with a photocatalytic application.* Nanoscale, 2014. **6**(21): p. 12740-12757.
7. M. Prekajski, A. Zarubica, B. Babić, B. Jokić, J. Pantić, J. Luković, and B. Matović, *Synthesis and characterization of Cr3+ doped TiO2 nanometric powders.* Ceramics International.

8. A. Trenczek-Zajac, M. Radecka, M. Jasinski, K.A. Michalow, M. Rekas, E. Kusior, K. Zakrzewska, A. Heel, T. Graule, and K. Kowalski, *Influence of Cr on structural and optical properties of TiO2:Cr nanopowders prepared by flame spray synthesis.* Journal of Power Sources, 2009. **194**(1): p. 104-111.

9. T.M. Breault and B.M. Bartlett, *Composition Dependence of TiO2:(Nb,N)-x compounds on the rate of photocatalytic methylene blue dye degradation.* The Journal of Physical Chemistry C, 2013. **117**(17): p. 8611-8618.

10. J. Navas, A. Sánchez-Coronilla, T. Aguilar, N.C. Hernández, M. Desireé, J. Sánchez-Márquez, D. Zorrilla, C. Fernández-Lorenzo, R. Alcántara, and J. Martín-Calleja, *Experimental and theoretical study of the electronic properties of Cu-doped anatase TiO 2.* Physical Chemistry Chemical Physics, 2014. **16**(8): p. 3835-3845.

11. B. Rajamannan, S. Mugundan, G. Viruthagiri, P. Praveen, and N. Shanmugam, *Linear and nonlinear optical studies of bare and copper doped TiO 2 nanoparticles via sol gel technique.* Spectrochimica Acta Part A: Molecular and Biomolecular Spectroscopy, 2014. **118**: p. 651-656.

12. J. Surmacki, P. Wroński, M. Szadkowska-Nicze, and H. Abramczyk, *Raman spectroscopy of visible-light photocatalyst–Nitrogen-doped titanium dioxide generated by irradiation with electron beam.* Chemical Physics Letters, 2013. **566**: p. 54-59.

13. W.Ma, Z. Lu, and M.Zhang, *Investigation of structural transformations in nanophase titanium dioxide by Raman spectroscopy.* Applied physics A: Materials Science and Processing, 1998. **66**: p. 621-627.

14. S.M. Soosen, K. Jiji, C. Anoop, and K.C. George, *Optical phonon confinement in ZnO nanorods and nanotubes.* Indian Journal of Pure & Applied Physics, 2010. **48**: p. 703-708.

15. W.F. Zhang, Y.LHe, M.S. Zhang, Z. Yin, and Q. Chen, *Raman scattering study on anatase TiO2 nanocrystals.* Journal of Physics D: Applied Physics, 2000. **33**: p. 912-916.

16. M. Dimitrievska, A. Fairbrother, V. Izquierdo-Roca, Perez-Rodrıguez, and E. Saucedo, *Raman scattering crystalline assessment of polycrystalline Cu2ZnSnS4 thin films for sustainable photovoltaic technologies: Phonon confinement model.* Acta Materialia, 2014. **70**: p. 272-280.

17. W.F. Zhang, M.S. Zhang, Z. Yin, and Q. Chen, *Photoluminescence in anatase titaniumdioxide nanocrystals.* Applied Physics B: Lasers and Optics, 2000. **70**: p. 261-265.

18. H.C. Choi, Y.M. Jung, and S.B. Kim, *Size effects in the Raman spectra of TiO2 nanoparticles.* Vibrational Spectroscopy, 2005. **37**: p. 33-38.

19. K.S.W. Sing, D.H. Everett, R.A.W. Haul, L. Moscou, R.A. Pierotti, J. Rouquerol, and T. Siemienewska, *Reproting physisorption data for gas/solid systems.* Pure and Applied Chemistry, 1984. **57**(4): p. 603-619.

20. J.R. De la Rosa, C.J. Lucio-Ortiz, A.H. Ramirez, G.A. Flores-Escamilla, and C.D. Garcia, *Photocatalytic degradation of trichloroethylene in a continuous annular reactor using Cu-doped TiO 2 catalysts by sol-gel synthesis.* Applied Catalysis B: Environmental, 2015.

21. J. Rouquerol, D. Avnir, C. Fairbridge, D. Everett, J. Haynes, N. Pernicone, J. Ramsay, K. Sing, and K. Unger, *Recommendations for the characterization of porous solids (Technical Report).* Pure and Applied Chemistry, 1994. **66**(8): p. 1739-1758.

22. Y. Zhang, G. Li, Y. Wu, Y. Luo, and L. Zhang, *The formation of mesoporous TiO2 spheres via a facile chemical process.* The Journal of Physical Chemistry B, 2005. **109**(12): p. 5478-5481.

23. R.S. Wong, J. Feng, X. Hu, and P.L. Yue, *Discoloration and mineralization of non-biodegradable azo dye orange II by copper-doped TiO2 nanocatalysts.* Journal of Environmental Science and Health, Part A, 2004. **39**(10): p. 2583-2595.

24. R. López, R. Gómez, and M.E. Llanos, *Photophysical and photocatalytic properties of nanosized copper-doped titania sol–gel catalysts.* Catalysis Today, 2009. **148**(1): p. 103-108.

25. G. Wang, L. Xu, J. Zhang, T. Yin, and D. Han, *Enhanced photocatalytic activity of TiO2 powders (P25) via calcination treatment.* International Journal of Photoenergy, 2012. **2012**: p. 9.

26. M. Feneberg, S. Osterburg, K. Lange, C. Lidig, B. Garke, R. Goldhahn, E. Richter, C. Netzel, M.D. Neumann, N. Esser, S. Fritze, H. Witte, J. Bläsing, A. Dadgar, and A. Krost, *Band gap renormalization and Burstein-Moss effect in silicon- and germanium-doped wurtzite GaN up to ${10}^{20}~\mathrm{cm}{}^{$-${}3}$.* Physical Review B, 2014. **90**(7): p. 075203.

27. H.P.D. Schenk, S.I. Borenstain, A. Berezin, A. Schön, E. Cheifetz, S. Khatsevich, and D.H. Rich, *Band gap narrowing and radiative efficiency of silicon doped GaN.* Journal of Applied Physics, 2008. **103**(10): p. 103502.

28. E. Burstein, *Anomalous Optical Absorption Limit in InSb.* Physical Review, 1954. **93**(3): p. 632-633.

29. K.F. Berggren, B.E. Sernelius, L. Engström, I. Hamberg, and C.G. Granqvist, *Bandgap widening in heavily Sn-doped In2O3*, in *Proceedings of the 17th International Conference on the Physics of Semiconductors*, J. Chadi and W. Harrison, Editors. 1985, Springer New York. p. 1051-1054.

30. B. Choudhury and A. Choudhury, *Luminescence characteristics of cobalt doped TiO2 nanoparticles.* Journal of Luminescence, 2012. **132**: p. 178-184.

31. B. Choudhury and A. Choudhury, *Oxygen vacancy and dopant concentration dependent magnetic properties of Mn doped TiO2 nanoparticle.* Current Applied Physics, 2013. **13**: p. 1025-1031.

32. B. Choudhury and A.Choudhury, *Tailoring luminescence properties of TiO2 nanoparticles by Mn doping.* Journal of Luminescence, 2013. **136**: p. 339-346.

33. Y. Lei, L.D. Zhang, G. W. Meng, G.H. Li, X.Y. Zhang, C.H. Liang, W. Chen, and S.X. Wang, *Preparation and photoluminescence of highly ordered TiO2 nanowire arrays.* Applied Physics Letters, 2001. **78**(8): p. 1125-1127.

34. M.A. Pugachevsky, *Effect of annealing on photoluminescent properties of titanium dioxide nanoparticles.* Journal of Applied Spectroscopy, 2012. **79**(5): p. 834-837.

35. M. Tahir and N.S. Amin, *Indium-doped TiO2 nanoparticles for photocatalytic CO2 reduction with H2O vapors to CH4.* Applied Catalysis B: Environmental, 2015. **162**: p. 98-109.

36. M.A. Henderson and M. A, *A surface science perspective on TiO 2 photocatalysis.* Surface Science Reports, 2011. **66**(6): p. 185-297.

37. P.A. Osorio-Vargas, C. Pulgarin, A. Sienkiewicz, L.R. Pizzio, M.N. Blanco, R.A. Torres-Palma, C. Pétrier, and J.A. Rengifo-Herrera, *Low-frequency ultrasound induces oxygen vacancies formation and visible light absorption in TiO2 P-25 nanoparticles.* Ultrasonics Sonochemistry, 2012. **19**(3): p. 383-386.

38. M.K. Nowotny, L.R. Sheppard, T. Bak, and J. Nowotny, *Defect chemistry of titanium dioxide. Application of Defect Engineering in Processing of TiO2-Based Photocatalysts.* journal of Physical Chemistry C, 2008. **112**: p. 5275-5300.

39. G. Liu, L. Wang, H.G. Yang, H. Cheng, and G.Q. Lu, *Titania-based photocatalysts—crystal growth, doping and heterostructuring.* Journal of Materials Chemistry, 2009. **20**: p. 831-843.

40. G. Liu, H.G. Yang, J. Pan, Y.Q. Yang, G.Q. Lu, and H.M. Cheng, *Titanium dioxide crystals with tailored facets.* Chem Rev, 2014. **114**(19): p. 9559-612.

41. L.G. Devi, B. Nagaraj, and K.E. Rajashekhar, *Synergistic effect of Ag deposition and nitrogen doping in TiO 2 for the degradation of phenol under solar irradiation in presence of electron acceptor*. Chemical Engineering Journal, 2012. **181**: p. 259-266.

42. L. Zeng, W. Song, M. Li, X. Jie, D. Zeng, and C. Xie, *Comparative study on the visible light driven photocatalytic activity between substitutional nitrogen doped and interstitial nitrogen doped TiO 2.* Applied Catalysis A: General, 2014. **488**: p. 239-247.

43. C. Di Valentin, G. Pacchioni, A. Selloni, S. Livraghi, and E. Giamello, *Characterization of paramagnetic species in N-doped TiO2 powders by EPR spectroscopy and DFT calculations.* The Journal of Physical Chemistry B, 2005. **109**(23): p. 11414-11419.

44. M. Gondal, S. Rashid, M. Dastageer, S. Zubair, M. Ali, J. Lienhard, G. McKinley, and K. Varanasi, *Sol–gel synthesis of nanocomposite and their morphological and optical properties.* Photonics Journal, IEEE, 2013. **5**(3): p. 2201908-2201908.

45. J. Surmacki, P. Wron´ski, M. Szadkowska-Nicze, and H. Abramczyk, *Raman spectroscopy of visible-light photocatalyst – Nitrogen-doped titanium dioxide generated by irradiation with electron beam.* Chemical Physics Letters, 2013. **566**: p. 54-59.

46. J.C. Yu, J. Yu, W. Ho, Z. Jiang, and L. Zhang, *Effects of F-doping on the photocatalytic activity and microstructures of nanocrystalline TiO2 powders.* Chemistry of materials, 2002. **14**(9): p. 3808-3816.

47. L.G. Devi and R. Kavitha, *Enhanced photocatalytic activity of sulfur doped TiO 2 for the decomposition of phenol: A new insight into the bulk and surface modification.* Materials Chemistry and Physics, 2014. **143**(3): p. 1300-1308.

48. P. Goswami and J.N. Ganguli, *A novel synthetic approach for the preparation of sulfated titania with enhanced photocatalytic activity.* RSC Advances, 2013. **3**(23): p. 8878-8888.

49. E.M. Rockafellow, L.K. Stewart, and W.S. Jenks, *Is sulfur-doped TiO 2 an effective visible light photocatalyst for remediation?* Applied Catalysis B: Environmental, 2009. **91**(1): p. 554-562.

50. J.C. Yu, W. Ho, J. Yu, H. Yip, P.K. Wong, and J. Zhao, *Efficient visible-light-induced photocatalytic disinfection on sulfur-doped nanocrystalline titania.* Environmental science & technology, 2005. **39**(4): p. 1175-1179.

51. W. Ho, C.Y. Jimmy, and S. Lee, *Low-temperature hydrothermal synthesis of S-doped TiO 2 with visible light photocatalytic activity.* Journal of solid state chemistry, 2006. **179**(4): p. 1171-1176.

Chapter 5 Photocatalytic Results

This chapter presents the photocatalytic degradation reactions of caffeine, aspirin, phenacetin and salicylic acid with the various catalysts synthesised as well as P25. The sections are divided as follows the copper doped catalysts and experimental controls are discussed first with each compound discussed separately in the order caffeine, aspirin, phenacetin and salicylic acid. The nitrogen and sulfur doped catalysts are then discussed with each compound discussed in the same order as the copper doped catalysts. Also presented in this chapter is the optimization of reaction parameters substrate concentration, solution pH and catalyst mass. All reactions shown in this chapter were done in duplicate. These reactions were done as a mixture with all four compounds in the same reaction medium, although each compound is discussed separately. All reactions were sonicated for 10 min and then stirred in the dark for 30 min and unless otherwise stated then irradiated for 120 min with a 32 W daylight lamp. The reactions were monitored by HPLC at a wavelength of 210 nm and a mobile phase of 40:60 methanol: pH 2.3 phosphoric acid water.

Emerging containments (ECs) are compounds that may persist in the environment for a long time and the knowledge on their effect on the ecosystem is limited. These chemicals can be man-made or naturally occurring; amongst them are pharmaceuticals, painkillers and personal care products which are of concern as they find their way into water bodies through discharges from households and various industries.

Caffeine is found in many items consumed on a daily basis such as coffee, tea, sweets and it can be found in various medications. Buerge *et al* studied caffeine as a chemical marker for the pollution of water [1]. Furthermore various studies have found caffeine in local waste water treatment plans as well as the effluent of waste water treatment plants which in turn finds its way into water bodies that provide drinking water [2-4].

Aspirin is commonly used as a painkiller and there is evidence that taking aspirin over prolong periods may prevent certain forms of cancer [5]. In high enough dosages aspirin can prove toxic (200-300 mg per a kg of mass) or even lethal (500 mg per a kg of mass) [6]. In a study done by Foluso *et al* on a number of water bodies in Kwa-Zulu Natal it was found that there is aspirin in water bodies that provide drinking water [4].

Phenacetin is used as a pain relieving and fever reducing drug, however it has been shown to cause kidney failure, due to this it has been banned in a number of countries [7, 8]. In countries where it has been banned it has been detected in water bodies and is therefore possible to consume [9].

Salicylic acid is a major metabolite of aspirin; it is also used in creams to treat pimples and blemishes [10, 11]. Salicylic acid has been found in effluent and influent in a number of places and may therefore find its' way into drinking water, hence it is of concern [12-14].

5.1 Copper doped TiO2

In this section the reactions of the control parameters namely reaction with catalyst (P25) in the absence of light, irradiation of the solution without catalyst and reactions with P25 are shown. The control parameters are compared to the reactions of the copper doped catalyst. The reactions which are labelled no light indicate that the solution was not irradiated during the course of the reaction.

5.1.1 Caffeine

Figure 5.1 (a) shows the degradation of caffeine with the control parameters, it can be seen that with catalyst and no light there is no degradation, very little absorption happens and the compound is not degraded without light. In red shows the degradation of caffeine without catalyst but irradiated, the compound seems to degrade slightly. Using P25 shows a major increase in the amount of caffeine degraded, with the caffeine degrading to 0.62 of its original concentration. These results show that the reaction is photocatalytic as with catalyst in the absence of light there is no degradation but under irradiation without catalyst there is a small amount of degradation, this degradation increases upon the addition of catalyst.

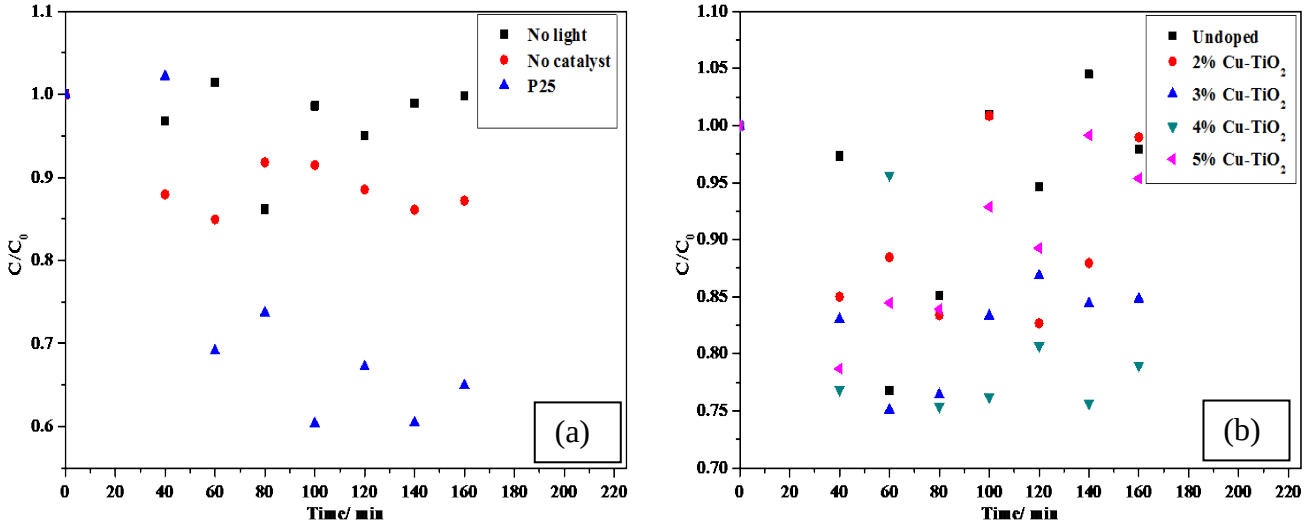

Figure 5.1: Caffeine degradation rate with control parameters (a) and with copper doped catalysts (b). Reaction mixture consisted of 5 ppm of each compound, 50 mg catalyst in 100 mL of solution. The reactions were monitored by HPLC at a wavelength of 210 nm.

Figure 5.1 (b) shows the performance of copper doped catalysts for the degradation of caffeine. The undoped catalyst shows little to no activity for the degradation of caffeine. Initially there is a decrease in the amount of caffeine, with the undoped catalyst, however

over time amount of caffeine increases in solution to the starting concentration. The caffeine therefore does not degrade with the undoped TiO_2 but rather adsorbs and then desorbs again. This can again be seen for the 2% Cu TiO_2 and 5% TiO_2 catalysts as there is an initial decrease in the amount of caffeine but after 160 min the concentration increases to the starting concentration. The 3% Cu TiO_2 and 4% TiO_2 catalysts however show degradation of caffeine. The 4% Cu-TiO_2 catalyst shows the best degradation of caffeine from all of the copper doped catalyst with caffeine degraded to 0.75 of its original concentration. However P25 has better activity than any of these synthesised catalysts for the degradation of caffeine.

5.1.2 Aspirin

Figure 5.2 (a) represents the control parameters for the degradation of aspirin. In the experiment for which there is catalyst but the solution is not irradiated aspirin does not degrade. When the compound is irradiated but there is no catalyst the aspirin degrades a little to a value of 0.90 of the original 5 $mg.L^{-1}$. There is an increase in the degradation rate of aspirin upon the addition of P25, with the final amount of aspirin being 0.76 of the original 5 $mg.L^{-1}$. From these results it is clear that this reaction is a photo-assisted reaction as the TiO_2 shows no activity without light.

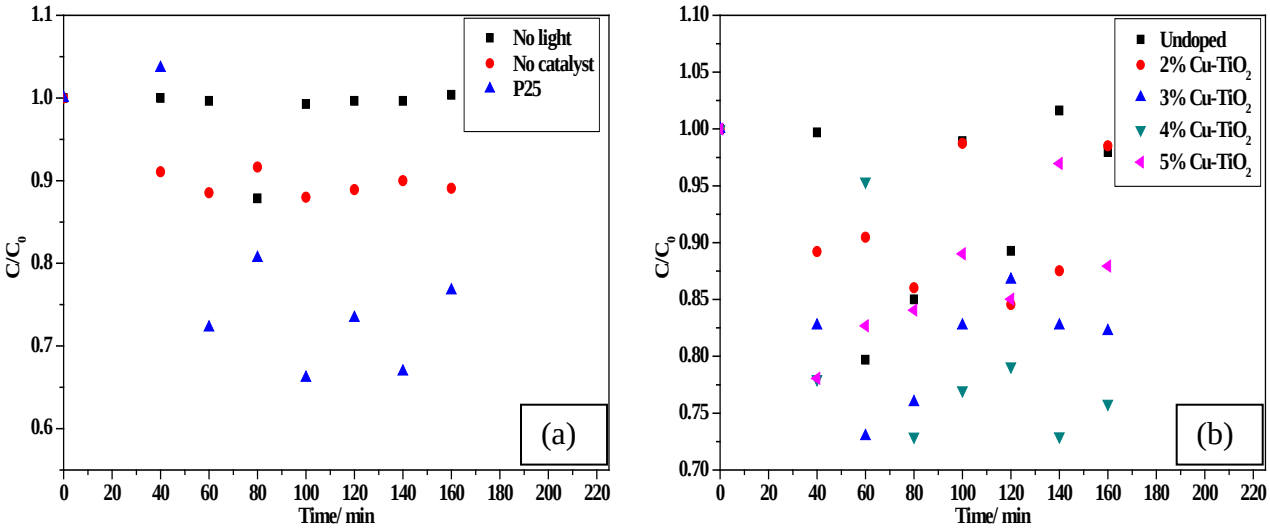

Figure 5.2: Aspirin degradation rate with control parameters (a) and with copper doped catalysts (b). Reaction mixture consisted of 5 ppm of each compound, 50 mg catalyst in 100 mL of solution. The reactions were monitored by HPLC at a wavelength of 210 nm.

Figure 5.2 (b) shows the degradation rates for aspirin using the copper doped TiO_2 catalysts. The undoped catalyst shows very little adsorption capacity and no photocatalytic activity as it can be seen that at the end of irradiation period the concentration of aspirin in solution is$C/C_0 = 1$. The 2% Cu-TiO_2 and the 5% Cu-TiO_2 catalysts have very little or no activity, with the 2% Cu-TiO_2 catalyst showing aspirin concentration of $C/C_0 = 1$ at the end of the reaction. The 5% Cu-TiO_2 shows desorption of aspirin despite the reaction ending with 0.87 of the original value. The 3%Cu-TiO_2 and 4% Cu-TiO_2 display removal of the compound, with the 3% Cu-TiO_2 degrading up aspirin to a final concentration of 0.82 and the 4% Cu shows the best activity degrading the aspirin to a final value of 0.75 of the original concentration. The degradation of aspirin for the by the 4% Cu-TiO_2 catalyst is lower than that obtained by using P25 for the degradation for aspirin.

5.1.3 Phenacetin

Figure 5.3 (a) shows the degradation reactions of phenacetin for the control parameters. Shown in **Figure 5.3** (a) is that in the absence of light in a solution containing catalyst, the phenacetin does not degrade. When the solution is irradiated but there is no catalyst there is a little degradation of the compound, with a final value of 0.85 of the original concentration. Upon addition of P25 the degradation amount increases greatly compared to irradiation with no catalyst, with a final value of 0.75 of initial concentration. This shows that the degradation is photocatalytic.

Figure 5.3 (b) shows the degradation reactions of phenacetin using copper doped catalyst. The undoped TiO_2 catalyst shows no photocatalytic activity, though upon initial irradiation (60 min) there is a drastic decrease in the amount of phenacetin the amount of phenacetin again increases to initial concentration. This is mostly likely due to adsorption of the substrate and then desorption. The 2% Cu-TiO_2 and 5% Cu-TiO_2 catalyst both show little photocatalytic activity; the 2% Cu TiO_2 catalyst has a final concentration of $C/C_0 = 1$ while the 5% Cu-TiO_2 shows a final concentration 0.94 of the original concentration. The 3% Cu-TiO_2 and 4% Cu-TiO_2 catalyst both show degradation of phenacetin with 0.82 and 0.80 of the initial concentration respectively. None of these synthesised catalyst show good catalytic activity compared to the reactivity of P25.

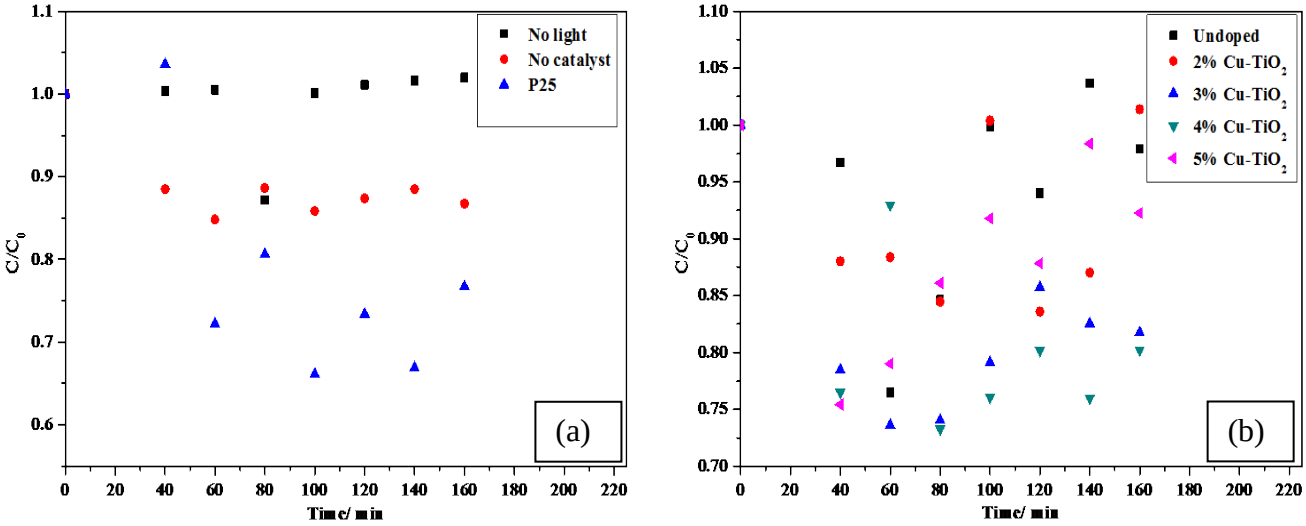

Figure 5.3: Phenacetin degradation rate with control parameters (a) and with copper doped catalysts (b). Reaction mixture consisted of 5 ppm of each compound, 50 mg catalyst in 100 mL of solution. The reactions were monitored by HPLC at a wavelength of 210 nm.

5.1.4 Salicylic acid

Figure 5.4 (a) shows the degradation rates of SA with the control parameters. The reactions with P25 in the absence of light show no degradation. The reactions with light but in the absence of catalyst showed some degradation of the substrate but this stays constant at 0.90 meaning that over time further degradation is not likely. When using P25 and irradiating the solution there is a greater amount of SA degraded, compared to the reactions with no catalyst, to a final value of 0.60. This shows that this reaction is photocatalytic as there is no degradation without light and there is only slight degradation in the absence of catalyst but with catalyst under irradiation there is degradation.

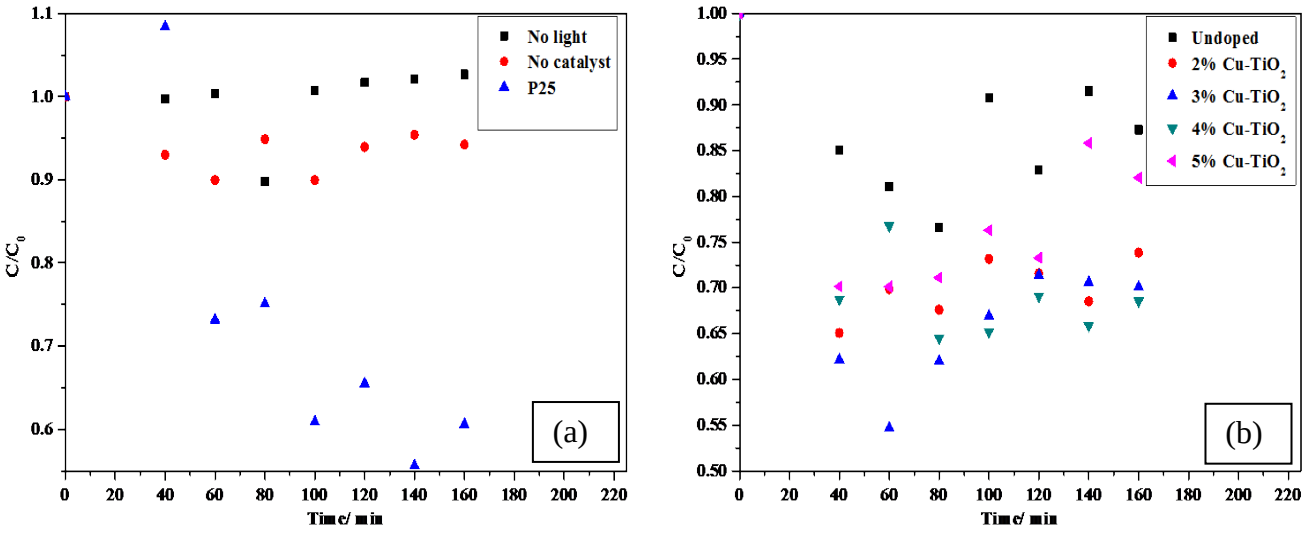

Figure 5.4: SA degradation rate with control parameters (a) and with copper doped catalysts (b). Reaction mixture consisted of 5 ppm of each compound, 50 mg catalyst in 100 mL of solution. The reactions were monitored by HPLC at a wavelength of 210 nm.

Figure 5.4 (b) shows the degradation rates of SA using copper doped catalysts. The undoped TiO_2 shows some degradation for SA as can be seen above the final amount is 0.87 of the initial concentration. For this compound the 2% Cu-TiO_2 catalyst showed better activity than the 5% Cu-TiO_2 catalysts 0.73 compared to 0.84 of the initial concentration. Once again the 3% Cu-TiO_2 and 4% Cu-TiO_2 catalysts showed very similar activity with the 4% Cu-TiO_2 catalyst having the best activity of all the catalysts. All catalyst had better activity toward SA than the comparative activity for any other compound.

5.1.5 Final Comments on the Photocatalytic Activity of Copper Doped TiO_2

For the control reaction in which there was catalyst used but there was an absence of light, at 80 min for all compounds there is a major reduction in the concentration of each compound.

This is most likely an outlier as it is present at the exact same time for all compounds and may be due to the low number of replicates used in this study with each reaction carried out in duplicate.

That SA was the compound degraded the most effectively can be understood by the fact that it is the smallest molecule out of all four compounds degraded this can be seen in chapter 2 section 2.8.4. In section 2.4 it was discussed that the greater the surface coverage the better the reaction rate. Smaller molecules have a higher driving force leading to better surface coverage compared to larger molecules. However if the degradation rates of the compounds was strictly determined by the size of the molecules then caffeine should show the slowest rate of degradation being the largest molecule. However caffeine, aspirin and phenacetin have similar rates of degradation for all catalysts this can be explained as steric also play a role in adsorption. It can be seen that for all graphs that the amount of any of the substrates do not decrease in a linear fashion over time and there is fluctuation in the amount of any of the substrates, this may be due to competitive absorption of substrate molecules. Competitive adsorption could also be between the original substrates and the degradation intermediates formed, this is as the degradation intermediates would form close to the catalyst surface and would be smaller than the original molecules. Of the copper doped catalysts 4% Cu-TiO_2 had the best activity of all, given that it had the second narrowest band gap of all 2.5 eV and the second lowest rate of electron-hole recombination rate (**Figure 4.22**) this was expected. All the copper doped catalyst showed improved activity when compared to the undoped TiO_2 catalyst. None of the copper doped catalyst had better activity than P25 though the 4% Cu-TiO_2 catalyst had similar activity to the P25 in all degradations.

5.2 Nitrogen Doped TiO_2

In this section the results of degradation reactions using nitrogen doped TiO_2 catalysts are presented.

5.2.1 Caffeine

Figure 5.5 shows the degradation rates of caffeine using the various nitrogen doped catalyst. In **Figure 5.5** it can be seen that the undoped catalyst does not degrade the caffeine but only adsorbs it before the caffeine is then desorbed, this shows that the catalyst is relatively inactive under reaction conditions. The TiO_2 N 1:2 catalyst shows a final amount of 0.88, while the concentration of caffeine increases to 1, after 100 min the general trend of the reaction is downward. The TiO_2:N 1:3 catalyst shows the best activity with a final concentration of 0.8 of the initial concentration and the TiO_2:N 1:4 catalyst shows almost no activity for the degradation of caffeine. P25 has better activity for the degradation of caffeine than any of the nitrogen doped catalysts.

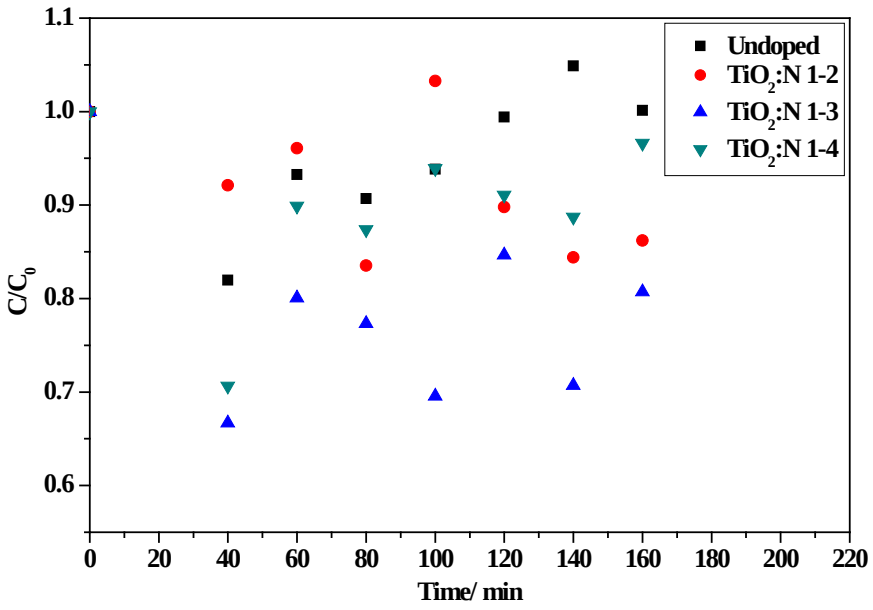

Figure 5.5: Photocatalytic degradation of caffeine with nitrogen doped catalysts. Reaction mixture consisted of 5 ppm of each compound, 50 mg catalyst in 100 mL of solution. The reactions were monitored by HPLC at a wavelength of 210 nm.

5.2.2 Aspirin

Figure 5.6 shows the degradation rates for aspirin using the various nitrogen doped catalysts. The undoped catalyst shows no activity for the degradation of aspirin despite initially adsorbing 20% of the starting concentration of aspirin. All the nitrogen doped catalysts showed high initial adsorption of the aspirin in solution however the final concentration of aspirin was greater than that after initial adsorption. It can be seen that all catalysts show a major spike in aspirin concentration at 60 min this is after initial irradiation, this shows that as degradation products are being formed the initial substrate (aspirin) desorbs. The TiO_2:N 1:2 catalyst shows the best final concentration of 0.81. For the degradation of aspirin none of the nitrogen doped catalyst has better activity than P25.

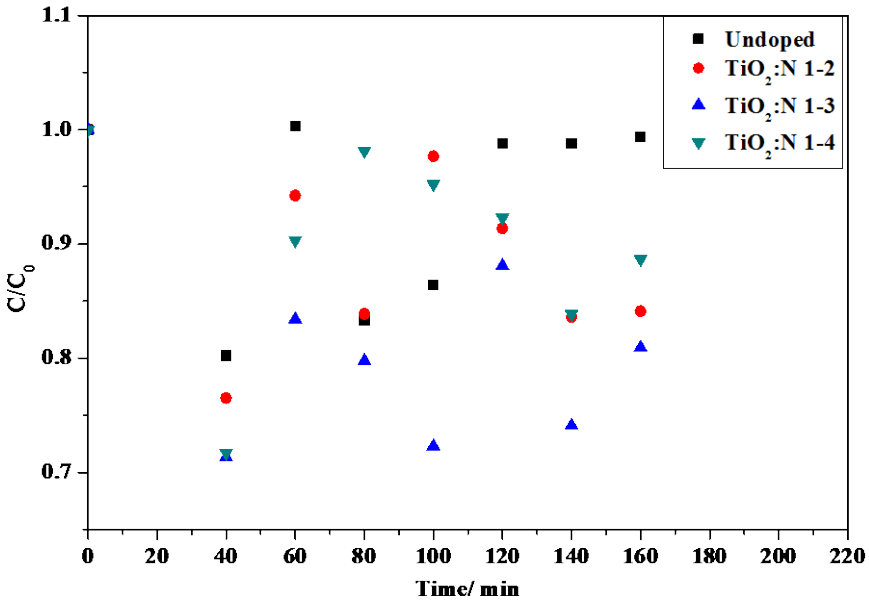

Figure 5.6: Photocatalytic degradation of aspirin with nitrogen doped catalysts. Reaction mixture consisted of 5 ppm of each compound, 50 mg catalyst in 100 mL of solution. The reactions were monitored by HPLC at a wavelength of 210 nm.

5.2.3 Phenacetin

Figure 5.7 shows the degradation reactions of phenacetin for nitrogen doped catalysts. All the nitrogen doped catalyst show strong initial adsorption of phenacetin between 15-30% of the initial concentration. After initial irradiation (60 min) of the solution all catalysts have a strong desorption of the phenacetin adsorbed onto the catalyst. The undoped TiO_2 and TiO_2:N 1:4 catalysts show no activity for the degradation of phenacetin with final concentration ,after 160 min, equal to the initial concentration. The TiO_2:N 1:2 and TiO_2:N 1:3 catalysts show the same activity with 0.85 final concentration.

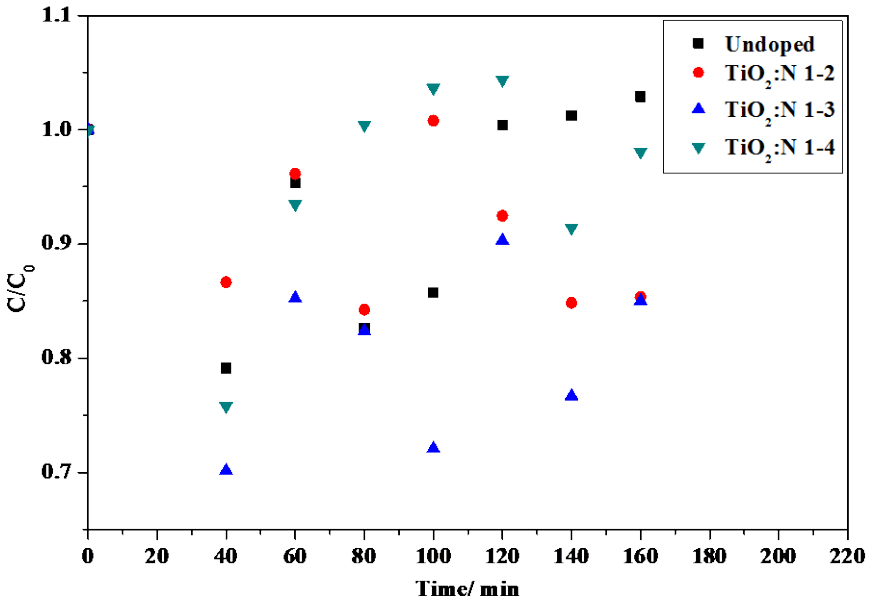

Figure 5.7: Photocatalytic degradation of phenacetin with nitrogen doped catalysts. Reaction mixture consisted of 5 ppm of each compound, 50 mg catalyst in 100 mL of solution. The reactions were monitored by HPLC at a wavelength of 210 nm.

5.2.4 Salicylic acid

Figure 5.8 shows the photodegradation reactions of SA with the various nitrogen doped catalysts. All catalysts show a large amount of adsorption after the solution was left to stir in the dark 10-35%, there can also be seen that after initial irradiation (60 min) there are varying degrees of desorption. The undoped catalyst showed no activity for the degradation of SA as the final concentration was equal to the initial concentration. The TiO_2:N 1:2 catalyst showed the lowest activity of all the nitrogen doped catalysts, also there seems to be complete desorb before some of the SA is removed to a value of 0.75 of the initial concentration. Both the TiO_2:N 1:3 and TiO_2:N 1:4 catalysts had linear degradation of SA, with the TiO_2:N 1:4 catalyst had the best activity to 0.52 of the starting concentration. Both TiO_2:N 1:3 and TiO_2:N 1:4 had better activity for the degradation of SA than P25.

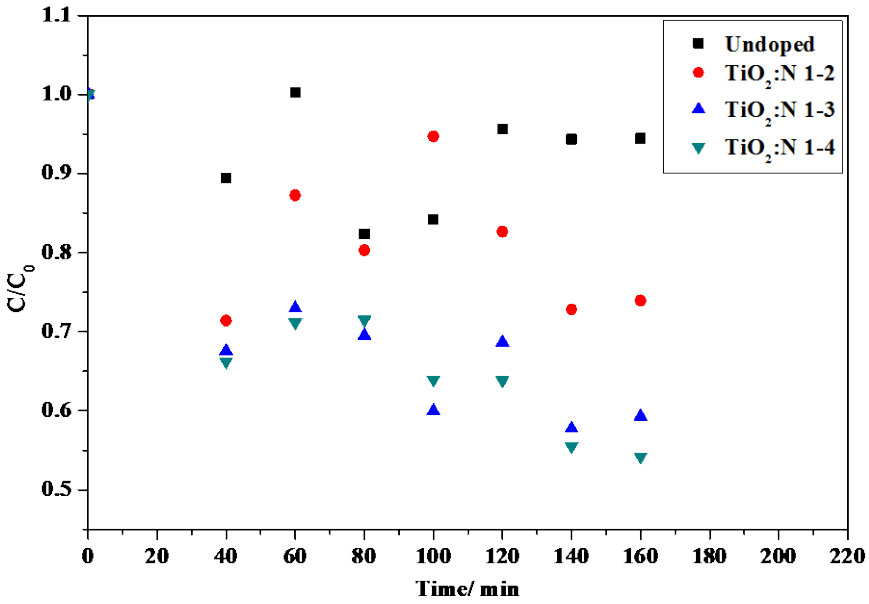

Figure 5.8: Photocatalytic degradation of SA with nitrogen doped catalysts. Reaction mixture consisted of 5 ppm of each compound, 50 mg catalyst in 100 mL of solution. The reactions were monitored by HPLC at a wavelength of 210 nm.

5.2.5 Final Comments on the Photocatalytic Activity of Nitrogen Doped TiO_2

From the results shown in **Figures 5.5-5.8** it can be seen that the undoped catalysts has no photocatalytic activity under the conditions of the experiment. For all of the substrates and for all of the nitrogen doped catalysts it can see that there is an increase in the amount of substrate in solution after initial irradiation (60 min) compared to after dark adsorption (40 min). The reason for this increase in substrate concentration would be that there is desorption of substrate from the catalyst. Given that the substrate desorbs from the surface of the catalyst upon irradiation the reason for this desorption may be due to the formation of degradation products. When the original substrates are degraded there will be new organic molecules formed near the surface of the catalyst. The reaction intermediates will compete

with the original substrates to adsorb onto the catalyst, considering that the intermediates may adsorb more strongly the original substrates will be displaced. The nitrogen doped catalysts offered better reactivity than the undoped catalyst, showing that nitrogen doping provides. Overall the TiO_2:N 1:3 catalyst shows the best activity with the TiO_2:N 1:4 catalyst having only slightly better activity for degradation of SA. This is odd as the TiO_2:N 1:4 catalyst has better physiochemical properties in all parameters that affect photocatalyst namely higher surface area (73 vs 65 m^2. g^{-1}), narrower band gap (2.7 vs 2.8 eV) and slower electron-hole recombination rate (**Figure 4.22**). Though for most of the degradations there is adsorption and desorption at various intervals making it difficult to determine if the final value for a given degradation is completely accurate. None of the catalysts synthesised showed better activity than P25 overall, TiO_2:N 1:3 and TiO_2:N 1:4 showed better activity only for the degradation of SA compared to P25.

5.3 Sulfur Doped TiO_2

The degradation reactions of the sulfur doped catalysts are described in this section. The undoped catalyst used in these reactions is the same as in section 5.2, so is not discussed. The undoped catalyst is only presented for the sake of comparison.

5.3.1 Caffeine

Figure 5.9 shows the photodegradation reactions of caffeine with sulfur doped catalysts. The TiO_2:S 1:2 and TiO_2:S 1:3 catalyst show strong adsorption after stirring in the dark (40 min) of caffeine while the TiO_2:S 1:4 catalyst shows no adsorption at all. After initial irradiation all sulfur doped catalyst show either a small decrease in caffeine content or the same amount

as before irradiation. The TiO_2:S 1:2 catalyst shows a linear decrease in the amount of caffeine until 100 min at which time caffeine begins to desorb from the surface of the catalyst until at 160 min the final value is C/C_0 =1. The TiO_2:S 1:3 catalyst has a similar trend as it can be seen that for the final two sample points after 140 and 160 min there is an increase in the amount of caffeine. The TiO_2:S 1:4 catalyst shows no activity for either adsorption or degradation of caffeine. P25 had better degradation efficacy for caffeine than any of the sulfur doped catalysts.

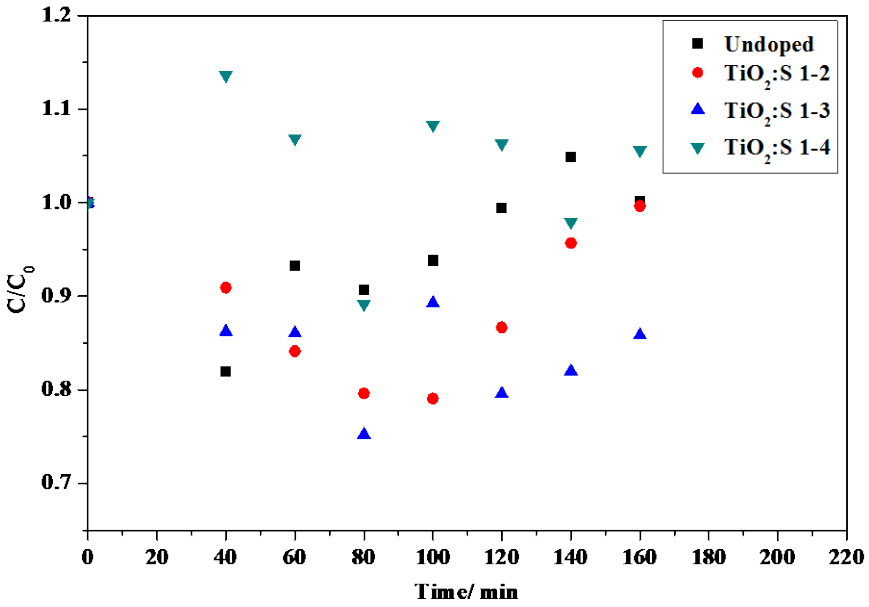

Figure 5.9: Photocatalytic degradation of caffeine with sulfur doped catalysts. Reaction mixture consisted of 5 ppm of each compound, 50 mg catalyst in 100 mL of solution. The reactions were monitored by HPLC at a wavelength of 210 nm.

5.3.2 Aspirin

Figure 5.10 shows the degradation reactions with various sulfur doped catalysts. The TiO_2:S 1:2 and TiO_2:S 1:3 catalysts show some adsorption of aspirin after stirring in the dark. After initial irradiation there is a slight decrease in the amount of aspirin for the TiO_2:S 1:2 catalyst

but a slight increase in the amount of aspirin for the TiO_2:S 1:3 catalyst. The TiO_2:S 1:2 catalysts shows a linear reduction in the amount of caffeine until the 100 min sample interval thereafter the amount of caffeine increases back to the initial concentration. The TiO_2:S 1:3 catalyst also shows desorption towards the end of the reaction going from 0.79 to 0.85. The TiO_2:S 1:4 catalyst shows no activity towards aspirin at all neither adsorbing the substrate nor degrading it. P25 performs better for the degradation of aspirin than any of the sulfur doped catalysts.

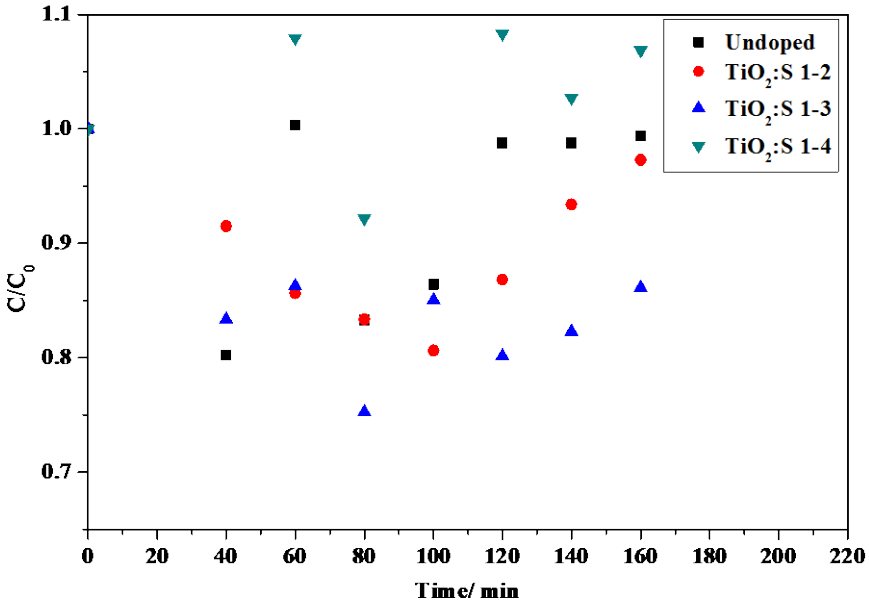

Figure 5.10: Photocatalytic degradation of aspirin with sulfur doped catalysts. Reaction mixture consisted of 5 ppm of each compound, 50 mg catalyst in 100 mL of solution. The reactions were monitored by HPLC at a wavelength of 210 nm.

5.3.3 Phenacetin

Figure 5.11 shows the photocatalytic degradation reactions of phenacetin using the various sulfur doped catalysts. Both the TiO_2:S 1:2 and TiO_2:S 1:3 catalysts show adsorption after dark stirring while the TiO_2:S 1:4 catalyst shows no adsorption after dark stirring. The

TiO_2:S 1:2 shows an increase in phenacetin concentration after initial irradiation while the TiO_2:S 1:3 shows a slight decrease in concentration. Once again the TiO_2:S 1:2 catalyst shows desorption of the substrate after 100 min to a final concentration, after 160 min, equal to the starting concentration. Unlike the reactions for aspirin and caffeine the TiO_2:S 1:3 catalyst does not show linear desorption after 120 min but rather fluctuation. The TiO_2:S 1:4 catalyst shows no activity for adsorption or degradation of phenacetin over the course of the reaction.

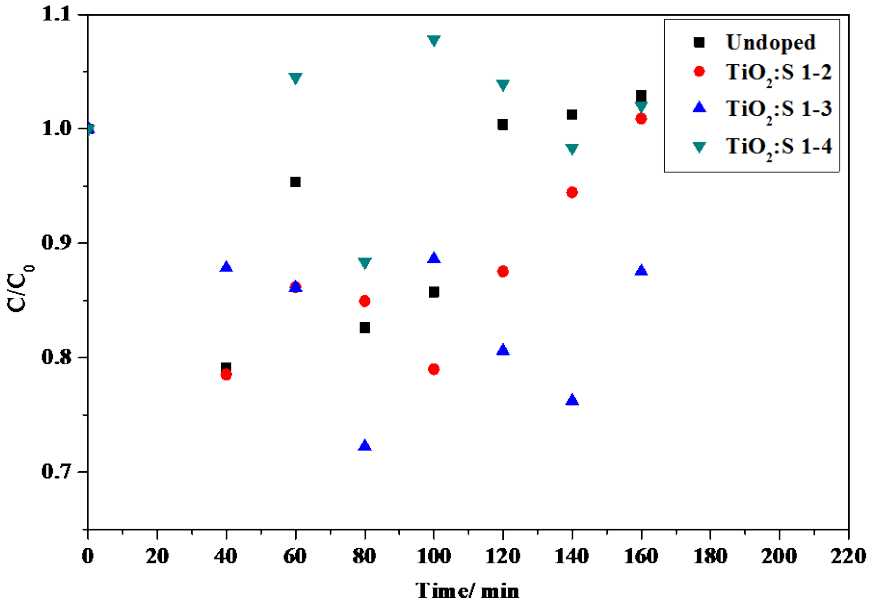

Figure 5.11: Photocatalytic degradation of phenacetin with sulfur doped catalysts. Reaction mixture consisted of 5 ppm of each compound, 50 mg catalyst in 100 mL of solution. The reactions were monitored by HPLC at a wavelength of 210 nm.

5.3.4 Salicylic Acid

Figure 5.12 shows the photocatalytic degradation of SA with the various sulfur doped catalysts. All of the sulfur doped catalysts show linear degradation of SA. The TiO_2:S 1:2 catalyst shows the lowest degradation of SA and TiO_2:S 1:4 catalyst has the best degradation

rate of SA. Catalysts showed very strong adsorption of SA after stirring in the dark adsorbing between 30-40% of the initial concentration of SA. All sulfur doped catalysts had better activity for the degradation of SA than P25.

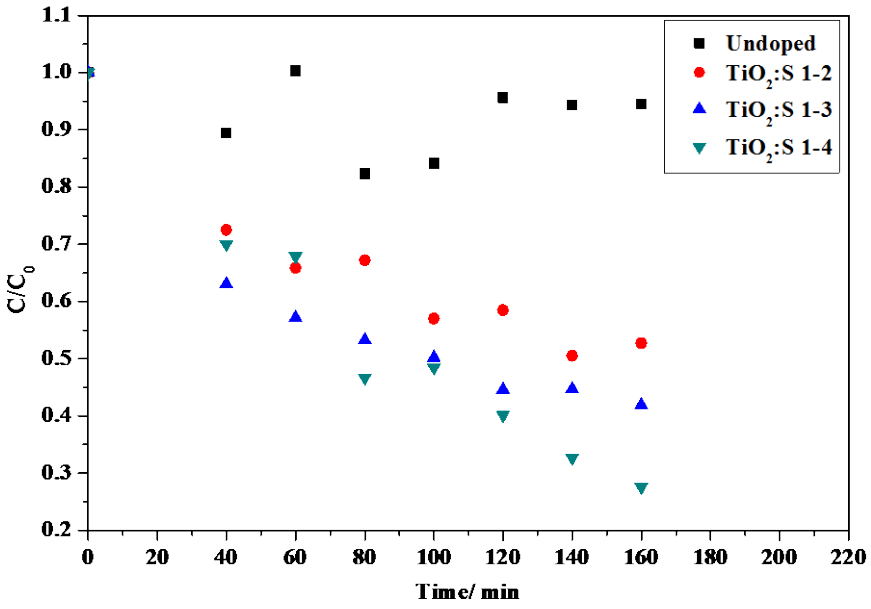

Figure 5.12: Photocatalytic degradation of SA with sulfur doped catalysts. Reaction mixture consisted of 5 ppm of each compound, 50 mg catalyst in 100 mL of solution. The reactions were monitored by HPLC at a wavelength of 210 nm.

5.3.5 Final Comments on the Photocatalytic Activity of Sulfur doped TiO_2

Looking at **Figures 5.9-5.11** all catalysts display a large amount of desorption this could be due to the former reasons proposed. The first reason proposed was competitive adsorption of substrate molecules. The second reason proposed was that degradation products would displace the original substrate molecules from the surface of the catalyst. This adsorption and desorption witnessed makes it difficult to accurately determine the activity of the catalysts for that particular molecule. That the highest amount of substrate degraded was again SA is predictable as previously stated being the smallest molecule should be the fastest to adsorb

and therefore degrade fastest. The TiO_2:S 1:2 catalyst shows no activity for 3 of the substrates (caffeine, aspirin and phenacetin) though for SA almost completely linear degradation and degrades 50%. This still indicates good photocatalytic activity for the TiO_2:S 1:2 catalyst as it is better than that of P25 for the same compound. All of the sulfur doped catalysts showed better activity than the undoped catalyst meaning that doping with sulfur improves photocatalysis of TiO_2. Overall the TiO_2:S 1:3 catalyst seems better than the TiO_2:S 1:4 catalyst. However the desorption of caffeine, aspirin and phenacetin seen in **Figures 5.8-5.11** place the actual amount of these substrates degraded into question. The final values taken as they are for all catalysts would suggest that the TiO_2:S 1:3 and TiO_2:S 1:4 have very similar activity; looking at the properties of each in chapter 4 this would make sense. The band gap for both catalysts is the same 2.4 eV, while the recombination rate for TiO_2:S 1:3 is low (**Figure 4.33**) the surface area for TiO_2:S 1:4 is higher (130 vs 69 $m^2 . g^{-1}$).

Given that the copper doped catalysts all showed adsorption and desorption for all substrates, it was determined that these catalysts should not be used to optimize parameters. Despite some positive results from the copper doped catalysts the fact that the final concentration may not be as accurate as seen in the graphs may prove detrimental to optimization. This meant that the best catalyst to optimize with should be chosen based on degradation of SA as for the nitrogen and sulfur doped catalysts linear degradation was obtained. Based on these criteria the best catalyst to optimize with was determined to be the TiO_2:S 1:4 catalyst as it had the highest degradation rate for SA.

5.4 Comparison of Obtained Results to Previous Results

5.4.1 Caffeine

Dalmazio *et al* reported the use of Degussa P25 for the degradation of caffeine, the operational conditions used was a 100 mL of 31 ppm caffeine solution with 0.1 $g.L^{-1}$ catalyst [15]. Marques *et al* studied the degradation of caffeine, with operational conditions of 250 mL of 50 ppm caffeine 1 $g.L^{-1}$ of P25 and continuously bubbling oxygen, the solution was irradiated with wavelengths over 350 nm [16]. Caffeine showed 10% degradation in 180 min with no catalyst and 100% degradation in 40 min with P25. The mixture was irradiated with a 254 nm lamp for 150 min, 90 % degradation was observed. Garcia *et al* conducted a study on the degradation 15 EC mixture, with caffeine being one of them, the concentration of each EC was 100 ppb with 5 $mg.L^{-1}$ of P25 in a 10L solar reactor [17]. The solution was irradiated for 60 min under solar light, caffeine was degraded completely in 25 min and all compounds showed significant reduction in 60 min. Klamerth *et al* studied the degradation of a mixture of 9 EC, of which one was caffeine, the initial concentration of each compound was 100 ppb and 5 $mg.L^{-1}$ of P25 was used in 22 L of solution [18]. The experiment was carried out under solar irradiation; caffeine was degraded completely in 120 min. Rey *et al* reported the degradation of caffeine in a mixture of 3 ECs; each EC was used at a concentration of 2 ppm and 0.5 $g.L^{-1}$ of catalyst in 500 mL of solution [19]. The solution was irritated with a 1500 W Xe arc lamp and 77% of caffeine was degraded in 120 min of irradiation.

The results obtained using the setup of this project do not provide results of a similar nature to work done previously. That is to say the amount of photodegradation using the setup of this project does not provide as great an amount of photodegradation seen in other works. Using P25 as the standard to compare to other work it can be seen that in the work done in this project P25 only provides 40% degradation of caffeine in 160 min, which is much lower

than in other works. One of the reasons for this may be the light source used, in the other works reviewed, the light source was one of, UV, solar irradiation or a high powered lamp, in this work a 32 W daylight lamp was used, with a much lower power output.

5.4.2 Aspirin

A slurry system similar to the experimental setup used for the photodegradation of aspirin could not be found in literature. Results obtained in this work, will therefore be compared to TiO_2 membranes and nanosheets used in other work for the photodegradation of aspirin.

Mukherjee *et al* immobilized P25 by 5 different procedures, the mass of P25 used was not given, and these films were used to degrade aspirin at a concentration of 2 ppm for 400 min under UV and solar irradiation separately [20]. Aspirin showed significant degradation under only UV or solar irradiation, the films had between 70-100% degradation under either form of irradiation. Li *et al* studied the effect of calcination temperature of TiO_2 nanosheets for the degradation of aspirin [21]. The mass of these nanaosheets was not given, the conditions for the photodegradation were as reported, 5 ppm (30 mL) of aspirin into which 1 nanosheet of the respective catalyst was placed the solution was irradiated with a 350 W Xe lamp. The best result was stated as 87.5 % degradation in 120 min of irradiation.

Considering that neither of the reviewed articles were slurry systems and the work of each article involved the degradation of only one compound, the results are difficult to compare to the work of this project. In the works of both articles the degradation rate of aspirin was greater than the degradation rate of aspirin seen in this project, the highest being 25% with P25. One of the reasons for the seemingly better activity of those systems may be that only

one compound is degraded. Another reason for the higher degradation may be that that high power lamps have been used in the other works compared to the one used in this project.

5.4.3 Phenacetin

Pervious work regarding a slurry setup for the photodegradation of phenacetin could not be found to compare to the work done in this project.

Giri *et al* used TiO_2 fibre sheets to degrade 16 EC of which one was phenacetin [22]. The reactions were carried out in 1.2 L of reaction medium with 1 ppm of each catalyst, the mass and number of sheets used was not stated, the solution was irradiated with a 10 W mercury vapour lamp for 60 min. After 60 min of irradiation there was very little change in the amount of phenacetin.

Compared to the results obtained of the above study in which phenacetin showed no degradation with TiO_2 and UV good degradation of phenacetin is observed in the work of this project. The mass of the fibre sheets are not given which makes comparison difficult however there is a relatively high concentration of all compounds in the work by Giri *et al* comparative to the overall concentrations used for this project.

5.4.4 Salicylic acid

Nagaveni *et al* used P25 to degrade salicylic acid, 30 ppm of salicylic acid was used and 1 $g.L^{-1}$ of catalyst was used in 400 mL [23]. The solution was irradiated with a 125 W mercury vapour lamp and 35% degradation of salicylic acid was seen in 200 min. Guo *et al* degraded salicylic acid with hydrothermal synthesised TiO_2 spheres, which were compared to P25 [24].

The reaction parameters were 0.2 g of catalyst in 100 mL of 10 ppm salicylic acid; this was allowed to equilibrate for 10 min in the dark and was irradiated for 140 min by a 300 W tungsten lamp. The P25 showed 46% degradation of SA and the synthesised catalysts showed between 55-81% degradation. Colon *et al* studied the degradation of salicylic acid with two commercial catalysts, one of which was P25, for this experimental setup $1 g.L^{-1}$ of catalyst was used and 4×10^{-4} M (55 ppm) of salicylic acid [25]. The solution was continuously bubbled with oxygen and was irradiated with a 400 W mercury lamp for 400 min, complete degradation was observed in 120 min. Adan *et al* studied the degradation of SA with TiO_2/SiO_2 fibres from UBE chemicals Ltd, the reaction condition were 100 ppm of SA and 2.5 $g.L^{-1}$ of catalyst in 1 L the reaction was irradiated with 500 W mercury vapour lamp [26]. Under these conditions with no external oxidant about 30 % degradation was noted in 250 min of irradiation.

The degradation of salicylic acid done in this work is comparable to the results achieved elsewhere. The best degradation amount achieved for SA for any of the catalysts used in this work was obtained with TiO_2:S 1:4 by the end of the reaction 75% of the initial concentration had been removed. The highest rates seen in the other catalysts set were 45% for TiO_2:N 1:4 and 35% for 4% Cu TiO_2, these are similar to results obtained elsewhere without an oxidant.

5.5 Variations of Reaction Conditions

This section describes the variation of reaction conditions in particular the parameters of substrate concentration, reaction medium pH and catalyst mass used. This was done in order to determine if there could be any improvement in reaction rates and if there is a change in the selectivity of the degradation. These reactions were all done using TiO_2:S 1:4.

5.5.1 Variation of Substrate Concentration

Figure 5.13 (a) shows the change degradation rate of caffeine with a change in the concentration of caffeine. There does not seem to be any correlation with the initial concentration of caffeine and the amount of caffeine adsorbed after stirring in the dark. The 10 ppm solution shows the highest adsorption and the 5 ppm solution the lowest adsorption. It be seen that for any initial concentration there is desorption of caffeine after the initial irradiation of the solution. Likewise there does not seem to any effect on the rate of caffeine degradation with a change in concentration, all initial concentration values show almost no degradation. This shows that change in concentration will not affect the degradation of caffeine with TiO_2:S 1:4.

Figure 5.13 (b) shows the change in the rate of degradation of aspirin with a change in the initial concentration of aspirin. The initial concentration of aspirin does not appear to affect the amount of aspirin adsorbed by the catalyst. The rate of aspirin degradation is also not effected by the initial concentration of aspirin. When the initial concentration is either 2 ppm or 10 ppm there seems to be adsorption of aspirin but there is no degradation as it can be seen that the aspirin the desorbs from the catalyst. The amount of aspirin degraded does not appear to be affected by the initial concentration of aspirin.

Figure 5.13 (c) shows the change in degradation rate of phenacetin with a change in the initial concentration of phenacetin. There initial concentration does not affect the amount of phenacetin initially adsorbed. The 10 ppm solution has the highest amount of adsorbed phenacetin and the 5 ppm the lowest. For all of the initial concentrations there is desorption of phenacetin after initially irradiation. There is no change in the amount of degradation with a change in concentration as can be seen for any of the any initial concentration by the end of the reaction almost all of the phenacetin has desorbed.

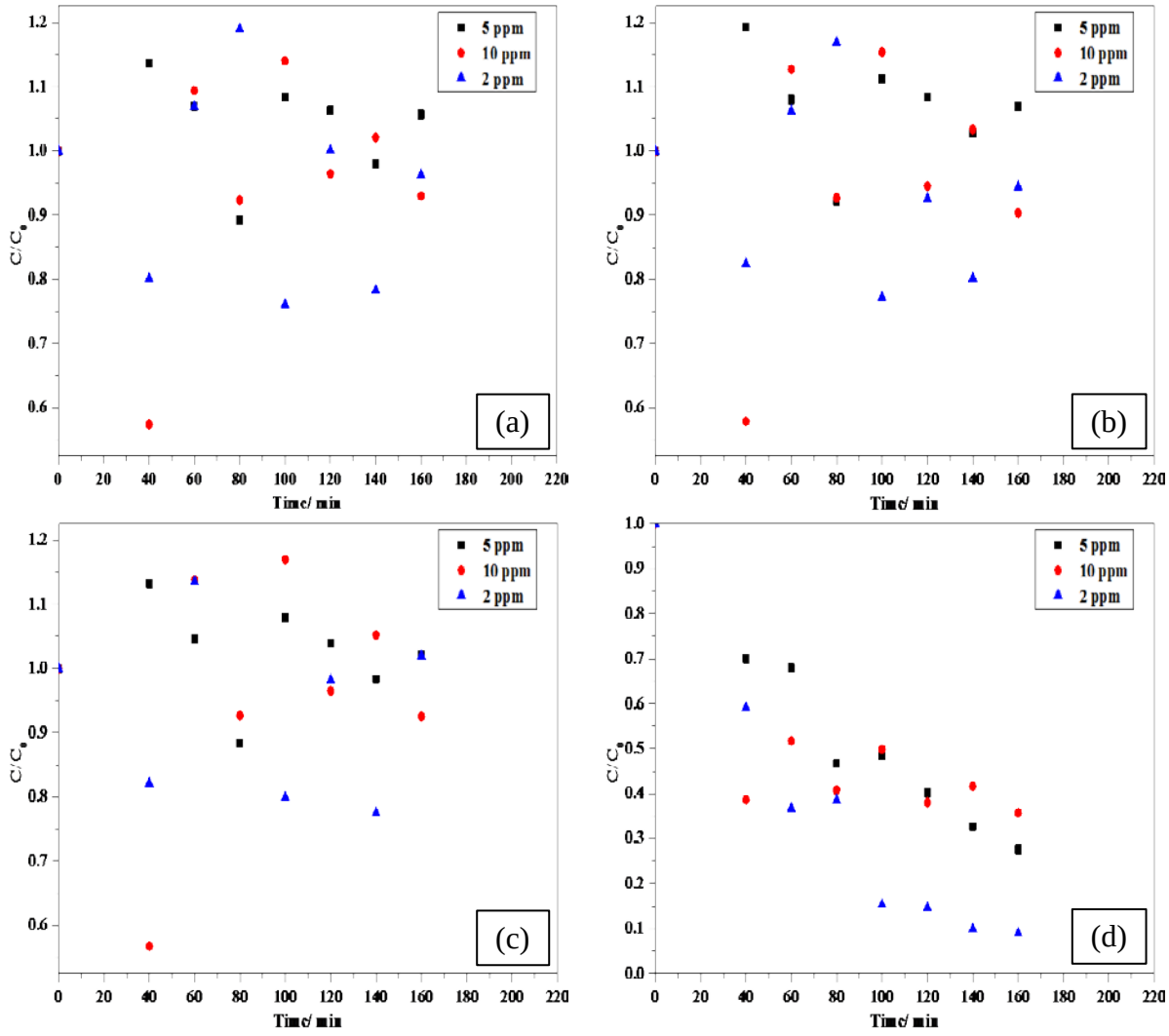

Figure 5.13: Effect of substrate concentration on the degradation rates of (a) caffeine, (b) aspirin, (c) phenacetin and (d) SA. These reactions where under natural pH using 50 mg of TiO_2:S 1:4 in a 100 mL of solution. Reactions were monitored by HPLC at 210 nm.

Figure 5.13 (d) shows the degradation rate of SA with a change in the initial concentration. There is no correlation of adsorption of SA with a change in initial concentration of SA. It seems that there is a decrease in the amount of SA degraded with an increase in the initial amount of SA. The solution with 10 ppm of SA shows the lowest rate of degradation and the solution with 2 ppm initial concentration shows the best reaction rate. In chapter 2 it was discussed that an increase in substrate concentration could result in lower reaction rate due to

the formation of degradation products which would lower the reaction rate. The 2 ppm solution is degraded to $C/C_0 = 0.1$, a major improvement over the other starting concentrations.

The results above are odd considering the only SA seems to be effected by the change in initial concentration, as all compounds should be affected by the change in concentration in some manner. Due to the lack of activity toward any of the other substrates the 2 ppm initial concentration was deemed to be the best as it showed a faster degradation rate for SA, in comparison to the other starting concentrations.

5.5.2 Variation of Reaction Medium pH

Figure 5.14 (a) shows the effect of the change in starting pH on the degradation rate of caffeine, the natural pH of the solution was 4.2. The initial pH does not seem to play a role in the amount of caffeine adsorbed initially as there is no clear pattern with an increase or decrease in pH. Under natural pH conditions and with a starting pH of 8.9 it can be seen after the initial irradiation there is desorption of caffeine form the catalyst, this is seen at 80 min for the pH 2.9 solution. For any pH tested the caffeine was found not to degrade, as there is a great fluctuation in the amount of caffeine over the course of time, at any pH tested. From these results it can be said that the variation in pH does not change the degradation of caffeine with TiO_2:S 1:4.

Figure 5.14 (b) shows the effect of the starting pH of the reaction medium on the degradation rate of aspirin. The starting pH of the solution does not appear to effect the rate at which aspirin adsorbs onto the surface of the catalyst. The final amount of aspirin degraded also does not appear to be effected by the starting pH of the solution, for any pH after initial

adsorption aspirin desorbs from the surface of the catalyst. These results show that caffeine degradation with TiO_2:S 1:4 is not effected by the starting pH of the solution

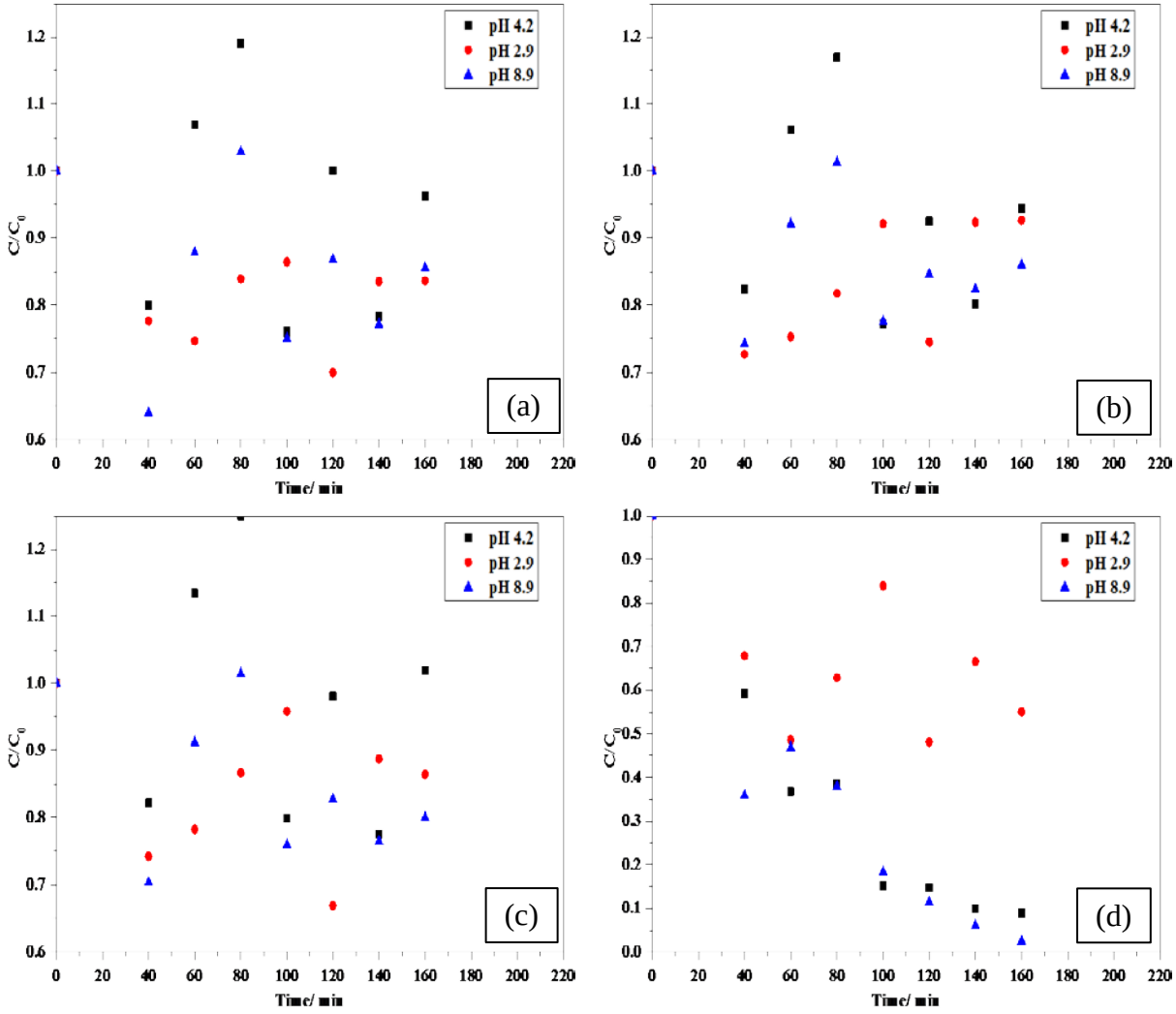

Figure 5.14: Effect of initial solution pH on the degradation rates of caffeine (a), aspirin (b), phenacetin (c) and SA (d). All reactions where done using 2 ppm of each substrate and 50 mg of TiO_2:S 1:4 in 100 mL of solution. Reactions were monitored by HPLC at 210 nm.

Figure 5.14 (c) shows the effect of the starting pH of the reaction medium on the degradation rate of phenacetin. It can be seen here that there is no effect of pH on the amount of adsorption of phenacetin on the surface of the catalyst. After initial irradiation there is

desorption of phenacetin from the surface of the catalyst, this can be attributed as previously to the formation of degradation products or competitive adsorption. The final concentrations for the pH 2.9 and 8.9 solutions can be seen as 0.85 and 0.77, however it can be seen that there is both adsorption and desorption over the course of the reaction hence these results may not be a true indication of activity. There does not appear that the pH affects the degradation rate of phenacetin with TiO_2:S 1:4.

Figure 5.14 (d) shows the effect of the starting pH of the reaction medium on the degradation rate of SA. From the results it appears that at higher pH values there is a higher amount of SA initially adsorbed. The reaction with a starting pH of 2.9 shows the lowest amount of adsorption and the solution with a starting pH of 8.9 shows the highest amount of adsorption. The pH 8.9 reaction medium shows the highest amount of degradation for SA reducing the concentration to $C/C_0 = 0.02$ by end of the monitoring period.

The change of the reaction medium pH did not appear to affect the adsorption or degradation of any of the compounds being studied aside from SA. It is odd that the reaction medium pH did not affect the degradation of the compounds as changing the reaction medium pH should affect the amount of substrate adsorbed. The reaction medium pH of 8.9 was chosen as the best as at this pH there was an improvement in the degradation of SA.

5.5.3 Variation of Mass of Catalyst Used

Figure 5.15 (a) shows the effect of the amount of catalyst used on the degradation rate of caffeine. There is greater adsorption of caffeine after stirring in the dark with a lower catalyst mass this can be seen as the amount of caffeine adsorbed decreases in the order 20 > 50 > 80 mg. This result is strange as greater catalyst mass should provide greater area for adsorption.

At all catalyst masses used it can be seen that after initial irradiation there is desorption of caffeine. The solution in which 20 mg of catalyst is used shows a rapid decrease in concentration between 100-160 min to a value of 0.7, though prior to this shows desorption of caffeine. It is possible the caffeine desorbed from the surface of the catalyst then adsorbs again.

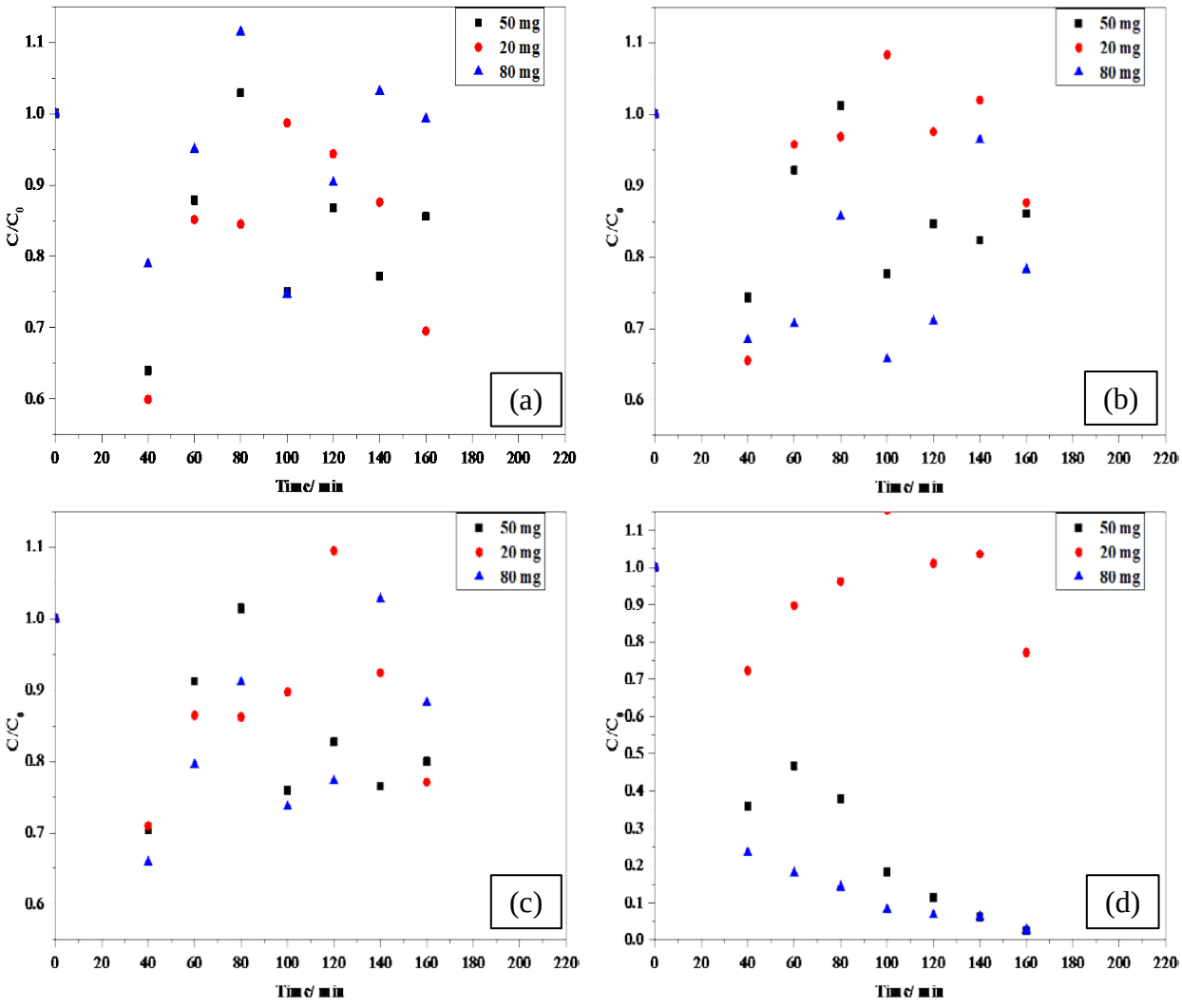

Figure 5.15: Effect of catalyst concentration on the degradation rates of caffeine (a), aspirin (b), phenacetin (c) and SA (d). All reactions were done using 2 ppm of each substrate the solution was at pH 8.9, the catalyst used was TiO_2:S 1:4, 100 mL of solution was used. Reactions were monitored by HPLC at 210 nm.

Figure 5.15 (b) shows the effect in the change of amount of catalyst used on the degradation rate of aspirin. The amount of catalyst used does seem to have an effect on the amount of aspirin adsorbed initially, with the 20 mg solution having the highest amount of adsorption and the 50 mg solution having the lowest amount of adsorption. The various amounts of catalyst do show some removal of aspirin from the solution at the end of the reaction, however the amount of adsorption and desorption make this difficult to judge the exact amount of substrate removed. The solution with 20 mg of catalyst shows a rapid decrease in aspirin between 100-160 min, this may be due to re-adsorption of the aspirin.

Figure 5.15 (c) shows the effect of the amount of catalyst used on the degradation rate of phenacetin. The amount of catalyst used does not seem to affect the amount of phenacetin adsorbed after stirring in the dark. For any of the given amounts of catalyst used there seem to be some removal of phenacetin; however the accuracy of this reduction is difficult to judge to adsorption and desorption of the substrate.

Figure 5.16 (d) shows the effect of the change in the amount of catalyst used on the degradation rate of SA. The amount of catalyst used clearly effects the amount of SA adsorbed after stirring in the dark. The amount of substrate adsorbed increases linearly with an increase in the amount of catalyst used. This is expected as greater mass should provide greater surface area and therefore result in a larger amount of adsorption. The solution in which 80 mg of catalyst is used shows the fastest degradation rate, though over the course of the reaction the solution using 50 mg shows the same amount of degradation. The solution using 20 mg of catalyst showed by far the lowest amount of degradation.

Given the amount of SA adsorbed (78%) when using 80 mg of catalyst, it may be understandable why there is a lack of adsorption of any of the other substrates. The surface of the catalyst may be saturated with SA and therefore cannot adsorb any of the other

substrates. It is expected once the SA is completely degraded, as can be seen in for the solutions using 50 and 80 mg of catalyst respectively, that the other compounds would then be degraded. The reason for this lack of activity may be due to the generation of degradation products which then occupy the surface of the catalyst. From the results presented above the optimum amount of catalyst was deemed to be 80 mg.

Oddly none of the parameters varied effected the degradation of any of the substrates tested aside for SA. The reasoning for this may be as stated before that SA being a smaller molecule compared to all the other substrates adsorbs first, and does not leave any space of the surface of the adsorption for the other substrates. Though for any of the substrates it can be seen that they do adsorb at least somewhat. However the original substrates may be forced off the surface of the catalyst by the formation of degradation intermediates. From the results above the optimum parameters chosen were 2 ppm of each substrate, pH 8.9 and 80 mg of catalyst, P25 was tested using these parameters to compare to the synthesised catalyst.

5.5.4 Comparison of Optimum Conditions

Figure 5.16 (a) shows the comparison of degradation rates of caffeine using P25 and TiO_2:S 1:4 under optimum conditions. P25 does not initially adsorb caffeine though it degrades caffeine in a very linear manner and very well, it decreases the concentration of caffeine by 70%. This is vastly better than the degradation of caffeine by TiO_2:S 1:4 under the same conditions. TiO_2:S 1:4 shows good adsorption of caffeine initially but does not degrade caffeine very well.

Figure 5.16 (b) shows the comparison of degradation rates of aspirin using P25 and TiO_2:S 1:4 under optimum conditions. It can be seen that P25 has better activity than TiO_2:S 1:4

with P25 degrading 70% of aspirin and TiO_2:S 1:4 having hardly any noticeable activity. The initial adsorbs of TiO_2:S 1:4 can be seen to be greater for aspirin than the adsorption of aspirin by P25.

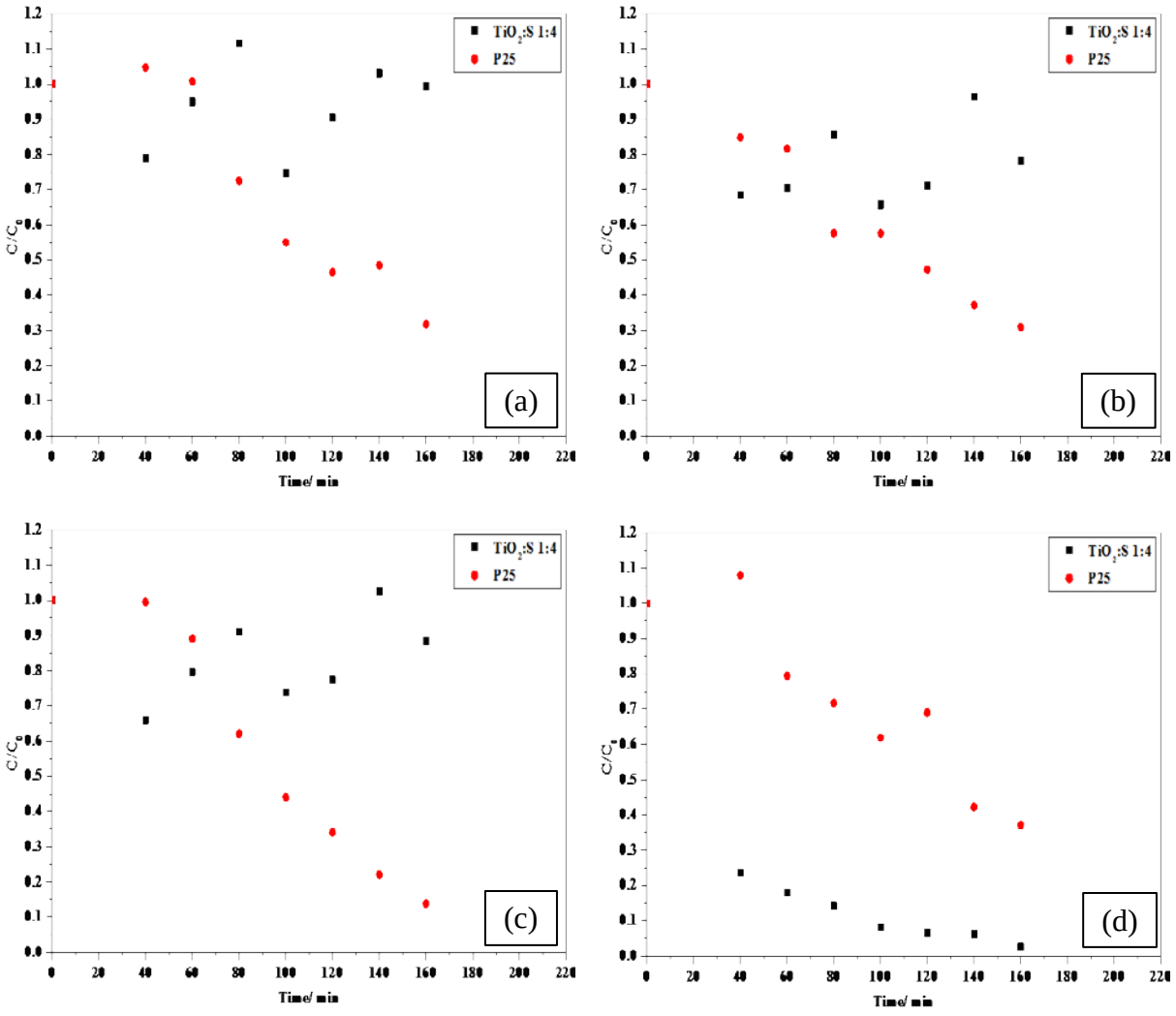

Figure 5.16: Shows the difference in photocatalytic activity between P25 and TiO2:S 1:4 for caffeine (a), aspirin (b), phenacetin (c) and salicylic acid (d). The conditions used for these reactions were 2 ppm of each substrate, reaction medium pH 8.9 and 80 mg of TiO_2:S 1:4.

Figure 5.16 (c) shows the comparison of degradation rates of phenacetin using P25 and TiO_2:S 1:4 under optimum conditions. P25 shows excellent photocatalytic degradation of

phenacetin degrading 90% of the starting concentration with in the 160 min of the reaction. This shows a great improvement compared to the active of P25 under the original conditions. TiO_2:S 1:4 shows very little activity for the degradation of phenacetin. Interestingly P25 does not adsorb any phenacetin after stirring in the dark whereas TiO_2:S 1:4 adsorbs up to 35% of phenacetin initial concentration.

Figure 5.16 (d) shows the comparison of degradation rates of SA using P25 and TiO_2:S 1:4 under optimum conditions. TiO_2:S 1:4 performs far better for the degradation of SA than P25 showing 100% degradation of SA in 160 min compared to the 65% degradation of SA with P25. P25 showed no adsorption for SA initially but TiO_2:S 1:4 on the other hand showed 80% adsorption of SA.

Although TiO_2:S 1:4 showed far greater adsorption than P25, which showed little to no adsorption, for all substrates P25 still had better activity overall. This is contrary to expectation as adsorption of the substrate on the surface of the catalyst is the first step in degradation. Although degradation could proceed through another pathway which is through the generation of hydroxyl radicals which will in turn react with the substrate and degrade it. Considering the difference in the behaviour of the catalyst it is possible that separate mechanisms are used by each catalyst. P25 most likely uses indirect oxidation of the substrates by producing hydroxyl radicals and therefore this would explain good degradation of all of the substrates. Hydroxyl radicals would reduce all organic compounds indiscriminately and therefore explain why substrates do not need to adsorb on to the catalyst to degrade. TiO_2:S 1:4 may use direct oxidation with substrates being oxidised by photogenerated holes. This would mean that only the substrates that are adsorbed on to the

surface of the catalyst would be degraded and that degradation products would form closes to the catalyst surface.

References

1. I.J. Buerge, T. Poiger, M.D. Müller, and H.-R. Buser, *Caffeine, an anthropogenic marker for wastewater contamination of surface waters.* Environmental Science & Technology, 2003. **37**(4): p. 691-700.
2. S. Matongo, G. Birungi, B. Moodley, and P. Ndungu, *Occurrence of selected pharmaceuticals in water and sediment of Umgeni River, KwaZulu-Natal, South Africa.* Environmental Science and Pollution Research, 2015: p. 1-11.
3. S. Matongo, G. Birungi, B. Moodley, and P. Ndungu, *Pharmaceutical residues in water and sediment of Msunduzi River, KwaZulu-Natal, South Africa.* Chemosphere, 2015. **134**: p. 133-140.
4. F.O. Agunbiade and B. Moodley, *Pharmaceuticals as emerging organic contaminants in Umgeni River water system, KwaZulu-Natal, South Africa.* Environmental monitoring and assessment, 2014. **186**(11): p. 7273-7291.
5. C. Bosetti, V. Rosato, S. Gallus, J. Cuzick, and C. La Vecchia, *Aspirin and cancer risk: a quantitative review to 2011.* Annals of Oncology, 2012. **23**(6): p. 1403-1415.
6. D.L. Seger and L. Murray, *Aspirin and nonsteroidal agents.* system (CNS), 2013. **4**: p. 5.
7. S. Antoni, I. Soerjomataram, S. Moore, J. Ferlay, F. Sitas, D.P. Smith, and D. Forman, *The ban on phenacetin is associated with changes in the incidence trends of upper-urinary tract cancers in Australia.* Australian and New Zealand Journal of Public Health, 2014. **38**(5): p. 455-458.
8. J.K. McLaughlin, L. Lipworth, W.-H. Chow, and W.J. Blot, *Analgesic use and chronic renal failure: A critical review of the epidemiologic literature.* Kidney Int, 1998. **54**(3): p. 679-686.

9. M. Kotti, E. Piliouris, and A. Vlessidis, *A new method for comparing hospital and municipal wastewater.* Journal of Environmental Science and Engineering. A, 2013. **2**(3A): p. 141.

10. S.K. Bae, K.A. Seo, E.J. Jung, H.-S. Kim, C.-W. Yeo, J.-H. Shon, K.-M. Park, K.-H. Liu, and J.-G. Shin, *Determination of acetylsalicylic acid and its major metabolite, salicylic acid, in human plasma using liquid chromatography–tandem mass spectrometry: application to pharmacokinetic study of Astrix® in Korean healthy volunteers.* Biomedical Chromatography, 2008. **22**(6): p. 590-595.

11. http://www.nlm.nih.gov/medlineplus/druginfo/meds/a607072.html. 10/07/15].

12. A.L. Spongberg and J.D. Witter, *Pharmaceutical compounds in the wastewater process stream in Northwest Ohio.* Science of the total environment, 2008. **397**(1): p. 148-157.

13. L. Lishman, S.A. Smyth, K. Sarafin, S. Kleywegt, J. Toito, T. Peart, B. Lee, M. Servos, M. Beland, and P. Seto, *Occurrence and reductions of pharmaceuticals and personal care products and estrogens by municipal wastewater treatment plants in Ontario, Canada.* Science of the Total Environment, 2006. **367**(2): p. 544-558.

14. H.-B. Lee, T.E. Peart, and M.L. Svoboda, *Determination of endocrine-disrupting phenols, acidic pharmaceuticals, and personal-care products in sewage by solid-phase extraction and gas chromatography–mass spectrometry.* Journal of Chromatography A, 2005. **1094**(1): p. 122-129.

15. I. Dalmázio, L.S. Santos, R.P. Lopes, M.N. Eberlin, and R. Augusti, *Advanced oxidation of caffeine in water: On-line and real-time monitoring by electrospray ionization mass spectrometry.* Environmental science & technology, 2005. **39**(16): p. 5982-5988.

16. R.R. Marques, M.J. Sampaio, P.M. Carrapiço, C.G. Silva, S. Morales-Torres, G. Dražić, J.L. Faria, and A.M. Silva, *Photocatalytic degradation of caffeine: Developing solutions for emerging pollutants.* Catalysis today, 2013. **209**: p. 108-115.

17. N. Miranda-García, M.I. Maldonado, J. Coronado, and S. Malato, *Degradation study of 15 emerging contaminants at low concentration by immobilized TiO2 in a pilot plant.* Catalysis Today, 2010. **151**(1): p. 107-113.

18. N. Klamerth, N. Miranda, S. Malato, A. Agüera, A. Fernández-Alba, M. Maldonado, and J. Coronado, *Degradation of emerging contaminants at low concentrations in MWTPs effluents with mild solar photo-Fenton and TiO2.* Catalysis Today, 2009. **144**(1): p. 124-130.

19. A. Rey, P. Garcia-Munoz, M. Hernandez-Alonso, E. Mena, S. Garcia-Rodriguez, and F. Beltran, *WO 3–TiO2 based catalysts for the simulated solar radiation assisted photocatalytic ozonation of emerging contaminants in a municipal wastewater treatment plant effluent.* Applied Catalysis B: Environmental, 2014. **154**: p. 274-284.

20. D. Mukherjee, S. Barghi, and A.K. Ray, *Preparation and characterization of the TiO2 immobilized polymeric photocatalyst for degradation of aspirin under UV and solar light.* Processes, 2013. **2**(1): p. 12-23.

21. D. Li, X. Cheng, X. Yu, and Z. Xing, *Preparation and characterization of TiO2-based nanosheets for photocatalytic degradation of acetylsalicylic acid: Influence of calcination temperature.* Chemical Engineering Journal, 2015. **279**: p. 994-1003.

22. R. Giri, H. Ozaki, S. Ota, R. Takanami, and S. Taniguchi, *Degradation of common pharmaceuticals and personal care products in mixed solutions by advanced oxidation techniques.* International Journal of Environmental Science & Technology, 2010. **7**(2): p. 251-260.

23. K. Nagaveni, G. Sivalingam, M. Hegde, and G. Madras, *Photocatalytic degradation of organic compounds over combustion-synthesized nano-TiO2.* Environmental science & technology, 2004. **38**(5): p. 1600-1604.

24. W. Guo, X. Liu, P. Huo, X. Gao, D. Wu, Z. Lu, and Y. Yan, *Hydrothermal synthesis spherical TiO2 and its photo-degradation property on salicylic acid.* Applied Surface Science, 2012. **258**(18): p. 6891-6896.

25. G. Colon, M. Hidalgo, and J. Navıo, *Photocatalytic deactivation of commercial TiO2 samples during simultaneous photoreduction of Cr (VI) and photooxidation of salicylic acid.* Journal of Photochemistry and Photobiology A: Chemistry, 2001. **138**(1): p. 79-85.

26. C. Adán, J.M. Coronado, R. Bellod, J. Soria, and H. Yamaoka, *Photochemical and photocatalytic degradation of salicylic acid with hydrogen peroxide over TiO 2/SiO 2 fibres.* Applied Catalysis A: General, 2006. **303**(2): p. 199-206.

Chapter 6 Conclusions and Outlook

6.1 Conclusions

Water is the most basic and important of resources, it is used for a variety of tasks in everyday life such as washing of clothes, basic sanitation, cooking and most importantly drinking. Clean drinking water is essential and in countries such as South Africa in which rainfall is low, it is difficult to deliver clean water to rural areas. There are many challenges to the delivery of clean drinking water one of which is pollution. ECs are organic pollutants and can be treated in number of ways, one method photodegradation with TiO_2 offers promise.

Titanium dioxide was doped separately with copper, nitrogen and sulfur via sol-gel methods, and studied for the photodegradation of 4 EC namely aspirin, caffeine, phenacetin and salicylic acid.

Copper doped catalysts were doped in a range of 2-5 mol% in relation to the moles of titanium present. The ICP-OES results showed that the amount of copper present in all the catalysts was lower than expected; this may be due to experimental error. From SEM and TEM results the catalyst appeared to be agglomerated and showed a wide range of particle sizes. The catalysts were shown to all be mesoporous with disordered pores, copper doping greatly improved surface area though after the 2% Cu TiO_2 sample surface area once again increased. Powder XRD showed that all samples only consisted of anatase phase TiO_2 which was confirmed by Raman. UV-DRS measurements showed that copper doping narrowed the band gap of TiO_2 however only up to a doping amount of 3% mol Cu thereafter an increase in band gap was seen. The amount of electron-hole recombination was reduced by doping with copper.

Nitrogen doped catalysts were doped in a range of 2-4 moles for every 1 mole of titanium dioxide used. From the results it was clear that nitrogen doping resulted in the narrowing of the TiO_2 band gap, increased the surface area in relation to the undoped catalyst and decreased the amount of electron-hole recombination. From XRD and Raman it was clear that all of the nitrogen doped catalysts consisted solely of anatase phase TiO_2. From nitrogen physisorption it was seen that the catalysts were all mesoporous with disordered pores. SEM and TEM micrographs showed that the catalysts consisted of agglomerates.

Sulfur doped catalysts were prepared in a range of 2-4 moles of sulfur for every one mole of titanium present in synthesis. It was found by ICP-OES measurements that the amount of sulfur present in the catalysts was much lower than was originally intended though this could be understood as sulfur may have formed SO_2 upon calcination. From SEM and TEM micrographs it appears as though the sulfur doped catalysts form agglomerates. From nitrogen physisorption measurements it was determined that, all of the catalysts were mesoporous with a Type IV isotherm and all the catalysts ha disordered pores. The surface of the catalysts showed a clear increase with an increase in the level of sulfur doping. XRD and Raman studies revealed that only anatase phase TiO_2 was present in all the catalysts. The band gap of the TiO_2 was greatly reduced through the addition of sulfur. From PL spectra it was clear that sulfur doping decreased the amount of electron-hole recombination but after a certain amount of sulfur was added the electron-hole recombination rate once again increased.

These catalysts were tested for photocatalytic activity by degrading 4 EC and compared to the activity of the commercial catalyst Degussa P25. The reaction was shown to be photocatalytic as there was no activity in the absence of light was the catalyst was present. Of the copper doped catalysts the 4% Cu TiO_2 was seen to have the best overall activity. Of the nitrogen doped catalysts the TiO_2:N 1:4 catalysts was shown to have the best overall

activity. From the sulfur doped catalysts it was determined the TiO_2:S 1:4 catalyst had the best activity. The doped catalysts all showed better activity for the degradation of the 4 compounds than the respective undoped catalyst. It was found that overall none of the synthesised catalysts had better activity than P25 for the degradation of all 4 compounds. However it was seen that the TiO_2:S 1:4 catalyst had far better activity than P25 for the degradation of SA, and it was for this reason that this catalyst was chosen to be used to optimise reaction conditions. The best reaction conditions were found to be 2 ppm of each substrate at pH 8.9 and with a catalyst mass of 80 mg. Upon testing P25 against these reaction conditions it was found that P25 still had better overall activity than the TiO_2:S 1:4 catalyst, but that the TiO_2:S 1:4 catalyst still had far greater activity for the degradation of SA.

Overall doping did not affect the selectivity of the degradation reactions and the variation of reaction parameters in the case of the TiO_2:S 1:4 catalyst also did not affect the selectivity of the degradation reactions.

6.2 Outlook and Challenges

This project has looked at doped TiO_2 for the degradation of pollutants found in water bodies; furthermore these degradation reactions were done on mixtures meaning they represented a realistic application of these catalysts for water remediation. It has been found that not all of the pollutants were degraded at the same time and to the same extent, the reason for this finding needs to be studied more carefully. Compounds should be degraded individually and in combinations (2 compounds in a mixture) so as to determine what factors control the selectivity of the degradation when degrading multiple compounds simultaneously.

Better results than those obtained in this study for the degradation of caffeine, aspirin and phenacetin have been reported in other studies. These studies used high power lamps or sunlight as a source of light. To generate a better idea of how well these catalysts may work for real world application, degradation of ECs with TiO_2 with sunlight as a light source should be done. Also other studies have used external oxidants to carry out degradation reactions, the effect of external oxidants on the degradation of ECs with doped TiO_2 should be studied.

Appendix A

Software Version	: 6.3.1.0504	Date	: 7/28/2015 11:32:01 AM
Sample Name	:	Data Acquisition Time	: 7/28/2015 11:06:44 AM
Instrument Name	: PE HPLC	Channel	: A
Rack/Vial	: 0/0	Operator	: manager
Sample Amount	: 1.000000	Dilution Factor	: 1.000000
Cycle	: 1		

Result File : C:\PenExe\TcWS\Ver6.3.1\Examples\10 ppm combined 1.rst
Sequence File : C:\PenExe\TcWS\Ver6.3.1\Examples\10 ppm combined 1.seq

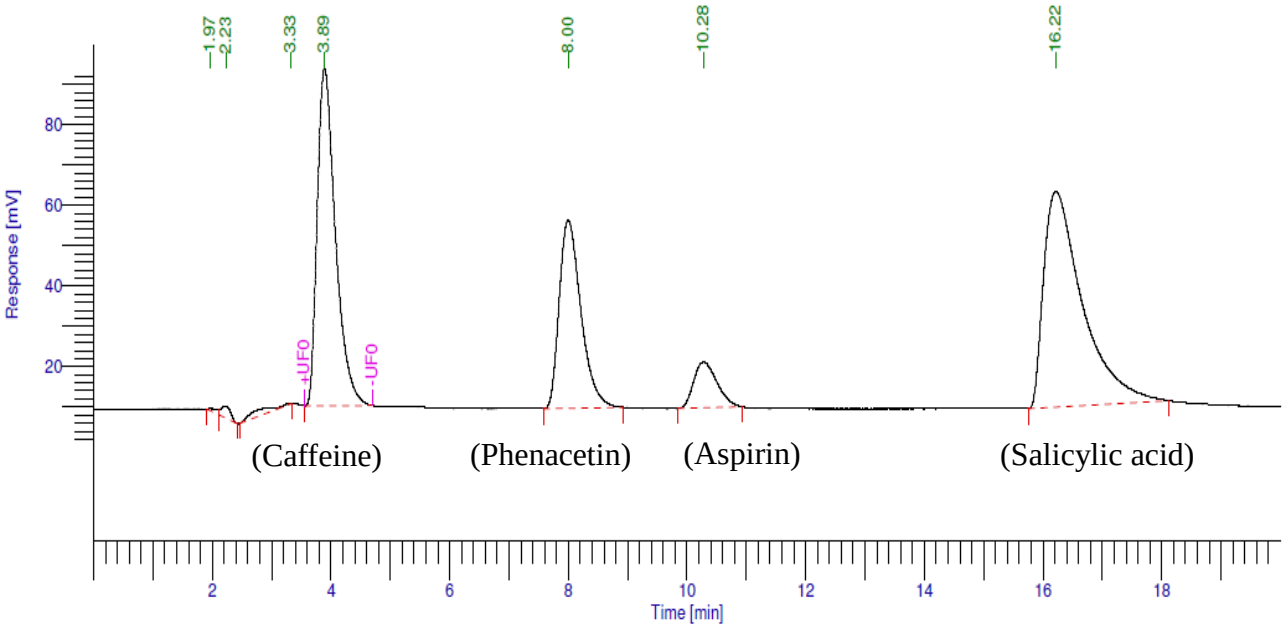

Caffeine REPORT

Peak #	Component Name	Time [min]	Area [uV*sec]	Height [uV]	Area [%]	Adjusted Amount
1		1.970	8800.06	529.23	0.15	0.0088
2		2.225	32902.80	3041.37	0.57	0.0329
3		3.327	42996.28	94.79	0.74	0.0430
4		3.888	1781822.10	83634.33	30.75	1.7818
5		7.996	1186729.39	46708.55	20.48	1.1867
6		10.281	310227.74	11417.50	5.35	0.3102
7		16.217	2430862.37	53468.79	41.95	2.4309
			5794340.74	198894.57	100.00	5.7943

Figure A1: Chromatograph showing the retention times of the ECs tested.

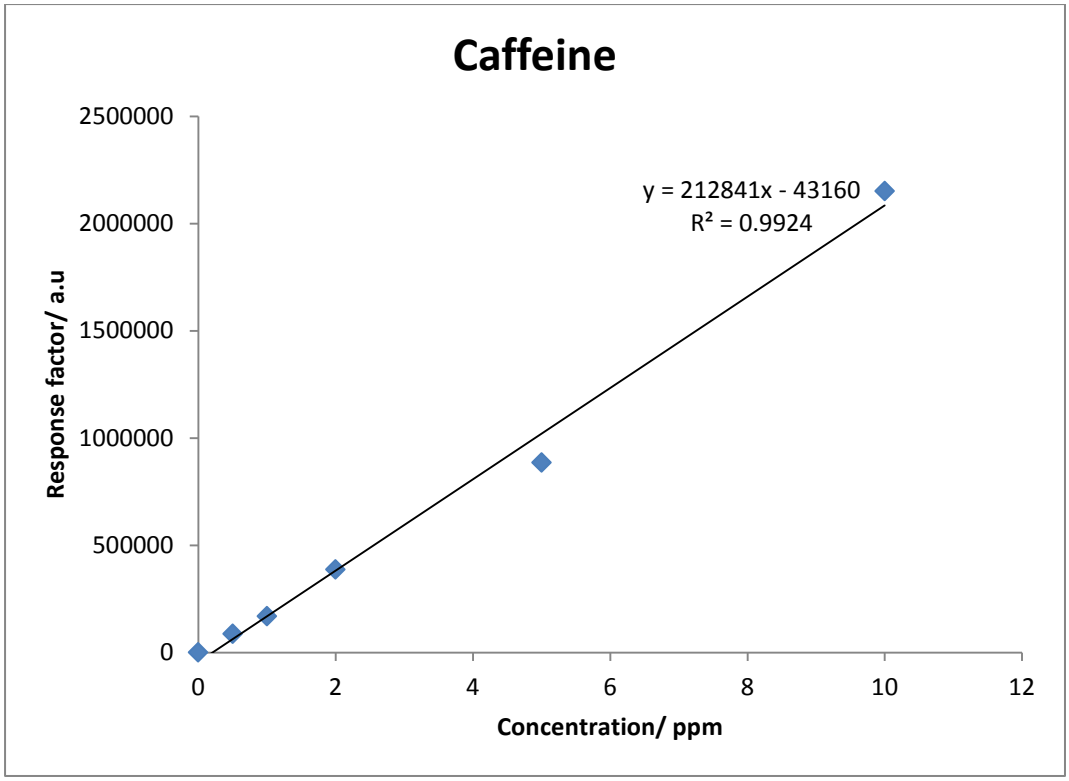

Figure A2: Calibration curve of caffeine as calculated from results obtained from HPLC.

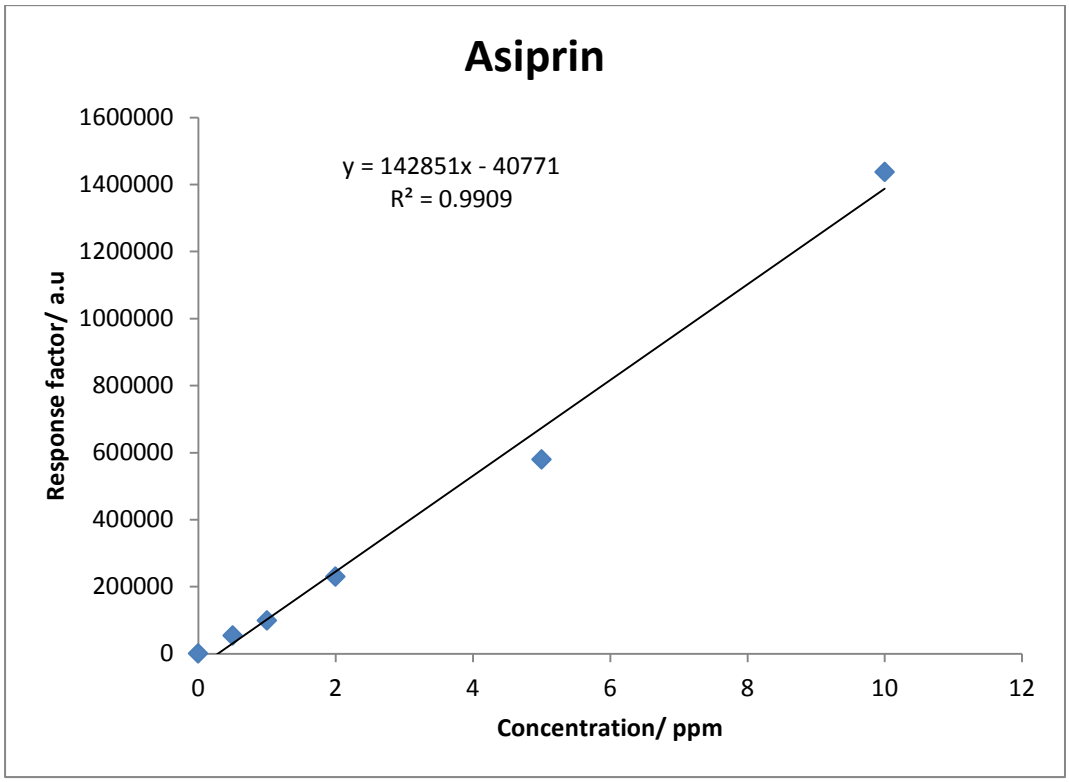

Figure A3: Calibration curve of aspirin as calculated from results obtained from HPLC.

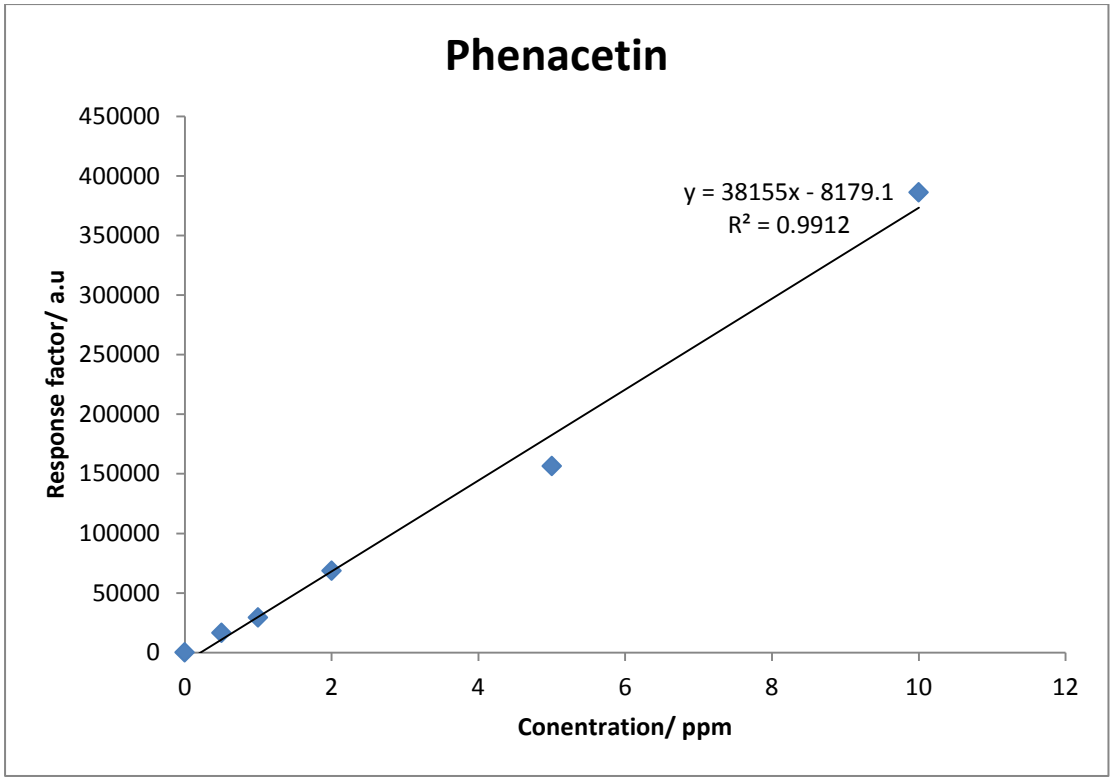

Figure A4: Calibration curve of phenacetin as calculated from results obtained from HPLC.

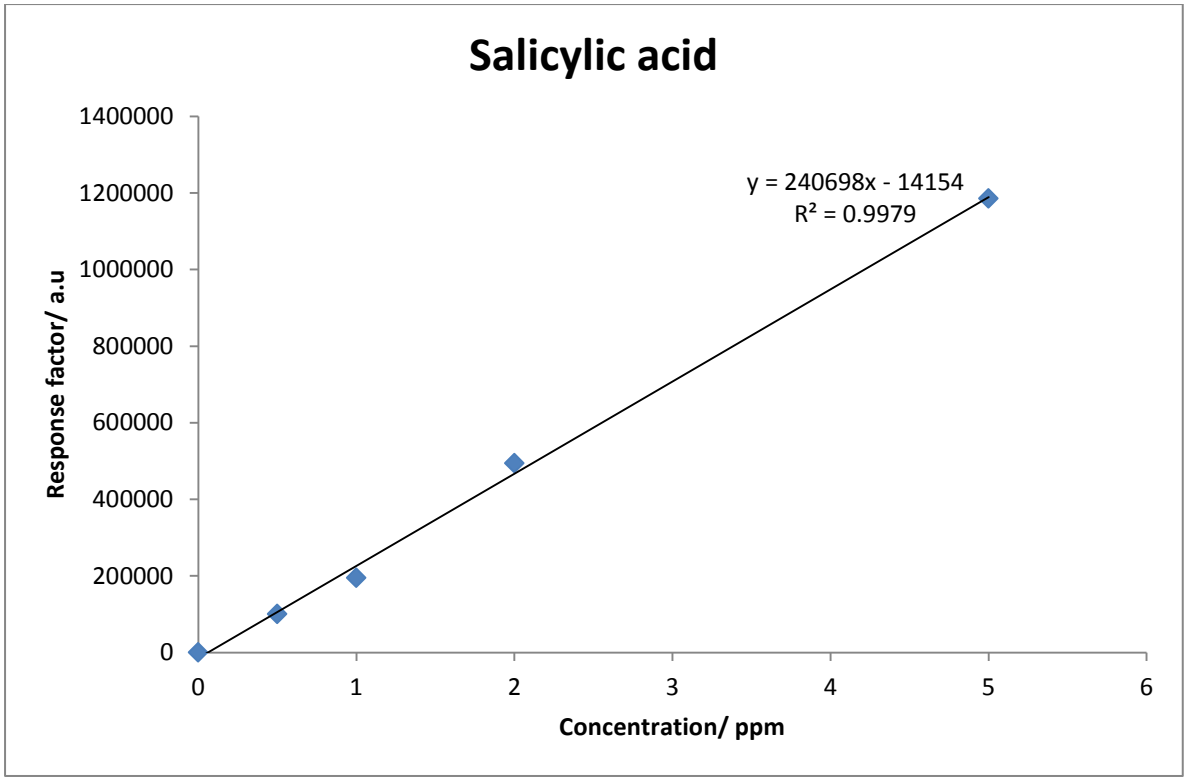

Figure A5: Calibration curve of salicylic acid as calculated from results obtained from HPLC.

A sample excel workbook of the calculations used for the reactions is provided on the CD accompanying the thesis.

Appendix B

These calculations are for the 2% Cu TiO_2 catalyst ICP-OES

$$Number\ of\ mols\ (Cu) = \frac{mass\ of\ copper}{Molar\ mass\ of\ copper}$$

$$\frac{3.3535*10^{-5}g}{63.546\ mol.g^{-1}} = 5.277\ x10^{-7}\ mol$$

$$Number\ of\ mols\ (Ti) =$$

$$\frac{mass\ of\ titanium}{Molar\ mass\ of\ titanium}$$

$$\frac{276.39*10^{-5}g}{47.867\ mol.g^{-1}} = 5.774\ x10^{-5}\ mol$$

$$n\ (Ti) = n\ (TiO_2)$$

$$\%\ mol = \frac{mol\ (Cu)}{mol\ (Ti)} * 100$$

$$\frac{5.277\ x10^{-7}}{5.774\ x10^{-5}} * 100 = 0.91\%$$

Bragg's law calculations copper undoped catalysts

$$d = \frac{n\lambda}{2Sin\theta}$$

$$\theta = \frac{25.345}{2} * \frac{\pi}{180}$$

$$\theta = 0.221 \text{ radian}$$

$$d = \frac{0.15405}{2*\sin(0.221)}$$

$$d = 0.352 \text{ nm}$$

"c" parameter calculation copper undoped catalyst

$$\frac{1}{d^2} = \frac{h^2+k^2}{a^2} + \frac{l^2}{c^2}$$

$$\frac{1}{0.2375^2} = \frac{0^2+0^2}{a^2} + \frac{4^2}{c^2}$$

$$0.05641 = \frac{c^2}{16}$$

$$0.05641 * 16 = c^2$$

$$\sqrt{0.9027} = c$$

$$c = 0.9501\ nm$$

Crystallite size calculation copper undoped catalyst

$$L = \frac{0.9\lambda}{\beta cos\theta}$$

$$\beta = \frac{FWHM*2*\pi}{360}$$

$$\beta = \frac{0.4592*2*3.14}{360}$$

$$\beta = 0.0081\ radian$$

$$L = \frac{0.9*0.15405}{0.00801\cos(0.221)}$$

$$L = 17.75\ nm$$